THE UPTAKE, TRANSPORT, AND STORAGE OF NICKEL IN CELLS:

A MODELING STUDY OF MN_2S_2 COMPLEXES AND THEIR DERIVATIVES

A Dissertation

by

JASON ADAM DENNY

Submitted to the Office of Graduate and Professional Studies of
Texas A&M University
in partial fulfillment of the requirements for the degree of

DOCTOR OF PHILOSOPHY

Chair of Committee,	Marcetta Y. Darensbourg
Committee Members,	David P. Barondeau
	Donald J. Darensbourg
	Timothy R. Hughbanks
	Sandun Fernando
Head of Department,	Francois P. Gabbai

August 2015

Major Subject: Chemistry

Copyright 2015 Jason Adam Denny

ABSTRACT

Nickel is an essential metal in biological systems and numerous studies have investigated the import, regulation, utilization, and export in cells and the proteins involved. Coordination complexes of nickel have been aimed at providing background information on exchange of nickel from N-rich binding sites used for import and storage to S-rich sites of the active enzymes. The model compounds were used to investigate a range of metal exchange reactions that are plausible during nickel homeostasis in cells.

A comprehensive review has examined the MN_2S_2 complexes that have been synthesized-to-date and their structural aggregation properties when two to four metals bind to the available lone pair on the thiolate in MN_2S_2 complexes. The review summarized a wide range of modifications that are possible for MN_2S_2 complexes ranging from the metal used to the organic linker between the N and S donor atoms. The aggregation modes are largely determined by the coordination number preferences of the secondary metal(s). Another project attempted to quantify the electron donor properties and steric requirements of such MN_2S_2 metalloligands. Electronic donor properties were measured using the IR stretches in metal carbonyl reporter units. Attempts to quantify the spacial requirements of MN_2S_2 metalloligands were challenging due to the asymmetry of such ligands and several approaches were utilized such as the ligand cone angles (related to the famous Tolman cone angle) for monodentate binding, wedge angles for bidentate binding, or percent buried volume computations for both cases.

A series of $MN_2S_2O_2$ complexes was synthesized and metal exchange properties examined. The complexes could be obtained from S-modification of MN_2S_2 compounds of from the free N_2S_2 ligand followed by metallation. The study showed the hierarchy of metal exchange followed the Irving-Williams series of stability for first row transition metals: $Fe^{2+} < Co^{2+} < Ni^{2+} < Cu^{2+} > Zn^{2+}$. The mechanism of exchange appears to occur through a ligand unwrapping/wrapping process similar to the previously investigated M(EDTA) systems by Margerum in the 1960's.

A wide range of biomimetic and inorganic compounds structures were solved using X-ray diffraction methods and figures for the finalized structures are presented.

DEDICATION

This dissertation is dedicated to my parents, Georgette, and all the friends I've made during my time in graduate school for their encouragement and occasional distractions that kept me going.

ACKNOWLEDGEMENTS

I would like to first thank my advisor Dr. Marcetta Y. Darensbourg for all the guidance and mentoring you have imparted on me throughout my time as an undergraduate and graduate student in your lab. You have always challenged and pushed me to improve my knowledge, understanding, and presentation of my work. I also can't thank you enough for standing in my corner and fighting for me when it came to various awards and career opportunities.

I would like to acknowledge my committee members Dr. David Barondeau, Dr. Tim Hughbanks, Dr. Don Darensbourg, and Dr. Sandun Fernando. I thank Dr. Nattami Bhuvanesh and Dr. Joesph Reibenspies for countless help teaching me crystallography, assisting me with troublesome structures, and of course the numerous times I came to bug the two of you with questions. Dr Clearfield, thank you for allowing me to teach and assist you with the inorganic teaching lab course and the multiple letters of recommendation you wrote for me over the years.

I wish to thank the current and past members in the MYD and DJD groups for your friendships and chemical discussions. In particular, Dr. Eric Frantz, Dr. Jeremy Andreatta, Dr. Ross Poland, Dr. Stephanie Poland (Wilson), Dr. Roxanne Jenkins, Dr. Elky Almaraz, Mr. William Foley, Dr. Jennifer Young (Hess), Dr. Scott Brothers, Dr. Danielle Crouthers, Rachel Chupik, and Allen Lunsford.

Danielle, Jen, and Scott I especially wish to thank you for your true friendship and help celebrating the highs and making it through the lows of grad school. Elky and

William I never would have made it anywhere without your guidance and friendships when I first started in the MYD group back in May 2007 as an undergraduate. I never would have made it where I am today without the two of you getting me started in lab. I also wish to thank the two undergraduate students that have worked for me during my time, Elizabeth Campbell and Alex Todd. Our reactions may not have always worked out as originally planned, but I am indebted to both of you for your hard work and am proud that both have moved on to start their own Ph.D. work.

Georgette, I know life hasn't always been easy being in a relationship with me and on top of that, dating a fellow chemistry graduate student, but I am forever thankful for your love and support. Thank you for the encouragement, venting sessions, and everything else I already thanked you for and for the things I forgot to thank you for. Soon we will both be doctors and moving on to the next stage, love you.

Of course I can't forget about all the friends I have made at A&M and their valued discussions and distractions from life. Last, but certainly not least, my parents for providing me with the values and opportunities that allowed me to get a strong education at every stage of my life as well as the encouragement and support to pursue my education and other opportunities during my lifetime such as sports and scouting.

NOMENCLATURE

1Fc	1-(ferrocenylmethyl)-3-methylimidazolate
2Fc	1,3-bis(ferrocenylmethyl)imidazolate
$\%V_{bur}$	percent volume buried
AA	acetamide
ACS	acetyl-CoA synthase
ATP	adenosine triphosphate
BArF	tetrakis[3,5-bis(trifluoromethyl)phenyl]borate
Bipy	bipyridine
bme-dach	N,N'−bis−2−mercaptoethylene−1,4−diazacycloheptane
bme-daco	N,N'−bis−2−mercaptoethylene−1,5−diazacyclooctane
bme*-daco	N,N'-bis(2-mercapto-2-methylpropylene-1,5-diazacyclooctane
CCDC	Cambridge Crystallographic Data Center
cif	crystallographic information file
CODH	carbon monoxide dehydrogenase
Cp	cyclopentadienyl
Cys	cysteine
DCM	dichloromethane
DFT	density functional theory
D-Hpen	D-penicillin
DMF	dimethyl formamide

DNA	deoxyribonucleic acid
DNIC	dinitrosyl iron complex
dppe	diphenylphosphinoethane
dppm	diphenylphosphinomethane
dppp	diphenylphosphinopropane
dsdm	N,N'-dimethyl-N,N'-bis(2-sulfanyl-ethyl)ethylenediamine)
EDTA	ethylenediaminetetraacetic acid
ema	N,N'−ethylenebis(2−mercaptoacetamide)
EPR	electron paramagnetic resonance
Gln	glutamine
H_2ase	hydrogenase
His	histidine
Hpn	*H. pylori* nickel storage protein
Hpn-like	*H. pylori* nickel storage protein; but larger than Hpn
HspA	heat shock protein for nickel storage
HypABCDEF	proteins for the maturation of [NiFe]-hydrogenase
IMe	1,3−bis(methyl)imidazolate
IMeMes	1−methyl−3−(2,4,6−trimethylphenyl)imidazolate
IMes	1,3−bis(2,4,6−trimethylphenyl)imidazolate
IMesiPr	1,3−bis(2,6−diisopropylphenyl)imidazolate
IPr	1,3−bis(isopropyl)imidazolate
IR	infrared spectroscopy

K_D	dissociation constant
KmtR	*M. tuberculosis* nickel regulator protein
M_{disp}	metal displacement
MeImid	methylimidazole
mese-daco	N,N'−(mercaptoethyl)(sulfinatoethyl)diazacyclooctane
MS	mass spectrometry
neocup	2,9-dimethyl-1,10-phenanthroline
NHC	N-heterocyclic carbene
NiCoT	nickel and cobalt transporter protein
NikABCDE	proteins for import of nickel into a cell
NikR	nickel regulator protein
NiSOD	nickel superoxide dismutase
NMR	nuclear magnetic resonance spectroscopy
NmtR	*M. tuberculosis* nickel regulator protein
pip	piperidine
pma	N,N'−phenylenebis(2−mercaptoacetamide)
PPN	bis(triphenylphosphine)iminium
PTA	1,3,5-triaza-7-phosphadamantane
Py	pyridine
RcnR	nickel regulatory protein
RND	resistance-nodulation-division protein for the efflux of nickel
SambVca	online software for percent volume buried calculations

SlyD	nickel storage protein
SP	square pyramidal
Stip	(2,4,6−tri−isopropyl)thiophenylate
TBP	trigonal bipyramidal
T_d	tetrahedral
THF	tetrahydrofuran
tsalen	thiosalen or 2,2'-ethylenebis(nitrilomethylidene)dithiophenol
TNIC	trinitrosyl iron complex
UreABCDEFG	proteins for the maturation of urease
XRD	X-ray diffraction

TABLE OF CONTENTS

Page

LIST OF FIGURES

Page

Page

Page

Page

Page

Page

Page

Page

LIST OF TABLES

1. INTRODUCTION AND LITERATURE REVIEW*

1.1 Introduction

Nature has had nearly four billion years to perfect the chemical reactions needed to sustain life in a diverse range of environmental conditions, while humans have only been working to mimic the natural systems for less than a hundred years. Enzymes are the reaction workhorses in the natural systems and utilize a range of metals from Ca to Mn to Zn in mediating, promoting and catalyzing the reactions required for life.[1] The most common metals in the active sites of the enzymes are iron and copper in various redox levels and coordination environments, however the major focus of my work is on the investigation and modeling of the enzymes which contain nickel in their active sites.

1.2 Nickel Containing Enzymes

Currently there are no known enzymes or nutritional requirements for nickel in animals; even though multiple proteins have been found capable of binding nickel.[2-4] However, uses for nickel in biological systems are found in prokaryotes and, more specifically, in the 8 nickel-containing enzymes that are currently known. These include methyl-CoM reductase, glyoxylase I, acireductone dioxygenase, urease, [NiFe]-hydrogenase, nickel superoxide dismutase, carbon monoxide dehydrogenase, and acetyl-CoA synthase.[5]

---

* Figures reproduced with permission from Li, Y.; Zamble, D. B. *Chem. Rev.* **2009**, *109*, 4617. Copyright **2009** American Chemical Society.

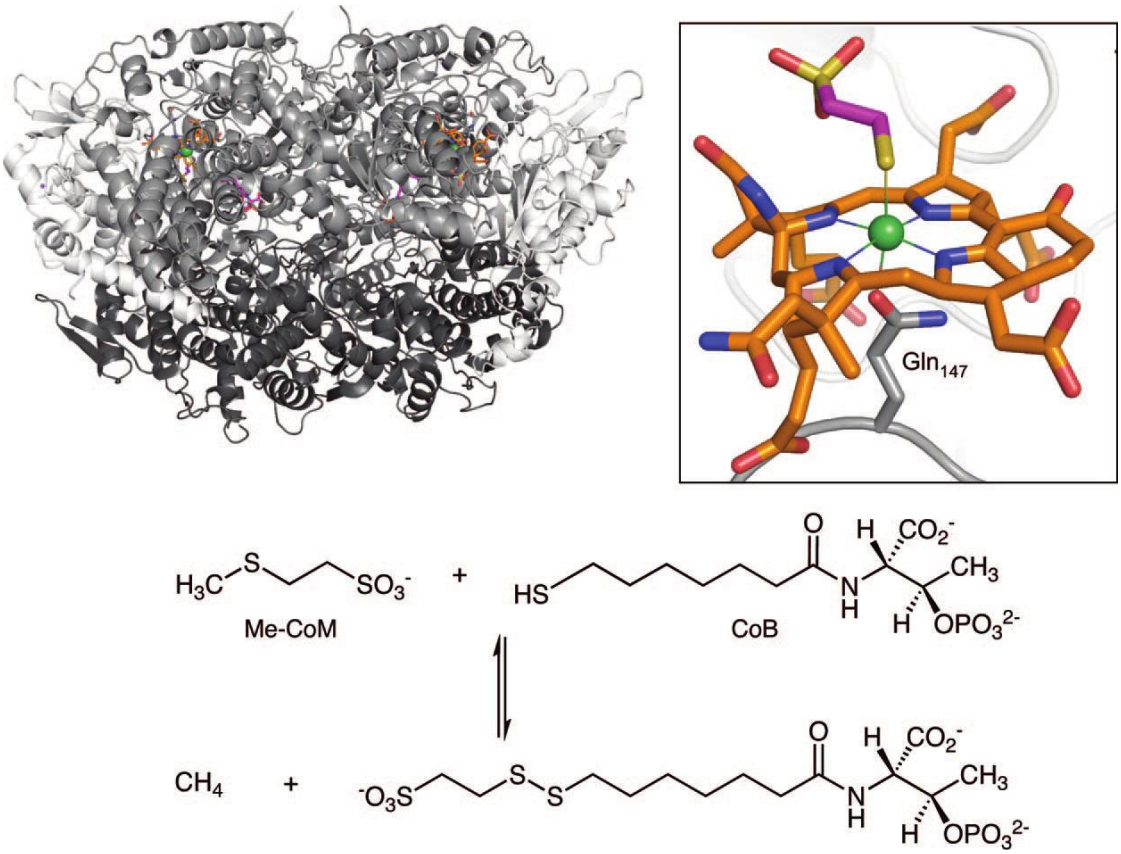

Figure 1-1. The crystal structure and active site of Methyl CoM reductase (pdb 1MRO) and the reaction catalyzed by the enzyme's nickel-containing active site. The color scheme is oxygen, red; nitrogen, blue; nickel, green; sulfur, yellow.[5]

Methyl-CoM reductase, Figure 1-1, is the final enzyme in methane biosynthesis of methanogenic and methanotrophic archaea.[1,6] The enzyme catalyzes the formation of methane through the fusion of Me-CoM and CoB to yield the disulfide CoM-CoB. The active site features a nickel-containing F430 corphin and was isolated with the axial ligands, Gln and CoM.[7-8] Acireductone dioxygenase, Figure 1-2, is the only known

nickel-containing oxygenase and is utilized in the methionine salvage pathway.[9] The active site consists of three histidines, a glutamate, and two water molecules.[10-13] Glyoxylase I is a cytosolic enzyme that removes toxic α-ketoaldehydes by eventual conversion to lactate.[14] The active site, Figure 1-3, contains an octahedral nickel bound to two water molecules, two histidines, and two glutamates.[15-16]

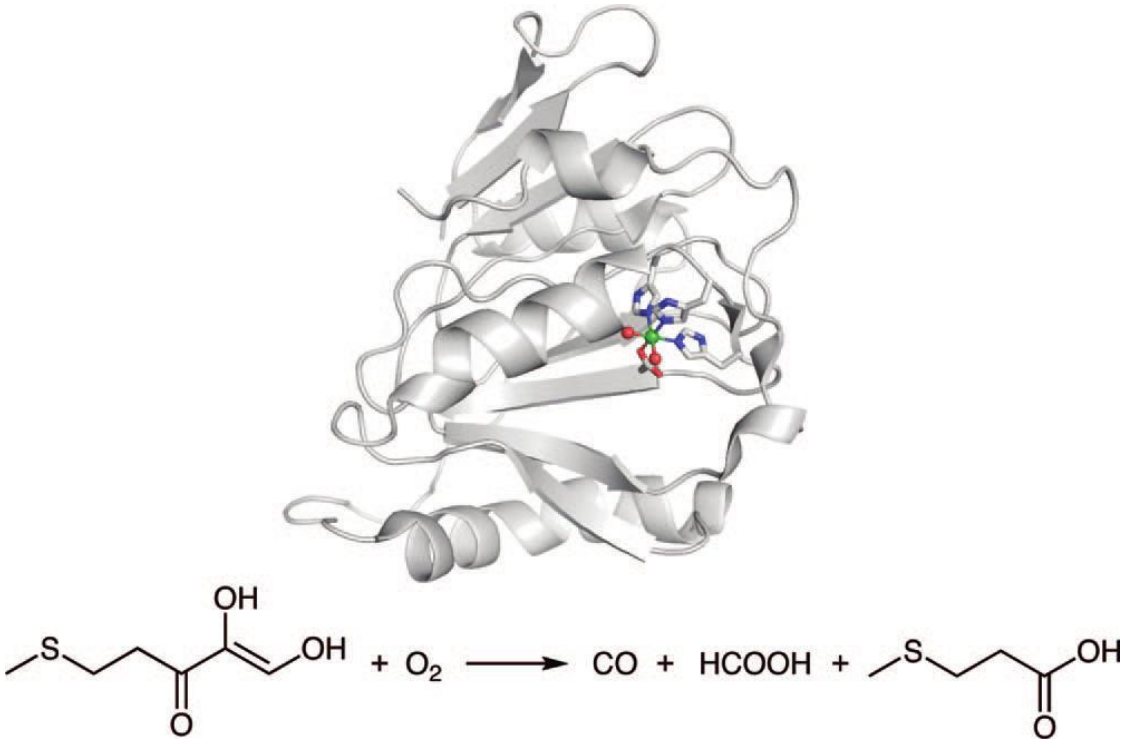

Figure 1-2. Protein crystal structure of acireductone dioxygenase (pdb 1ZRR) showing the nickel of the active site bound to 3 histidines, a glutamate, and a water ligand. The reaction catalyzed is also shown.[5]

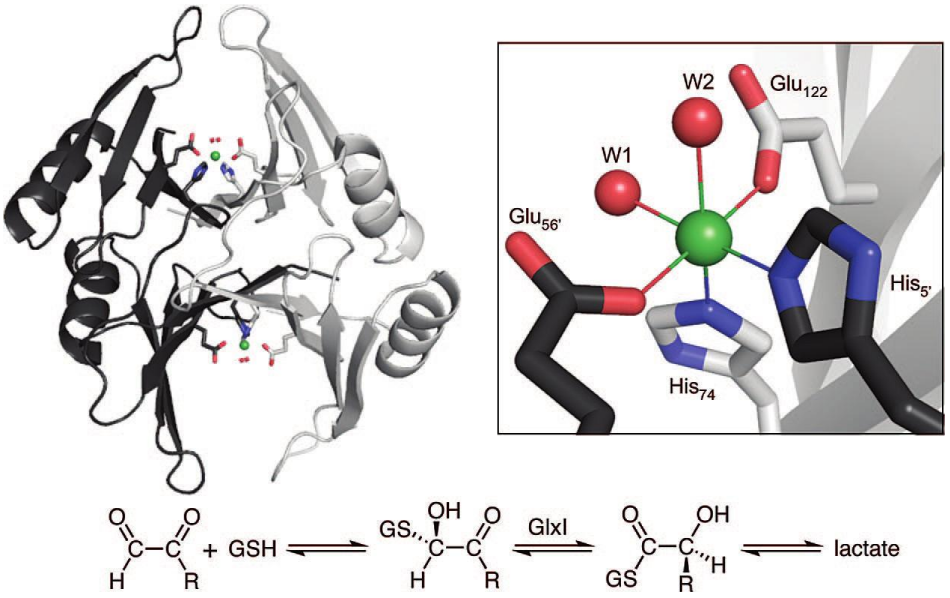

Figure 1-3. Crystal structure of glyoxalase I (pdb 1F9Z) with an inset showing the binding environment of the active site as well as the reaction it catalyzes.[5]

Urease, the first enzyme ever crystallized,[17] catalyzes the hydrolysis of urea into ammonia and carbonic acid; urease plays a key role in nitrogen metabolism of many organisms.[18] The active site, Figure 1-4, features two nickel centers bridged by a carbamylated lysine and hydroxide and each nickel has a water molecule and two N-donors from histidine residues.[19] One of the nickel centers also contains a terminal aspartate. Urease is assembled by four main proteins UreDEFG with the nickel ions being delivered to the active site by UreE.[20] UreE has a His-rich C-terminus tail that can bind 5-6 nickel ions in octahedral O/N donor sites with 10 μM affinity. A conserved histidine on the surface of the protein binds nickel to form protein dimers or tetramers.[21-23] However, the nickel ions of the active site are believed to arise from a Ni-O-Ni moiety located in the C-terminus region.[22,24]

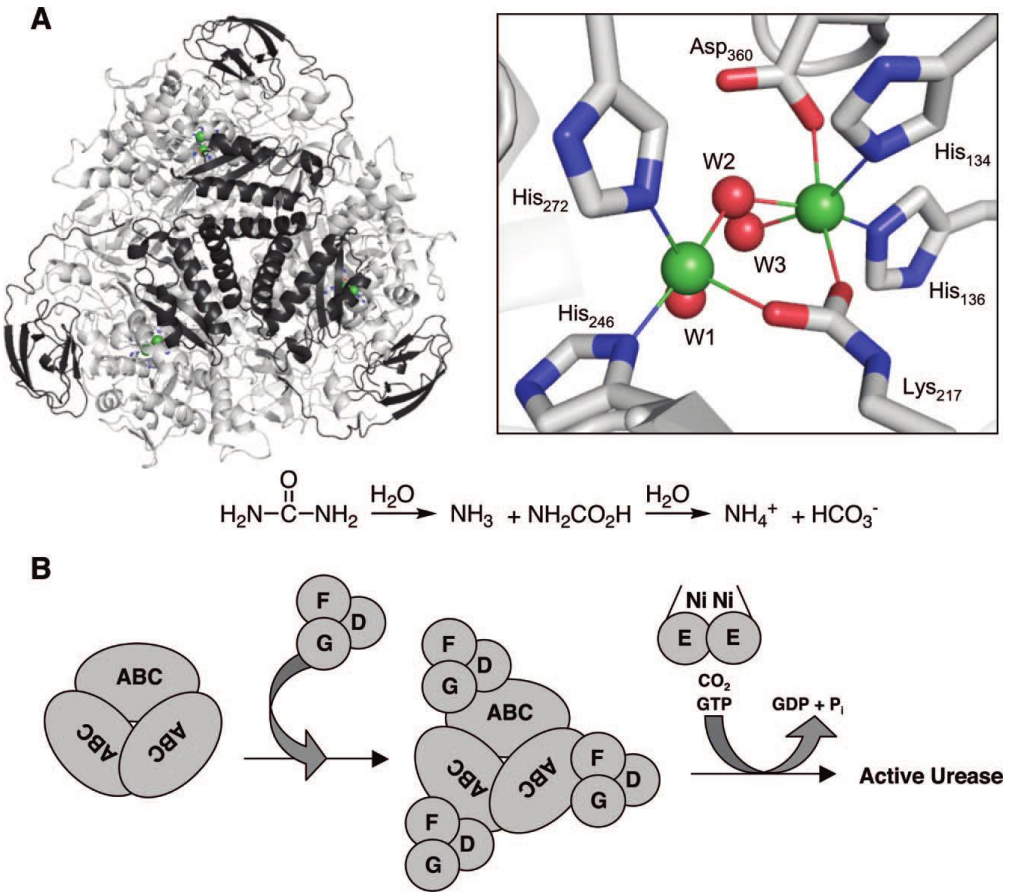

Figure 1-4. A) Protein crystal structure of urease (pdb 1FWJ) with inset showing the binuclear nickel active site and the catalyzed hydrolysis of urea. B) Biosynthesis of urease using UreABCDEFG maturation proteins.[5]

In addition to the UreDEFG proteins the [NiFe]-H_2ase proteins HypA, HypB, and SlyD described below have shown enhancement in nickel transfer to urease[25-26] but the reverse cannot be said for the UreDEFG proteins on the [NiFe]-H_2ase maturation process. That observation implies that the nickel in UreE is specifically intended for insertion into urease.[5]

Three additional storage proteins linked to the biosynthesis of urease are HspA, Hpn, and Hpn-like. HspA is a heat-shock protein (implies ability to form protein-protein complexes) that contains a C-terminus with eight histidine and four cysteine residues that can bind two nickel ions with 1-2 μM affinity.[27] Hpn is a 60-residue protein comprised of 28 histidine, 4 cysteine, and 8 carboxylate amino acids and is known to form large aggregates and bind multiple nickel ions with micromolar affinities. It provides nickel toxicity resistance.[28] The Hpn-like protein exhibits similar binding properties for nickel but contains more amino acids. Its composition is roughly 50% glutamines and 33% histidine residues. The Hpn and Hpn-like proteins are proposed to play a role in long-term nickel storage.[29-30]

The [NiFe]-hydrogenase (H_2ase) enzyme is biased towards the oxidation of hydrogen into protons and electrons, Figure 1-5. The [NiFe]-H_2ase enzyme is wide spread in bacteria and archaea and contain up to 13 iron atoms with only one nickel in the active site along with several iron-sulfur clusters, Figure 1-5.[31-33] The bimetallic, Ni-Fe active site is located in the large subunit of a heterodimeric protein with the small subunit containing a chain of FeS clusters for electron transport to and from the active site.[34] The nickel is bound to two terminal and two bridging thiolate cysteine residues with one of each originating from a CxxC motif. The iron is ligated by the two bridging cysteines as well as three poisonous diatomic ligands (two cyanides and one carbon monoxide). A third bridging ligand is observed but the exact identity is unknown but hypothesized to be a water or hydroxide ligand.[34]

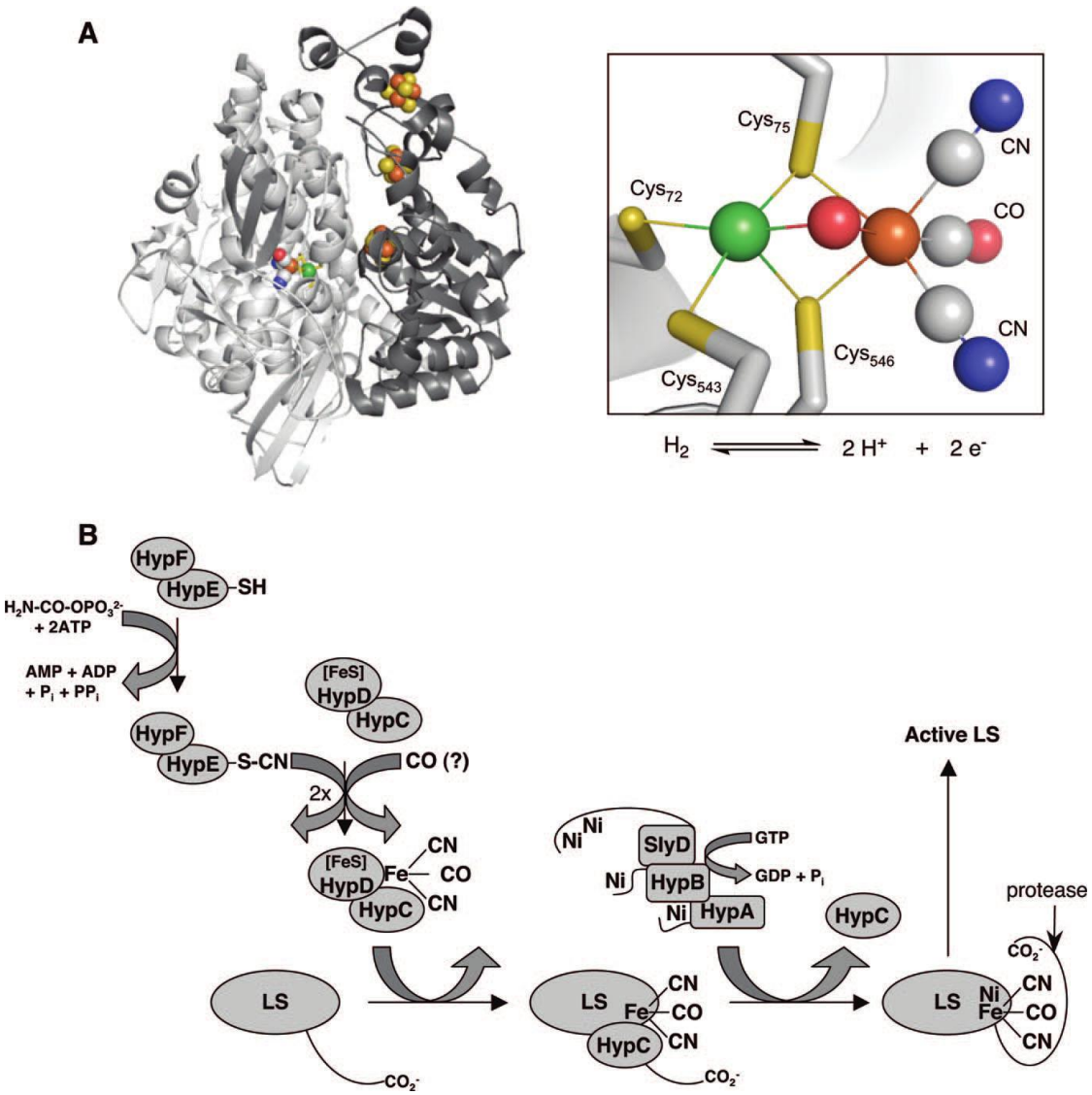

Figure 1-5. A) Crystal structure (pdb 1YRQ) of [NiFe]-hydrogenase showing the active site and reaction catalyzed. The large subunit is shown in light gray and the small subunit in dark gray. B) Maturation scheme to produce the large subunit, which after a protease cleaves the C-terminus, the small unit, containing the iron-sulfur clusters, can bind to form the active heterodimer of [NiFe]-hydrogenase. The iron is shown in orange.[5]

The maturation of [NiFe]-H_2ase involves at least 6 metallochaperones beginning with a complex of HypF and HypE for the synthesis of the CN^- ligand. HypF and HypE synthesize an SCN group by transfer of a carboxamide group from carbamoylphosphate to a cysteine in HypE followed by dehydration.[35] HypE can then form a complex with HypC and HypD to transfer the cyanide ligands to the iron.[36] The source of the CO ligand is not fully understood but once the diatomic ligands have been transferred to the HypC/HypD complex the metallochaperones can dock with the large subunit and transfer the $Fe(CN)_2(CO)$ unit.[37-38] The HypC protein remains bound to the large subunit maintaining an open conformation allowing direct access to the active site for nickel insertion.[39]

Two to three proteins can facilitate nickel insertion into the active site; however, none are required for nickel insertion to occur and form active enzyme.[40-48] The maturases are able to enhance nickel insertion as well as accomplish it at low-non-toxic levels of nickel.[49] The first protein, SlyD, is for nickel storage and contains a 50-residue C-terminus comprising 15 histidine, 6 cysteines, and 7 carboxylate amino acids capable of binding multiple metal centers.[50-51] There are indications that when SlyD forms a complex with HypB it increases the rate of nickel transfer compared to HypB alone.[26,52-53] Organisms without SlyD exhibit a modified HypB protein that has a His-rich region near the N-terminus for nickel storage.[45,47,54] HypA is believed to organize the interaction between the HypB/SlyD complex and the large subunit to transfer nickel from HypB to the active site.[55-59]

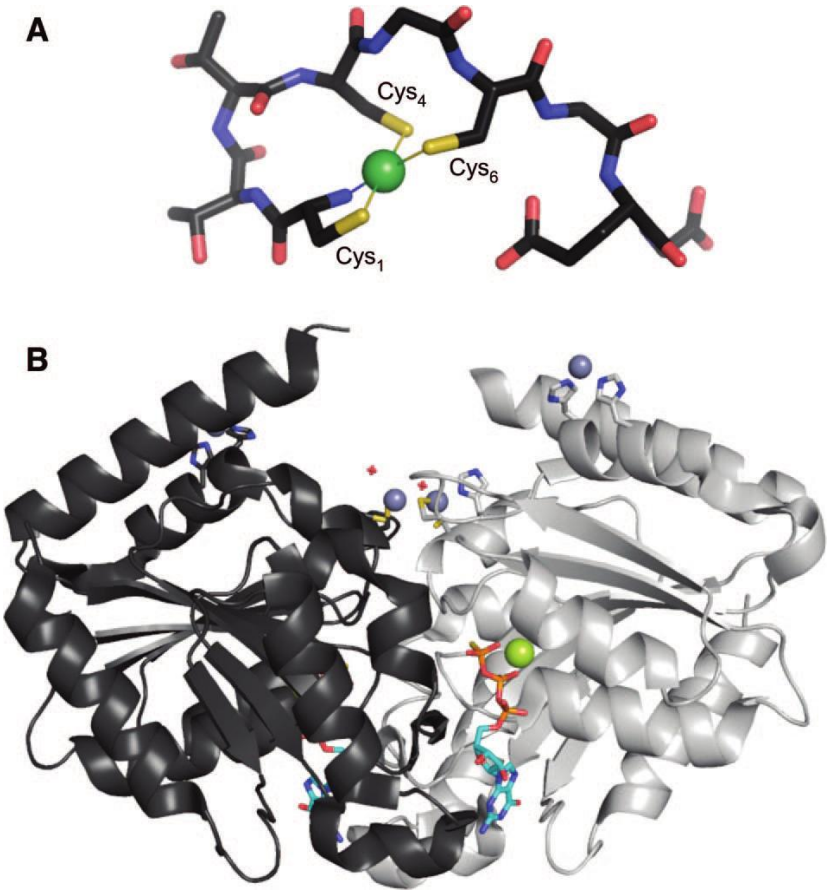

Figure 1-6. A) DFT calculated structure for the nickel high-affinity binding site of the N-terminus. B) Protein crystal structure of dimeric HypB (pdb 2HF8) showing the two zinc ions (light blue/gray) needed to form the dimeric interface of the two protein units. The zinc ions are tetrahedral with a bridging Cys_{95}, a terminal Cys_{127}, a water molecule, and the fourth binding site occupied by His_{96} or a terminal Cys_{95} for the respective zinc centers.[5]

The dimeric structure of HypB is shown in Figure 1-6 along with the high-affinity nickel binding site of the N-terminus which features a CxxCGC motif that binds the nickel in a square planar $S_3N_{terminus}$ fashion with 0.1 pM affinity.[60-61] At the dimer

interface is a dinuclear zinc site that has been shown to bind zinc an order of magnitude more strongly than nickel.[60,62] However, upon nickel binding, a conformational change is believed to occur which leads to protein-protein interactions. Alternatively, the protein-protein interactions could cause the conformational change which leads to nickel binding at the observed bimetallic zinc site.[60,62]

Once the nickel has been transferred to the active site the metallochaperones undock from the large subunit activating a protease that cleaves off the C-terminus of the large subunit.[63-67] Once the cleavage occurs a conformational change occurs which causes the large subunit to close around the active site and allow binding of the small subunit and formation of the active heterodimer of [NiFe]-H_2ase.[34]

The NiSOD enzyme, Figure 1-7, catalyzes the disproportionation of superoxide into oxygen and hydrogen peroxide by cycling between Ni^{2+} and Ni^{3+}.[68] The active site features an N-terminus His-Cys-X-X-Pro-Cys-Gly-X-Try motif where the nickel binds to the amino-terminus, two cysteines, and a backbone amide in a planar fashion.[69-70] The axial position of the square pyramidal nickel binds to His_1 which may dissociate and bind reversibly during catalysis as the nickel cycles between redox states; however, there are reports that the histidine remains bound.[71-74]

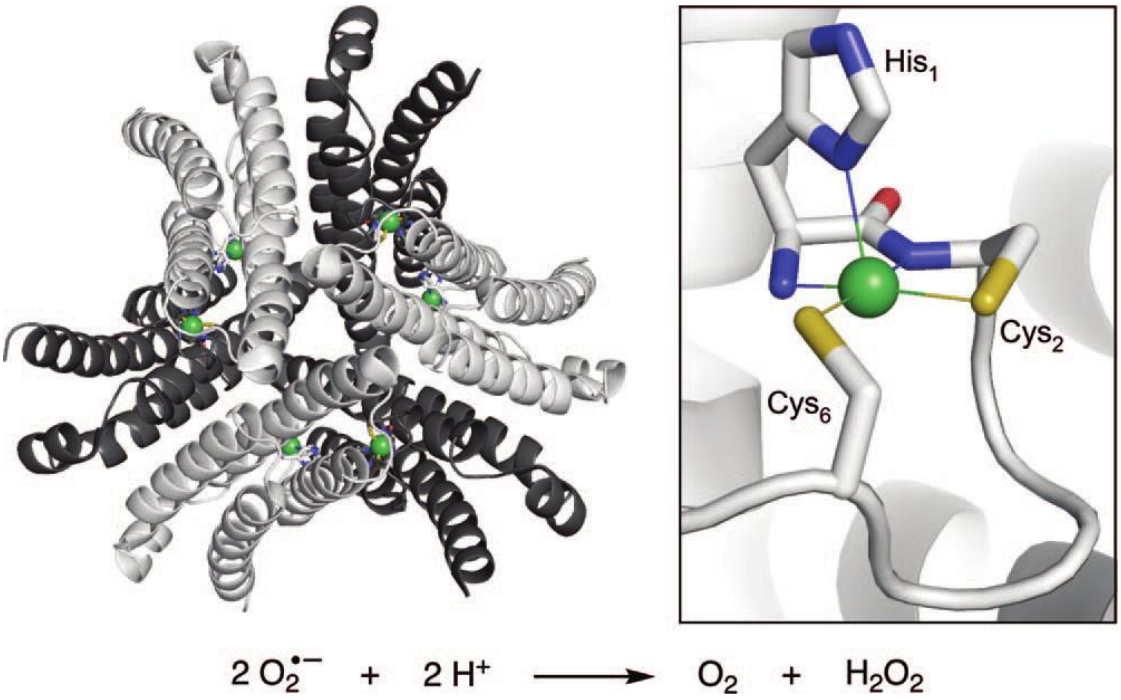

Figure 1-7. Crystal structure of the hexameric protein nickel superoxide dismutase with the NiN_3S_2 active site shown at right and the catalyzed disproportionation of superoxide shown below.[5]

The carbon monoxide dehydrogenase (CODH) and acetyl-CoA synthase (ACS) are the last of the known nickel-containing enzymes discussed herein. The crystal structure of the dimeric A- and C-cluster subunits, ACS and CODH respectively, is shown in Figure 1-8.[75-80] The CODH catalyzes the reversible conversion of CO to CO_2 using a series of 4Fe4S clusters for electron shuttling and an unusual open 4Fe4S cluster with a nickel ion.[81] A long channel connects the CODH and ACS active sites allowing for transport of CO to the ACS site.[81] The ACS active site features a NiN_2S_2 metalloligand to a second nickel which is bound to a 4Fe4S cluster and a fourth ligand

presumed to be water.[81-82] The distal NiN_2S_2 site is comprised of two amide backbone nitrogens and two cysteine residues that bridge to the proximal nickel which is also the site for the catalytic conversion of CoASH, methyl, and carbon monoxide to CoAS-CO-CH_3.[81-82]

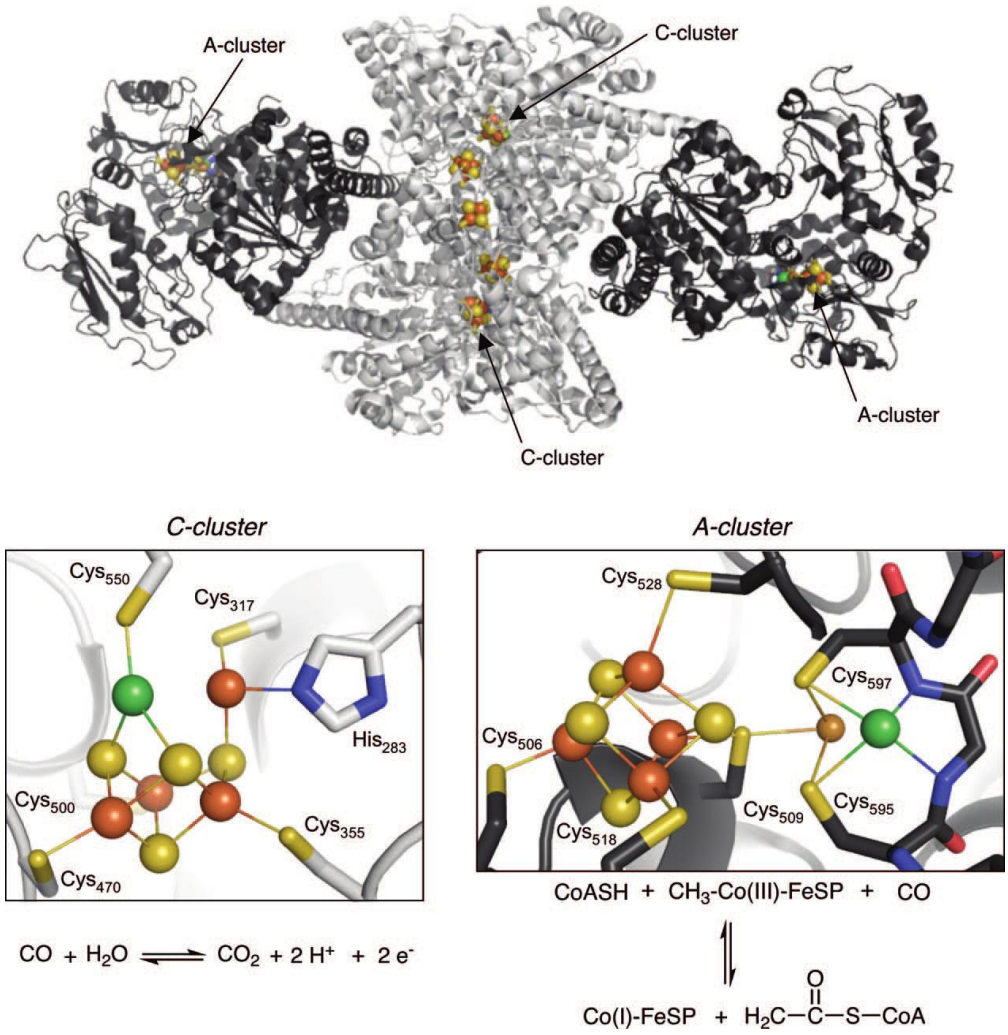

Figure 1-8. Protein crystal structure of the carbon monoxide dehydrogenase and acetyl-CoA synthase subunits (pdb 2Z8Y) with insets of the respective active sites and reactions shown below. Copper is shown in tan in the A-cluster but the active form contains nickel.[5]

1.3 Nickel Transport and Regulation

In addition to the proteins already mentioned above for nickel storage there are multiple proteins and mechanisms geared up for nickel transport into a cell. One such pathway involves the NikABCDE family that couples transport of nickel into the cell with ATP hydrolysis, Figure 1-9.[83-84] NikA is a periplasmic protein that binds nickel with six oxygen donors,[85] however other experiments have indicated a binding site of two histidines and four water molecules.[86] NikA transports nickel to the transmembrane proteins NikB and C, which are coupled to the cytoplasmic nucleotide-binding proteins, NikD and NikE.[87]

There are also permeases such as NiCoT and other less known mechanisms for nickel uptake by cells, Figure 1-9. Additionally, routes to export nickel are vital and there have been several pumps shown to remove nickel out of the cytoplasm or periplasm;[88-89] nevertheless, few nickel specific exporters are known.[89]

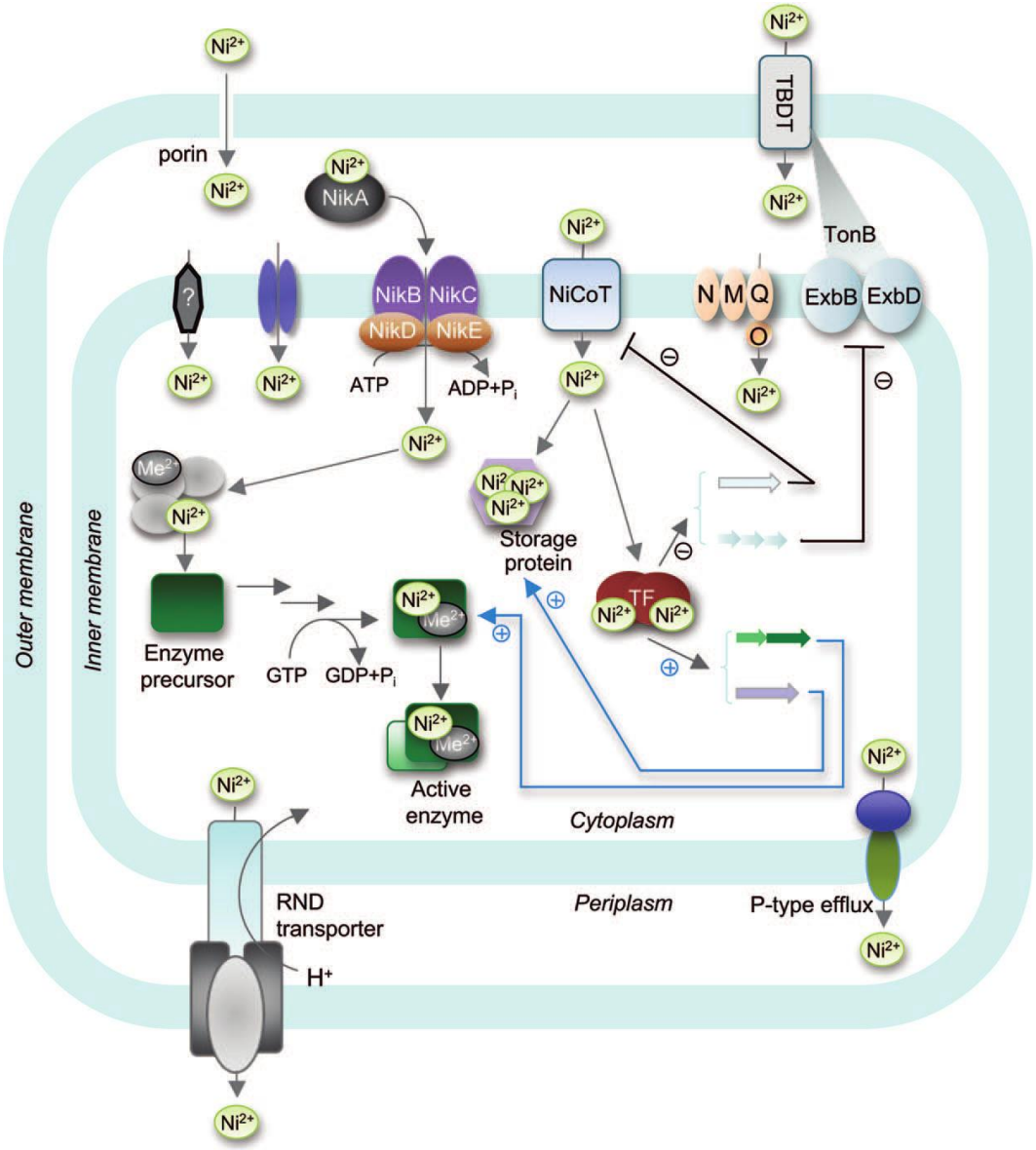

Figure 1-9. Schematic showing the homeostasis and regulation of nickel in biological systems beginning with the import of nickel by NikABCDE, NiCoT, and other import proteins. Once in the cell nickel can be stored in storage proteins such as SlyD or enzyme precursors such as HypB until it is needed to produce the active forms of nickel-containing enzymes. Nickel export is shown by means of an efflux pump or RND transporter.[5]

Nickel regulation must be a fundamental requirement in these systems to prevent nickel toxicity but preserve enzyme activity. One of the primary nickel transcription factors is the NikR protein which is found in a variety of bacteria and archaea and has been shown to bind to the major grove of DNA to suppress transcription of nickel import genes.[90-92] In the crystal structure, four nickel ions are shown to bind to residues at the interfaces of a tetramer which is bound to a short segment of DNA, Figure 1-10. The square planar coordination environment consists of two histidines and one cysteine from one monomer and a third histidine from another monomer.[93-94] This high affinity site binds nickel with nanomolar affinity and will subsequently bind to DNA with a K_D of 5 nM.[95-97] However at elevated nickel levels NikR will bind a second nickel at an octahedral, 2 histidine, 4 N/O donor site that has yet to be resolved in the XRD structures but increases the binding of DNA by NikR from 5 nM to 20 pM completely turning off expression of nickel importer genes.[95-96,98]

If excess nickel is present in the cellular environment, nickel binding to RcnR, NmtR, or KmtR will lead to expression of genes in the DNA that code for nickel efflux pumps. RcnR has been found to bind nickel with a K_D of 25 nM in a octahedral binding site that includes the N-terminus, a backbone amide, a cysteine and two histidine residues.[99] NmtR binds nickel with a K_D of 20 μM in an octahedral site comprised of five histidine and one aspartame ligand.[100-101] KmtR has a higher nickel affinity than NmtR indicating it is activated under at lower concentrations of nickel and if higher levels are present the secondary mechanism of NmtR is activated. The nickel binding site of KmtR is octahedral by means of four histidines, one glutamate, and one

aspartame residue.[102] Thus, a very sensitive nickel import and export mechanism is present in these organisms to maintain the biosynthesis of nickel containing enzymes but prevent toxic levels being reaching.

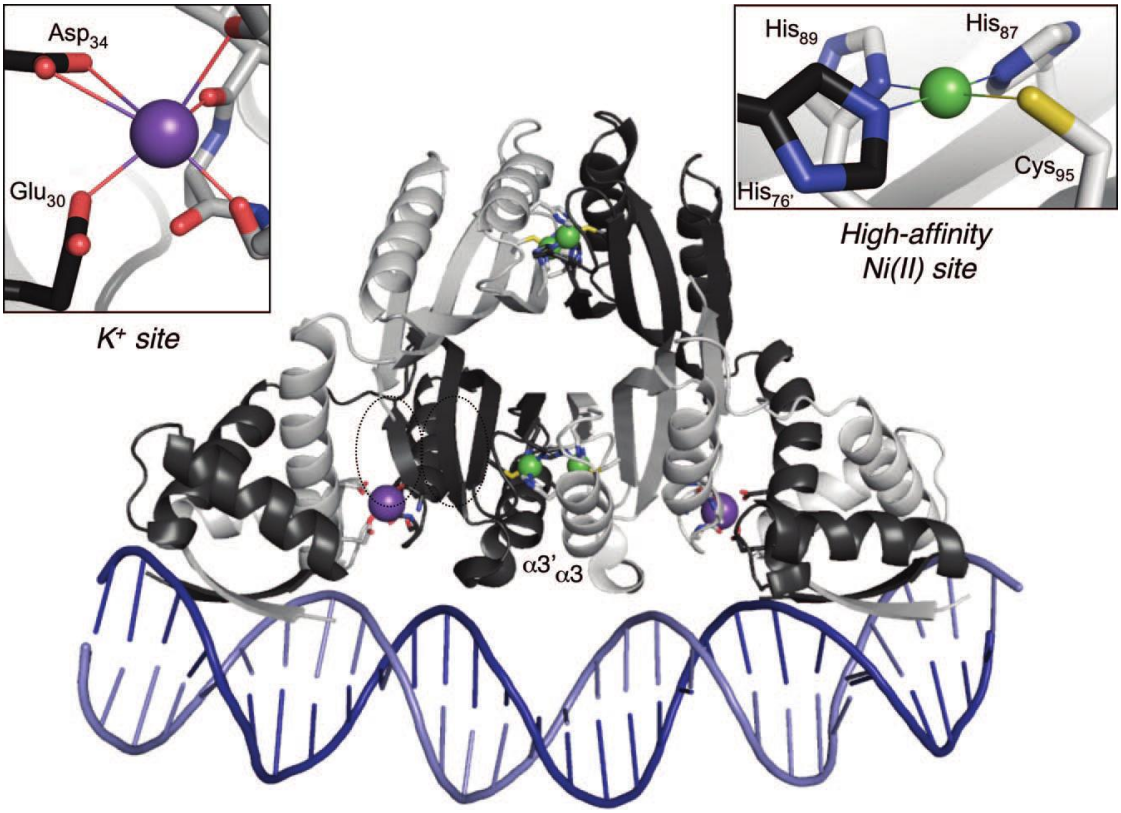

Figure 1-10. Protein crystal structure of the tetrameric *E. coli* NikR nickel regulation protein (pdb 2HZV). A high affinity nickel site is observed along with a potassium site which are shown in the insets. The tetramer was isolated bound to a strand of DNA representative of the *nik* operon. The potassium is shown in purple.[5]

1.4 Non-Nickel Containing N_2S_2 Binding Sites

In addition to the ACS and NiSOD active sites covered above there are three other major enzymes which contain N_2S_2 binding sites that are known to bind iron and cobalt. The iron-containing nitrile hydratase and thiocyanate hydratase are shown in Figure 2-2 along with the reactions catalyzed by each enzyme.[103-104] Note the iron containing nitrile hydratase contains an NO ligand bound to the iron when the analogous cobalt-containing enzyme is isolated a water molecule occupies the axial position.[105] A unique feature of these enzymes is the post-translational modification of the sulfurs by partial oxygenation to RSO and RSO_2. This S-oxygenation was first observed in NiN_2S_2 model compounds.[106]

1.5 Biological Trends and Relating Them to Model Compounds

The biological studies about nickel discussed above show common trends. For nickel trafficking into the cell and storage, ligand binding sites largely feature histidine and O-donors from water and/or amino acid side chains in octahedral sites. The nickel binding sites are also solvent accessible and generally on the protein surface or at a flexible terminus. Nickel can be transferred from the storage protein to the metallochaperons and eventually into the enzyme active sites. In the process of nickel trafficking, the nickel starts at N-rich binding sites with coordination numbers between 4 and 6, and a gradual increase in the number of cysteine thiolate donors eventually results in square planar coordination modes; using [NiFe]-H_2ase maturation as an example: N_4 (NikA-E) to N_3S (SlyD) to NS_3 (HypB) to S_4 ([NiFe]-H_2ase).[5] Throughout these

transfers the nickel maintains a 2+ oxidation state and is found in square planar or octahedral binding sites as is the preference for d^8 metals with N/O/S donor ligands.[5] It is only during the different enzyme catalytic processes that the oxidation state of nickel changes to Ni(I) or Ni(III).

Despite the wealth of information from protein studies there remains a lack of studies that examine such transfer reactions using model compounds; specifically needed are example of the transfer of nickel from a ligand to another or the exchange of one metal in a binding site for another. Thus, the work of my dissertation has focused on using model compounds to examine the biological trafficking of nickel from binding site to binding site as well as transmetallation reactions keeping the binding site constant.

A review and analysis of various compounds that have been synthesized to model some of the nickel and MN_2S_2 binding sites observed in biology, described above, are presented in Section 2. The major focus of the section is on the various metals inserted and modifications that have been made to the N_2S_2 ligands. As well as the aggregation of MN_2S_2 complexes with exogenous metal ions to form multi-metallic clusters.

Section 3 is an investigational study into methods of measuring and quantification of the electronic and steric properties of MN_2S_2 complexes that serve as mono- and bidentate metalloligands to a secondary metal center.

Section 4 is an experimental investigation into the metal exchange reactions and binding preferences of $MN_2S_2O_2$ complexes to undergo clean metal exchange with

exogenous metal. The complexes were synthesized through thiolate modification with acetyl- and acetylamide reagents to form $MN_2S_2O_2$ complexes.

Section 5 is a compilation of the XRD crystal structures that the author has solved during his PhD work. Some of the compounds were synthesized by the author but the majority were synthesized by coworkers in the M.Y. Darensbourg laboratory. Some structures were already published, some subsequently published, and the remainder awaits publication as private communications or in peer-reviewed journals with myself as a co-author.

2. METALLODITHIOLATES AS LIGANDS IN COORDINATION, BIOINORGANIC, AND ORGANOMETALLIC CHEMISTRY*

2.1 Introduction

In a series of notable manuscripts in the early 1960's, Daryle H. Busch and coworkers described reactions of coordinated ligands, particularly choosing mercaptoamines (NS) to demonstrate the scope of electrophilic reactions that might occur at the sulfur of metal−bound thiolates.[107-108] Such reactivity was the genesis of extensive studies in nickel−templated macrocyclization reactions that yielded tetradentate heterocyclic ligands.[109-110] A byproduct of the reaction of nickel−bound mercaptoamines (as well as $Pd^{II}N_2S_2$ analogues) with alkylating agents was an S−bridged trimetallic, $[(Ni^{II}N_2S_2)_2Ni^{II}]^{2+}$, presumably arising via an intermediate thioether complex, $[Ni^{II}(N-S-R)_2]^{2+}$.[108] Rapid release of Ni^{2+} within the labile thioether and its capture by the nickel−bound thiolate of the $Ni^{II}N_2S_2$ precursor accounted for the trimetallic, and prompted the comment that "bridging sulfur atoms are stronger ligands than thioether groups."[108] Dahl and Wei's report of the molecular structure of the "Busch−Jicha complex," Figure 2-1, described the framework as arising "…from chelation of two identical $Ni(NH_2CH_2CH_2S)_2$ entities to a third Ni^{2+} ion."[111]

---

* Reproduced with permission from Denny, J. A.; Darensbourg, M. Y. *Chem. Rev.* **2015**, in press. Copyright **2015** American Chemical Society.

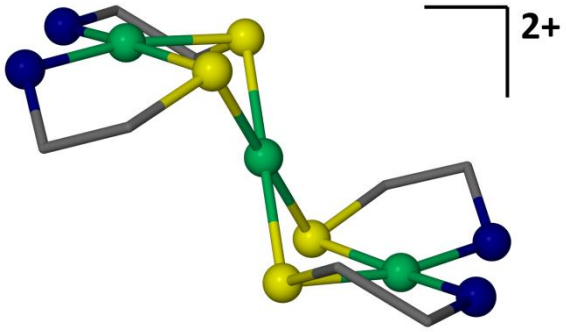

Figure 2-1. Framework of the bis−ethylmercaptoamine nickel complex, bound to a central Ni^{2+}, the Busch−Jicha complex.[111] The dihedral angle between the N_2S_2 and S_4 square planes is 109°.

Thus the concept of square planar cis−dithiolates of Ni^{2+} as metalloligands in coordination chemistry was acknowledged. While Busch correctly foresaw that "reactivity towards nucleophiles by the coordinated sulfur atom might be expected to yield results of broad significance to reactions that occur in living organisms,"[108] it was several decades before such post−translational modification, i.e., reactivity at metal−bound sulfur subsequent to metalloprotein assembly of an enzyme active site, was discovered. Most obvious in this class are the contiguous N_2S_2 metal−binding sites derived from Cys−X−Cys tripeptide motifs, utilizing deprotonated peptide amido nitrogens as well as cysteine sulfurs, which may adopt a square planar configuration. In the nitrile and thiocyanate hydratases, S−oxygenation tunes the Lewis acidity of iron and cobalt for optimal function in the hydration of nitriles to amides and thiocyanate to ammonia and carbonylsulfide, respectively, Figures 2-2A and B.[103-104] The acetyl−CoA

synthase, ACS, active site structure, Figure 2-2C, is more clearly related to that of the Busch−Jicha complex.[112] Two nickels are involved; the nickel distal to the 4Fe4S cluster, Ni_d, is in a tight tripeptide binding site consisting of two amido−N and two thiolato−S, producing an overall dianionic nickel metallodithiolate ligand that binds a second nickel. The nickel that is proximal to the cluster, Ni_p, may be in a square planar or tetrahedral coordination, both of which are accommodated by the bidentate NiN_2S_2 ligand, which, according to the computational mechanism may swing open to reveal an available reactivity site.[113] Interestingly, the first reported crystal structures identified copper and zinc as the proximal metal, reflecting the promiscuity of such thiolate sulfurs in the NiN_2S_2 metalloligands exposed to various metals.[5,77,114] Later studies confirmed that nickel in that site, rather than copper or zinc, is required to perform the organometallic processes that convert CH_3^+, CO, and the thiolate, Co−A, to acetyl−CoA, an organometallic process of ultimate importance to biochemistry.[5,82,113] The reactivity of the A−cluster of ACS has prompted its description as "Nature's Monsanto acetic acid catalyst."[115]

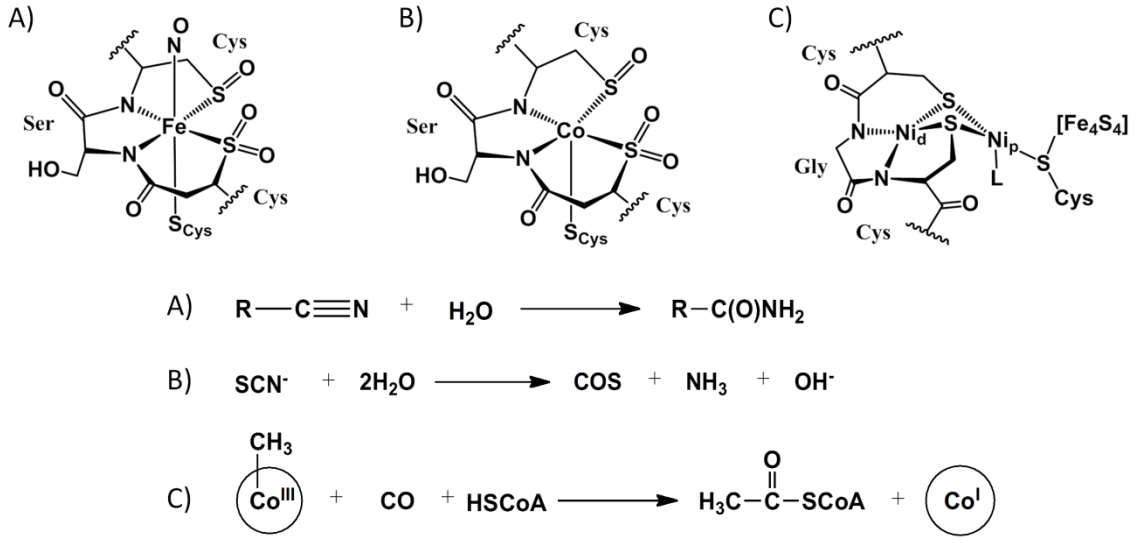

Figure 2-2. Enzyme active site structures and catalyzed reactions of A) nitrile hydratase (as isolated with iron an NO ligand is attached; as isolated with Co, a water molecule is attached);[104] B) thiocyanate hydratase;[103] and C) acetyl Co−A synthase.[112] Ni_p is that nickel proximal or closest to the 4Fe4S cluster, while Ni_d is distal.

Doubtless the Cys−X−Cys motif, wherever it is found within a protein, should be considered as a potential site for N_2S_2 metal binding, resulting in thiolate S−protection and/or for control of subsequent S−based reactivity of consequence to reactions in metallobiochemistry. In addition, the N_2S_2 complexes of nickel, designed to mimic the distal nickel site of ACS, themselves constitute a broad class of versatile S−donor metalloligands, with properties that may be varied by the carbon frameworks that connect the N and S sites, as well as the central metal of the MN_2S_2 coordination unit. In illustration, the neutral NiN_2S_2, N,N'−bis(mercaptoethylene−1,4−diazacyclooctane nickel(II), Ni(bme−daco), listed below as **2**, has been shown to support olefin/CO

coupling on palladium, via the $[Ni(bme{-}daco){\bullet}Pd^{II}(CH_3))OEt_2]^+$ catalyst, Figure 2-3.[116] In this case, the Ni(bme−daco) mimics the bipyridine ligand in Brookhart's palladium catalyst developed for the production of polyketoethylene.[117] Further, Ogo and coworkers have shown that the NiN_2S_2 metalloligand bound to Ru^{2+} serves as a functional model of [NiFe]−hydrogenase, Figure 2-4.[118-119]

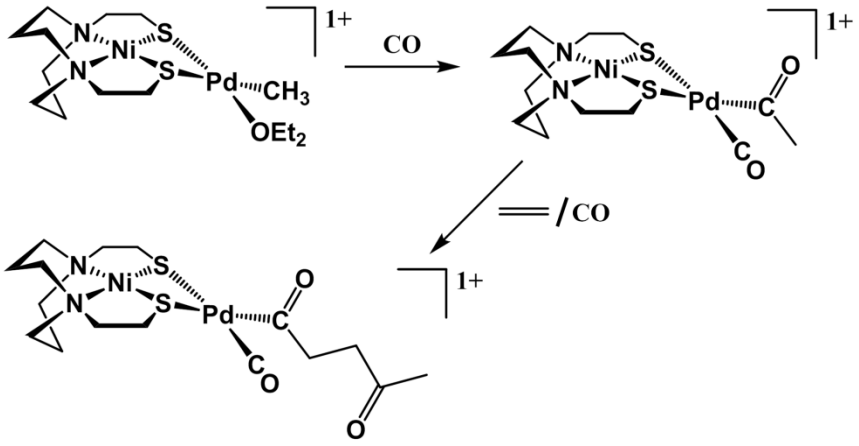

Figure 2-3. Steps in the assembly of polyketones with palladium (II) as catalyst, supported by Ni(bme-daco), metalloligand **2**.[116] The CO-bound acyl complex is the resting state. When the olefin is captured, olefin insertion is fast; double CO insertion does not occur.

In the following pages, we review numerous MN_2S_2 complexes and their application as metallodithiolate ligands. We have focused on contiguous S−N−N−S tetradentate ligands that largely accommodate square planar binding and present the thiolate sulfurs in the cis− configuration that is conducive for them serving as bidentate

S−donor ligands. We have mined the Cambridge Crystallographic Data Base,[120] finding the complexes reported herein; we expected the d^8 nickel family to be the largest contributor. Nevertheless, another prominent class is the metal oxo complexes, Re=O, Tc=O, or V≡O. Of the ~165 monomeric MN_2S_2 complexes, ~50 are metal oxo containing, while ~50 have nickel or palladium as M. The remainder contains various transition metals, and may be multi−metallic as well as L or X type ligand−cleaved, monometallic compounds.

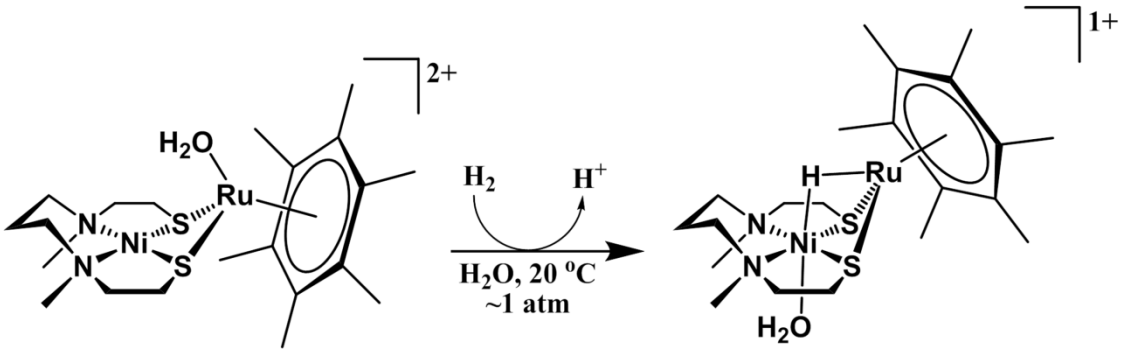

Figure 2-4. The open chain NiN_2S_2, complex **19** is a metalloligand to Ru^{2+} and serves as a functional mimic of the [NiFe]−H_2ase active site that facilitates heterolytic H_2 cleavage with formation of a bridging hydride.[118-119]

Distinguishing features of the MN_2S_2 class of ligands that are used in the organization of this review are as follows:

a) M−S−C_x−N and M−N−C_x−N ring size, determined by the number of C atoms in the connectors between donor atoms;

b) The S−M−S, S−M−N, and N−M−N angles, and resultant S to S distances, relating to bite angle of the MN_2S_2 in a bidentate binding mode;

c) The overall ligand charge; and,

d) Modifications for steric, electronic, and photochemical properties.

Published works that review parts of this subfield of coordination chemistry include that from R. H. Holm and coworkers in 2004.[121] In the course of exploring the synthesis of $Ni(\mu{-}SR)_2M$ rhombs as analogues of the ACS active site, Figure 2-2C, planar NiN_2S_2 complexes with "physiologically credible coordination" led to >20 new complexes from the Holm laboratory whose structures were categorized somewhat similarly to the organization we have used here. In particular, an instructive figure, for which Figure 2-5 is a modified version, lays out the ring sizes within NiN_2S_2 metalloligands, 5−5−5, 5−6−5, 5−5−6, and 6−5−6, representing the Ni−S−C_x−N, Ni−N−C_x−N, and Ni−N−C_x−S connectivities, respectively.[121] The Cys−X−Cys motif thus produces the 5−5−6 arrangement in the square planar NiN_2S_2 binding of the ACS active site A−cluster. As there are two N to N connectors in some ligands, they are doubly designated with the central number in parentheses. For example, complex **1**, the bismercaptoethanediazacycloheptane nickel complex, Ni(bme−dach), with a mesocyclic diamine framework, is described as a 5−5(6)−5 complex or metalloligand. Note that we also encounter complexes with no N to N connection. In such cases the free metalloligand $M(NS)_2$ may be found as the trans−isomer, but in the presence of

exogenous metals converts to the cis−isomer, e.g., similar to the Busch−Jicha complex shown in Figure 2-1.

Two micro−reviews of Ni(μ−SR)$_2$Fe complexes as synthetic analogues of the [NiFe]−hydrogenase active site by Bouwman[122] in 2005 and Ohki and Tatsumi in 2011,[123] further demonstrates the synthetic utility of the metallodithiolate in ligand design approaches.

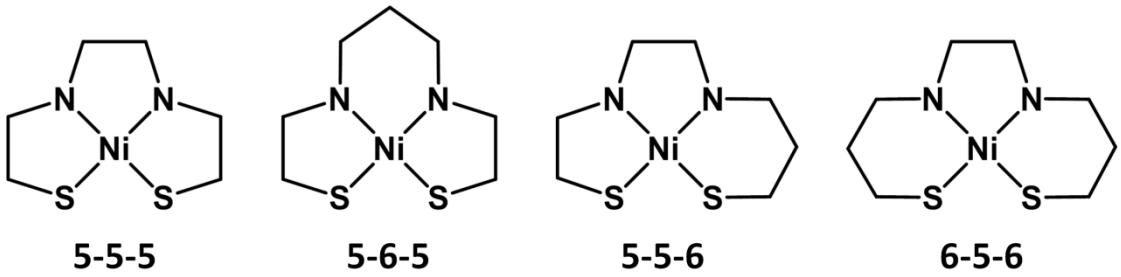

Figure 2-5. Examples of the various chelate ring sizes observed in the complexes featured in this review with 5−5−5 and 5−6−5 representing the largest contributions.

2.1.1 Strategy to Correlating and Reporting Complexes

Individual entries in the tables and figures within this review are given identifying numbers as well as the 6−letter code from the CCDC database.[120] Access to the structure, the cif file, as well as the corresponding literature report can be obtained by entering the 6−letter code into the CCDC webpage. Both "ChemDraw" stick structures and ball and stick renditions of the actual X−ray crystallographic structure are presented herein. Tables A1 and A2 contain ν(CO) and ν(NO) IR data for complexes shown in section 2.3. Compilations of metric parameters are listed in Tables A3 − A23.

The organization of this review in terms of structural categories found within specific figures is largely based on the chelate ring pattern as well as the metal center in the metallodithiolate ligands. Aliphatic vs. aromatic donor linkages influence division into sub−categories. As described above, the known chelate ring patterns are primarily 5−5−5 and 5−6−5, with smaller contributions from the 5−5−6 and 6−5−6 patterns.

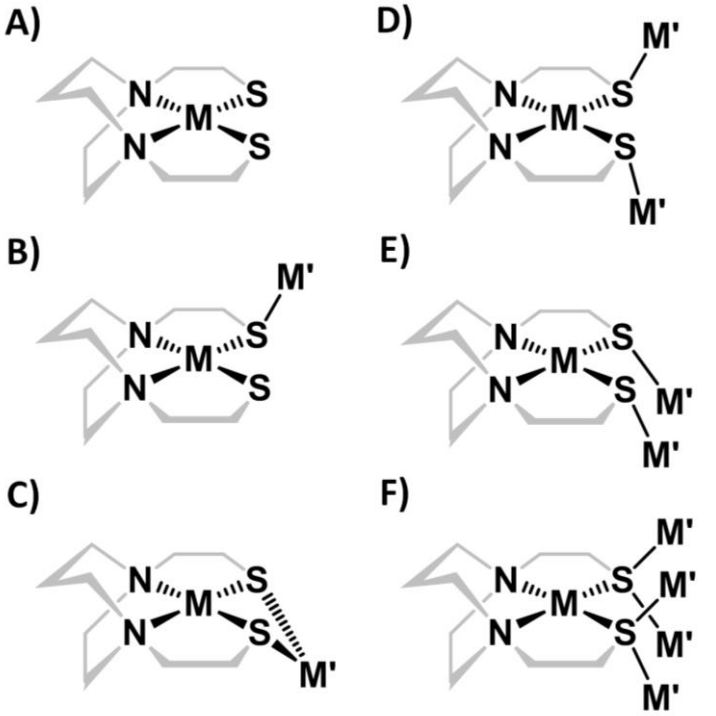

Figure 2-6. Examples of the various S−directing orientations in thiolate bridges between metal centers; the shaded N_2S_2 ligand, bme−dach, is used as an example.

Section 2 describes the monomeric MN_2S_2 complexes that are notable as metallodithiolate ligands. As nickel plays a starring role in this field, descriptions of

NiN_2S_2 complexes dominate. Further derivatives include numerous iron, cobalt, and copper complexes, several of which have not been explored as metallodithiolate ligands.

Section 3 describes bimetallic complexes evolving from MN_2S_2 metalloligands in combination with a transition metal acceptor bearing diatomic ligands as reporter groups of the electron donating ability of the MN_2S_2 ligands. To date those acceptors proven most useful are $W(CO)_4$ and $Fe(NO)_2$; their ν(CO) and ν(NO) stretching frequencies and associated force constants distinguish members within a range of MN_2S_2 metalloligands. The steric character of the ligands is assessed from X−ray diffraction data for which there are ample entries for comparison.

Sections 4−6 review various structural forms that result in trimetallics to large clusters, depending on the extent to which available lone pairs on the cis−dithiolates are engaged in the aggregation process. Figure 2-6 displays the Ni(bme−dach) complex as paradigm for the structural connections possible for M' binding. Figure 2-6B is for a single metal attachment while Figure 2-6C is the signature bidentate binding as is found in the Busch−Jicha trinickel complex of Figure 2-1. Structure D in Figure 2-6 uses the MN_2S_2 as a metalloligand which spans two metals in transoid configuration. The arrangement that places the two pendent metals on the same side of the MN_2S_2 plane, Figure 2-6E, generates the propeller and paddlewheel complexes described in Sections 5 and 6; while the involvement of 3 or more lone pairs on S leads to larger clusters, Figure 2-6F. The latter are described in Section 6.

Despite this attempt to place possible interactions within such a geometric rubric determined by S−lone pair orientation, the specific coordination requirements of some

metals and the geometrically promiscuous sulfurs lead to unusual geometries not covered by the prototypes of Figure 2-6. The reader is forewarned!

2.2 Monometallic Systems or the Metalloligands

2.2.1 NiN_2S_2 Complexes

Much of the driving force for the continued investigation of NiN_2S_2 complexes over the last ~25 years comes from the structural identification of the ACS/CODH,[5,112,115] NiSOD,[5,69] and [NiFe]−hydrogenase[5,124-125] enzymes whose active sites feature Ni in various sulfur ligated modes. Thus, the need to better understand the chemical properties of nickel−sulfur bonding has led to the impressive series of compounds whose structures are presented here, with smaller emphasis paid to the various physical techniques that have been used in their characterization. Not all of the NiN_2S_2 complexes were prepared as synthetic analogues of enzyme active sites. Kawamoto and coworkers used the NiN_2S_2 framework in combination with an extended π–conjugated system to prepare near−infrared absorbing dyes.[126] These were synthesized through a unique carbon−carbon bond forming reaction of Schiff base−containing NiN_2S_2 complexes, thus forming a link between the nitrogen donors. This same reaction has more recently been utilized to demonstrate transfer of chirality at the molecular level based on the reversibility of the C−C bond forming reaction.[127]

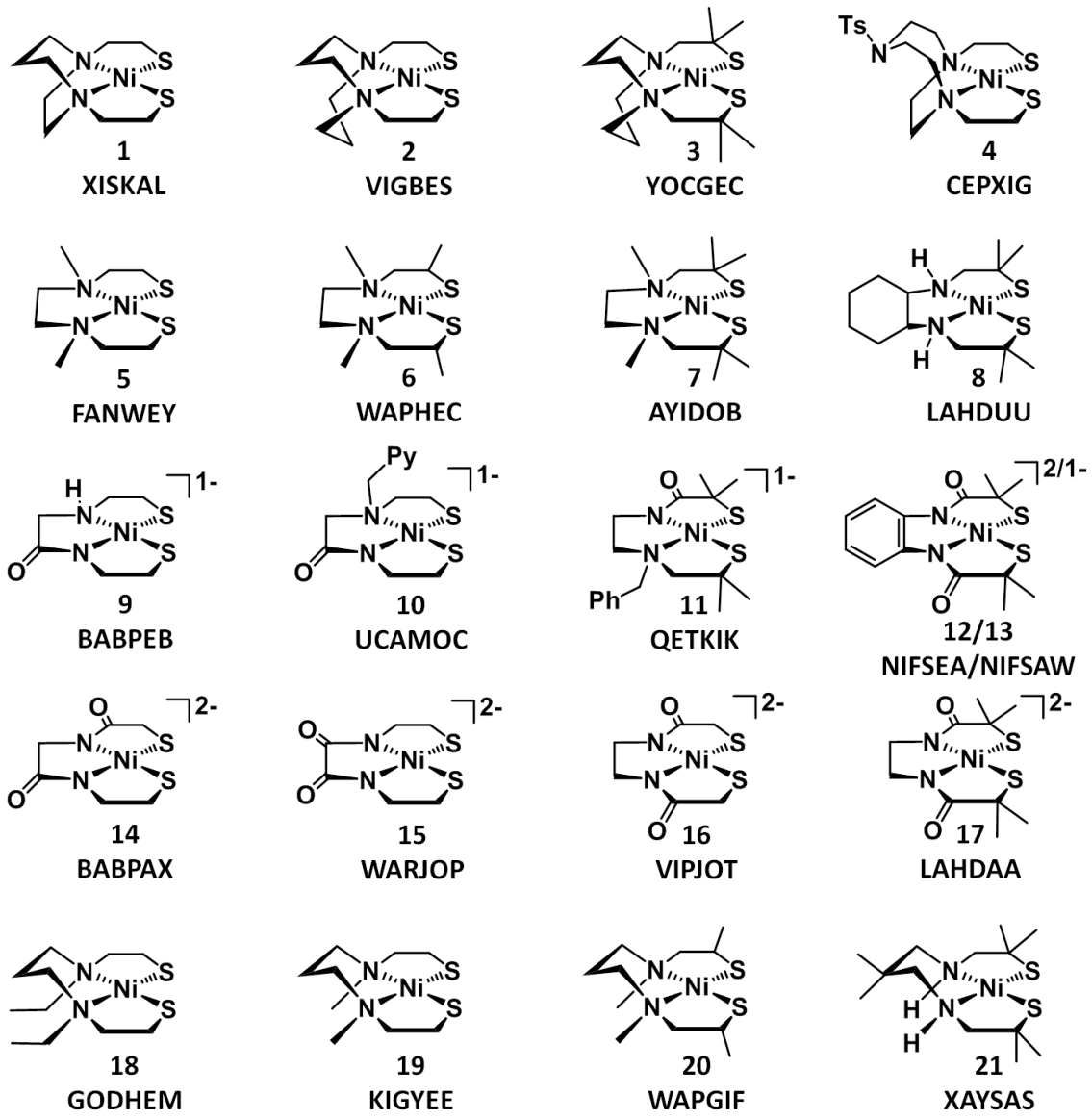

Figure 2-7. NiN_2S_2 complexes that feature a 2−carbon alkyl chain between the N and S donors, with N to N connectors of various types; i.e., of the 5−X−5 metallo−ring forms.

The twenty−one NiN_2S_2 complexes shown in Figure 2-7 (complexes **12** and **13** are the same N_2S_2 ligand) are illustrative of this class. In these, two carbons connect N to S in 5−membered, Ni−N−C−C−S rings; the N to N linkers vary. Complexes **1** through **4**

are based on mesodiazacycles as frameworks, resulting in tertiary nitrogen donors in the patterns of 5−5(6)−5 and 5−6(6)−5, respectively.[128-133] Complexes **5** through **8** also have 3° nitrogen donors, with two−carbon linkers between N−donor atoms, of 5−5−5 form.[121,134-136] Complexes **9** − **11** contain one amido N−donor and one pyramidal, 2° or 3°, N−donor.[137-139] Complexes **12** through **17** have two amido donors and exist in dianionic form.[121,137,140-142] Complex **13** is the one−electron oxidized form of **12** and the only isolable Ni^{3+} complex of this type thus far reported.[140] Complexes **18** − **21** are neutral and contain a 3−carbon, open chain, linker between the N donors, i.e., 5−6−5.[135,143-145] All of these, **1** − **21**, are square planar with any distortion tending towards a slight tetrahedral twist of the ligand set. The metric data, Table A3, show similar Ni−N and Ni−S distances (1.8 − 2.0 Å and 2.1 − 2.2 Å, respectively) with a slightly shorter (by ~0.1 Å to 0.2 Å) Ni−N distance in the amido−nitrogen containing, anionic species.

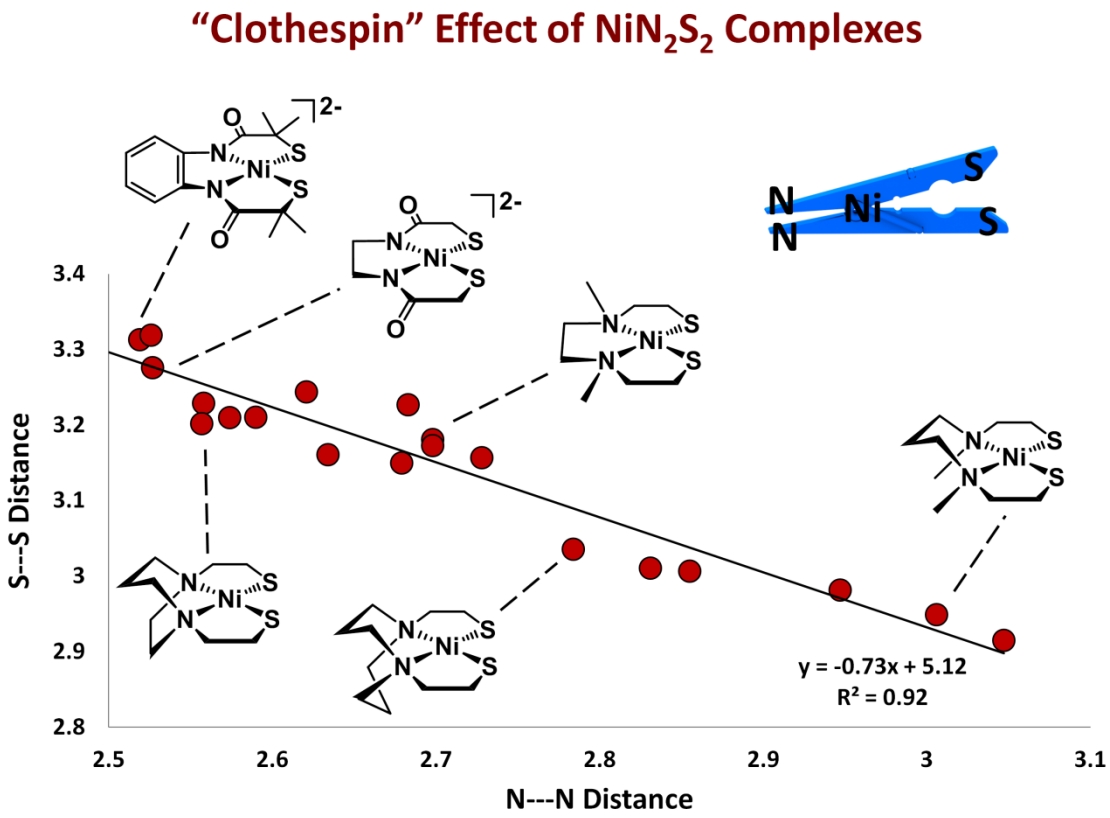

Figure 2-8. Plot of the S to S vs. N to N distances of complexes **1**−**21** which illustrates the "clothespin effect" observed for the monomeric complexes.[145]

The S−Ni−S angle varies inversely with the N−Ni−N angle in the compounds of Figure 2-7. The correlation is shown in Figure 2-8 as a plot of S to S distance vs. N to N distance. The distances range over ~0.4 Å and ~0.6 Å for the S − S vs. N − N, respectively. The pinning together of the nitrogens generally opens the S−Ni−S bite angle; this rather linear correlation has been termed the "clothespin effect" by Schugar, Potenza, *et al.*[145] Further influences on the S−Ni−S angle can come from modification of the N to S linker; i.e., changing from a 2 to 3 carbon linker will increase the N−Ni−S

angle and as a result decrease the S−Ni−S bite angle. There are further S−Ni−S bite angle influences when the N to S linkers differ within a complex, Figure 2-9.

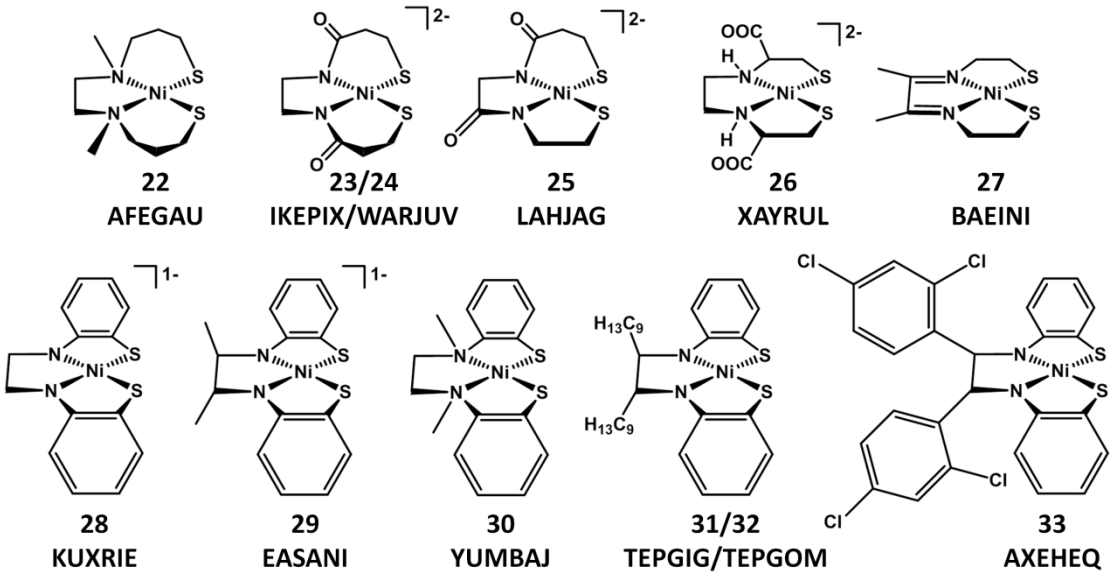

Figure 2-9. Complexes **22−33** are monomeric NiN_2S_2 complexes with 3−carbon alkyl chains or a phenylene ring between the N and S donors.

Figure 2-9 contains NiN_2S_2 with N to S linkers of varying types. Compounds **22** through **25** have at least one 3−carbon chain between the N and S donors.[121,141,146-147] This has the effect of opening the N−Ni−S angle as compared to the complexes with a two carbon linker between the N and S, which in turn decreases the S−Ni−S angle; i.e. 94° for **5** and 83° for **22**. Complex **26** is dianionic by virtue of substituent carboxylates on the N to S linker.[145] Complex **27** has a conjugated N to N linker, which leads to a smaller N to N distance and opens the sulfurs as compared to **5**; the N to N and S to S distances are 2.45 and 3.24 Å in **27,** respectively, and 2.70 and 3.17 Å in **5**.[148]

Complexes **28** through **33** bear ortho−substituted thiophenylates with a 2−carbon linker between the nitrogen donors.[127,149-152] The non−innocence of such ligands, with redox−activity similar to that of the metal, renders the nickel oxidation state assignment ambiguous. The anionic complexes, **28** and **29**, are S = ½ complexes, while **30** − **33** are diamagnetic. Complexes **31** and **32** are isolated as optical isomers with highly similar metric data, Table A4. Figure 2-10 offers a detailed look at the bond distances of complexes **5**, **29**, and **31**. From this analysis, complex **5** contains an innocent ligand that has the sulfurs carrying the negative charge (shown in red). Complex **31** can be viewed as a dianionic ligand in that each phenyl ring is a radical anion, resulting in an oxidation state of +2 for the nickel.[127] This is also the case for **30**, **32** and **33**. However complex **29** contains a trianionic ligand by virtue of a radical on one half of the ligand and the other half having anionic nitrogen and sulfur donors.[150] These are highlighted in red in the bottom right of Figure 2-10.

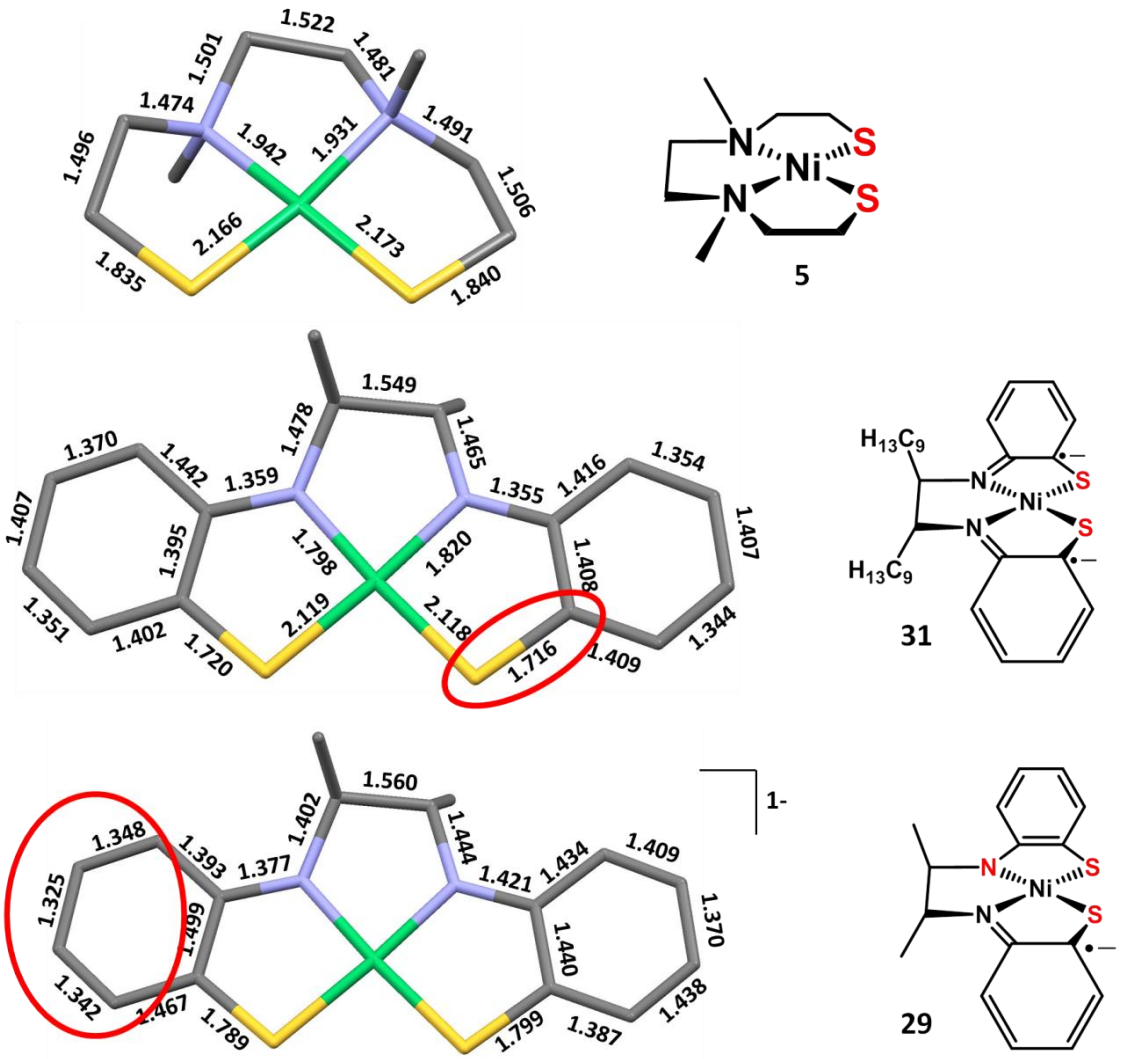

Figure 2-10. A closer look at the bond lengths from complexes **5**(top), **31**(middle), and **29**(bottom) to highlight the non−innocent ligand and the metric data that is evidence for ligand−based radicals. Note the alternating bond lengths in the arene connector between N and S in **31**.

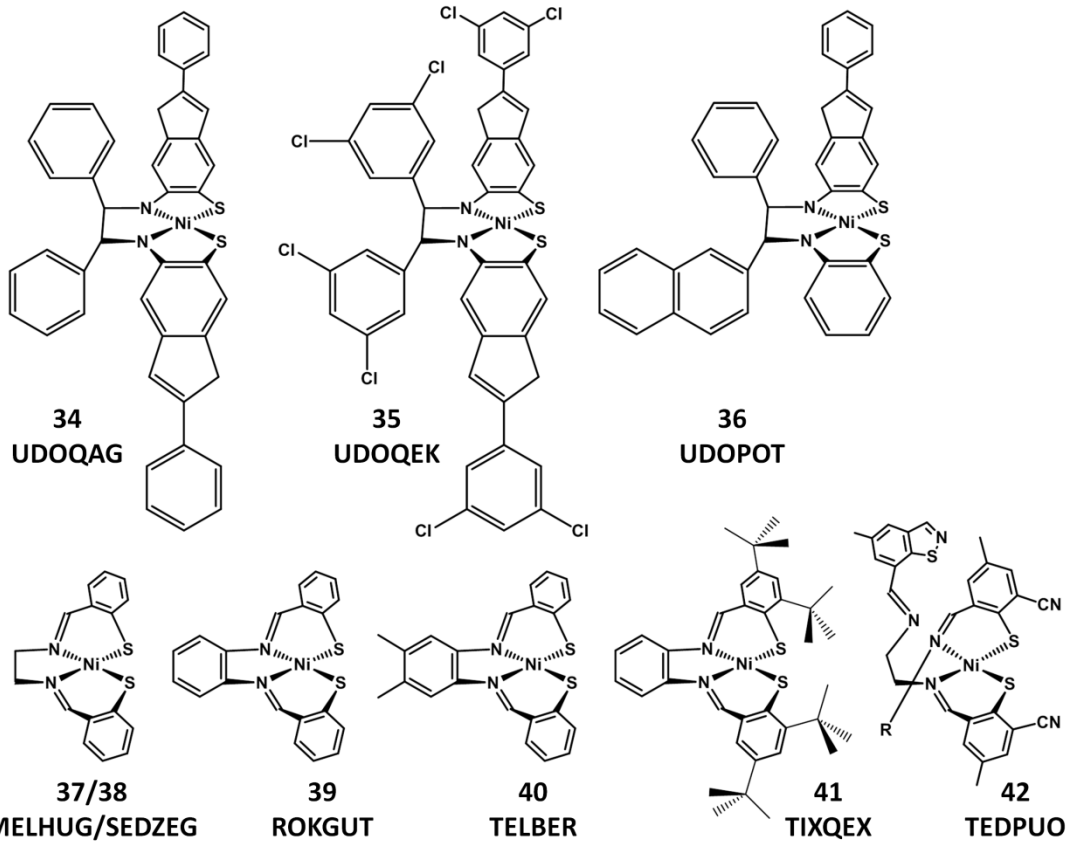

Figure 2-11. NiN_2S_2 complexes based on N/S donors within an extended π−system and thio−salen type ligands.

Reported by Kawamoto, complexes **34** through **36** of Figure 2-11 contain extended π–conjugated systems that are near−infrared absorbing dyes, *vide supra*.[126] Six monomeric NiN_2S_2 salen−type complexes (**37** − **42**) have been reported, the simplest of which, shown in Figure 2-11, contain 6−membered $NiNC_3S$ rings with a phenylene ring within the N to S linker.[153-158] These complexes were prepared by Shiff base condensation of a thiophenolate and the respective diamine. Such N_2S_2 ligands can be readily modified by substituents on the phenyl thiolate as well as the diamine.

In an interesting template reaction, one N_2S_2 thiosalen ligand of **42**, Figure 2-11, converts into a thiazole upon connection of a thiolate sulfur with the adjacent cyanide on the phenylene ring, leaving only one N/S donor site for binding to the nickel and requiring two such salen ligands to complete the N_2S_2 donor set.[158]

All the complexes thus far in this section demonstrate 4−coordinate, square planar binding of nickel. Complexes **43** and **44**, Figure 2-12, are pentacoordinate nickel complexes with cis−dithiolates, analogous to complex **4**. In the case of complex **43**, the base of the square pyramidal ligation is formed by the N_2S_2; the mesocycle ring contains a third nitrogen that interacts with the nickel in the axial position.[133] The Ni−N_{ax} distance is 2.207 Å and leads to a distorted TBP/SP geometry with $\tau = 0.48$ (defined by Addison, τ is a measure of the relationship between square pyramidal and trigonal bipyramidal, $\tau = 0$ for the former and $\tau = 1$ for the latter).[159] Complex **44** is of a similar motif with a thioether in the mesocycle ring. The weak thioether S−Ni interaction of 2.824 Å is consistent with the $\tau = 0.05$; i.e., the NiN_2S_2 is largely a plane.[160]

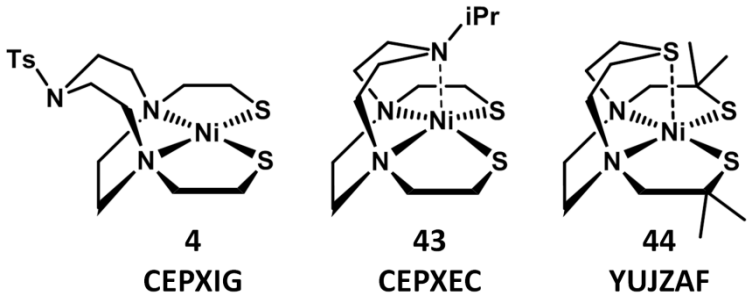

4 CEPXIG **43** CEPXEC **44** YUJZAF

Figure 2-12. Two examples of NiN_2S_2 complexes containing a 5th donor site within a 9−membered mesodiazacycle.

2.2.2 $M[N_2S_2]_x$ Complexes: M ≠ Ni, M=O, or V≡O

Monomeric MN_2S_2 and $[MN_2S_2]_2$ where M ≠ Ni make up a group of over 90 compounds that have been crystallized and subjected to X−ray diffraction analysis to date. The range of metals capable of binding within the N_2S_2 pocket include metal oxo units, such as $V{\equiv}O^{2+}$, $Re{=}O^{3+}$ and $Tc{=}O^{3+}$, which are not included; instead complexes of the form $[MN_2S_2]_{1,2}$ with M other than Ni, M=O, or V≡O are in this section. Those based on familiar diazamesocycle frameworks, bme−dach and bme−daco, are shown in Figures 2-13 and 2-14, respectively.

As displayed in Figure 2-13, there are ten M(bme−dach) structures that have been crystallized and subjected to X−ray diffraction analysis thus far; the seven complexes based on M(bme−daco) are shown in Figure 2-14. Complexes **1** and **45** – **47** of Figure 2-13 and **2** and **54** of Figure 2-14 contain d^8 metal ions Ni^{2+}, Pd^{2+}, Pt^{2+}, and Au^{3+} in the N_2S_2 framework forming rigorously square planar complexes with very similar metric parameters.[128-129,161-163] Specifically, with increasing atomic number of the metal (increasing thiophilicity) the metals shift slightly towards the sulfur (away from the nitrogen) resulting in a systematic increase of N to N distances overall of ca 0.2 Å. Concomitantly, the S to S distances increase from 3.2 to 3.6 Å in the group 8 divalent metals, however the Au^{3+} complex, **47**, shows an S to S distance less than that found for the analogous Pt^{2+} complex, **46**, consistent with the smaller ionic radius of Au^{3+}. Note that the metallodiazacyclohexane ring in the bme−dach derivatives is routinely in the chair conformation; in contrast, the bme−daco derivatives contain a mixture of chair/boat and chair/chair conformers.

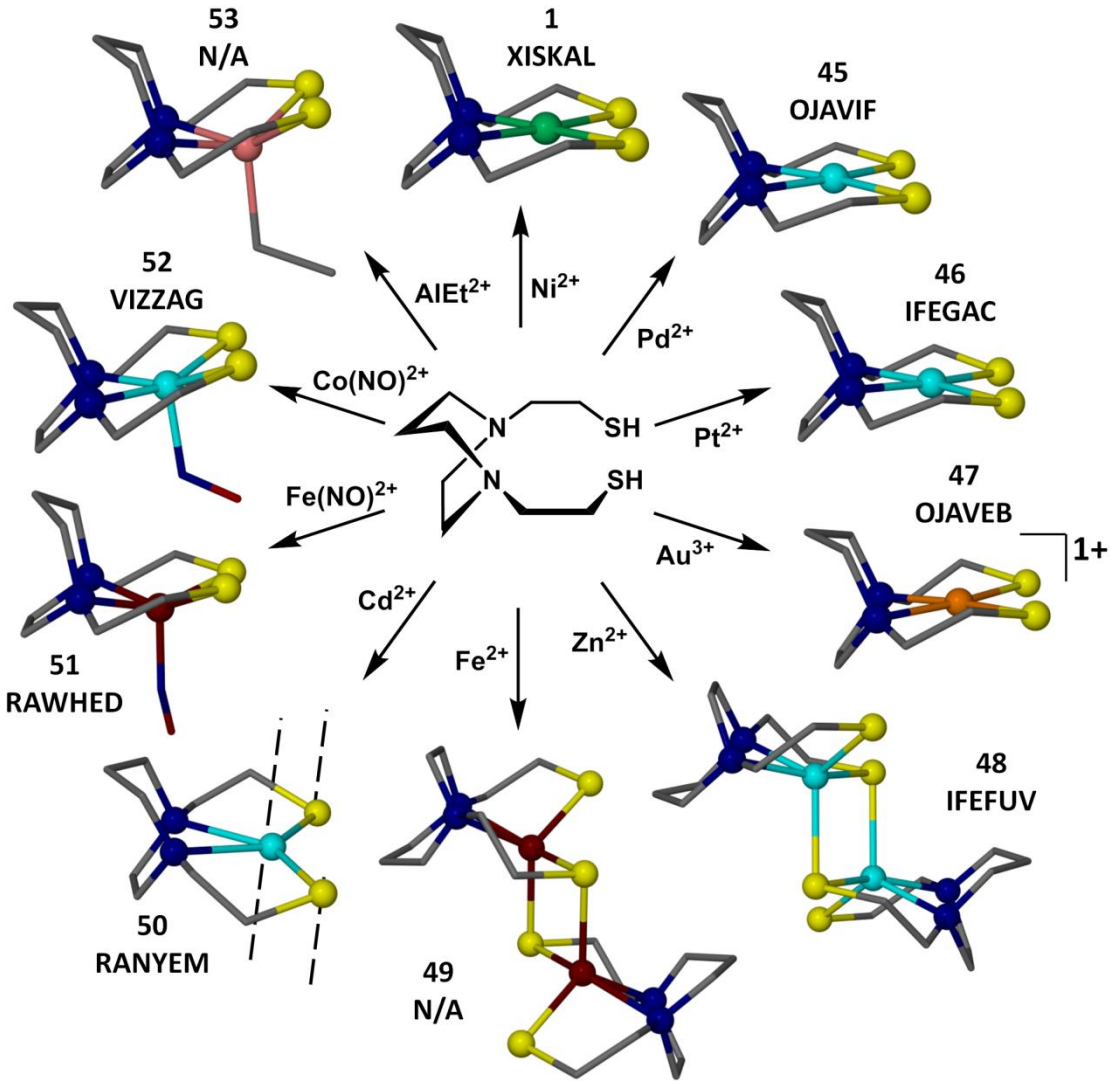

Figure 2-13. Complexes **1** and **45**−**53** are the group of $[M(bme-dach)]_x$ (x = 1, 2, and polymeric) complexes crystallized to date.

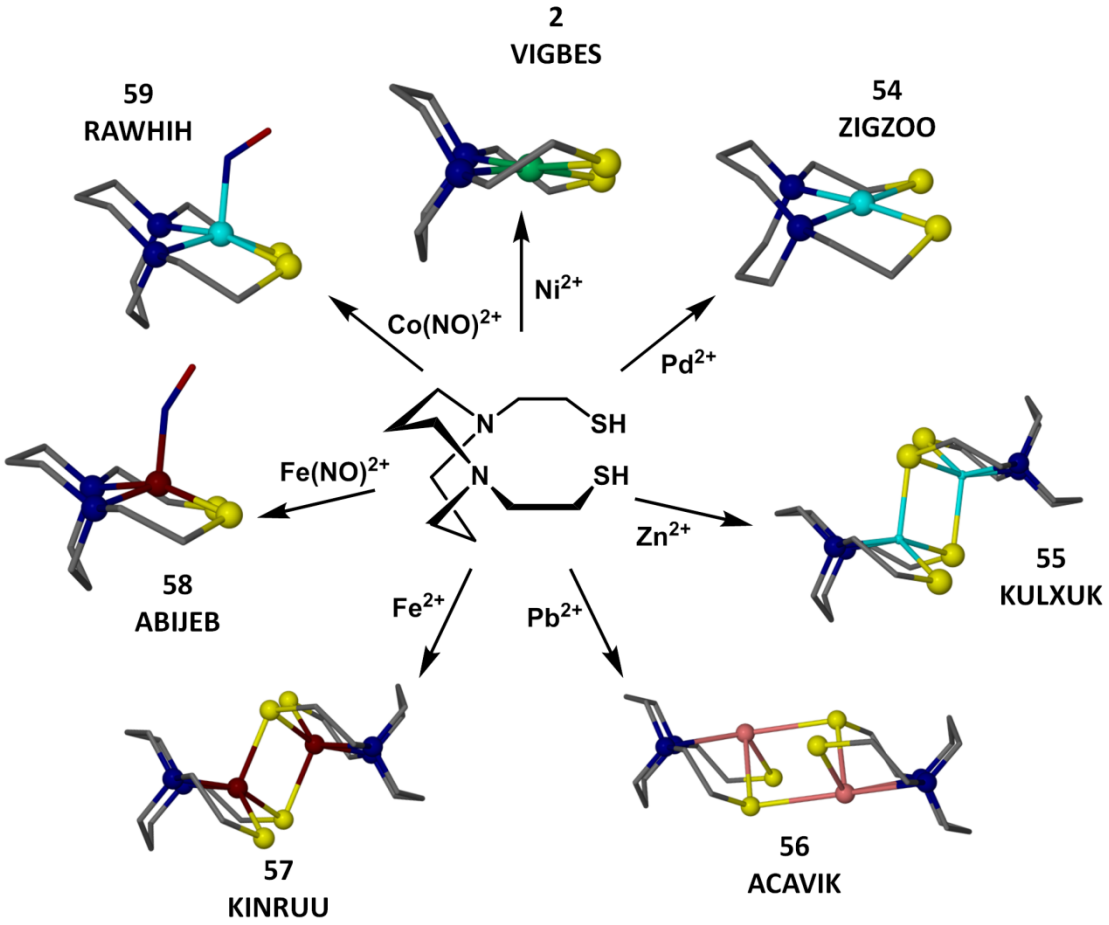

Figure 2-14. Complexes **2** and **54−59** represent the $[M(bme{-}daco)]_x$ (x = 1,2) crystallized to date.

Other MN_2S_2 complexes shown in Figures 2-13 and 2-14 have pentacoordinate M, either by 1) addition of an exogenous ligand in the apical position of a square pyramid; or 2) dimerization with formation of two bridging thiolates leading to a diamond M_2S_2 core. The latter structures are seen for M = Zn and Fe. All show pentacoordinate binding about the first row transition metal with geometries exhibiting various degrees of square pyramidal and trigonal bipyramidal character. In pentacoordinate complexes (with the

exception of $[CdN_2S_2]_x$ and $[PbN_2S_2]_2$, but including the metal oxos), the metals are displaced out of the best N_2S_2 planes. The displacement parameter, M_{disp}, ranges from 0.3 to 0.7 Å; however, the N_2S_2 "plane" is no longer regular. The shift of the bridging thiolates towards the adjacent metal can be so severe that the $MN_2S_2(\mu-S)$ geometry becomes distorted between square pyramidal and trigonal bipyramidal.

In the case of $[ZnN_2S_2]_2$, complexes **48** and **55**, Addison's τ values are 0.47 and 0.31, respectively, suggesting a distortion from square pyramidal towards trigonal bipyramidal.[162,164] If regarded as square pyramidal, the zinc of complex **48** would be displaced by 0.582 Å out of the best N_2S_2 plane toward the sulfur in the second ZnN_2S_2 unit. The Zn−S distance within the N_2S_2 binding site of **48** is 2.308 Å and that between the Zn and the S of the second ZnN_2S_2 is 2.496 Å.[162] Complex **55** has a similar Zn displacement and Zn−S distances of 0.567 Å, 2.327 Å, and 2.493 Å, respectively.[164] However, complex **55** has more square pyramidal character, $\tau = 0.31$. Similar to these two structures are the iron−containing analogs, $[Fe(N_2S_2)]_2$, complexes **49** and **57**; complexes **49** and **57** have Fe−S distances in intra−N_2S_2 and inter−N_2S_2 of 2.315/2.346 and 2.409/2.420 Å, and $\tau = 0.16/0.29$, respectively.[165-166]

Complex **50** represents an example, possibly the only one, of an MN_2S_2 coordination polymer that exists in the absence of additional modification of the ligand framework with carboxylate groups.[167] As Cd^{2+} is highly thiophilic, a drastic shift away from the nitrogen toward the sulfur donors generates the largest S−M−S angle observed in contiguous S−N−N−S square planar complexes, 132.50°. The end result of the large thiophilic metal center is a pseudo octahedral coordination polymer featuring intra and

intermolecular M−S distances of 2.562 and 2.842 Å, respectively. Complex **56**, M = Pb^{2+}, displays a unique MN_2S_2 complex geometry. The lead is prominently displaced from the best N_2S_2 plane by 1.393 Å, in a dimeric $[Pb(N_2S_2)]_2$ form within a pseudo−see−saw geometry. The irregularity in this structure was ascribed to the stereoactivity of the Pb^{2+} lone pair.[168]

Complexes **51/58**[169-170] and **52/59**[169,171] contain $Fe(NO)^{2+}$ and $Co(NO)^{2+}$ moieties within the bme−dach/daco frameworks, respectively. Formally the paramagnetic iron complexes **51** and **58** have been assigned to an Fe^{2+} attached to an •NO radical; the iron is 0.490/0.480 Å above the N_2S_2 best plane and τ = 0.11/0.17.[169] In contrast the diamagnetism of complexes **52** and **59** is attributed to a Co^{3+} center bound to NO^- with the cobalt displaced from the N_2S_2 plane by 0.334/0.372 Å and τ = 0.04/0.23.[169,171] Supporting these assignments are Fe−N−O angles of 152° and 151° that contrast with Co−N−O angles of 124° and 129°, respectively. It should be noted that the electronic configurations of such nitrosyls are widely described by the Enemark−Feltham (E−F) notation that combines the number of NO π^* electrons with the valence electrons of the metal ion in an oxidation state prescribed by the innocent ligands within the coordination sphere.[172] In these cases, the E−F notation is $\{Fe(NO)\}^7$ and $\{Co(NO)\}^8$.

Complex **53** expands the M(bme−dach) structures into main group metals and is the only example in the Cambridge data base of a N_2S_2 framework with an aluminum metal center. The Al^{3+} is raised by 0.650 Å out of the N_2S_2 plane and an ethyl fragment is bound in the axial position (τ = 0.0). Complex **53** was prepared from reaction of the deprotonated bme−dach N_2S_2 ligand and $Al(Et)_2Cl$ in toluene.[173]

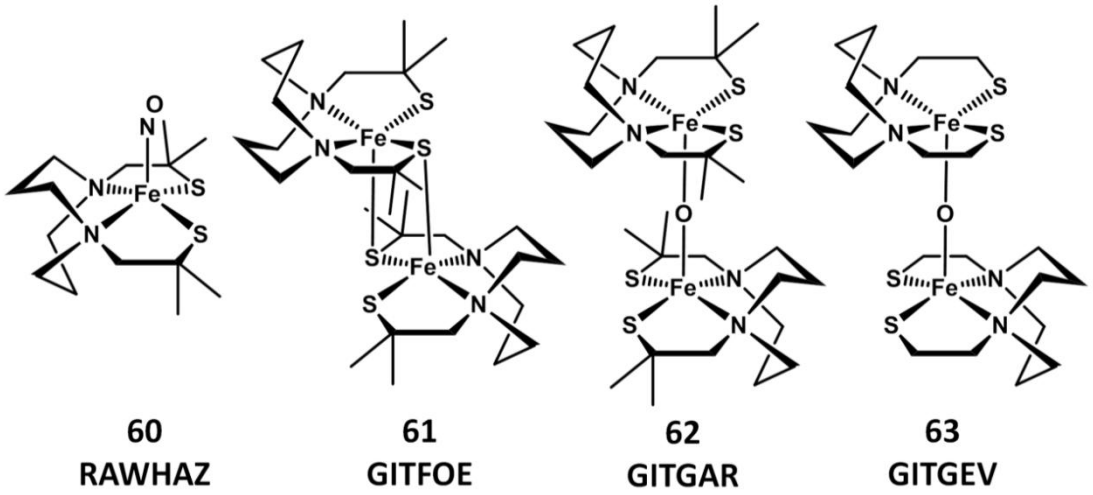

Figure 2-15. Complexes **60−63** are various Fe(bme−daco) complexes with gem−dimethyl groups and/or bridging oxo's.

Structures **60 − 62** of Figure 2-15 are of pentacoordinate iron within an N_2S_2 ligand containing gem−dimethyl groups on the carbon alpha to the thiolate sulfurs. Complex **60** is analogous to **58** with very minor differences in the Fe−S distances.[169] Likewise the steric bulk within the N_2S_2 ligand does not significantly alter the metric parameters of **61** as compared to **57**.[174] Complexes **62** and **63** are μ–O analogs of **61** and **57**, respectively.[174] Formation of the μ–O results in a shift of the N_2S_2 ligand such that the two irons align and the N_2S_2 donor sets are in reverse formation. The best N_2S_2 planes are 3.107 Å and 4.820 Å from each other in **61** vs. **62**, respectively. They are 3.126 Å and 4.768 Å apart in **57** and **63**, respectively. Note that while O_2 leads to S−oxygenation products with NiN_2S_2 compounds, it oxidizes the $Fe^{2+}(\mu\text{−}SR)_2Fe^{2+}$ system to $Fe^{3+}(\mu\text{−}O)Fe^{3+}$ with loss of the bridging thiolates.[106]

Open chain versions of N_2S_2 ligands offer flexibility in coordination geometry, which is sometimes observed; however, the geometries in the solid state structures of complexes **64**−**68**, Figure 2-16, are analogous to the constrained mesocycle derivatives described above. For example, complexes **64** and **65** are the open chain,[169,175] 5−6−5, analogues of **52/59** and **51/58** in Figures 2-13 and 2-14, respectively, for which the stick drawings that are biased towards square pyramidal character are accurate. Complex **66** is similar to **64** and **65** with a difference being that the NO is oriented on the N−Me side of the N_2S_2 ligand.[176]

Complexes **67** and **68**, Figure 2-16, are the precursors to the monomeric FeNO complexes **65** and **66**, respectively, derived by addition of NO gas to the dimeric starting material.[177] If NO^+, as in the $NOBF_4$ salt, is added to **68**, the cationic diiron μ–NO complex **69** is obtained.[178] Substantial reorganization of the S−N−N−S chain in **69** orients the N−Me groups anti, and the sulfur donors are trans to each other, one of which is also bridging to the adjacent Fe. As shown in **69**, the μ–NO completes an octahedral geometry about Fe, with angles in the range of 85 – 95°. Nevertheless, there is a short Fe−Fe distance of 2.47 Å that is well within metal−metal bonding distance, and was interpreted as such by the authors.[178] That is, the authors suggest NO^+ has oxidatively added to **68**, generating μ–NO^- and two low−spin d^5 Fe^{3+} metal centers in a spin−coupled diamagnetic complex. This argument is strengthened by the characterization of the cobalt analogue, complex **70**, where the same geometry is observed but the Co−Co distance of 2.77 Å indicates a non−bonding repulsion along the Co−Co axis.[179] In **69** and **70**, the NO distances of 1.193 and 1.211 Å, respectively, the

ν(NO) values of 1553 and 1545 cm^{-1}, respectively, and the M−N−O angles of 134° and 130°, respectively, are consistent with a reduction of bond order ($N{\equiv}O^+$ to $N{=}O^-$).[178-179]

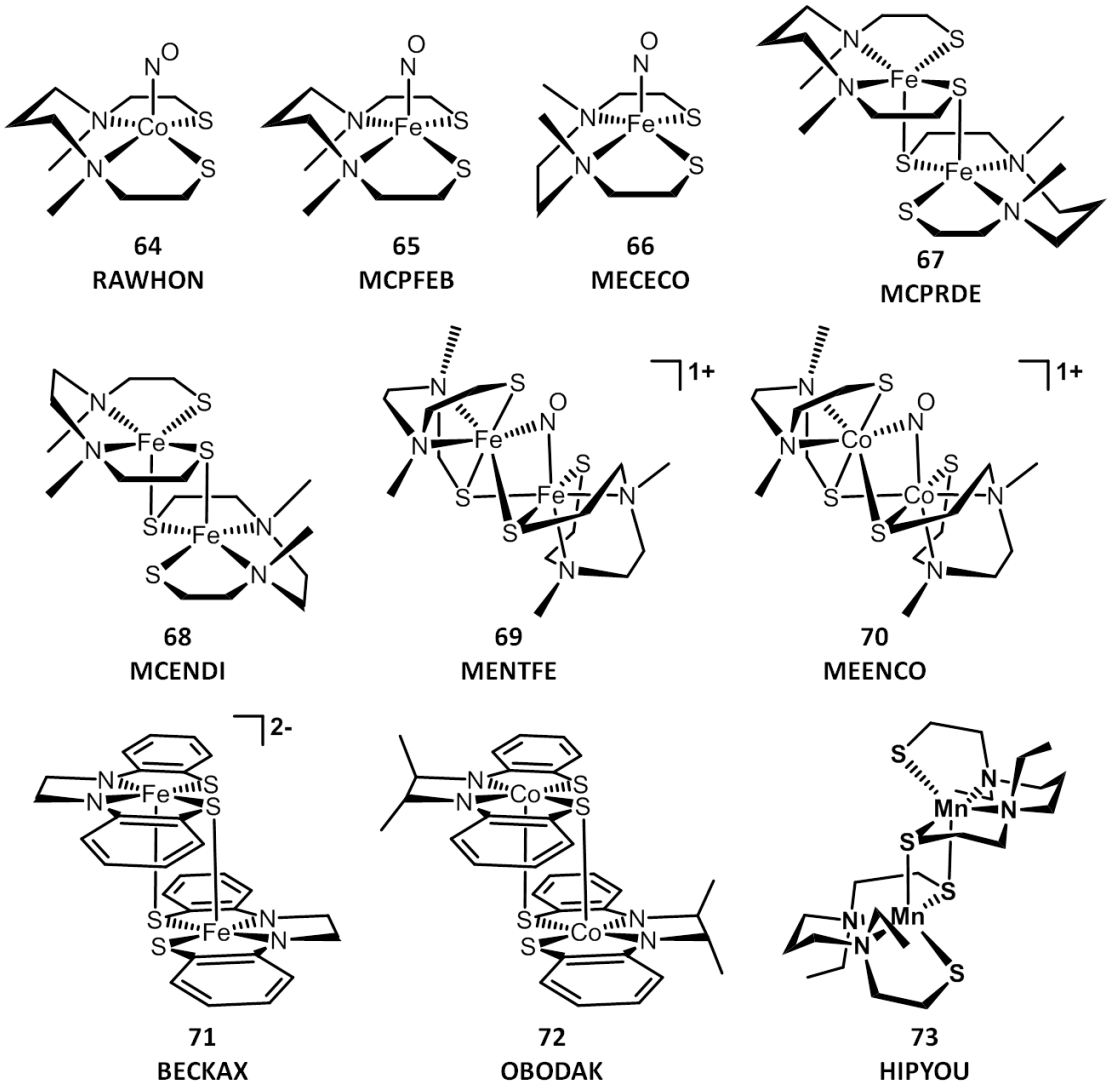

Figure 2-16. Open chain MN_2S_2 complexes **64**−**73** where M = Fe, Co, and Mn.

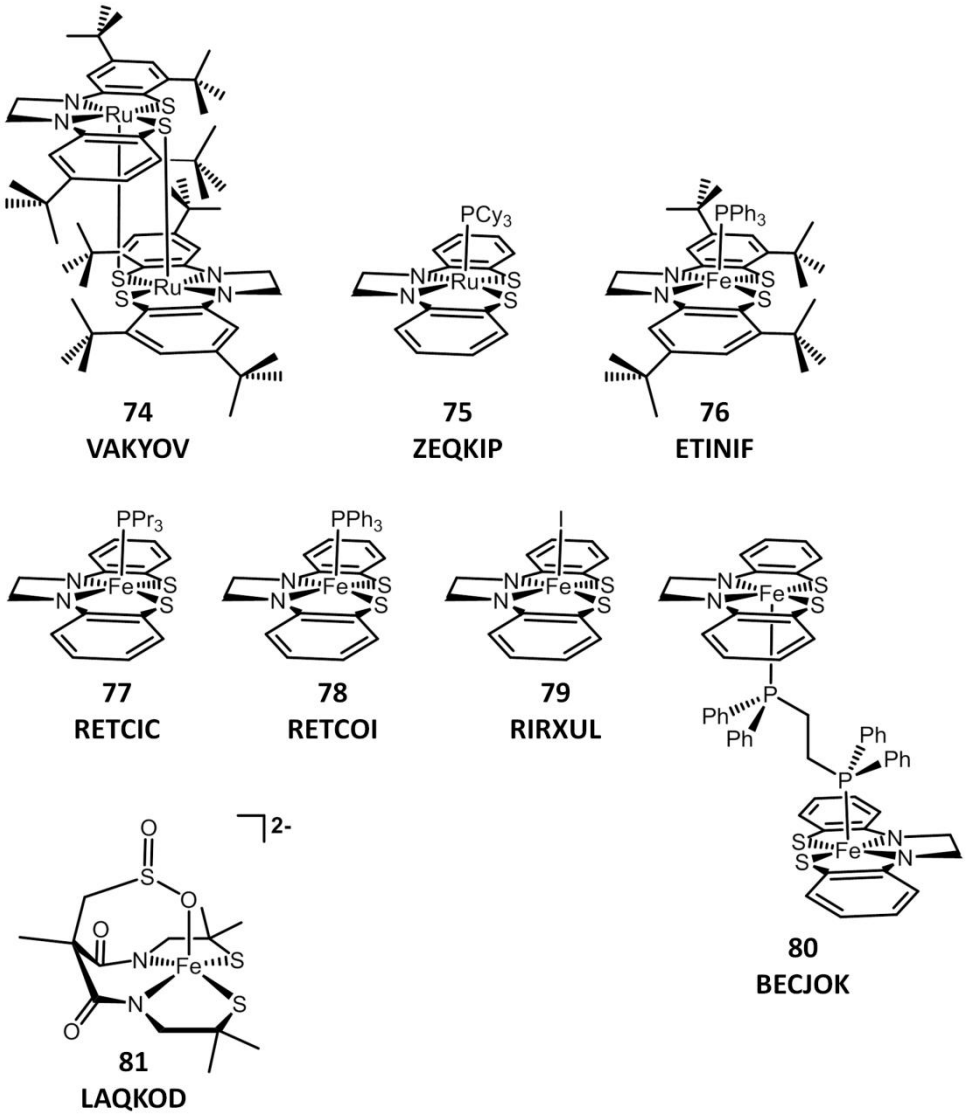

Figure 2-17. Group 8 MN_2S_2 complexes **74−81** all of which have 5−coordinate geometries.

The N_2S_2 ligand in which the N to S linker is a phenylene is found in complexes **71** and **72**.[180-181] The stick drawings of these complexes indicate similarity to the alkyl chain N_2S_2 ligands, however the non−innocence of such 1,2−mercaptoaniline units has

shown these ligands are actually $[N_2S_2]^{3-}$ radicals bound to Fe^{2+} in **71**; in **72,** the $[N_2S_2]^{2-}$ diradical is bound to low spin Co^{2+}. Anti−ferromagnetic coupling accounts for the lack of an EPR signal in complex **72**. The non−innocence of these ligands has been further established through computational investigations by Wieghardt, *et al.*[182-184]

Complex **73** crystallized in an isomeric form in which the N−Et groups are in the anti orientation and the overall coordination geometry is TBP (τ = 0.74) with apical positions occupied by a bridging S and a N.[185] This is the sole MnN_2S_2 complex that was found in the CCDC.

Decoration of the 2−aminothiophenolate units with tert−butyl groups has led to the diruthenium complex **74** (Figure 2-17),[186] analogous to the 2−electron oxidized form of **71**. To our knowledge, the precise electronic structure of this complex has not been determined; however, the expectation is that both metals are Ru^{2+}, with the ligand in the dianionic state. Complex **75** is synthesized from a one−pot reaction of Ru^{3+} with the dianionic ligand in the presence of the tris−cyclohexylphosphine ligand.[187] Described in the original report as having a Ru^{4+} center, Wieghardt, *et al.* have suggested that the electronic structure and oxidation state assignment should be reconsidered.[182-184]

Several pentacoordinate $(L)FeN_2S_2$ complexes of the 2−aminothiophenolate ligand are listed as complexes **76−80**.[180,184,188-189] As shown in Figure 2-17, the fifth coordination site may be occupied by phosphines; in **80** a diphosphine spans two FeN_2S_2 units. A neutral product, complex **79**, was isolated from the binuclear oxidative addition of I_2 to **77**. In this case, Mössbauer, EPR, and DFT studies concluded that the oxidation state of the iron was Fe^{3+}, with an intermediate spin state, anti−ferromagnetically

coupled to two N_2S_2 ligand−based π−radicals. Complex **81** contains an Fe^{3+} stabilized by an N_2S_2 ligand different from those of complexes **76−80**; a built in sulfinic acid functionality in the N to N linker maintains five coordination.[190]

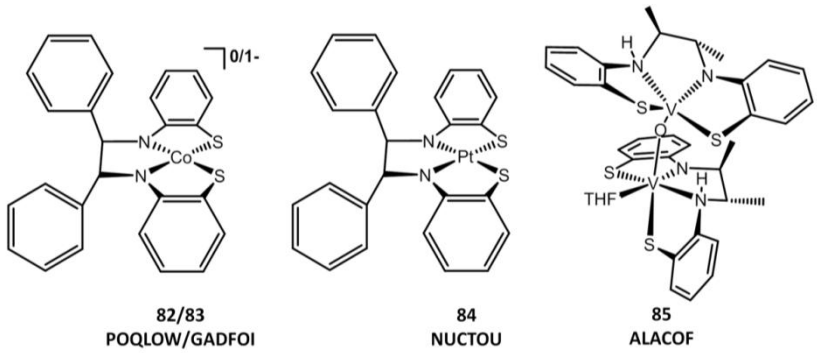

Figure 2-18. MN_2S_2 complexes **82−85** where M = Co, Pt, and V and the ligand is comprised of the non−innocent aminothiophenol unit.

The similar 2−aminothiophenolate N_2S_2 scaffold has been used to chelate Co^{3+}, Figure 2-18, in a neutral complex **82**,[183,191] and in the monoanion, complex **83**.[183] Spoules, Wieghardt, *et al.*, maintain the oxidation state of cobalt is still Co^{3+}, while the ligand has been reduced from −3 in **82** to −4 in **83**.[183] The geometries of **82** and **83** are largely square planar with T_d twists of 8° and 2°, respectively. The platinum analogue to **82**, complex **84**, has also been crystallized.[192] On the lighter side of the d−block series, the di−vanadium complex **85** is an unusual $V^{4+}(\mu{-}O)V^{4+}$ complex of the singly protonated mercaptoaniline N_2S_2 ligand.[193] Note that one V^{4+} is octahedral by means of a bound THF molecule; a second THF of crystallization is H−bonded to one of the amido nitrogens.

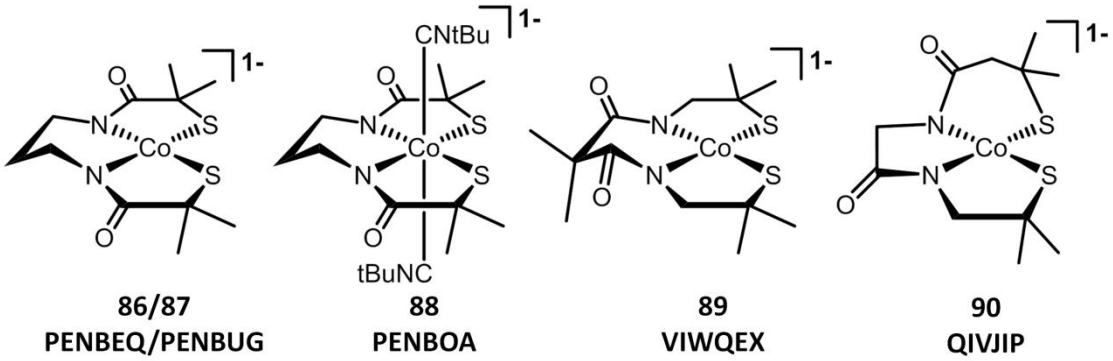

Figure 2-19. Complexes **86−90** are monomeric CoN_2S_2 mimics of the nitrile hydratase active site.

A three−carbon linker connects the nitrogens in complexes **86−89**, Figure 2-19.[194-195] The N donors are amidates in each case with the carboxyl group either in the N to S or the N to N linker. In **90**, a carboxyl group is in both positions, reminiscent of the Cys−X−Cys tripeptide motif, see Figure 2-2.[196] The unusual N_2S_2 ligand shown in Figure 2-20 derives from thiomorpholine, condensed with 1,3−dibromopropane to yield a 3−carbon linker between the nitrogens, and two 2−carbon links between the N and S; i. e., a 5(5)−6−5(5) arrangement describes the connectivity in the ligand. Tertiary nitrogens and thioethers are arranged to yield a square planar N_2S_2 binding set with highly pinched N−M−S bite angles (~75°), resulting in a S−M−S angle of 110° and 104° for complexes **91** and **92**, respectively.[197]

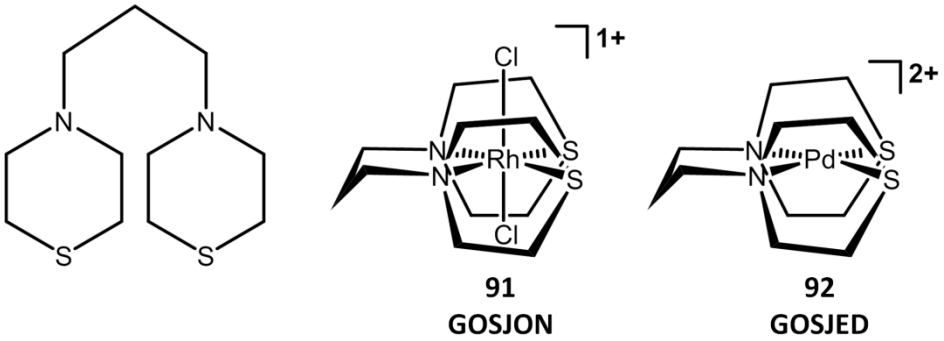

Figure 2-20. Complexes **91** and **92** feature two thiomorpholine rings linked by an alkyl chain. The connectivity within the free N_2S_2 ligand is shown left.

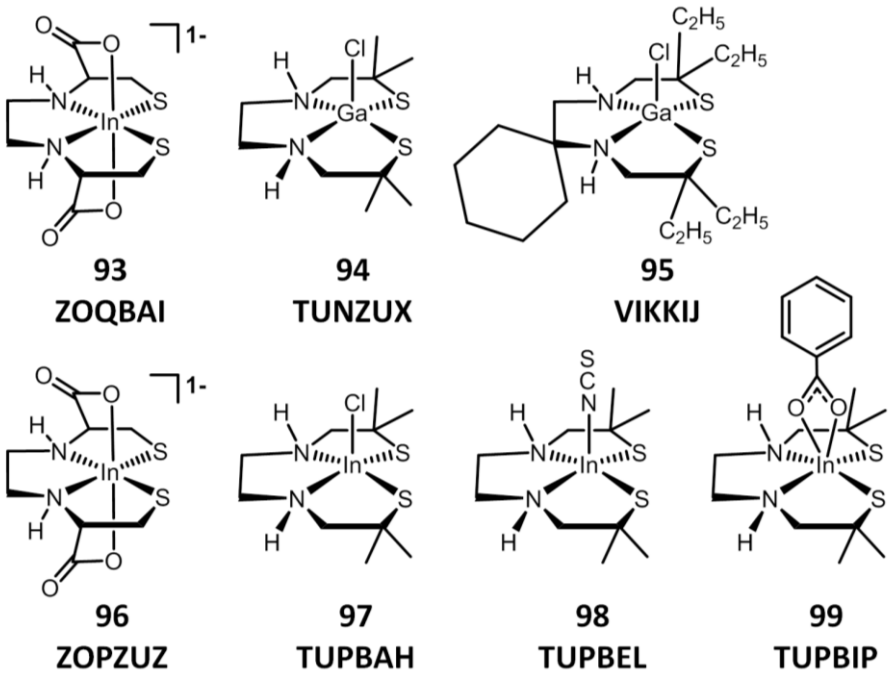

Figure 2-21. Complexes **93−99** represent examples of MN_2S_2 complexes with M = Ga^{3+} or In^{3+}.

Non−transition metal N_2S_2 derivatives are found in Figure 2-21. Complexes **93−99** represent the 5− or 6− coordinate examples of MN_2S_2 complexes where M = Ga^{3+} or In^{3+}. The axial ligands may be built into the N_2S_2 framework as found in the carboxylates of **93** and **96**.[198] The preference of Ga^{3+} and In^{3+} for penta−coordination is met by a bound counterion or anionic ligand as in **94**, **95**, and **97 – 99.**[199-200]

The pentacoordinate zinc of complex **100**, Figure 2-22, has τ = 0.46 and is analogous to the nickel complex, **44,** but with far greater geometrical distortion about the metal center.[201] While the nickel analogue (complex **7**) of complex **101**, Figure 2-22, has a minimal tetrahedral twist (15°), the preference of Zn^{2+} for tetrahedral coordination results in a significant distortion and a 72° T_d twist.[136] The Cu^{2+} complex **102** has a 21° T_d twist, somewhat similar to the Ni^{2+}, d^8 complexes.[202-203] The similar 5−5−5 chelate pattern in **103** includes a Cu^{3+} and is rigorously square planar.[204]

The ZnN_2S_2 complexes **104−106** differ by substituents on the N and/or the N to N alkyl linker. Pentacoordination about Zn in **104** results in dimer formation with the less sterically bulky ligand[205] while tetracoordination and largely tetrahedral geometries exist for **105** and **106**.[193,205]

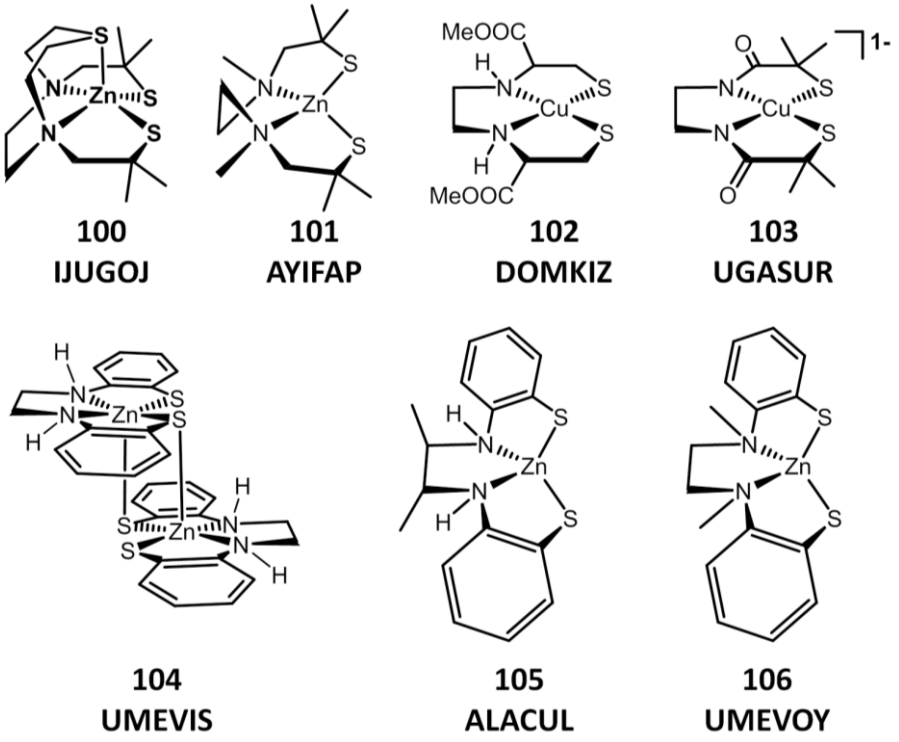

Figure 2-22. Complexes **100−106** represent examples of MN_2S_2 complexes with M = Zn or Cu.

Complexes **107−113**, Figure 2-23, have the 5−5−5 chelate ring pattern in which the N to N link is either phenyl or cyclohexyl. Copper (II) and (III) derivatives, **107** and **108**/**109**, exist as analogues of Ni^{2+} and Ni^{3+} complexes, **12** and **13**, respectively.[204,206] The same N_2S_2 ligand accommodates pentacoordinate iron in **110** and **111**.[207] As the ligand is −4, the oxidation level of iron is clearly +3 in **110**; by this electron counting, the redox level of the Fe(NO) unit in **111** should be an unusual $\{Fe(NO)\}^6$. However, the Mössbauer parameters and ν(NO) IR values do not match with other reported $\{Fe(NO)\}^6$ complexes.[208]

Complexes **112** and **113** for Cu^{2+} and Zn^{2+} show tetrahedral twists of 33° and 71°, respectively.[209-210] Complex **114** has a 6−5−6 chelate ring pattern allowing for a greater T_d twist of 67°.[211]

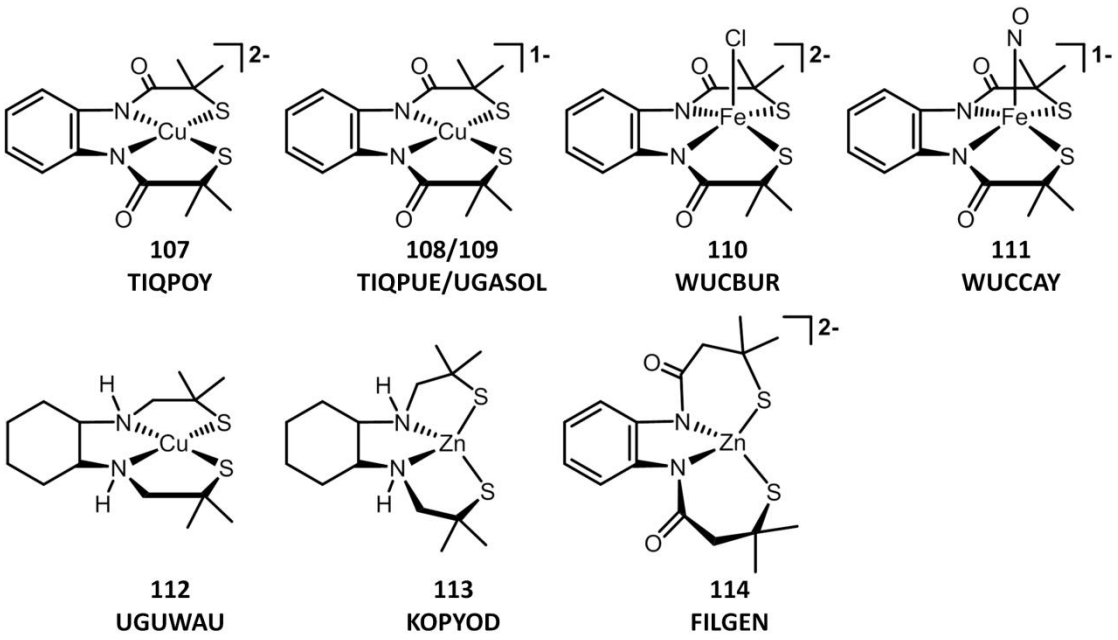

Figure 2-23. Complexes **107−114** are MN_2S_2 complexes with diaminocyclohexane or diamidobenzene N to N linkers.

Figure 2-24 displays variations of metal and substituents on the thiosalen (tsalen) ligand, leading to the complexes **115−120**, which are analogous to the nickel complexes of Figure 2-11. Complex **115** contains Cu^{2+} and has a T_d twist of 23°.[153] The Co^{2+} complex **116** is dimeric with a Co_2S_2 diamond core.[212] A chloride completes the pentacoordination environment about Fe^{3+} in **117**,[213] while a μ–O bridges two $Fe^{III}N_2S_2$ units of **118**.[214] The hexacoordinate, octahedral complex **119** features the thiosalen

ligand with a CO and pyridine ligand in the axial positions.[215] Complex **120** is a dimeric ZnN_2S_2 with the familiar Zn_2S_2 core lending pentacoordination to Zn.[156]

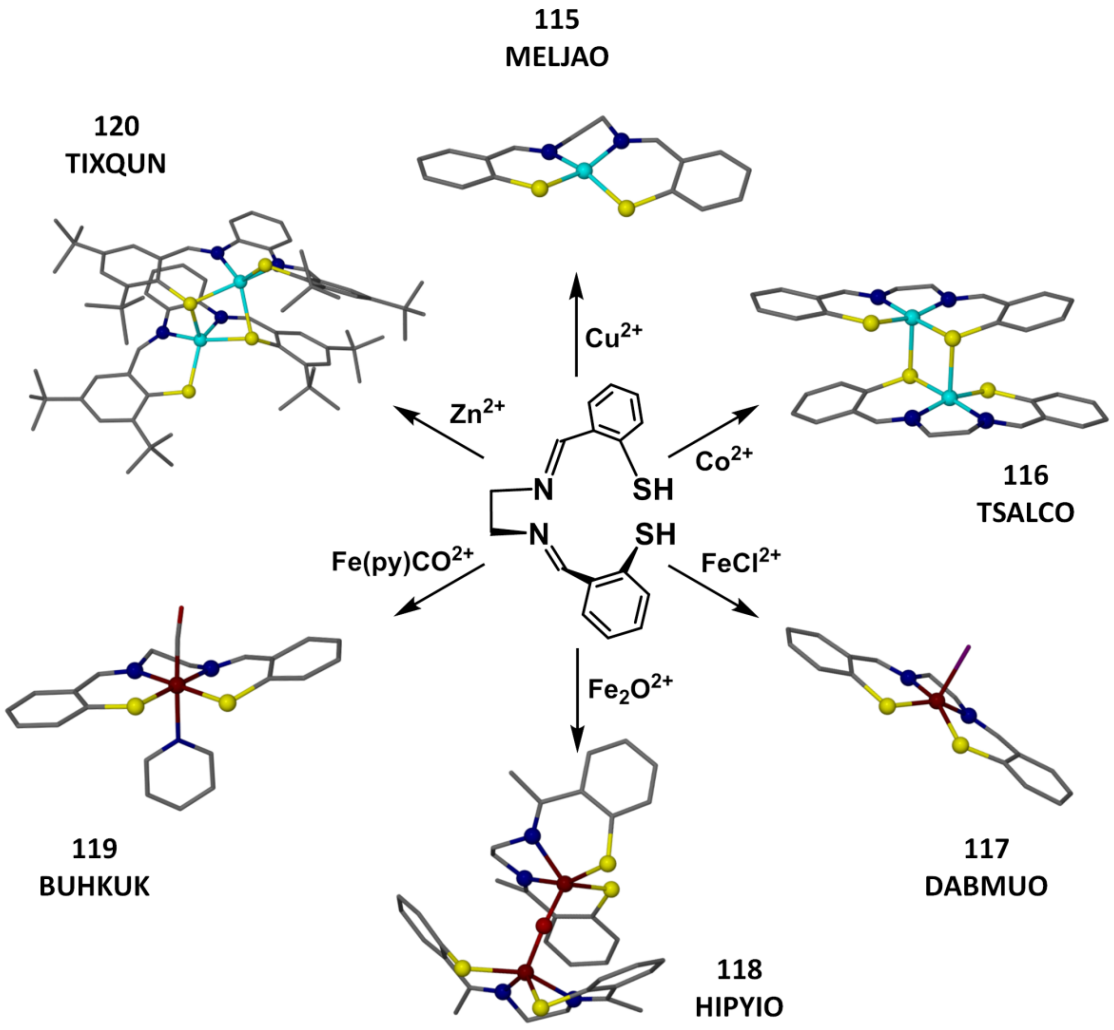

Figure 2-24. Complexes **115−120** represent the M(tsalen) complexes crystallized to date, where M ≠ Ni.

2.3 Bimetallic Systems

2.3.1 $MN_2S_2W(CO)_x$ Complexes and the Definition of Steric and Electronic Factors

There are many approaches to descriptions of ligand properties and their corresponding influences on transition metal properties and reactivities.[216] With classical, Werner−type coordination complexes, the coordinating abilities of hard, first−row donor ligands are typically compared by their pK_a values, i.e., their relative abilities to be protonated.[217] Myriad approaches for comparisons of electron donor effects of softer donors of importance to organometallic chemistry and homogeneous catalysis, such as phosphines, N−heterocyclic carbenes, π−ligands, etc., have been reported. Nevertheless, the Tolman electronic parameter, derived from ν(CO) IR values in a standard $LNi^0(CO)_3$ complex has retained usefulness for nearly a half−century.[218] Likewise, the simple Tolman cone angle, originally developed for phosphines,[218] is a standard whose values other approaches are expected to match. Clearly the "cone" that emanates from the metal and encompasses the outer reaches of PR_3, $P(OR)_3$, or π−ligands such as η^5−C_5R_5 is reasonably symmetrical. However, other approaches must be taken for two dimensional ligands such as the N−heterocyclic carbenes or pyridines and derivatives. This has been pursued by computational modeling that takes bond stretching and wagging into account.[219-220] A solid cone angle approach which addresses multiple conformers and compressibility was adopted by Musco, et al. to describe phosphine ligands.[221] Nolan used the concept of percent buried volume to define the

steric character of NHC ligands.[222] We have used crystallographic parameters to identify steric impedance of the MN_2S_2 ligands in our study, *vide infra*.

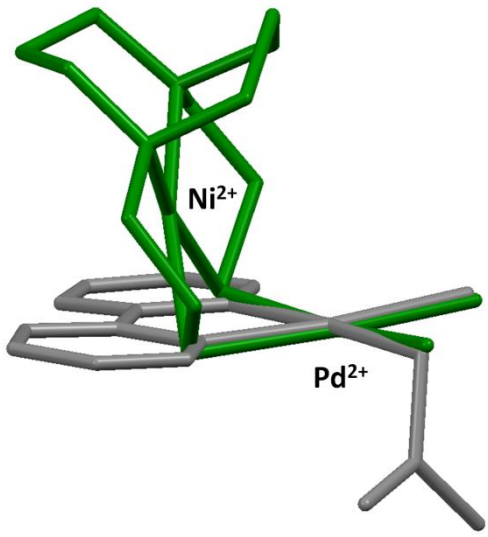

Figure 2-25. Structural overlay of Ni(bme−daco)Pd(CH_3)Cl,[116] green, and (bipy)Pd(CH_2COCH_3)Cl,[223] grey.

Anionic S−donor thiolates are intermediate in the hard/soft description of Lewis bases; thiophilic metals are in the intermediate to soft category of Lewis acids. Nevertheless, the π−donor ability of RS^- is substantial, and thereby stabilizes first−row transition metals in higher oxidation states, such as $Fe^{III}(SR)_4^-$. In contrast, thioethers, RSR, neutral and with two lone pairs, are soft donors, and have poor binding ability to first row transition metals in positive oxidation states. Thiolates that are bound by transition metals retain lone pairs that, in comparison to the free RS^- or R−S−R, are of intermediate binding ability, as evidenced by published precedents of isolated

complexes. The tight binding sites that result in the contiguous arrangement of S−N−N−S donors produce terminal thiolate sulfurs that retain lone pair reactivity. Their cis orientation is suitably available for further binding without complications of extreme aggregation. In fact, the orientation of the lone pairs on adjacent sulfurs within the largely planar MN_2S_2 unit is similar to those of common bidentate N− and P−donor ligands such as bipyridine or bis−1,2−diphenylphosphinoethane, dppe. A difference is that the residual lone pair, that remains after one is used to bind to a second metal, has a stereochemical preference that dictates what we have loosely described below as "hinge angle" for the bidentate MN_2S_2M' and $MN_2S_2M'_2$ systems. Despite the difference in stereochemical orientational effect found for the MN_2S_2M' and bipyridine•M' arrangements,[117,223] most dramatically illustrated by the overlay of structures in Figure 2-25, complexes of MN_2S_2M' may be designed as if the metallodithiolate ligands were simple diamine or diphosphine ligands. A likely explanation is that the bite angles and donor abilities of such bidentate ligands are quite similar.

As stability is a requirement of any analytical standard or chemical analysis tool, the $[W(CO)_4]$ platform is particularly attractive for its ability to form bidentate $MN_2S_2W(CO)_4$ adducts that are available as crystalline materials whose molecular structures are consistent with the vibrational spectroscopy in the ν(CO) region of the infrared spectra. A series of such adducts has been developed, Figure 2-26, and ν(CO) IR values were taken as spectroscopic reporters of the relative donating abilities of MN_2S_2 metallodithiolate ligands. Nonetheless, discrimination between the various neutral NiN_2S_2 complexes by the $W(CO)_4$ reporter unit is minimal and other reference moieties

are found to be useful for corroboration. The dinitrosyliron unit, $Fe(NO)_2$, a transition metal acceptor fragment that is unusually stable (even in two redox levels), has also been shown to bind to metallodithiolate ligands and have less steric hindrance; results from this spectroscopic probe will be discussed in Section 3.3.

Figure 2-26 displays ten structures of MN_2S_2 adducts of $W(CO)_4$: M = Ni^{2+}, $V{\equiv}O^{2+}$, $ZnCl^{+}$, $Fe(NO)^{2+}$, and $Co(NO)^{2+}$, imbedded in various N_2S_2 ligands.[171,226-229] Most of the structures are of C_s symmetry with a mirror plane containing W, the axial CO's, and the M of the N_2S_2 metalloligand. All structures show that the bridging dithiolates impose a butterfly arrangement where the dihedral angle between the best N_2S_2 plane and the $S_2W(CO)_2$ plane, the hinge angle, varies over a range of 103−134° as listed in Figure 2-26. Additional metric parameters are listed in Table A15. It should be noted that for the $NiN_2S_2W(CO)_4$ adducts this definition of hinge angle is the same as the intersection of the NiS_2 and WS_2 planes. For non−planar MN_2S_2 metallodithiolate ligands, where the M center is displaced out of the N_2S_2 plane, the latter description, the intersection of the MS_2 and $M'S_2$ planes, leads to larger hinge angles. Hence, for consistency we will report the dihedral angles using the best N_2S_2 plane, *sans* M, all of which refer to crystallographic data.

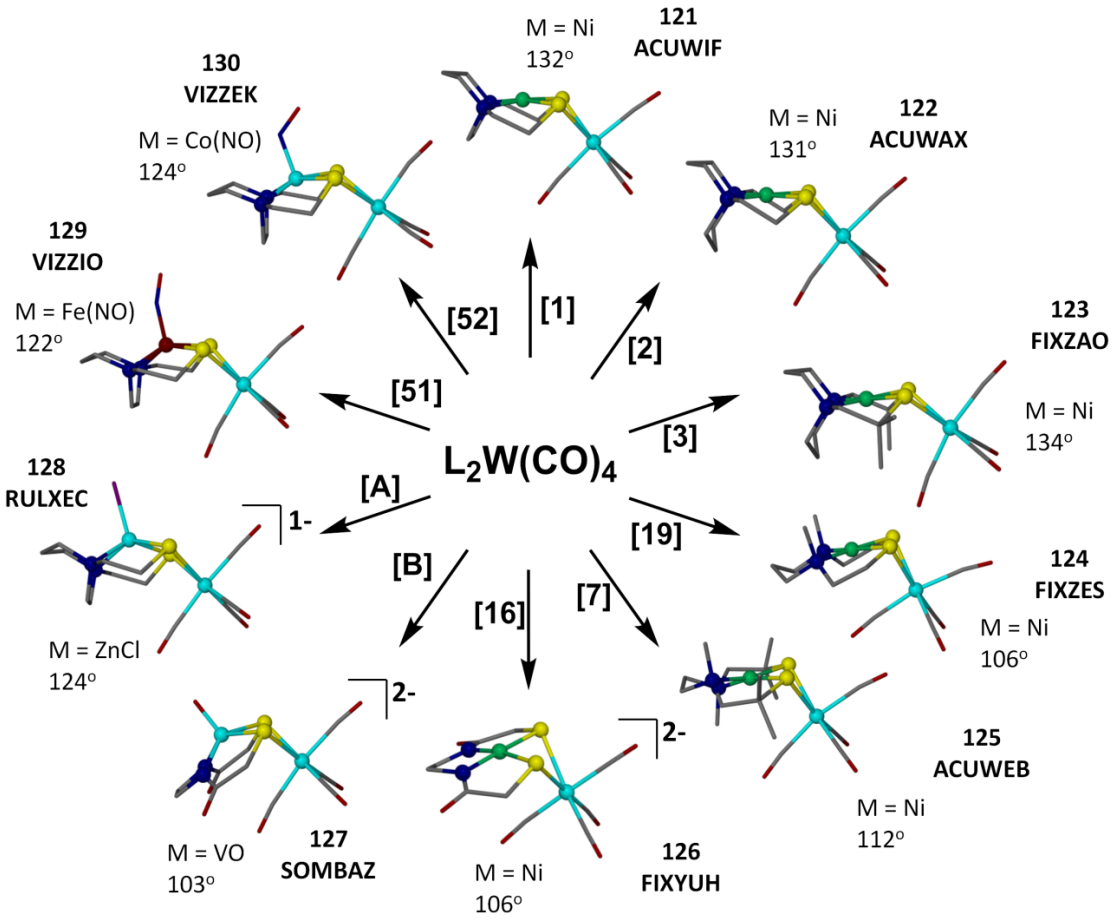

Figure 2-26. Complexes **121**−**130** are the $MN_2S_2W(CO)_4$ structures typically derived from thermal replacement of piperidine in the labile ligand complex, cis−$(pip)_2W(CO)_4$.[224] Numbers in brackets over the arrows represent monomeric MN_2S_2 complexes defined above. The MN_2S_2 complex [A] that leads to **128**, monomeric $[Zn(Cl)N_2S_2]^-$, has not been structurally characterized; and the $V(O)N_2S_2$ structure [B] that leads to **127** is known but not presented herein.[225] The hinge angles of each complex are also given.

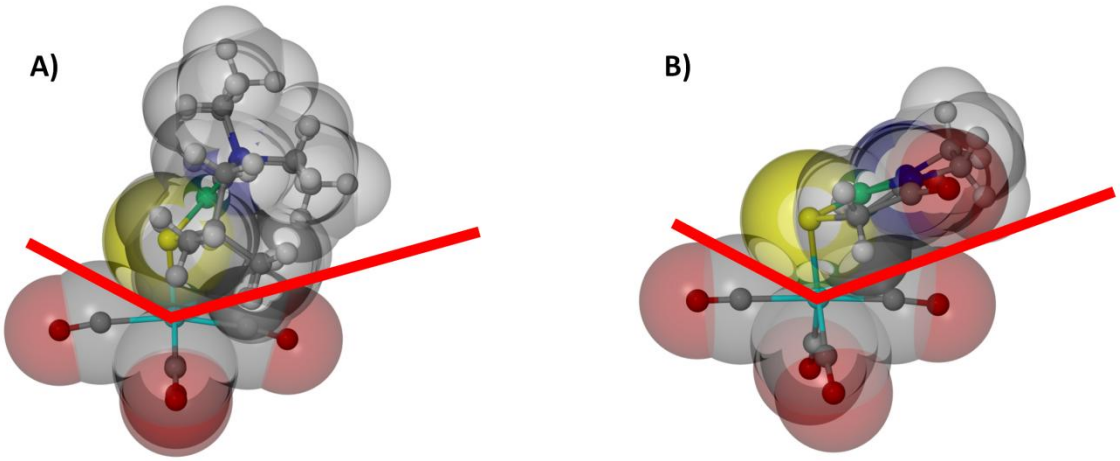

Figure 2-27. Space filling models of complexes A) **123** and B) **126** with vectors superimposed that relate to steric factors. In both examples the left vectors are based on the van der Waals radius of the sulfur (yellow atom) and the right vector is based on the hydrogen atom that is directing the greatest amount of steric encumbrance on the $W(CO)_4$ unit. Note that the sulfurs (yellow) as well as the nitrogen atoms (blue) are eclipsed.

The steric encumbrance of the MN_2S_2 ligands is felt mostly by the proximal CO ligands on the $W(CO)_4$ unit of the $M(N_2S_2)$ adducts of $W(CO)_4$. Here the hinge angle is influenced by both the N to S and N to N hydrocarbon linkers in the N_2S_2 unit, and any substituents on these connectors. Figure 2-27 displays space−filling models of complexes **123** and **126**. The former has gem−dimethyl groups alpha to the S donor, increasing steric bulk, and the latter is derived from the largely planar $(ema)^{4-}$ ligand. In both cases, the red vectors prescribe the wedge filled by the surface of the metalloligands in the two−dimensional representation (140° for **123** and 128° for **126**).[227] The angle

defined by the vectors in each are directed towards the broadest (largest hydrocarbon encumbrance) portion and the sulfur portions of the bound ligand. Nevertheless, the carbonyl ligand closest to the MN_2S_2 ligand is actually flanked by the gem−dimethyl groups of **123**, hence the vector is drawn tangent to that sphere of the H atom closest to the CO ligand.

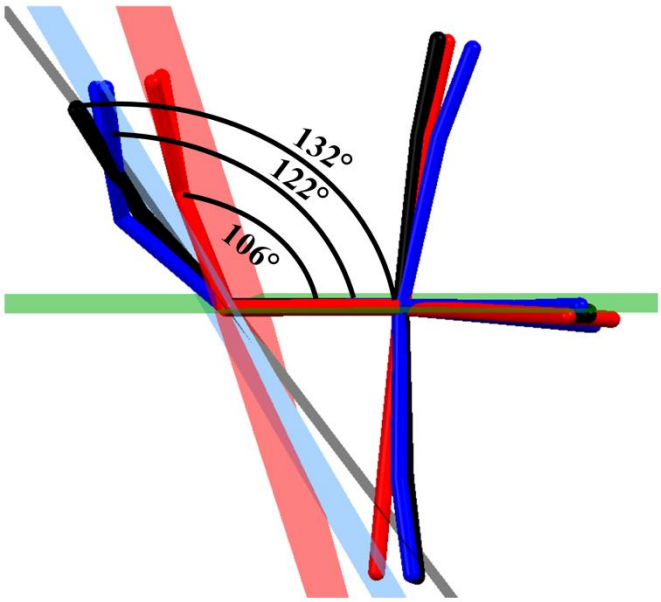

Figure 2-28. Overlay of complexes **121** (black), **129** (blue), and **126** (red) showing the range of hinge angles (132°, 122°, and 106° respectively) observed for the $MN_2S_2W(CO)_4$ complexes, presented as a side profile with the S_2WC_2 unit (green) horizontal. For clarity only the Ni, N, S, and W atoms and CO ligands are shown.

Figure 2-28 presents stick structural overlays of intersecting best N_2S_2 / WS_2 planes derived from three complexes found in Figure 2-26. The smallest hinge angle

seen here is from the $Ni(ema)^{2-}$ adduct, 106°, while the largest is from the mesocyclic Ni(bme−dach) metalloligand, 132°. We will see below that these angles are largely maintained in the $Fe(NO)_2$ derivatives, i.e., where less steric encumbrance from the iron and its remaining coordination sphere allows smaller hinge angles on the order of 5° or less.

The rigidity of the $W(CO)_4$ unit prevents major distortions in W−C−O angles, however the CO groups trans to each other are slightly bent away from the metallo ligand, with little differences between that which is proximal or more sterically encumbered by the MN_2S_2 ligand and that which is influenced by the repulsive interaction of the residual lone pairs. Interestingly, such a slight distortion from linearity of the trans CO groups is also seen in the X−ray structure of the bipyridine•$W(CO)_4$ complex.[230] This is presumably a result of interelectronic repulsion of π−density on the N−donors of bipyridine and the adjacent carbonyl ligands, similar in their influence as the electronic sphere about sulfur, Figure 2-27. The electronic asymmetry in the $W(CO)_4$ portion of the $NiN_2S_2W(CO)_4$ complex is confirmed by the observation of three signals in the CO region of the C−13 NMR spectrum with evidence of coalescence at ~90° and an estimated barrier of 15 − 16 kcal/mol for complex **123**.[226] The high barrier to up/down flapping of the metallodithiolate ligand, which would equilibrate the CO ligands that are trans to each other, reflects the secure orientational effect of the residual lone pairs on the sulfur bridges.

The smallest hinge angles are seen in complexes **124 − 127**,[226-227] and those of intermediate values are the ones with $ZnCl^+$, $Fe(NO)^{2+}$, and $Co(NO)^{2+}$, i.e., complexes

128 − 130,[171,229] where the pentacoordinate metals bearing apical Cl^- or NO ligands are displaced out of the N_2S_2 plane by 0.744 Å, 0.552 Å, and 0.385 Å, respectively. Compared to the free nitrosylated metalloligand the displacements for the Co(NO) and Fe(NO) are slightly larger in the $W(CO)_4$ adducts, by ca. 0.05 Å; see Figures 2-13 and 2-26 and Tables A6 and A15.

The $W(CO)_4$ adduct of a vanadyl−N_2S_2 could only be obtained with the tetraanionic $(ema)^{4-}$ ligand, generating a dianionic $[(V{\equiv}O)N_2S_2]^{2-}$, complex **127** of Figure 2-26. In comparison to the $Ni(ema)^{2-}$, complex **126**, the hinge angle of **127** is smaller by 3° apparently as a result of displacement of $V{\equiv}O^{2+}$ out of the N_2S_2 plane by 0.7 Å, whereas the analogous metal displacement in $Ni(ema)^{2-}$ is only 0.1 Å.[228] The additional consequence is in M−W distances of 3.29 Å for **127** and 2.93 Å for **126**. As expected, the largest M−W distance in this set is in complex **128**, 3.51 Å.[229] The two open chain N_2S_2 derivatives of Ni, complexes **19** and **7**, bind to $W(CO)_4$ with small hinge angles, 106° and 112°, for **124** and **125**, respectively.[226-227] Contrasting significantly, complexes **121 − 123** derived from mesocyclic diamine frameworks have more open hinges of 131−134°.[226-227]

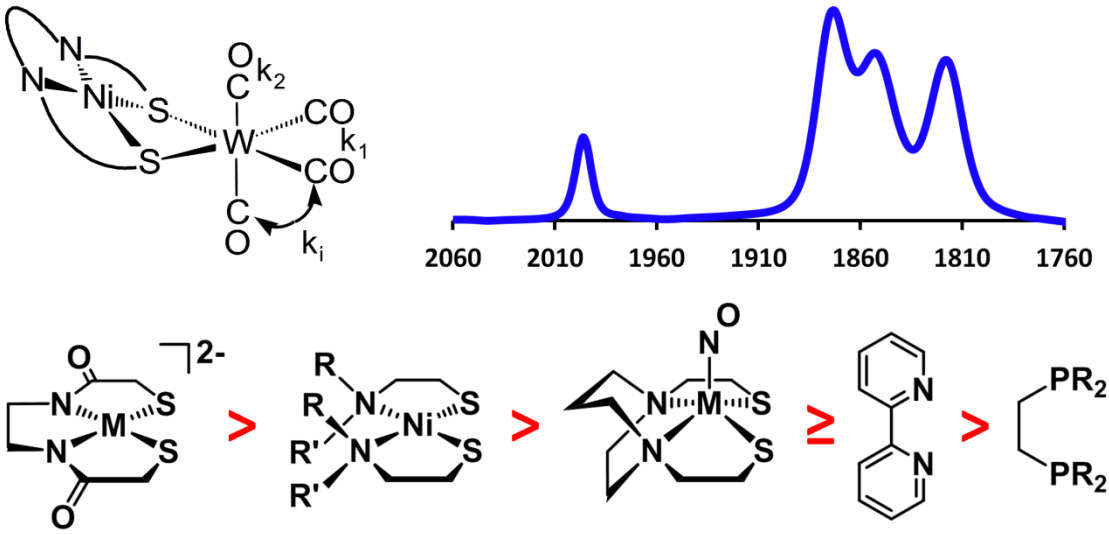

Figure 2-29. Hierarchy of donation strength for MN_2S_2 metalloligands as compared to traditional bipyridine and diphosphine ligands. As an example, the ν(CO) IR spectrum is shown for complex **121**, Ni(bme−dach)W(CO)$_4$, recorded in DMF solution.

Table A1 contains solution data in the ν(CO) region of the infrared spectrum with assignments and related Cotton−Kraihanzel force constants as indicated.[231] The listing is in order of diminishing k_1 values, which are expected to be influenced most by the donor strength of the MN_2S_2 metalloligand. Also listed are averages of all ν(CO) values which, as shown in Table A1, largely track with calculated k_1 values. As expected, dianionic complexes made with the ema^{4-} ligand are the best donors (lowest ν(CO) and smallest k_1 values), and the monoanionic complex, [ZnCl(bme−dach)]$^-$, is also amongst the best. All neutral Ni^{2+} complexes are roughly equivalent, while the $Co(NO)^{2+}$ and $Fe(NO)^{2+}$ are slightly weaker with donor strengths comparable to bipyridine. According to the ν(CO) reporter data, all the cis−dithiolate metalloligands are better donors than the diphosphine

ligands such as dppe, dppm, etc.[226] Figure 2-29 contrasts the donor abilities of the metal dithiolates and such traditional ligands.

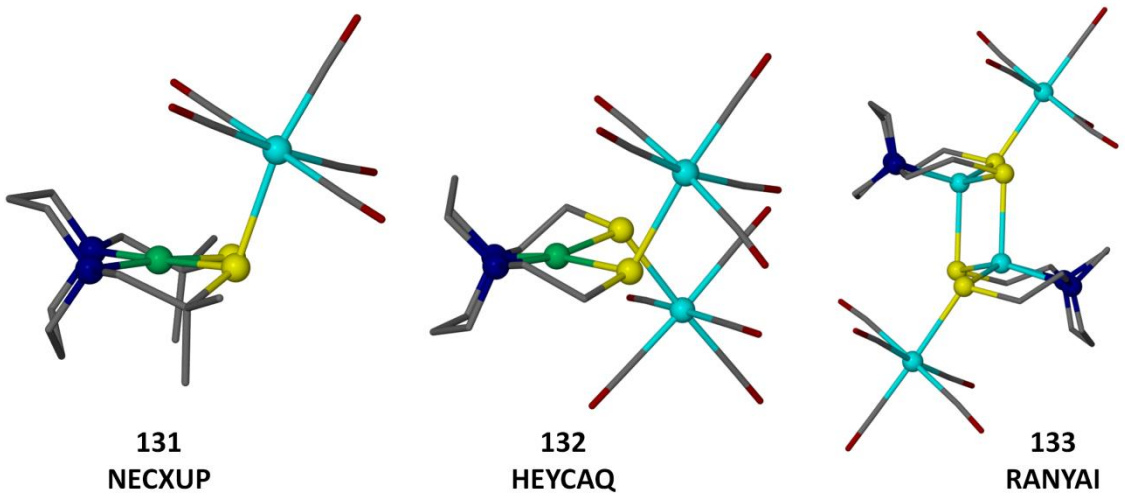

Figure 2-30. Examples of $MN_2S_2W(CO)_5$ complexes; M = Ni^{2+} for **131** and **132**; M = Cd^{2+} for **133**.

Several members of the series in Figure 2-26 have been used to establish reactivity with CO to yield $MN_2S_2W(CO)_5$ complexes in which the metallodithiolate serves as a monodentate S−donor ligand. In no cases thus far reported has complete CO replacement of the MN_2S_2 ligand to generate $W(CO)_6$ been observed, even under CO pressures of up to 1400 psi. Hence the MN_2S_2 ligands are designated as hemi−labile, becoming more strongly bound following the ring−opening (W−S bond−breaking) process,[232] and generating products such as those in Figure 2-30. The complexes may also be prepared by the photolysis of $W(CO)_6$ in THF to yield solvated $[W(CO)_5]$ followed by addition of the MN_2S_2.[233] Figure 2-31 shows an overlay of complex **3** as a

monodentate metalloligand to $W(CO)_5$ (complex **131**)[232] and the analogous PPh_3 derivative[234] that demonstrates the similarity in steric encumbrance. Also listed in Figure 2-31 are ν(CO) IR values for the two complexes from which the better donating ability of **3** over PPh_3 can be inferred.

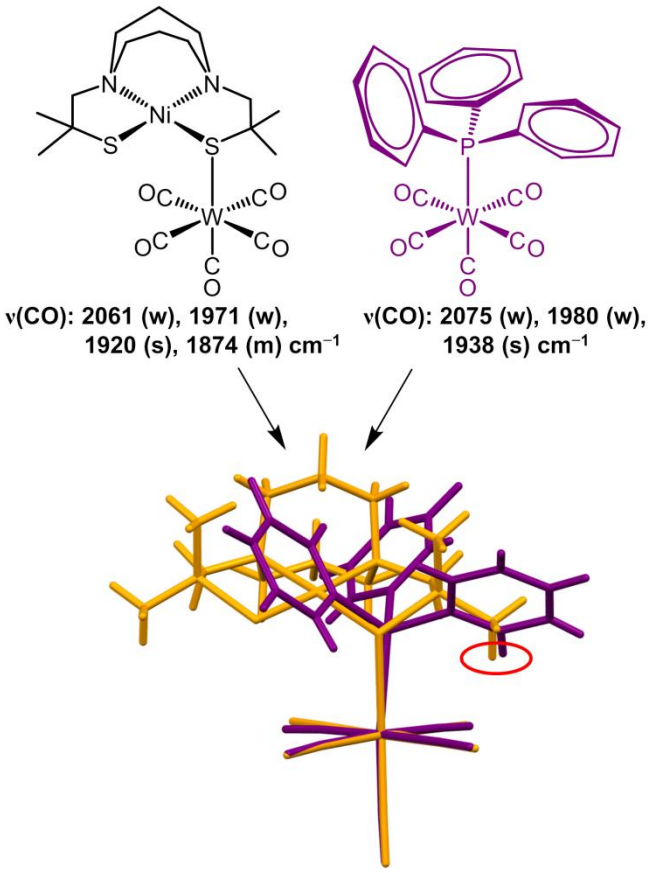

Figure 2-31. Overlay of molecular structures of PPh_3 and **3** as monodentate ligands showing similar steric requirements (red circle) to $W(CO)_5$; ν(CO) IR data recorded in DMF.

Another example of a $W(CO)_5$ derivative of NiN_2S_2 in Figure 2-30 is complex **132** which has two $W(CO)_5$ units bound to complex **2** in a transoid arrangement. We conclude that, in the absence of the steric hindrance from the gem−dimethyl groups that are on the complex **3** metalloligand, the nucleophilicity of the second thiolate is retained for a double adduct formation.[233] Even the sulfinyl derivative of Ni(bme−daco), Figure 2-32, shows reactivity at the available thiolate. The ν(CO) values indicate the S−oxygenated or $NiN_2S(SO_2)$ complex is a slightly weaker donor (ν(CO) IR: 2066 (w), 1977 (w), 1924 (s), 1876 (m) cm^{-1}) as compared to the NiN_2S_2 complex.[233]

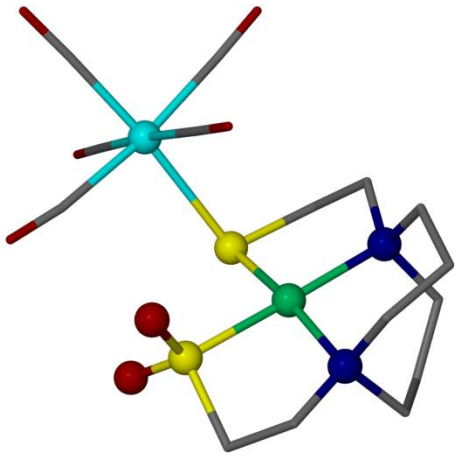

Figure 2-32. Molecular structure of Ni(mese−daco)$W(CO)_5$ with one thiolate and one sulfinyl.[233]

Complex **133** of Figure 2-30 is derived from $[Cd(bme−dach)]_x$ shown earlier as it is in the solid state, a coordination polymer, complex **50**, Figure 2-13.[167] In the presence of $(THF)W(CO)_5$ in THF/DCM solution, complex **50** deaggregates to a dimer, whose

core structure is similar to the $[MN_2S_2]_2$ dimeric complexes of Fe, Co, and Zn. Two $W(CO)_5$ moieties are bound to the free thiolates on each CdN_2S_2 in **133**, while the second thiolates on each are engaged in the dimeric $Cd_2(\mu-S)_2$ core.

2.3.2 Other Metal Carbonyl Containing MN_2S_2 Complexes

Additional metal carbonyl adducts of NiN_2S_2 are found in Figure 2-33 along with two examples, **142** and **143**, of $[FeN_2S_2]_2$ as metallodithiolate ligands. Trigonal bipyramidal complexes of $LFe(CO)_4$ are formed with Ni(bme−daco) and Ni(bme−dach) serving as monodentate S−donor ligands to iron, **134** and **135**.[235-236] As expected, given their lack of π−backbonding ability, the NiN_2S_2 occupy the axial position of the trigonal bipyramid. The Ni−S−Fe angles in complexes **134** and **135** are 113.4° and 115.3°, respectively, and Ni−Fe distances are 3.762 Å and 3.791 Å, respectively.

Oxidation of complex **134** results in a low yield of **136** with rearrangement of the dithiolate to bidentate binding and the assembly of two Ni(bme−daco) metalloligands about $[Fe(CO)_2]^{2+}$; the average Ni−Fe distance is 3.094 Å.[235] A simple combination of the NiN_2S_2 with $Fe_2(CO)_9$ yields monodentate, monoiron products **134** and **135** with the rigid diazacycle derivatives; the more flexible open chain nickel precursor creates the trimetallic product, **137**, in which the NiN_2S_2 serves as a bidentate bridge between two $Fe(CO)_3$ units, but with a significant distortion from square planar to T_d (T_d twist of ~85°).[237] Short Ni−Fe distances, avg. 2.510 Å, are within M−M bonding possibility.

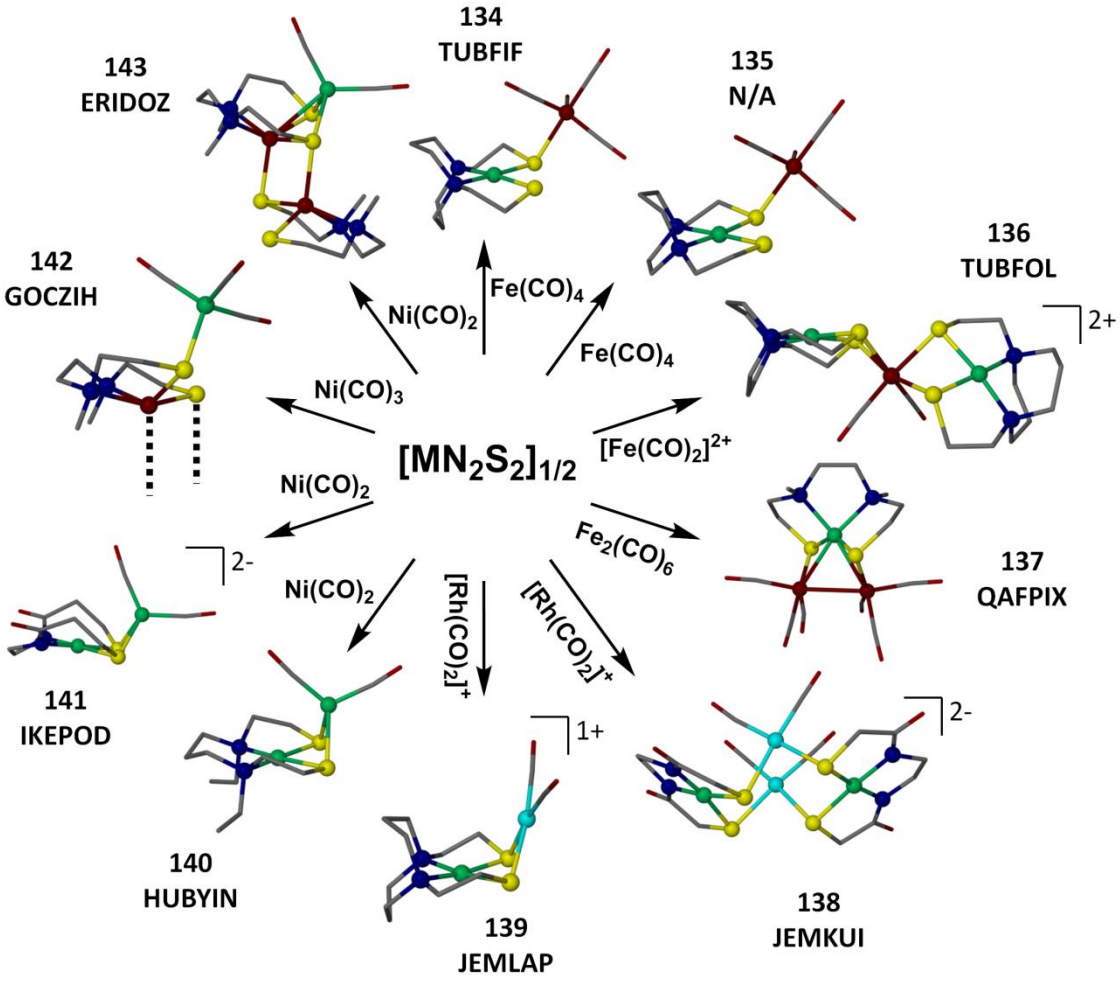

Figure 2-33. Various $MN_2S_2M'(CO)_x$ examples shown by complexes **134**−**143**. M' equals Fe^0 in **134**−**135** and **137**, Fe^{2+} in **136**, Rh^+ in **138**−**139**, and Ni^0 in **140**−**143**. The structure of complex **135** has not been published.

The rhodium dicarbonyl chloride dimer, $(\mu\text{−}Cl)_2[Rh(CO)_2]_2$ is the precursor to complexes **138** and **139**.[238] In **138**, two dianionic $Ni(ema)^{2-}$ are bridging bidentate ligands that permit square planar $RhS_2(CO)_2$ coordination with the square planes of the rhodium units roughly parallel and eclipsed. The Rh−Rh distance in **138** is 3.211 Å; for

each nickel there is one short and one long Ni−Rh distance which average to 3.292 and 3.539 Å, respectively. The Ni/Rh bimetallic, complex **139**, finds two square planes with a dihedral angle 112° and a Ni−Rh distance of 2.871 Å. The S−Ni−S angle is 84.64° in **139** and diminishes in **140** to 82.45°, despite the fact that the bidentate nature of the NiN_2S_2 metalloligand is used in a tetrahedral coordination complex to $Ni(CO)_2$ in **140** vs. square planar in **139**. The Ni−S−Ni angle of **140** is 71.2°, bringing the two nickel atoms to 2.660 Å, arguably within bonding distance. A $Ni^0 \rightarrow Ni^{2+}$ Lewis acid/base interaction is an attractive description of this molecule.[239]

Complex **141** is derived from an analogue of $Ni(ema)^{2-}$, the $Ni(pma)^{2-}$ metallodithiolate ligand, complexes **23/24** found in Figure 2-9.[147] When bound to $Ni(CO)_2$, a very similar bimetallic geometry to that found for neutral **140** is obtained, now with a Ni−Ni distance of 2.835 Å. In **142**, the $Ni(CO)_3$ fragment binds to $[FeN_2S_2]_2$ with retention of the dimeric structure of the iron metalloligands, making use of the available thiolate sulfur on the two FeN_2S_2 units of the dimer.[240] By comparing the Tolman electronic parameter of complex **142** to analogous phosphine complexes, the FeN_2S_2 metalloligand is found to be the stronger donor. Complex **142** was obtained from an unplanned metal exchange between $HFe(CO)_4^-$ and the appropriate NiN_2S_2.[240] Another product of Ni/Fe "reshuffling" led to the final complex of this series, **143**, which is also based on dimeric $[FeN_2S_2]_2$.[241] In this case a $Ni^0(CO)_2$ binds to only one FeN_2S_2 unit, via both the terminal and bridging thiolate sulfurs, analogous to complexes **140** and **141**. The Ni−Fe distances in **143** are 2.851 ($Ni-Fe_{proximal}$) and 3.095 ($Ni-Fe_{distal}$) Å.

2.3.3 $MN_2S_2Fe(NO)_2$

The dinitrosyl iron unit presents a unique opportunity to explore MN_2S_2 complexes as metalloligands. It may be isolated in two redox levels $\{Fe(NO)_2\}^9$ and $\{Fe(NO)_2\}^{10}$; i.e. oxidized and reduced, respectively. As described above for the mononitrosyl iron and cobalt compounds, the even greater complexities of oxidation state assignment of the dinitrosyl iron complexes (DNIC's) are addressed by the Enemark−Feltham notation. Although the electron density of the $Fe(NO)_2$ unit is highly delocalized, spectroscopic/computational interpretations suggest the oxidized, S = ½, $\{Fe(NO)_2\}^9$ unit has large contributions of Fe^{2+}, NO^-, and NO• as well as Fe^{3+} and $2NO^-$ resonance forms, while the reduced form is mainly Fe^{2+} and 2 NO^-, spin paired to render the unit diamagnetic.[242-243] Hence stabilization of the former by good anionic and neutral donor ligands is expected, and found, while the paradigm (and usual synthon) for the reduced form is $Fe(NO)_2(CO)_2$. Both redox levels are found in the $MN_2S_2Fe(NO)_2$ derivatives; in fact the $Fe(NO)N_2S_2$ metalloligand, **51**, serves as an uncommon example of a bidentate ligand to both oxidized and reduced forms of $Fe(NO)_2$, complexes **145** and **146**, respectively, Figure 2-34.[244-245] An open chain $Fe(NO)N_2S_2$, metalloligand **66**, is known to form the cationic complex **144**,[246] analogous to **145**. By the E−F notation, the neutral $Fe(NO)N_2S_2$ contains $\{Fe(NO)\}^7$ while the analogous cobalt metalloligand is $\{Co(NO)\}^8$. The hinge angle that is analogous to the $MN_2S_2W(CO)_4$ complexes of section 2.3.1, is defined in the $Fe(NO)_2$ complexes as the dihedral angle between the N_2S_2 best plane and the S_2Fe plane. Trends in the values are consistent with those in the tungsten analogues, and in general, ~5° smaller, presumably due to the decreased steric

impedance of the acceptor unit. Complex **149** has a hinge angle that is 11° smaller than its tungsten analogue.

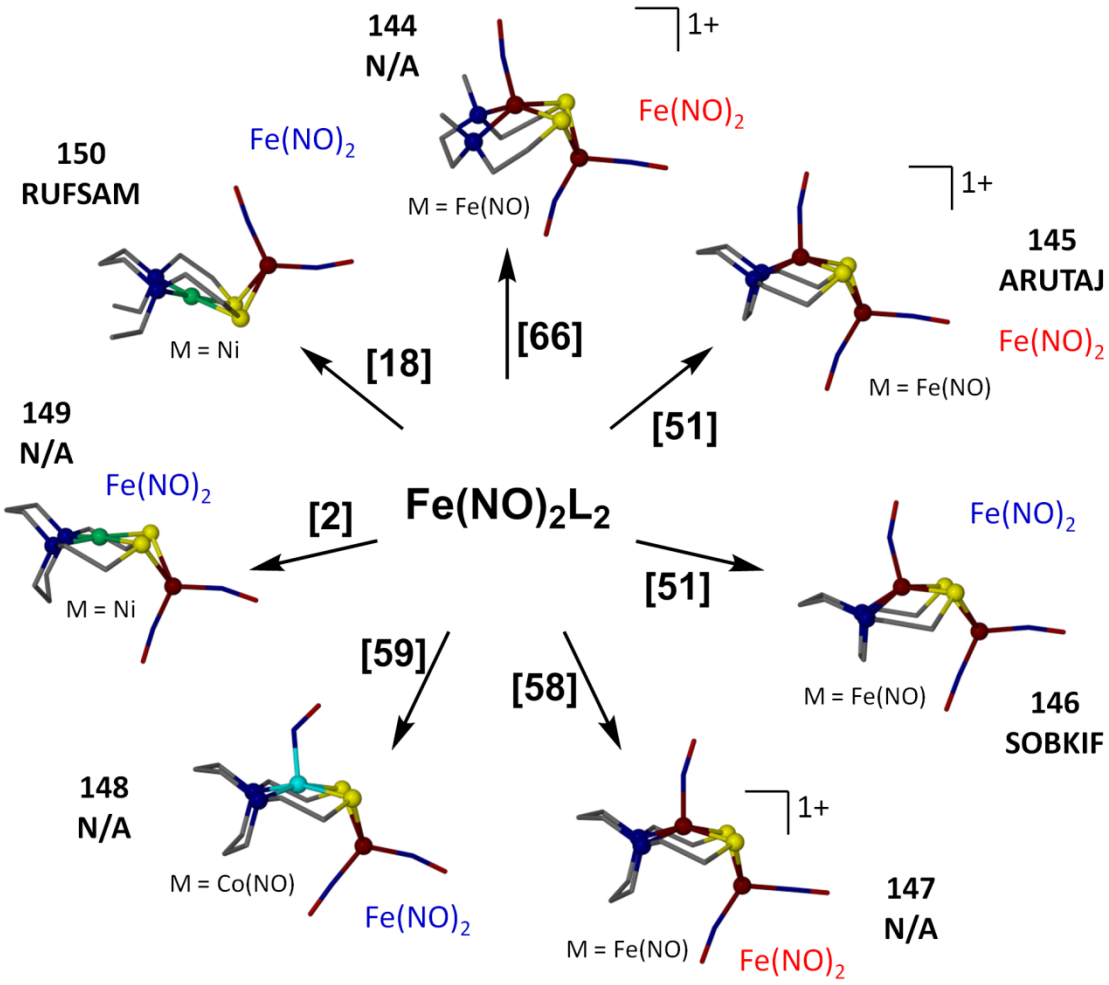

Figure 2-34. $Fe(NO)_2$ adducts of MN_2S_2 complexes, **144**−**150**. Bracketed numbers on the arrows represent the monomeric metalloligands described earlier. Represented by the red color are $Fe(NO)_2$ units in the oxidized form, $\{Fe(NO)_2\}^9$; by blue, the $\{Fe(NO)_2\}^{10}$ in the reduced form. Complexes **144** and **147**−**149** have not been published.

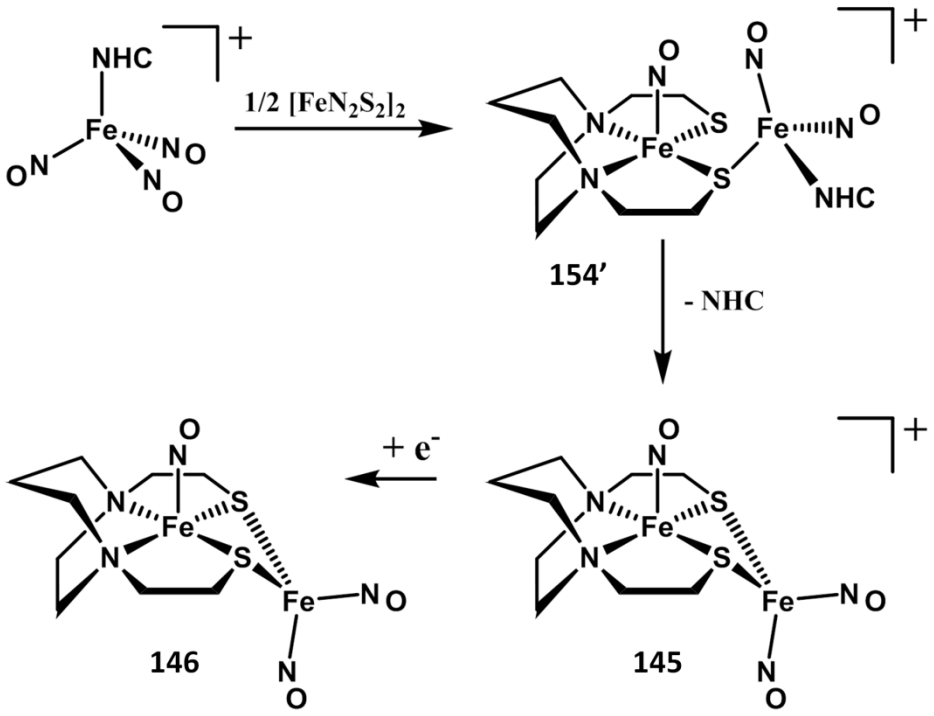

Figure 2-35. Synthetic scheme showing the stepwise reaction of $[FeN_2S_2]_2$ with a TNIC, $(IMes)Fe(NO)_3$, to form complex **145** and the subsequent reduction to **146**.[244-245] The **154'** designates the analogue to **154** of Figure 2-36.

Other examples of MN_2S_2 serving as bidentate ligands to $Fe(NO)_2$ are complexes **147**, **148**, and **149**.[247-249] These use the bis−mercaptoethane diazacyclooctane binding site for $Fe(NO)^{2+}$, $Co(NO)^{2+}$, and Ni^{2+} in the formation of M−Fe heterobimetallics. An interesting feature is that the more stable $Fe(NO)_2$ redox level is $\{Fe(NO)_2\}^{10}$ for M = Ni^{2+} and $Co(NO)^{2+}$, while the oxidized form, $\{Fe(NO)_2\}^9$, is of greater stability for M = $Fe(NO)^{2+}$. Spin pairing renders the $\{Fe(NO)\}^7$−$\{Fe(NO)_2\}^9$ bimetallic to be diamagnetic, while the one−electron reduced form, has been characterized as

paramagnetic $\{Fe(NO)\}^7$−$\{Fe(NO)_2\}^{10}$. At this point an oxidized version of the Co−Fe derivative, **148**, has not been fully characterized.

The NiN_2S_2−$\{Fe(NO)_2\}^{10}$ complex **149** was prepared as an analogue to the open chain NiN_2S_2 complex, **150**. The latter was originally targeted by Osterloh, Pohl, *et al.* as a [NiFe]−hydrogenase active site biomimetic.[250] There are notable differences in the metric parameters of **149** vs. **150**; in particular the Ni−Fe distance is 0.2 Å longer in **149**, thus implicating a role for the central methylene unit in the NiN_2C_3 6-membered ring. To our knowledge, no hydrogenase−like functional properties of **150** and **149** have been established; however, the diiron complexes **145** and **146** are known to engage in electrochemical, H_2 evolution activity.[244-245]

As established in the $W(CO)_4$ derivatives, hemi−lability is also implicated in the synthetic and structural studies of reaction intermediates of the $Fe(NO)_2$ complexes. For example, complex **154** was isolated in the $\{Fe(NO)_2\}^9$ form en route to complex **147** via the synthetic scheme shown in Figure 2-35. Complex **154** suggests a similarity in binding ability of the N−heterocyclic carbene and the $Fe(NO)N_2S_2$ monodentate metalloligand, Figure 2-36.[251]

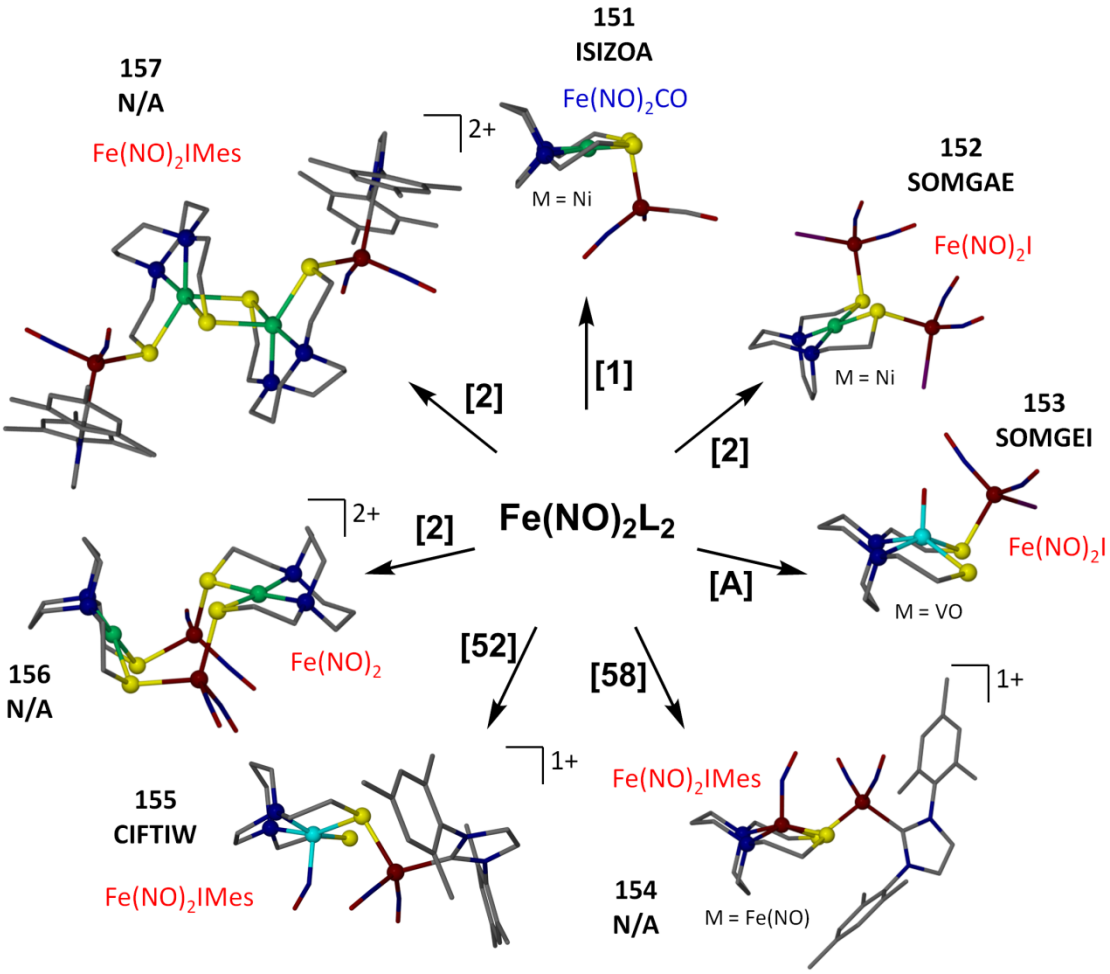

Figure 2-36. Complexes **151**−**157** are further examples of MN_2S_2 compounds that serve as monodentate metalloligands to DNICs. Bracketed numbers on the arrows represent the monomeric metalloligands described earlier. Represented by the red color are $Fe(NO)_2$ units in the oxidized form, $\{Fe(NO)_2\}^9$; blue is the reduced form, $\{Fe(NO)_2\}^{10}$. The structures of complexes **154**, **156** and **157** have not been published. [A] represents the (V≡O)(bme−daco) metalloligand.[225]

Monodentate MN_2S_2 metalloligands to the $Fe(NO)_2$ unit are seen in **151**−**153**, Figure 2-36. The CO adduct of **151** represents conversion of the Ni(bme−dach) analogue of **149** from bi− to monodentate on the $\{Fe(NO)_2\}^{10}$ reduced species.[252] The better acceptor ability of $\{Fe(NO)_2\}^9$ permits two $Fe(NO)_2I$ units to bind to Ni(bme−daco) in a transoid fashion, **152**.[228] Only one $Fe(NO)_2I$ unit is found to bind to the poorer donor, (V≡O)(bme−daco), **153**.[228] Thus, the $Fe(NO)_2$ system connected to MN_2S_2 metalloligands provide examples of electronic control exercised by both the donor and acceptor units.

Complex **155** is analogous to **154** and obtained by the same synthetic approach, substituting $[Co(bme-dach)]_2$ instead of the $[FeN_2S_2]_2$ used for **154**.[253] Complexes **156** and **157** represent an oxidized DNIC bound to complex **2** and result from different oxidized $Fe(NO)_2$ starting materials: $Fe(CO)_2(NO)_2^+$ for **156** and a TNIC,[244] $(IMes)Fe(NO)_3^+$, for **157**.[249] Complex **157** is a rare example of a pentacoordinate Ni^{2+}, seriously distorted towards TBP, $\tau = 0.31$.

As shown in Table A2, the ν(NO) stretches from the $Fe(NO)_2$ units indicate that the donating ability of MN_2S_2 metalloligands may be ranked as was done for the $W(CO)_4$ reporter. Consistently, the best donors are the NiN_2S_2 complexes followed closely by the $Co(NO)N_2S_2$ and $Fe(NO)N_2S_2$ complexes. For the same metalloligand, the DNIC unit shows approximately a 100 cm^{-1} wavenumber difference between the reduced and oxidized forms. By this approach, the order of ligand donating abilities within each redox level is MN_2S_2 ~ NHC > PPh_3; however, further analysis of the data is hampered by inconsistencies in the media used for recording the spectra.

2.3.4 $MN_2S_2M'L$

There are approximately 80 complexes of the structural type $MN_2S_2M'L$ analogous to Darensbourg's complex in Figure 2-3 or Ogo's complex in Figure 2-4. These complexes will be discussed in detail in a separate review.

2.4 Trimetallic Systems

2.4.1 Stair−step or $[MN_2S_2]_2M'$ Complexes

The group of trinickel structures shown in Figure 2-37 relate to the original paradigm for the ligating ability of cis−dithiolates in NiN_2S_2 square planar complexes; i.e. the Busch/Jicha complex shown in Figure 2-1, and again as complex **163** in Figures 2-37 and 2-38.[111] This structural family in the so−called "stair−step" configuration consists of three square planes, two NiN_2S_2 and one $Ni'S_4$, intersecting with dihedral angles ranging from 101° to 146°, resulting in Ni−Ni' distances of 2.67 to 3.15 Å. The reaction wheel shown in Figure 2-38 places the monomeric metalloligand building block, described in earlier sections, over the arrow originating at the nickel ion at the center. Note that the stair−step angles of complexes containing metalloligands common to those in the $W(CO)_4$ examples, **160**/**161** (comparable to **124**),[254-255] **162** (comparable to **125**),[256-257] and **169** (comparable to **126**) are within 5° of the hinge angles earlier defined for the tungsten bimetallics.

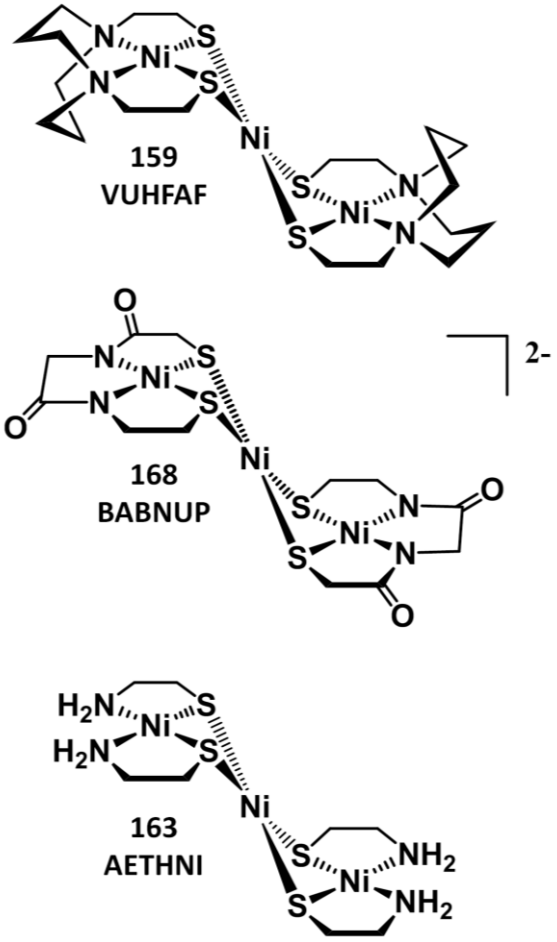

Figure 2-37. ChemDraw representation of complexes **159**, **168**, and **163** from Figure 2-38.

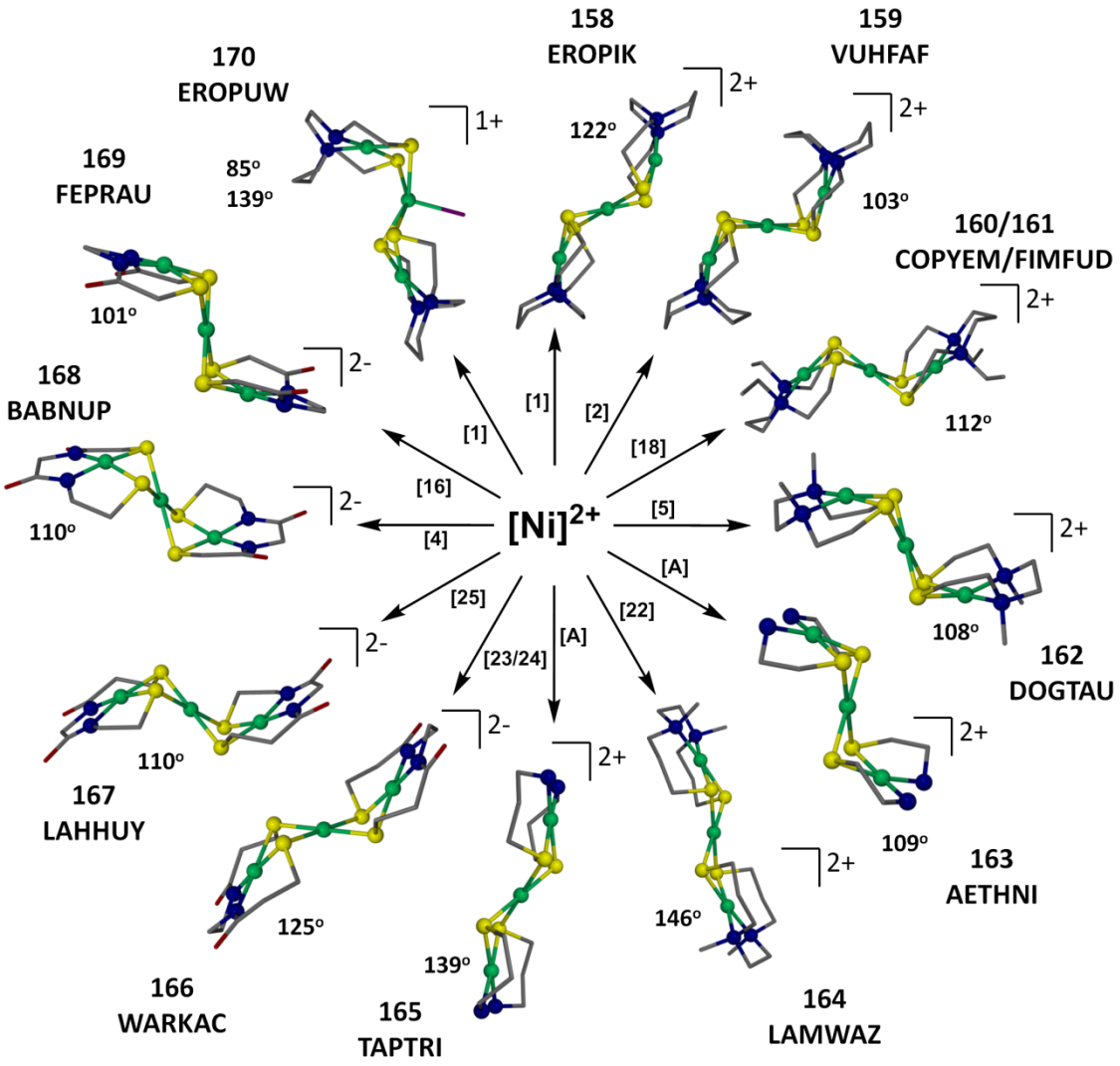

Figure 2-38. Complexes **158–170** are the tri–nickel "stair–step" family of N_2S_2 compounds. Numbers in brackets by each arrow refer to the monomeric NiN_2S_2 structures found in Figures 2-7 and 2-9. The stoichiometry of the reaction is two NiN_2S_2 to one aggregating metal. The angles listed refer to the dihedral angle between the best N_2S_2 and S_4 planes. The free $Ni(NS)_2$ complexes that form **163** and **165** are found only as the trans–isomer and represented as [A].

In contrast to the open chain NiN_2S_2 complexes **5**, **16**, and **18**, those with Ni(bme−dach) and Ni(bme−daco) metalloligands in the stair−step complexes, **158** and **159**, respectively, have quite different hinge angles from their $W(CO)_4$ counterparts.[106,258] The former, **158**, is about 10° smaller, while that in **159** is 31° smaller, Figure 2-39. Note that the single NiN_2C_3 metallodiazacyclohexane unit in each Ni(bme−dach) metalloligand of complex **158** is in the chair conformation. The Ni(bme−daco) contains both chair and boat NiN_2C_3 metallodiazacycle rings with the boat conformation orienting the central methylene group towards both nickels with a Ni'−C distance of 3.67 Å and a Ni−C distance of 2.80 Å. The former suggests the possibility of a stabilizing C−H anagostic interaction and the latter an agostic interaction that is not possible in the $W(CO)_4$ complex.[259-260]

Complexes **164** and **165** contain 3−carbon linkers between the N and S donors of the NiN_2S_2 metalloligands.[261-262] In **164**, the N donors are connected by a 2−carbon linker as in complex **162**. In **165**, similar to **163**, the nitrogens are not linked and are primary amines. Complexes **164** and **165** have the largest step angles of all in this class, 146° and 139°, respectively. There are no obvious intra− or intermolecular solid state interactions that would account for the large step angles. As all other step angles are within ±10° of the average 109°, we surmise that the torsion angles within the 3−carbon N to S linker direct the sulfur lone pairs differently from the 2−carbon N to S linker.

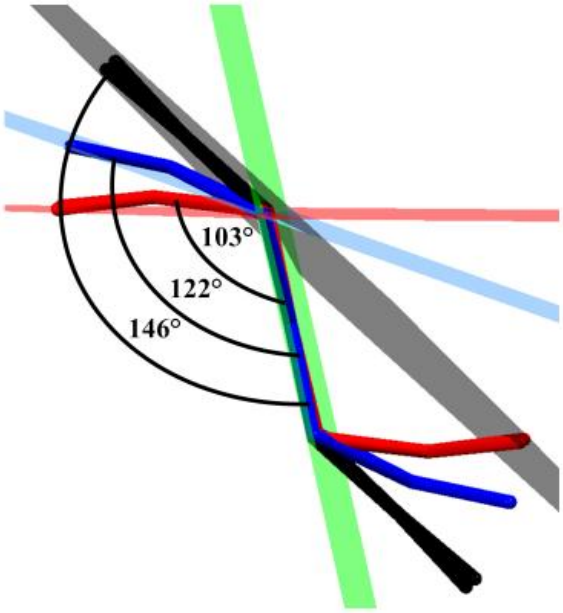

Figure 2-39. Overlay of planes derived from complexes **158** (blue), **159** (red), and **164** (black) showing the range of hinge (or step) angles (122°, 103°, and 146° respectively) observed for the $[NiN_2S_2]_2Ni^{2+}$ stair−step complexes. As viewed from a side profile with the NiS_4 plane (green) vertical.

Complexes **166−169** are dianionic as a result of deprotonated amido nitrogens as well as the cis−dithiolates within the metalloligands that were described in Figures 2-7 and 2-9.[121,137,141,263] A consequence of the negative charge is a shorter Ni−N bond as compared to the dicationic stair−step complexes, while the Ni−S and Ni'−S distances are largely the same.

Complex **170**, in which the Ni' is pentacoordinate, was prepared by reaction of **1** with $NiCl_2$ rather than the $NiBr_2$ source that was used in the synthesis of complex **158**. The penta−coordination of the central nickel, Ni', in **170** is unusual and is not likely to

persist in solution.[258] The positioning of the Ni' out of the S_4 plane (0.520 Å) results in longer Ni'−S distances and a loss of the inversion center that is in **158**.

Figure 2-40 displays products of first row transition metal−N_2S_2 complexes that serve as metallodithiolate ligands to palladium (II) and platinum (II). Complex **171** is analogous to **159** of Figure 2-38.[264] The metric parameters within the NiN_2S_2 are largely the same and the Pd−S distances are, as expected for the second row metal, ca. 0.15 Å larger than the Ni'−S distances found in the previously described Ni−trimetallic stair−step complexes of Figure 2-38.

The open chain NiN_2S_2 metalloligand in **173** generates a 5−6−5 ring pattern and has an almost identical structure to that of **171**.[265] In contrast, in complex **172** the Ni(bme−dach), metalloligand **1**, crystallizes as a unique structural form that is described as a basket in which the bottom is the square planar PdS_4 and the sides are the NiN_2S_2, with the 2−carbon N to N links facing towards each other, giving the illusion of handles.[258]

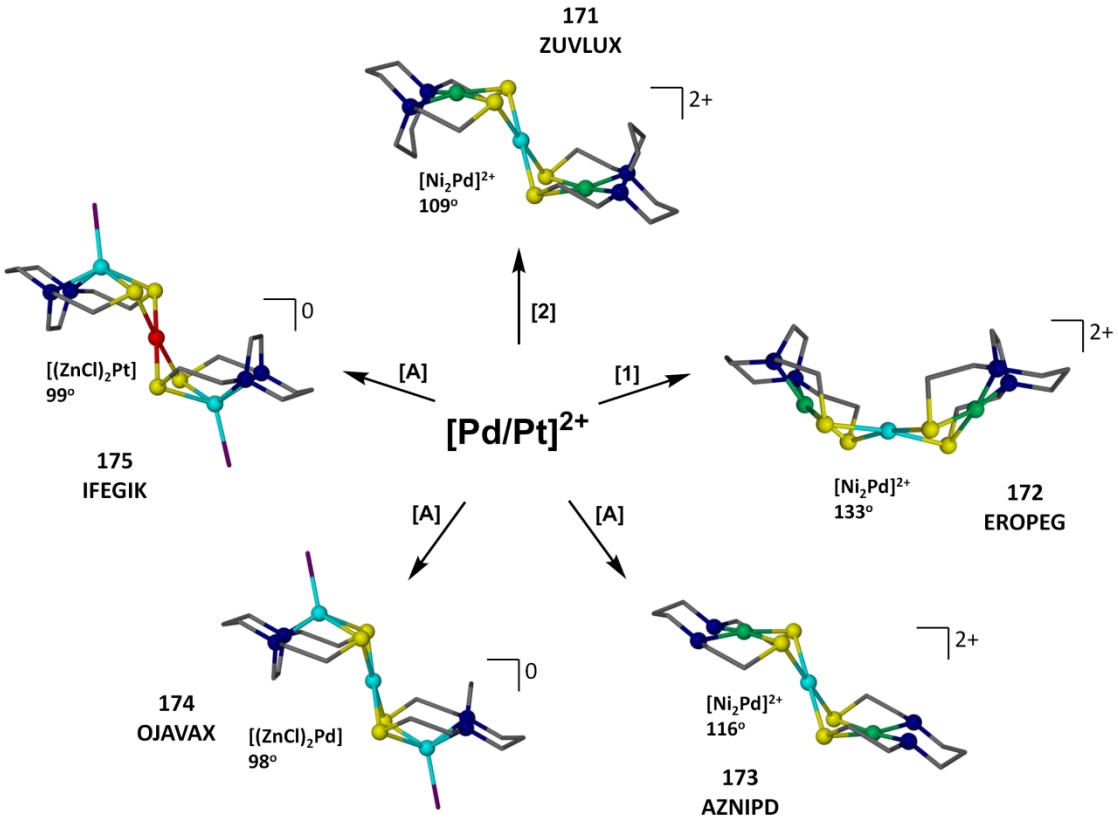

Figure 2-40. Complexes **171−175** are the Pd and Pt tri−metallic "stair−step" structures, with NiN_2S_2 metalloligands in **171−173**, and $[Zn(Cl)N_2S_2]^-$ metalloligands for **174** and **175**. The dihedral angles between the best N_2S_2 and S_4 planes are listed. The monomeric NiN_2S_2 and $Zn(Cl)N_2S_2$ metalloligands, which are contained in **173** and **174/175**, respectively, are represented by [A] and have not been crystallized.

The remaining two structures of Figure 2-40, **174** and **175**, utilize $ZnCl^+$ within the N_2S_2 binding site, generating a pentacoordinate Zn^{2+} displaced by 0.871 Å out of the N_2S_2 planes, and an overall anionic $Zn(Cl)N_2S_2$ metalloligand.[161-162] Similar complexes with the stair−step structure arising from Pd^{2+} and Pt^{2+} binding were cited as evidence

for the potential of S−rich zinc fingers to aggregate with platinum (II) in tertiary adducts of DNA−Pt−zinc finger proteins, potentially relating to Cisplatin© resistance or DNA repair mechanisms.[162,266]

2.4.2 Other Trimetallic Complexes

The trimetallic complexes shown in Figure 2-41 are based on four different NiN_2S_2 metalloligands. With the dianionic metalloligand **25**, a copper (II) aggregate generates complex **176**, of stair−step configuration analogous to those of Figure 2-38, with a step−angle of 109°.[121] It is interesting that the Ni_2Cu complex of **176**, composed of a dianionic NiN_2S_2 ligand and Cu^{2+}, is a discrete trimetallic stair-step, as it contrasts to the neutral NiN_2S_2 metalloligands and Cu^{2+} synthons. The latter form penta− or hexa−nuclear clusters resulting from reduction of Cu^{2+} to Cu^{+} with concomitant formation of disulfides (*vide infra*).

The $[Ni_2Ag]^{3-}$ structure **177,** derived from metalloligand **16**, shows a linear S−Ag−S arrangement with the two NiN_2S_2 planes roughly parallel to each other.[121] Complex **177** is unusual in that C_3 paddlewheels comprised of $[Ni(N_2S_2)]_3Ag_2$ typically assemble on mixing of similar components, see Section 2.6.1.

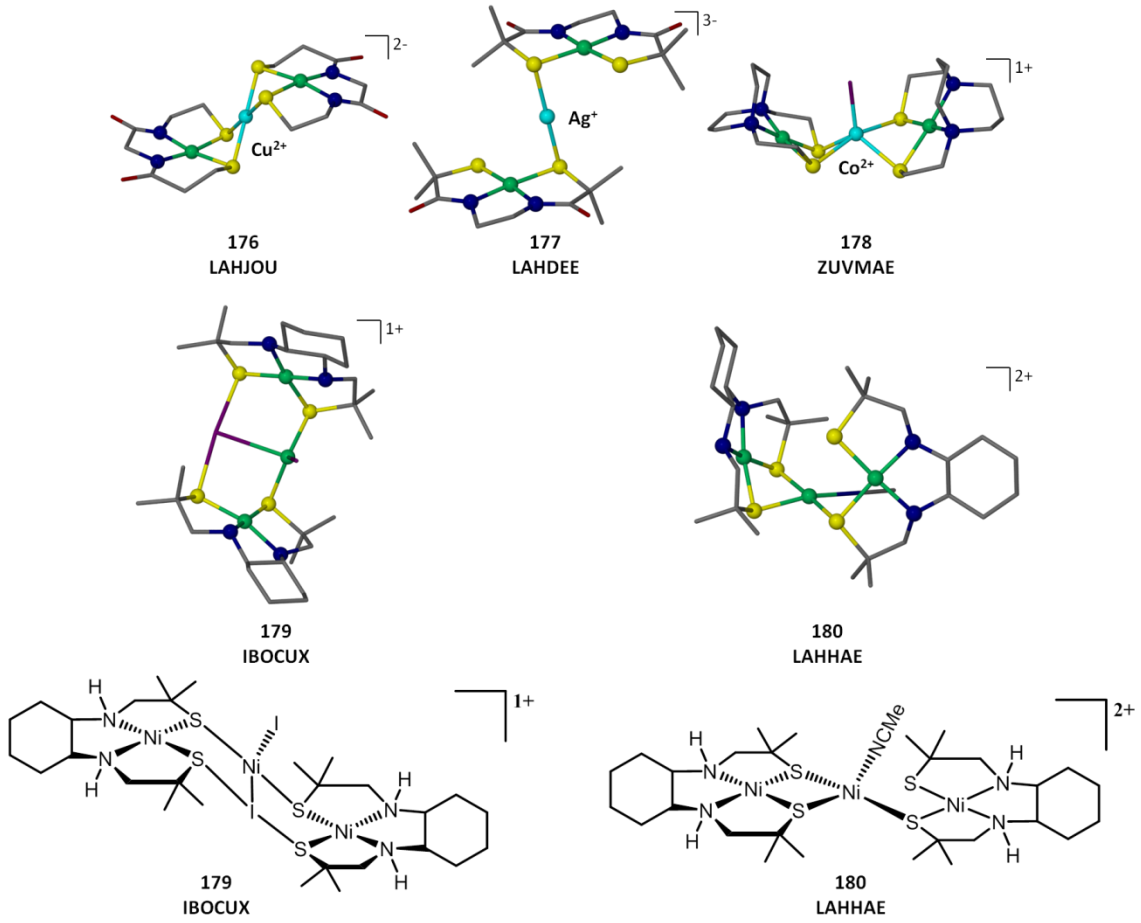

Figure 2-41. Other examples of trimetallic NiN_2S_2 metalloligands flanking the central metal are shown in complexes **176**–**180**. The central metal coordination sphere is completed by Cl^- in **178**, by a terminal I^- and a μ_3–I^+ ligand in **179**, and by MeCN in **180**. The last two are also shown as ChemDraw structures.

Complex **178** has a pentacoordinate cobalt, CoS_4Cl, at the center, in which the sulfur donors of the two NiN_2S_2 metalloligands each occupy an axial and equatorial site of the distorted TBP (τ value of 0.69) coordination geometry about Co^{2+}.[264] The NiN_2S_2 metric parameters are largely the same as those of the free metallodithiolate ligand,

differing only in a shrinking of the S−Ni−S angle (86°) to accommodate the 4−membered CoS_2Ni chelate ring.

Complex **179** of Figure 2-41 results from the reaction of the NiN_2S_2 complex, **8**, with I_2. Formally the complex can be described as two neutral $Ni^{II}N_2S_2$ metalloligands bridging a $[NiI_2]^+$ unit. The authors interpreted this unusual unit as consisting of a Ni^+, a bridging iodonium ion (I^+), and a terminal iodide (I^-).[267] Complex **180** is analogous to the stair−step complexes of Figure 2-38, but one of the NiN_2S_2 units is now monodentate with the fourth position of the central nickel occupied by an acetonitrile molecule, thus highlighting the hemi−lability, or ring−opening possibility, of the MN_2S_2 metalloligands.[121]

2.5 Tetrametallic Systems

2.5.1 Pinwheel Complexes and non−C_2 Propellers

While complex **181** in Figure 2-42 is not of the pinwheel geometry described below, it is nevertheless a tetrametallic complex and can be viewed as a modification of the stair−step complexes described in Figure 2-38. A $[Ni_2S_2]$ butterfly core has been inserted between two NiN_2S_2 metalloligands yielding the expanded stair−step complex $[NiN_2S_2]NiS_2Ni[NiN_2S_2]$.[121]

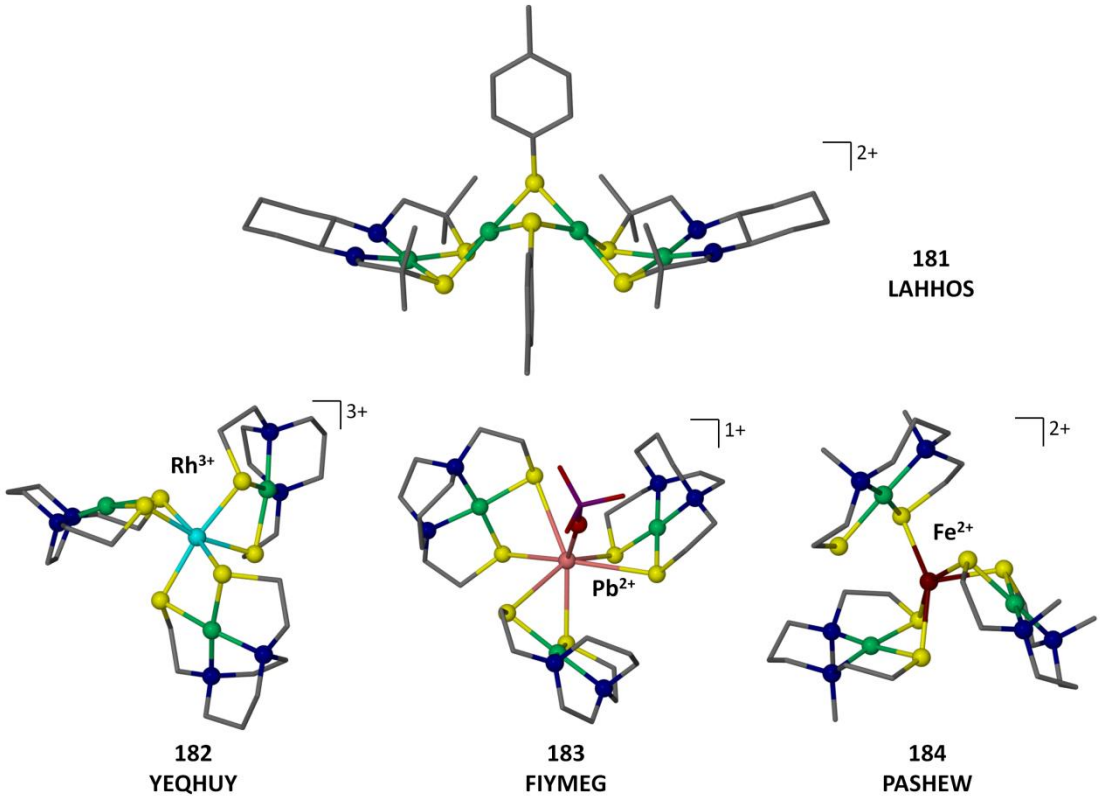

Figure 2-42. Complex **181** is a rare example of a Ni_4S_6 structure which contains 4 square planar nickel centers edge bridged in a zigzag fashion. The pinwheel motif is shown in complexes **182**−**184** with formulas of $[NiN_2S_2]_3M$'.

The ability of the NiN_2S_2 to adapt to higher coordination numbers can be seen in the tetrametallics of Figure 2-42. The octahedral RhS_6, **182**, engages three NiN_2S_2 ligands in a pinwheel geometry. Here the S−Ni−S angle decreases from that in the free metallodithiolate ligand (~95°) to an average of 89.7° in **182**, generating S−Rh−S angles of 79.3° and Rh−Ni distances of 3.13 Å.[268]

Three NiN_2S_2 metalloligands also aggregate about Pb^{2+} (**183**) and Fe^{2+} (**184**). In the latter, one NiN_2S_2 is a monodentate ligand, resulting in penta−coordination for the Fe^{2+}. While the τ value of 0.11 suggests a square pyramidal description of the coordination geometry about iron, the $Fe-S_{unbound}$ and $Fe-S_{bound}$ distances of 3.20 and 2.48 Å, respectively, suggest hemi−labile character and the possibility of a hexacoordinate intermediate or transition state.[269]

The lead derivative, **183**, finds the Pb^{2+} surrounded by six S-donors where three Pb−S distances are > 3 Å and three are ~0.2 Å shorter. Assuming all sulfurs are in coordinate covalent bonding, the overall geometry is a highly distorted octahedron or trigonal antiprism. A large S−Pb−S angle suggests an open site presumably dictated by the steroactive lead lone pair. Interestingly, one of the perchlorate counterions sits above this position, that is opened by the lone pair giving a Pb−O distance of 2.78 Å.[270]

2.5.2 C_2 Propeller (Paddlewheels) or $[MN_2S_2]_2M'_2$ Complexes

Tetrametallic complexes based on NiN_2S_2 which bind gold(I) or copper(I) with C_2 symmetry, Figure 2-43, result in an overall geometric form similar to the stair−step complexes of Figure 2-38. That is, an inversion center exists at the single metal connecting the two MN_2S_2 planes in the latter and between the two metals of the former. The stereochemical preferences of gold(I) and copper(I) dictate linear S−M'−S arrangements leading to Au−Au and Cu−Cu average distances of 3.09 and 2.86 Å, respectively. The Au−Au distances of complexes **185−188** are typical of aurophilic interactions and match almost precisely the S to S distances of the bidentate bridging

NiN_2S_2 metalloligands (average S to S distance of 3.18 Å).[271-272] The smaller Cu−Cu distances of complexes **189** and **190** place the 2Cu unit slightly inside the NiS_2 "bites".[147,273] Note that the ligand charge has no influence on the M'−M' distances.

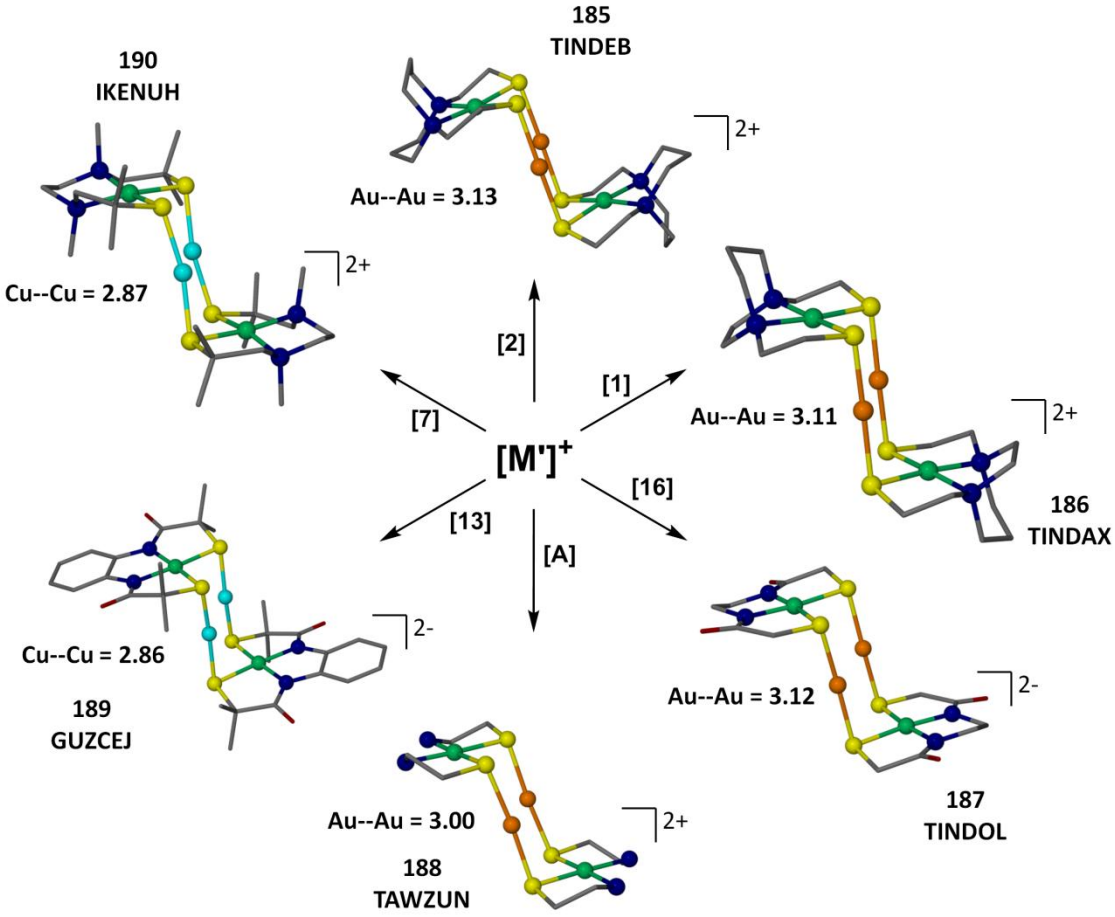

Figure 2-43. Complexes **185−190** of the form $[NiN_2S_2]_2M'_2$ represent regular C_2 paddlewheels with gold(I), **185–188**, and copper(I), **189−190**. [A] The monomeric $Ni(H_2N(CH_2)_2S_2)$ has not been crystallized as the cis−isomer.

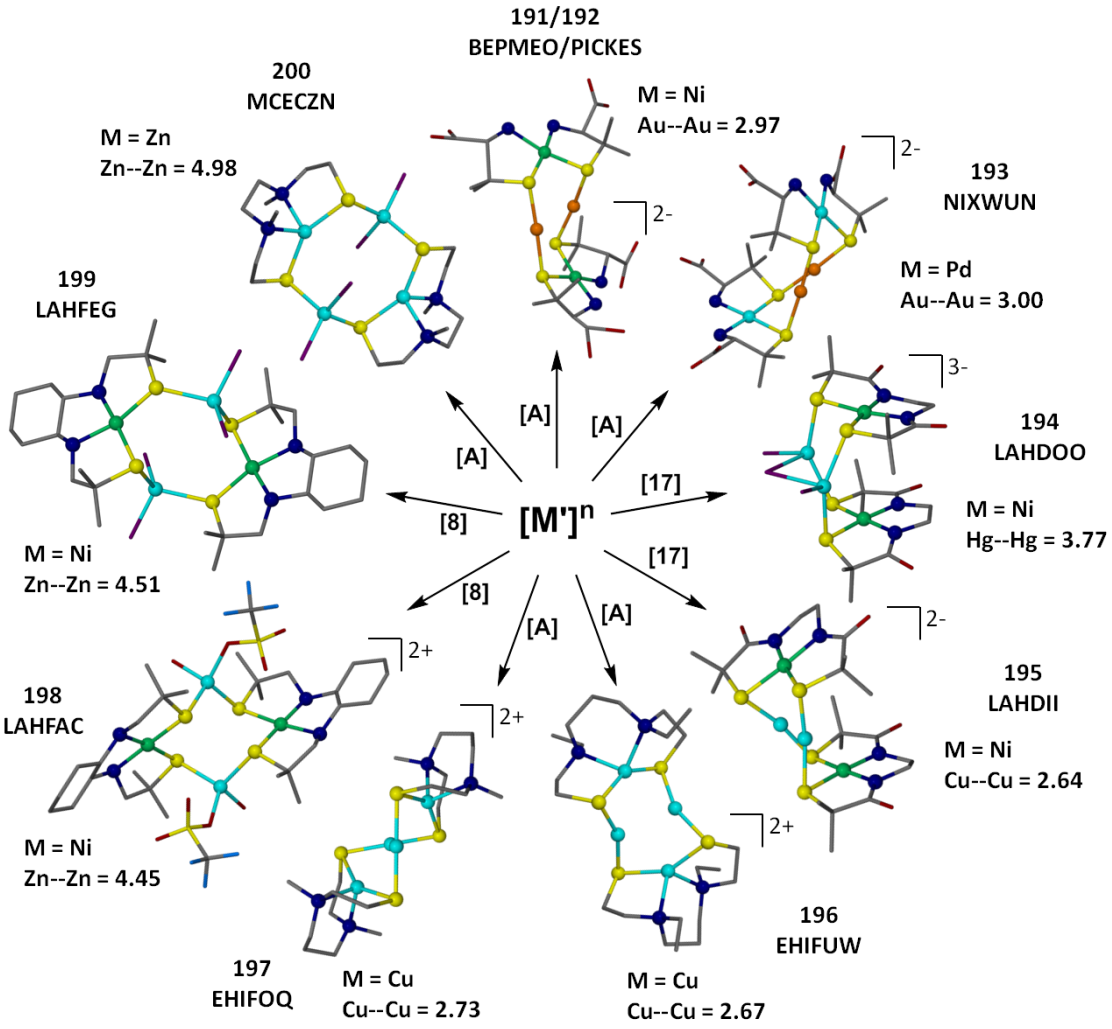

Figure 2-44. Complexes **191−200** of the form $[MN_2S_2]_2M'_2$ represent distorted, irregular C_2 paddlewheels. The symbol [A] over the reaction arrow represents monomeric MN_2S_2 complexes that have not been structurally characterized.

Figure 2-44 displays tetrametallics of various metals that are substantially distorted from the propeller or C_2 paddlewheels of Figure 2-43. A simple rendition of some motifs found in this set of $M_2M'_2$ complexes is given in Figure 2-45. Complexes **191/192** are the same dianion structures found when crystallized with different alkali

metal counterions.[274-275] The N,S ligand *D*−Penicillaminate, (*D*−Hpen), of biological significance, yields interconvertible polynuclear structures derived solely from Ni^{2+} and Au^{+}. Complexes **191/192** have a twist from the C_2 paddlewheel structures likely caused by counterion interactions that generate an extended structural array, a coordination polymer, in the solid state.[274-275]

Complex **193** uses the *D*−Hpen N,S ligand bound to Pd^{2+}.[276] The PdN_2S_2 ligands are now in a pseudo cisoid conformation, in which the ligand planes are on the same side (i.e., this is not a stair−step complex which has a pseudo−transoid ligand arrangement), center of Figure 2-45. This structural motif is more clearly seen in complex **194** where the two NiN_2S_2 ligands are parallel and almost eclipsed providing an S_4 binding environment for the $[Hg_2Cl_3]^{+}$ unit.[121] The larger S to S distance of 3.3 Å accommodates the Hg(μ−Cl)Hg distance of 3.77 Å. At the 4 o'clock position of Figure 2-44, two dianionic metalloligands are found to bind two Cu^{+} in a cisoid fashion in complex **195**.[121]

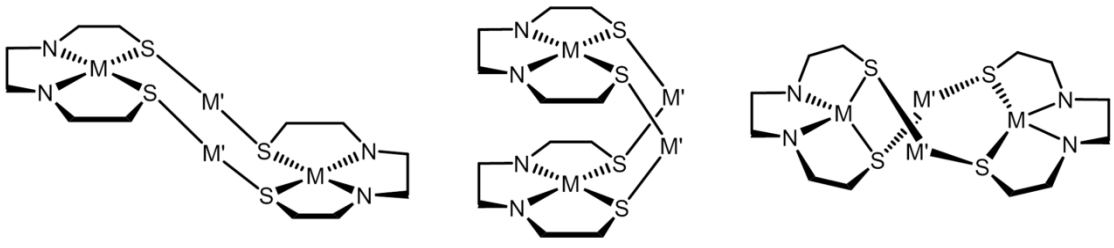

Figure 2-45. Representations of three possible isomers observed in the C_2 propeller structural class. The left structure is analogous to complexes **185−190**; center (**194−195**); and right (**196−197**).

The open chain $-S(CH_2)_2NR(CH_2)_3NR(CH_2)_2S-$ (R = Et, **196**; Me, **197**) ligand bound to Cu^{2+} presents a bidentate, bridging S−donor metalloligand to two Cu^{+} ions, at an average Cu−Cu distance of 2.70 Å and with S−Cu−S angles of ~160°.[277] As a result of the tetrahedral geometry about the Cu^{2+} centers, the complexes are of D_{2d} symmetry, Figure 2-45 (right).

Complexes **198**−**200** represent three irregular C_2 propeller structures that feature zinc as the bridging metal. Complexes **198** and **199** utilize metalloligand **8** and differ in the ligands that complete the tetrahedral zinc coordination environment: triflate/water and chlorides respectively.[121] Complex **200** is formed from two $ZnCl_2$ units bridging between two metalloligands, complex **101** without gem−dimethyl groups, Figure 2-22. Due to the tetrahedral coordination environment about the four zinc ions, complex **200** displays the largest M'−M' distance in this class.[278]

2.6 Larger Multimetallic Systems

2.6.1 C_3 Paddlewheels or $[MN_2S_2]_3M'_2$ Complexes

Stereochemical requirements of trigonal planar or tetrahedral about the two metals (M') that will become the axles of the paddlewheels are essential to the assembly of C_3 paddlewheels. Structures **201**−**206** of Figure 2-46 have Ag^{+} and Cu^{+} as the aggregating metal in trigonal planar arrays.[121,270,273,279-281] The metalloligand "paddles" in **201**, **203**, **204** and **205** are neutral NiN_2S_2. Complex **205** is quite distorted from C_3 symmetry, with roughly a 30° twist along a very short Cu−Cu distance within the axle (2.64 Å).[273] The $Fe(NO)N_2S_2$ units serve as the metalloligand paddles to $Ag^{+}-Ag^{+}$ in

202; the paramagnetism of the $\{Fe(NO)\}^7$ unit leads to an overall S = 3/2 for the Ag_2Fe_3 pentametallic cluster.[279] Complex **206** is a mixture of three Cu^{2+} (within the N_2S_2 paddles) and two Cu^{+} ions bound in trigonal planar sulfur, S_3, arrays as the axle.[281]

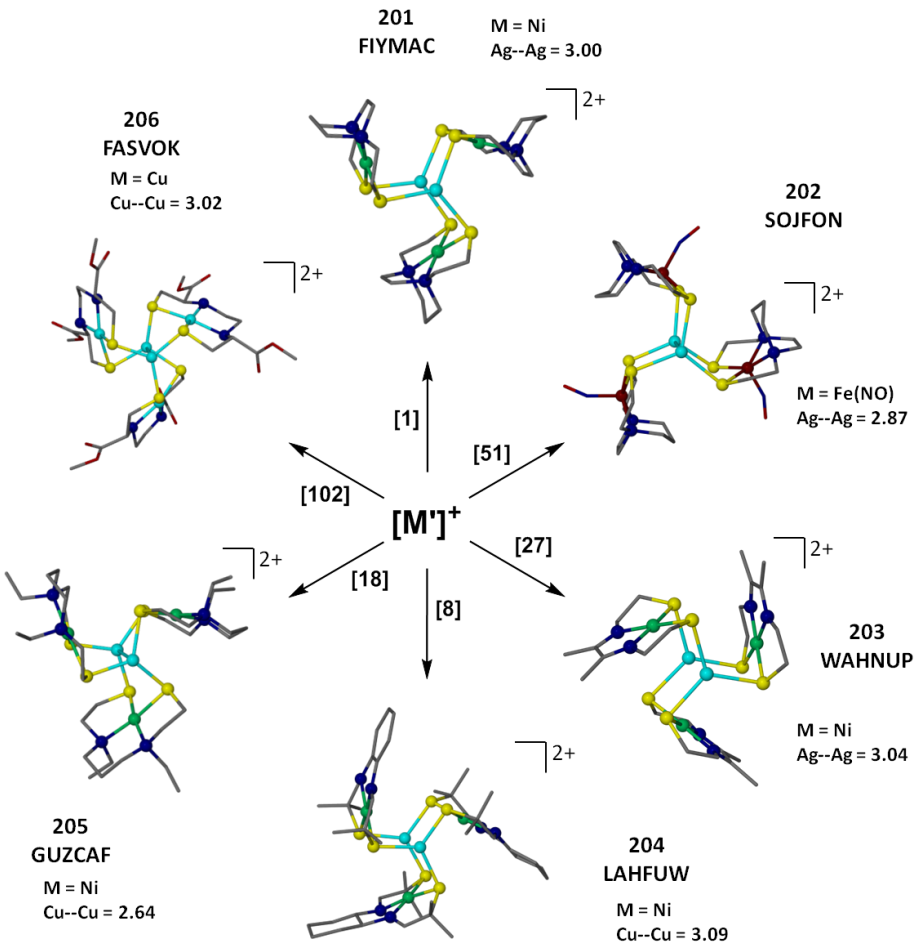

Figure 2-46. Complexes **201**−**206** of the form $[MN_2S_2]_3M'_2$ are of the C_3 paddlewheel structural motif and contain trigonal planar $M'S_3$ units. Numbers in brackets represent the metalloligand used to synthesize the respective complex.

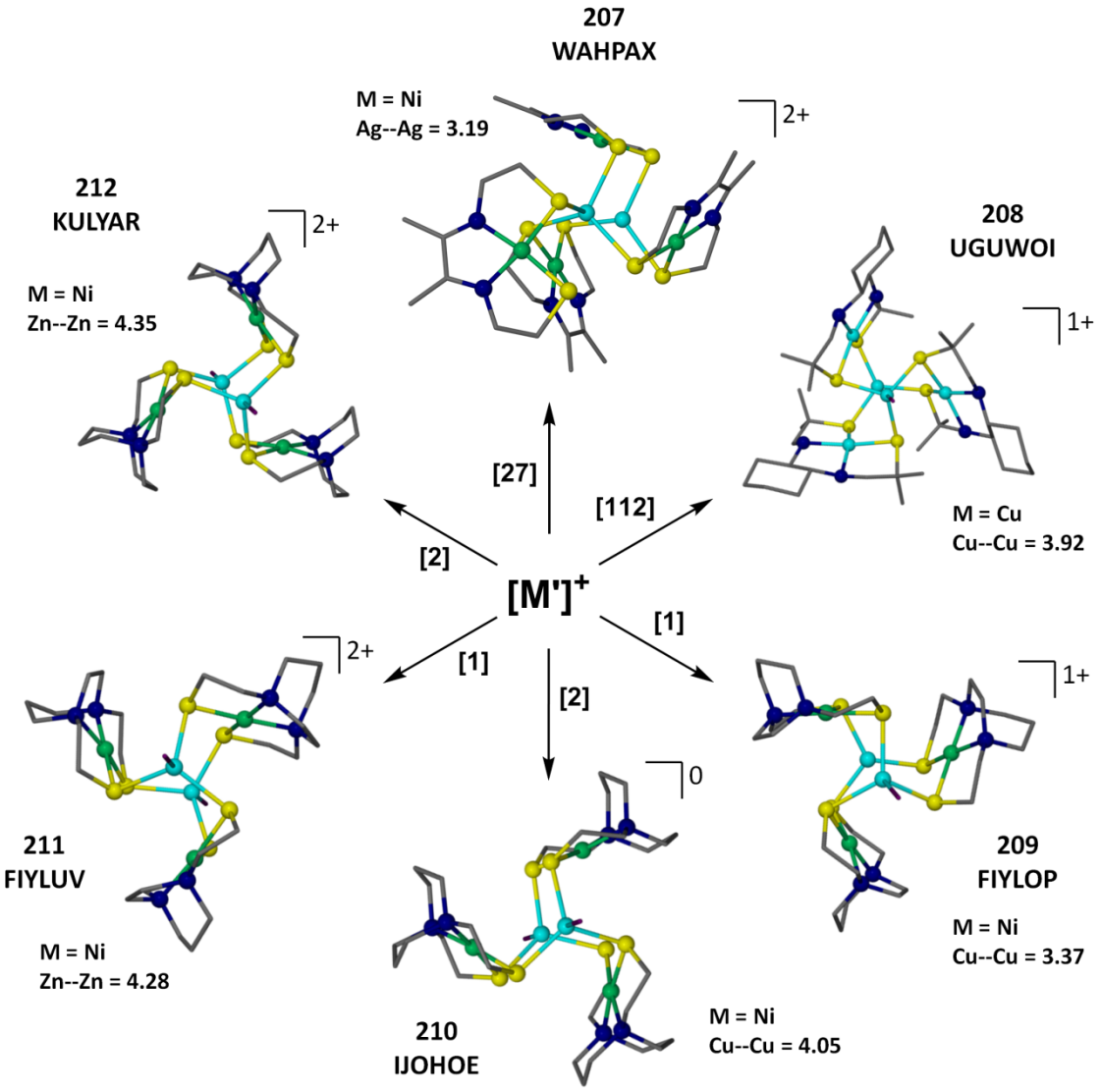

Figure 2-47. Complexes **207−212** of the form $[MN_2S_2]_3[M'X]_2$ are of the C_3 paddlewheel structural motif and contain one or two tetrahedral $S_3M'X$ units. Numbers in brackets by each arrow are the MN_2S_2 metalloligands used to derive the respective complexes.

Complexes **207**−**209** contain one trigonal planar S_3Cu and one tetrahedral S_3CuX site, Figure 2-47. This has the effect of increasing the M^+−M^+ distance from an average of 3.06 Å to 3.19, 3.92 and 3.37 Å for **207**, **208**, and **209**, respectively. Complex **207** is analogous to the silver complexes of Figure 2-46, but one of them is now four−coordinate by means of a fourth NiN_2S_2 metalloligand that serves as a monodentate ligand in the axial position.[280] As a result, **207** has a longer Ag−Ag distance than that found in **201** and **202**. The longer distance in **208** is accompanied by a large trigonal twist of ~50°,[209] whereas in **209** the twist is only ~20°.[270]

The C_3 paddlewheels with S_3MX coordination of the metals within the axles are **210 – 212**, Figure 2-47. Complex **210** is a neutral C_3 paddlewheel with two $[CuBr]^0$ units serving as the axle.[282] The Cu−Cu distance of 4.05 Å and the displacement of Cu out of the S_3 plane of 0.5 Å and away from the second Cu clearly indicate a lack of Cu−Cu dispersive (attractive) interactions. Zinc chlorides with metalloligands **1** and **2** are regular with T_d twists of 26° for **211** and 3° for **212**.[164,270] The Zn−Zn distance is 4.3 Å in both.

2.6.2 C_4 Paddlewheels or $[MN_2S_2]_4M'_2$ Complexes

The C_4 paddlewheel structures are derived from metal ions with square planar geometry preferences and those with M−M bonds. Examples of the latter are **213**−**215** of Figure 2-48; **213** and **214** find the Mo_2^{4+} unit with a formal quadruple bond at a Mo−Mo distance of 2.15 Å, supported by metalloligands **2** and **1**, respectively.[283] The Mo_2^{4+} unit

is well within the S−S bridging−bidentate bite as the S to S distance is 3.0 Å. Complex **215** has a Rh−Rh distance of 2.89 Å and a formal Rh−Rh single bond.[268]

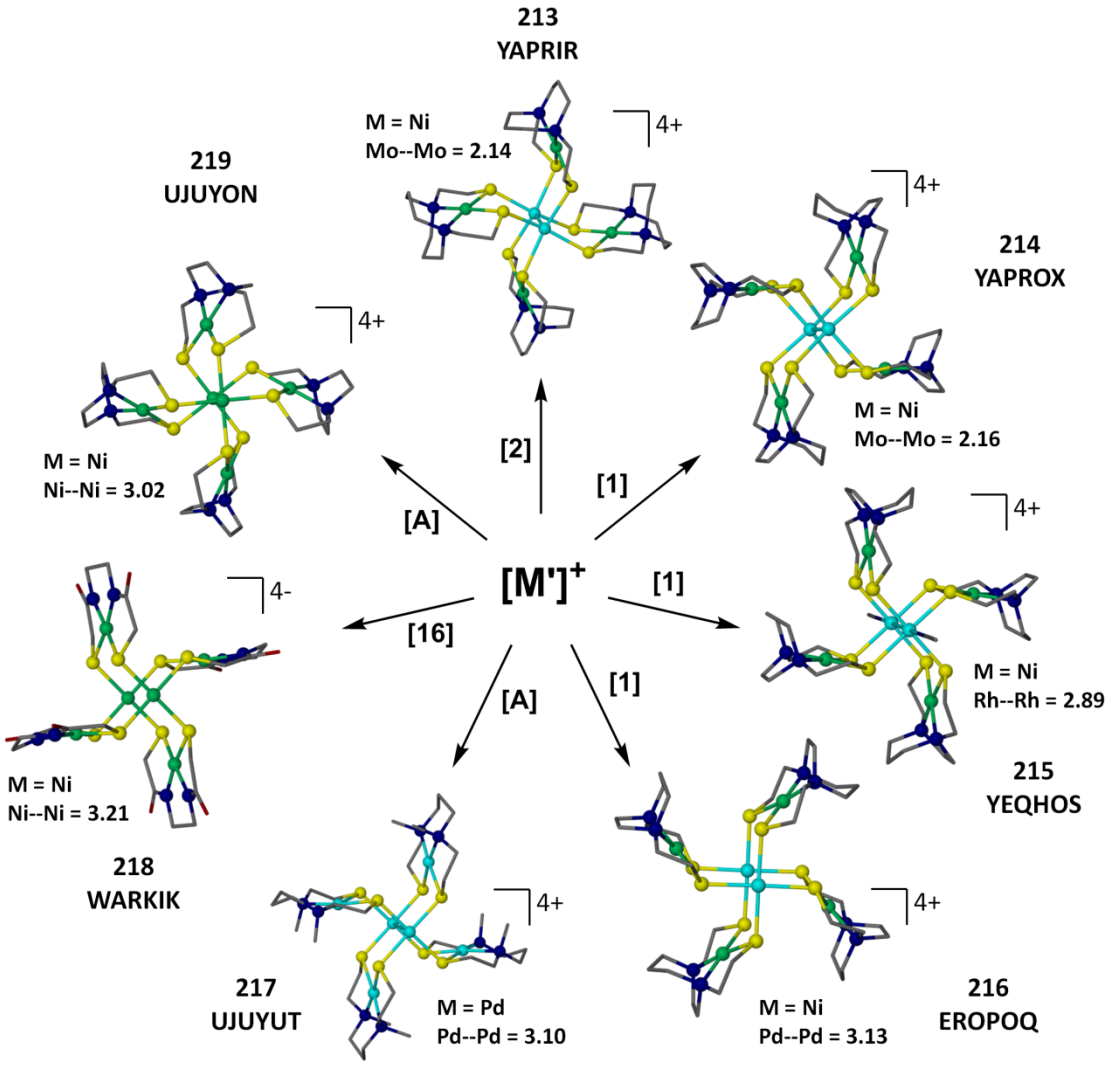

Figure 2-48. Complexes **213−219** of composition $[MN_2S_2]_4M'_2$ are of the C_4 paddlewheel structural motif. The M'−M' distances are listed for each complex, varying from 2.14 Å (Mo^{2+}—Mo^{2+}) to 3.21 Å (Ni^{2+}—Ni^{2+}).

The Pd−Pd distance in **216** of 3.13 Å is taken as indication that there is no metal−metal interaction.[258] Palladium (II) is used both for the N_2S_2 paddles and in the axle in complex **217**, derived from the open chain N_2S_2 ligand and carrying a 4+ overall charge.[284] Six Ni^{2+} ions comprise **218**, where the paddles are dianionic and based on metalloligand, **16**.[141] All in this class are highly regular with twists no larger than 2°. The last paddlewheel, complex **219**, is however highly distorted (twist of 32°) possibly deriving from the 6−membered diazacycle, piperazine, forming the backbone of the N_2S_2 ligand.[284]

2.6.3 Adamantane−like Clusters or $[MN_2S_2]_2M'_{3/4}$ Complexes

Yet another interesting structural type arises from the engagement of both lone pairs of the terminal thiolate sulfur with exogenous metals as indicated in Figure 2-6, paradigm F.

The cage like structure **220**, Figure 2-49, is comprised of two perpendicular NiN_2S_2 units with a Ni to Ni spacing of 5.54 Å. Four Cu^+ ions link the NiN_2S_2 units rendering roughly trigonal planar geometry about each Cu^+ and an overall adamantane−like topological form.[285] In Figure 2-50, the core of complex **220** has been highlighted as A) to point out the four 6−membered NiS_2Cu_2S cyclohexane−like rings that when combined together form the adamantane structure,[286] shown in Figure 2-50 B). Complex **221** is the analogous $[Cu^{II}N_2S_2]_2[Cu^{I}Cl]_4$ structure.[285] The remaining structures in Figure 2-49 are similar, however there is a hole or open space in the adamantane core as only 3 metals bridge the MN_2S_2 caps. Complex **222** is identical to **221** but with one

less CuCl, i.e., $[Cu^{II}N_2S_2]_2[Cu^{I}Cl]_3$.[285] The unoccupied adamantane site is clearly seen in the overlay of the cores of structures **221** and **222**, Figure 2-50 C).

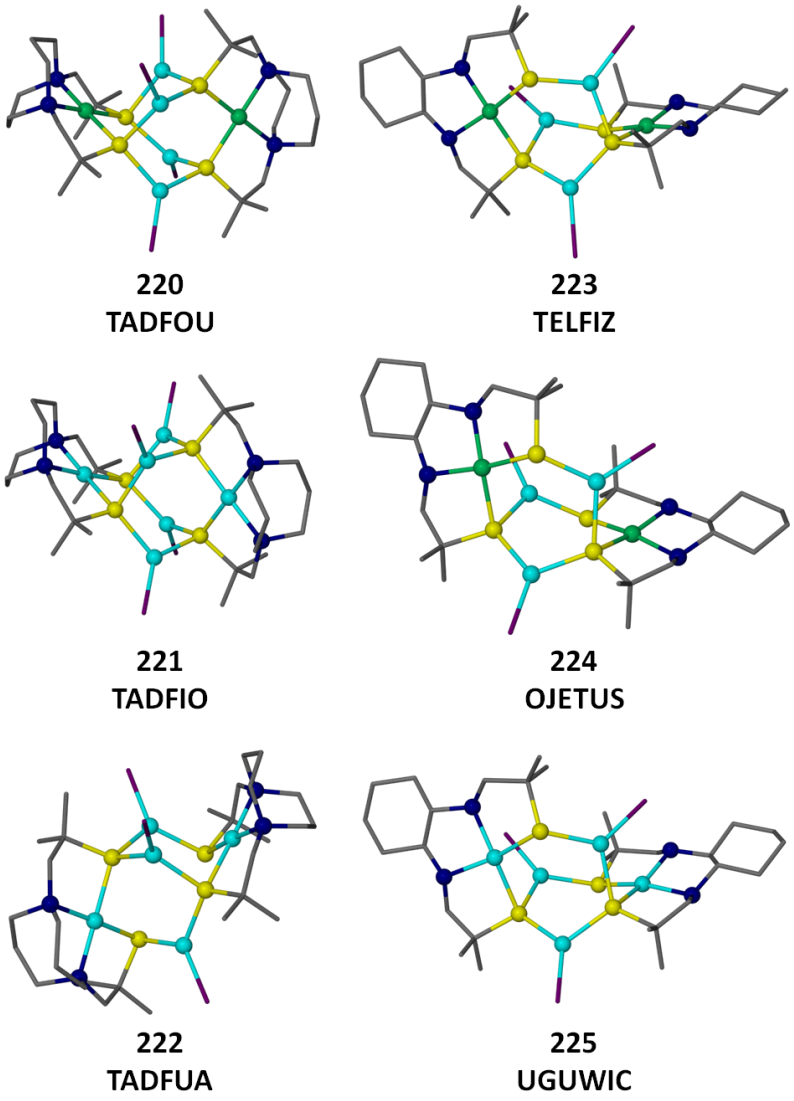

Figure 2-49. Complexes **220**−**225** are examples of structures with adamantane−like cores of formula $[MN_2S_2]_2M'_{3\text{ or }4}$.

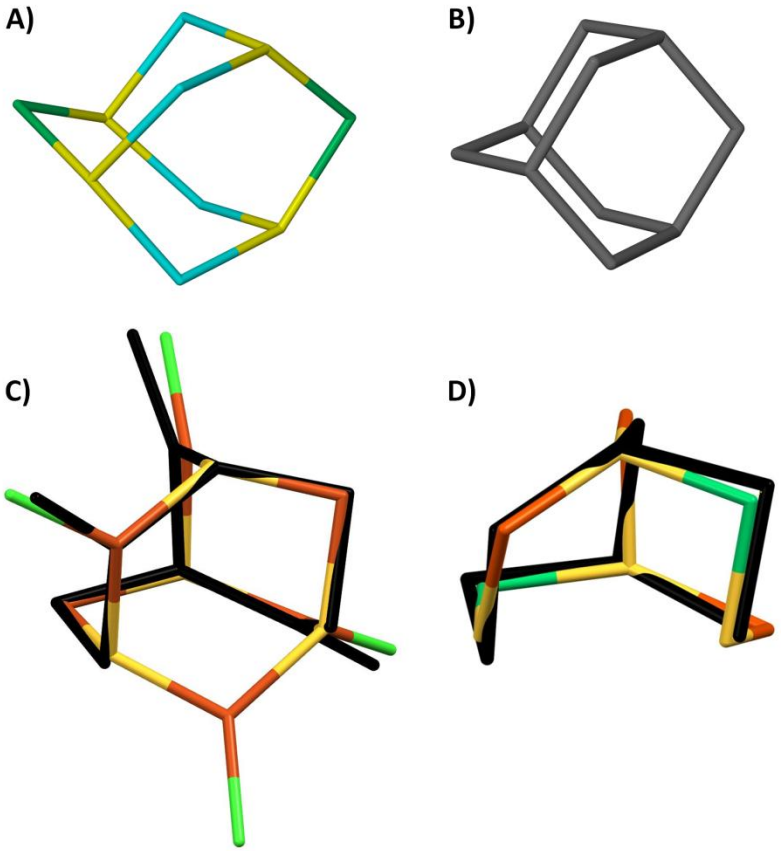

Figure 2-50. A) Adamantane−like core of complex **220** and B) adamantane. C) Overlay of complexes **221** and **222** (black) showing the complete vs. incomplete adamantane core structure. D) Complexes **222** (black) and **226** are overlaid, highlighting the structural similarities between Cu^{+} and the reduced $\{Fe(NO)_2\}^{10}$ fragment as bridges to the two MN_2S_2 adamantane caps.

Complexes **223** and **224** utilize complex **8** as the NiN_2S_2 metalloligand[287-288] and **225** uses the same N_2S_2 binding site but for Cu^{2+}.[209] Both contain three bridging $Cu^{I}X$ units, yielding the incomplete adamantane core. The greater flexibility of the N_2S_2 ligands in **223**−**225**, as contrasted to the rigid mesocyclic N_2S_2 framework utilized in

220−222, leads to distortion in the $M_2S_4M'_3$ core presumably in response to the open site.

Complex **226**, Figure 2-51, has complex **1** as NiN_2S_2 metalloligand to $Fe(NO)_2$ in the reduced form, $\{Fe(NO)_2\}^{10}$, generating a $[NiN_2S_2]_2[Fe(NO)_2]_3$ cluster that is related to **222**, i.e., analogous to the $[CuN_2S_2]_2[CuCl]_3$.[252] The incomplete adamantane cores of **222** and **226** overlay almost precisely, Figure 2-50 D). Such interesting structural similarity suggests that the analogy of the $\{Fe(NO)_2\}^{10}$ and the Cu^+−d^{10} electronic configurations induces similar assembly propensities and similar structural parameters in the $M_2S_4M'_3$ core. Complex **227**, is composed of a less common N to N linker in the N_2S_2 binding site for Cu^{2+} in a $Cu_2S_4Cu_3$ incomplete adamantane core, analogous to **225**.[289]

In illustration of the commonality of the adamantane−like $M_2S_4M'_4$ composition, complex **228**, Figure 2-51, has such a core in which three dppm ligands form a partial outer shell, linking the Cu^+ ions such that they are 4−coordinate and tetrahedral.[290] Were there four dppm ligands, the four Cu^+ ions would be symmetric. However, a NiN_2S_2 is used as a bidentate bridging ligand in place of the fourth dppm, rendering a hetero−heptanuclear cluster complex, $(NiN_2S_2)_2Cu_4(dppm)_3(NiN_2S_2)$. This formulation emphasizes the different roles of the NiN_2S_2; two are involved in the adamantane core structure and the third serves as a pseudo dppm ligand. Two renditions of **228** are given in Figure 2-51 to clarify the connectivities. Complex **228** has luminescent properties.[290]

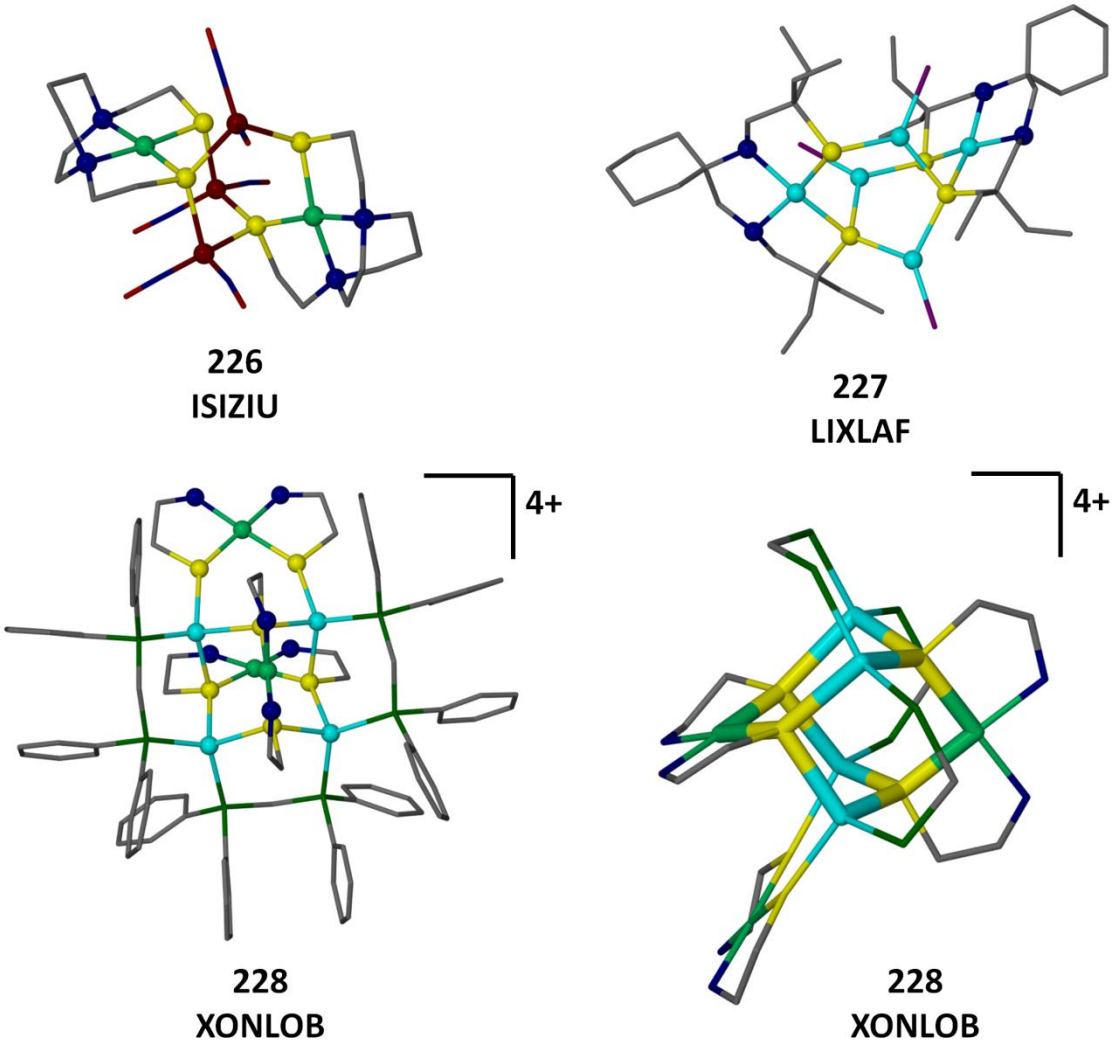

Figure 2-51. Complexes **226**−**228** are further examples of adamantane−like structures. Complex **228** is shown twice; on the left is the full molecule and the right is a different angle with the adamantane core highlighted and the phenyl rings of the dppm removed for clarity.

2.6.4 Other Large Clusters

Figure 2-52 displays multi−metallic clusters containing ≥ 6 metals bridged by thiolates; each cluster is presented in a second style that emphasizes the M−S(R)−M' connections. Complex **229** uses the NiN_2S_2 unit in the transoid S−metallation motif of Figure 2-5, with $HgCl_2$ moieties generating a 16−membered ring structure of composition $[HgSNiS]_4$.[121] The asymmetric unit of **230** likewise suggests a 10−membered ring structure, a result of aurophilic interactions of two $(Ph_3PAu)_2NiN_2S_2$ units wherein the Ph_3PAu electrophilies are within 3.1 Å.[271] Structure **231** is made up of four NiN_2S_2, complex **27**, linked together with four Au^+ ions.[272] It may be considered as a dimer of structural type **188**, Figure 2-43, rendering the Au^+ in a parallelogram with distances in the 3.15 to 3.29 Å range and Au−Au−Au angles of 126° and 59°.

The interplay of iron−sulfur clusters in the active sites of the bifunctional ACS/CODH enzyme is an exacting challenge for synthetic bioinorganic chemists. Figure 2-53 shows successful strategies. Holm prepared a site−differentiated 4Fe4S cluster which has three of the irons capped by a tridentate S_3 ligand, permitting the ligand on the fourth iron to be varied.[291] Complex **232** of Figure 2-53 shows that the fourth iron may be capped by a bidentate NiN_2S_2 metalloligand.[255] Osterloh, Saak, and Pohl reported a simpler 4Fe4S cluster precursor, $[Fe_4S_4I_4]^{2-}$, that could be used to illustrate attachment of complex **18**, of NiN_2S_2, in bidentate fashion to two irons as in complex **233**.[292-293] With the $[Fe_4S_4I_2(Stip)_2]^{2-}$ (Stip = tri−isopropyl phenylthiolate) reagent, two NiN_2S_2 units, complex **18**, displace the iodides and bind in a monodentate fashion, generating complex **234**.[293]

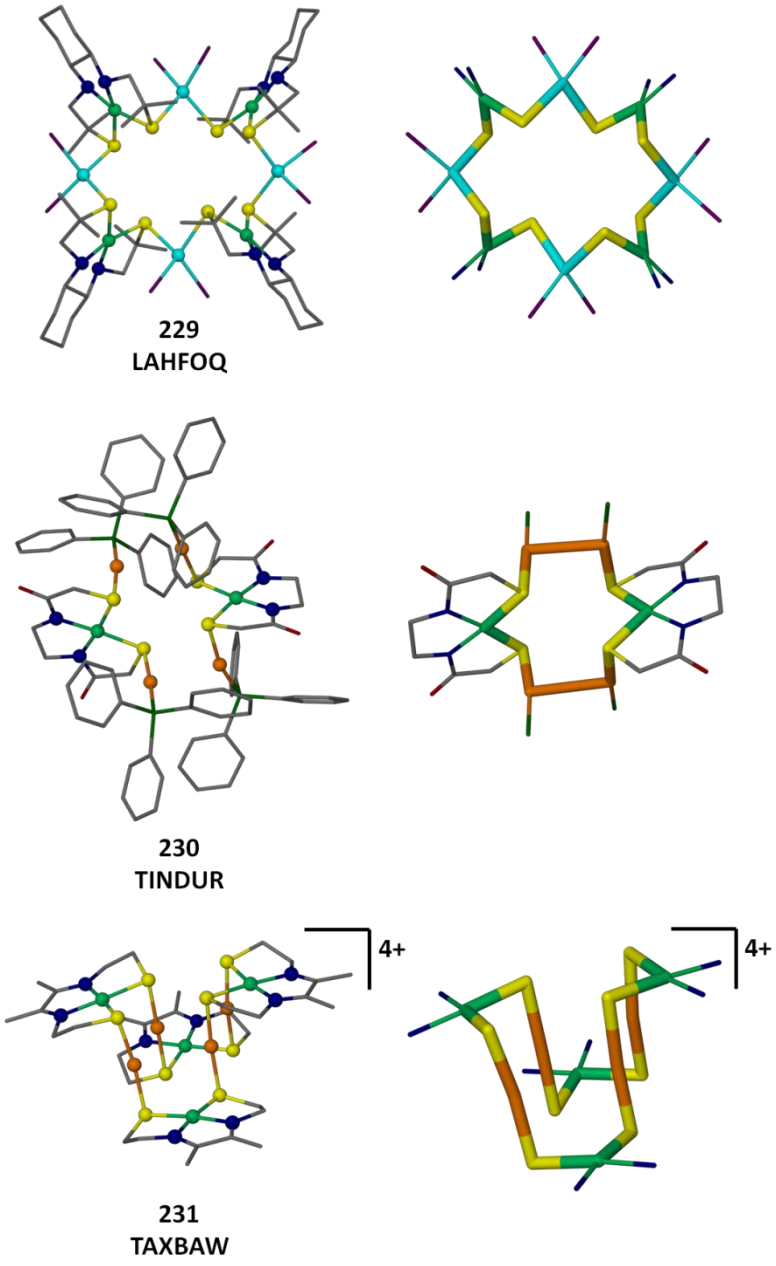

Figure 2-52. Complexes **229−231** are examples of larger multi−metallic complexes with bridging thiolates. For clarity, the core atoms are extracted from each structure and shown to the right.

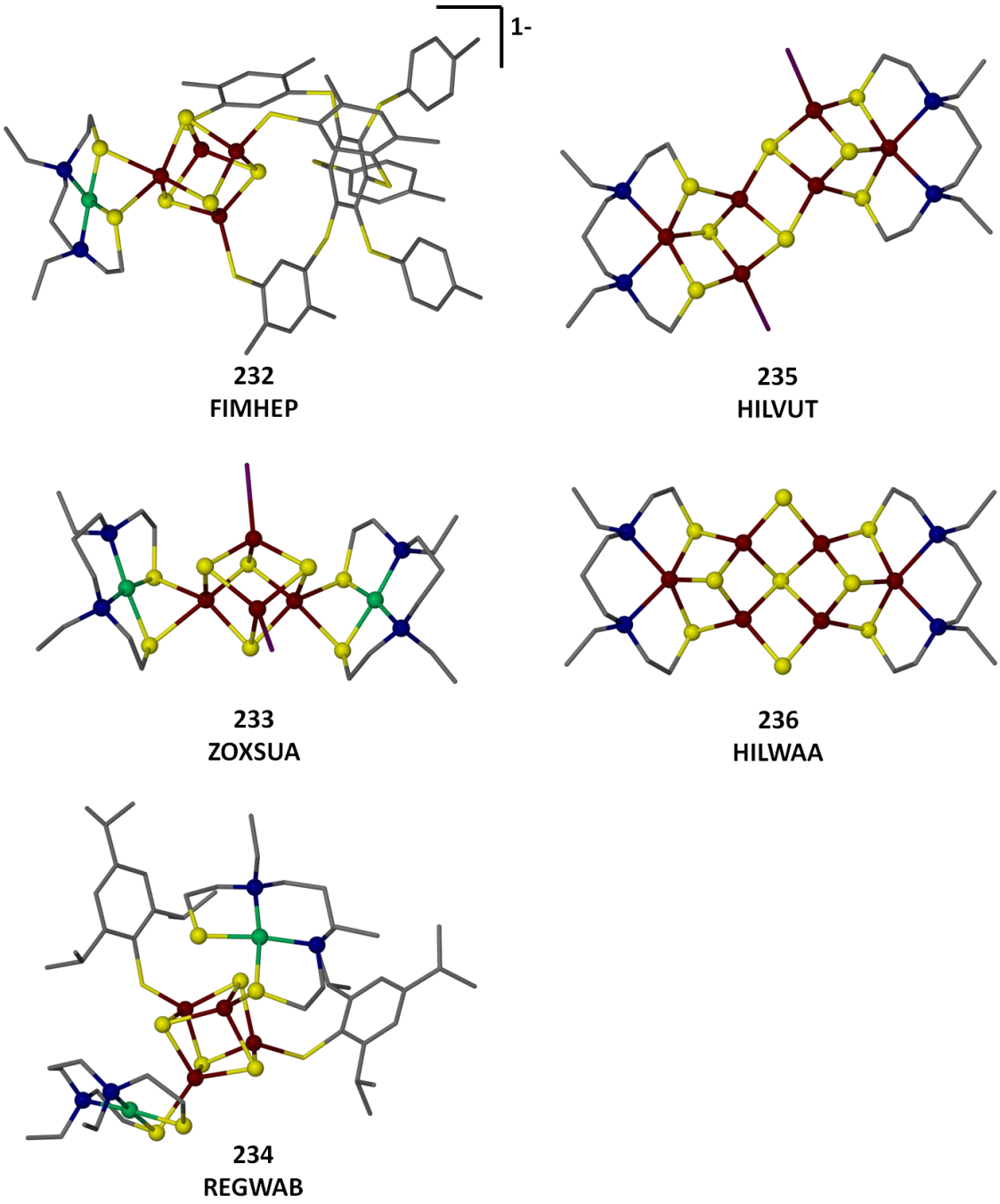

Figure 2-53. Complexes **232−236** are examples of MN_2S_2 compounds thiolate−S−bridged into iron−sulfur clusters.

Complex **235**, Figure 2-53, was assembled from the $[Fe_4S_4I_4]^{2-}$ synthon in combination with an $[FeN_2S_2]_2$ dimer that is analogous to complex **67**.[294] The product, **235**, contains two iron atoms in N_2S_2 coordination and four irons surrounded by sulfur: four thiolates and four sulfides that are bridging between irons. Two irons are in tetrahedral FeS_3I coordination, and two have a FeS_4 tetrahedral coordination. On change of solvent from DCM to DMF, a conversion to complex **236** occurs.[294]

2.7 Conclusions

Only the bravest of synthetic inorganic chemists (Richard Holm, Dieter Sellmann, and Dimitri Coucovanis, for example) have attempted to address the notorious reputation of sulfides and thiolates as ligands that engage in difficult−to−avoid, and even more difficult−to−predict, self assembly processes, that might reproduce the metal−sulfur clusters achieved by nature via intricate, step−by−step biosynthetic pathways.[295] The preassembly of cis−dithiolates attached through carbon linkers to nitrogen donors in tetradentate N_2S_2 complexes of Ni^{2+}, Pd^{2+}, $Fe(NO)^{2+}$, $Co(NO)^{2+}$, etc., seems to tame or control the sulfur lone pairs, orienting them in appropriate positions, and, as described in this review, leading to aggregative reactivity with appropriate metal acceptors of, if not always predictable, at least readily categorizable types. In donor ability and steric requirements, such MN_2S_2 complexes as ligands, similarly to cyanides,[296] may truly fulfill the description of "Nature's Phosphines," perhaps originally deriving from prebiotic, reducing atmospheric conditions on earth for the early CO/CO_2 conversion catalysts,[297-299] and evolutionally morphing into certain biological

specialist catalysts in today's microorganisms. The characterization of donor ability of these MN_2S_2 complexes as ligands has been defined by the diatomic CO−reporter approach, thereby finding that they are indeed better donors than phosphines.

The largely structural overview above emphasizes the unique forms of multimetallic clusters that have been sighted thus far. Presumably the diffuse binding surface of the S lone pairs in cis configuration accounts for the range of metal−metal distances that can be accommodated when the highly versatile MN_2S_2 complexes−as−ligands are asked to span two metals as in the propeller and paddlewheel complex structures. Figure 2-54 presents a graphic of paddlewheel complexes described above that highlights the core M_2S_x (x = 6 or 8) units, noting that the S to S distances in all are largely the same, 3.1 to 3.2 Å. That is, the S − S bidentate binding surface easily connects metals that lie outside the MS_2 span, as in the tetrahedral zinc units bound to three Ni(bme−dach) units, **211**. In complex **214**, we see that the Ni(bme−dach) is equally proficient at housing those metals that engage in strong M−M bonding of very short M−M distances, such as found in the $[Mo]_2^{4+}$ unit.

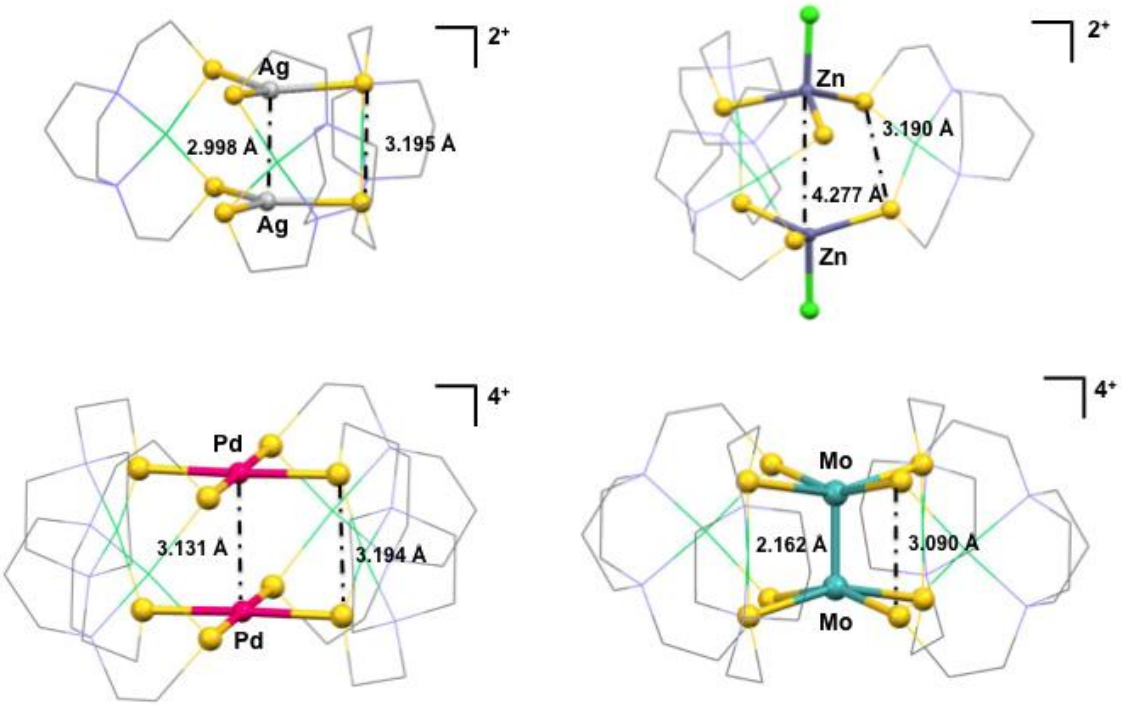

Figure 2-54. A selection of paddlewheel complexes with the NiN_2S_2 metalloligand "paddles" drawn in transparent relief. Note the S to S distances are relatively constant despite dramatic differences in M to M distances.

The stereochemical orientation of the lone pairs that engenders a variable hinge at the cis−dithiolate binding site and a butterfly type structure in the heterobimetallic MN_2S_2−M' complexes invites explorations of bimetallic redox chemistry, and small molecule capture by such bifunctional reagents. Reports of these, some very promising, have however thus far been limited. We anticipate that this area might be greatly expanded in the future.

3. AN APPROACH TO QUANTIFYING THE ELECTRONIC AND STERIC PROPERTIES OF METALLODITHIOLATE LIGANDS IN COORDINATION CHEMISTRY

3.1 Introduction

Complexes of first row transition metals in secure, tetradentate N_2S_2−binding represent a unique class of ligands in that the lone pairs of the sulfurs in such cis−dithiolates are ideally oriented to participate as bidentate ligands to a single or multiple exogenous metals, Figure 3-1.[300] When available sites are limited, monodentate coordination is also possible. In comparison to anionic thiolates without such coordinate covalent bonds, these S−donors are "tamed" by the transition metal, with donor abilities lying between those of RS^- and RSR.[301] In fact, studies of a series of $(L-L)W(CO)_4$ complexes that report the effect of ligand on CO stretching frequencies, similarly to the Tolman electronic parameter approach,[218] concluded that $Ni(N_2S_2)$ ligands were better donors than conventional bidentate ligands such as bis−1,2−diphenylphosphinoethane, dppe, or bipyridine, Table 3-1.[226] The metallodithiolate ligands differ from the latter in that there are two lone pairs on each sulfur site leading to geometrically ordered aggregation and yielding various topological forms, Figure 3-1.[300] Importantly, the more or less regular square planar binding conformation of the N_2S_2 donor set can accommodate a range of metals and ion fragments such as the other group VIII divalent metal ions, Pd^{2+} and Pt^{2+} , as well as species such as $[V=O]^{2+}$ ion, $[ZnCl]^+$, $[Fe(NO)]^{2+}$, and $[Co(NO)]^{2+}$ in which the metal achieves pentacoordination in the N_2S_2 environment.

The latter ions rely on the versatility of the N_2S_2 donor set that permits such metals to sit above the N_2S_2 plane to achieve optimal overlap in their square pyramidal geometry. Thus the indirect interactions of steric and electronic effects of what we will define as the endo metal (that within the N_2S_2 site) on the residual S-donor ability to the exo metal (that attached to one or both of the cis dithiolates) is of significance, and questions related to this coordination environment are the object of this report.

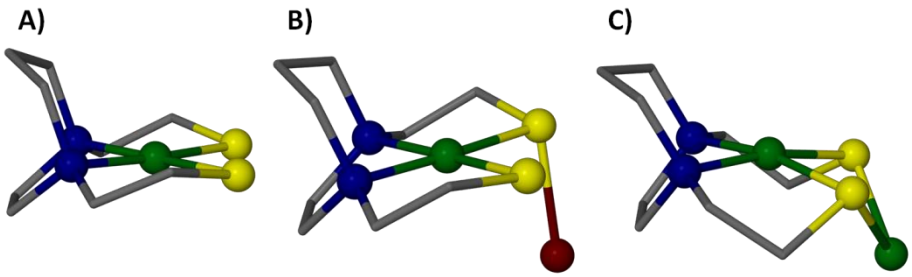

Figure 3-1. Crystal Structure representations of A) a free MN_2S_2 metalloligand; B) monodentate binding of a MN_2S_2 metalloligand to a secondary metal center (M'); and C) bidentate binding to the secondary metal center.

Table 3-1 contains a selection of such metallodithiolates as bidentate donors to $W(CO)_4$, (expanded from that in the literature),[171,226-229] and as monodentate ligands to $W(CO)_5$,[232] $Fe(CO)_4$,[235] and $Ni(CO)_3$ acceptors,[240] wherever valid comparisons may be found. Values derived from three methods of quantifying steric bulk are listed in Table 3-1: the "solid angle";[221] our modification of Tolman's ligand cone angle; and Nolan's percent buried volume ($\%V_{bur}$).[222] The application of each of these approaches for the irregular metallodithiolate ligands will be described below.

3.2 Electron Donor Ability

The electronic parameter originally established by Tolman for phosphine ligands of $LNi^0(CO)_3$, assumed that the donor ability of L was revealed through back-bonding on the ν(CO) A_1 vibrational mode, the lower the ν(CO) value, the better the donor. Table 3-1 contains solution data in the ν(CO) region of the infrared spectrum with assignments as indicated. By this measure, the N-heterocyclic carbene, NHC ligand, IMes, is a better donor by ca. 20 cm^{-1} over that of the PPh_3 ligand. Currently the only known MN_2S_2 metalloligand bound to a $Ni(CO)_3$ fragment is that of a dimeric $[FeN_2S_2]_2$ complex, whose structure leaves one thiolate sulfur in a terminal position that is capable of binding as a monodentate ligand to another metal. As indicated in entries **1 - 3** of Table 3-1, the ν(CO) A_1 value is similar to that of the NHC ligand, and possibly a bit lower.[218,240,302]

Using the $Fe^0(CO)_4$ fragment as acceptor, entries **4 - 9** of Table 3-1, the data again show the IMes, NHC, ligand to be a better donor than PPh_3, with the ν(CO) values for the NiN_2S_2 as monodentate S-donor even lower, entry **9**, Table 3-1.[235,303-307] Another comparison of a phosphine and NiN_2S_2 as monodentate ligands to $W(CO)_5$ as acceptor and reporter unit consistently finds the latter to lower the ν(CO) values by ca. 10 – 20 cm^{-1} as compared to PPh_3, entries **10** and **11**.[232,234]

In bidentate coordination we have used the stable and well-characterized $MN_2S_2W(CO)_4$ series of compounds for examination of the donor strength of the MN_2S_2 metalloligands as well as for codifying steric parameters. Earlier the ν(CO) IR values of several NiN_2S_2 derivatives were reported and these are repeated here.[226-227] To that list

we add several pentacoordinate complexes, entries **15**, **16**, **20**, and **21**.[171,228-229] The ν(CO) IR values for the neutral M(NO)(bme-dach) (M = Fe and Co) derivatives of $W(CO)_4$ are slightly more positive than the analogous Ni^{2+} complexes **17 - 19** which are roughly equivalent. Placing the dicationic $[V=O]^{2+}$ into the tetraanionic ema ligand results in a dianionic $W(CO)_4$ derivative with lower ν(CO) IR values, entry **20**, while the anionic $ZnCl(bme\text{-}dach)^-$ and the dianionic $Ni(ema)^{2-}$ metalloligands, entries **21** and **22**, respectively, have the lowest ν(CO) IR values of all. Again we note that even the neutral metallodithiolate ligands rank higher in donor abilities than do the classical diphosphine (dppm) and bipyridine ligands, entries **12 - 14**.[224,230,308] While the donor ability of ligands does not necessarily correspond to binding ability, the former has been successful to gage the ligand's ability to stabilize higher oxidation states as might be intermediates in catalytic processes involving oxidative addition reactions.

The extent to which the MN_2S_2 ligand is a Lewis base to an exogeneous metal may also be monitored by electrochemical events. Using the $W(CO)_4$ unit as acceptor, the reversible one-electron reduction potentials of M(bme-dach), M = Ni^{2+}, $Co(NO)^{2+}$, and $Fe(NO)^{2+}$, are observed to shift from their free ligand values by +0.47 V (-2.11 → -1.64 V); +0.49 (-1.08 → -0.59 V); and, +0.61 (-1.08 → -0.47 V), respectively. The differences in free ligand values of the $Ni^{II/I}$ vs. the $[M(NO)]^{2+/1+}$ derivatives is ascribed to the delocalization possible in the latter nitrosyl derivatives. The positive shifts on binding to the $W(CO)_4$ unit is a result of electron density drained from the dithiolates by the soft Lewis acid acceptor. The similarity in the positive shifts of the three ligands is largely consistent with the ν(CO) IR data. It should be noted that such simple

interpretations of metallothiolates as ligands may be questioned in thiolate-bridged complexes where the two transition metals are of equal thiophilicity. That is, the assignment of X and L character to the thiolate bridge in a particular M-(μ-SR)-M' arrangement will not always be straightforward.

3.3 Steric Effects

Tolman's steric parameter, the angle of the cone that emanates from the metal and encompasses the bulk of ligands, originally applied to monodentate phosphines anchored on a pyramidal $Ni(CO)_3$ unit, has remained as a standard comparison of ligand steric properties since its first report in 1970.[218] Other approaches have been developed for less symmetric and two dimensional ligands, such as N−heterocyclic carbenes (NHCs) or pyridines and derivatives. Immirzi and Musco defined a ligand angular encumbrance similar to Tolman's coe angle, and a "solid cone angle", Ω, derived from X-ray structural data and space-filling models, in attempts to account for multiple conformers and compressibility of asymmetric phosphine ligands.[221] Importantly this approach demonstrated differences (albeit small) in ligand steric features with coordination environment on the metal acceptor. Nevertheless there is a general correlation with the simpler Tolman cone angle.

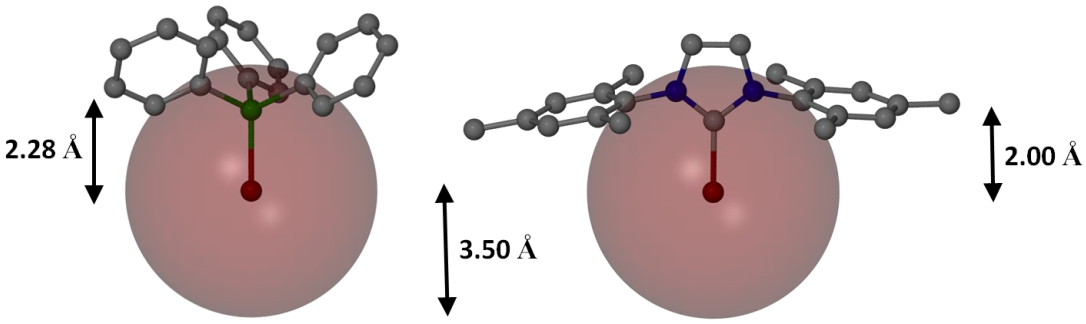

Figure 3-2. Models of percent volume buried calculations on PPh3 and IMes ligands based off a P-M bond length of 2.28 Å and a C-M bond length of 2.00 Å. The center of the sphere (red) of radius 3.5 Å is placed that distance from the ligand and an axis to define in what direction to place the center of the sphere is based off the 3 carbon atoms bound to the phosphorus or the two nitrogens of the carbene ligand.

Clavier and Nolan explored the concept of percent buried volume, %Vbur, as might be appropriate for phosphines and the highly asymmetric and widely used N-heterocyclic carbenes, Figure 3-2.[222] This approach imbeds the ligand within a sphere of set radius from the metal center and, from the van der Waals radius of each atom within the sphere, the percent volume occupied by the ligand is calculated making use of available software, SambVca.[309] Once again, for phosphines, a linear correlation with Tolman cone angles was observed, (R^2 = 0.96), at M-donor atom distances of 2.00 and 2.28Å. The extension of the approach making use of Au^+ as a reference metal of low coordination number for NHC's, obviated steric encumbrance from other ligands. From values determined here, the coauthors could assess the effect of "spectator" ligands on the $\%V_{bur}$ of the NHC, finding variability in the orientation of the N-substituents of the

NHC, with concomitant differences in the $\%V_{bur}$. Ligands that have multiple conformers such as phosphines or NHC's and flexibility in their steric requirements are noted by Clavier and Nolan as having potential for enhancing catalysis by transition state stabilization.

Such approaches as described above have not been applied to the more complex, highly asymmetrical metalloligands such as the MN_2S_2 complex ligands. As noted in Figure 3-1, the orientation of the lone pairs on the sulfur donor of metalloligand renders a highly angular hinge at the $M(\mu{-}SR)_2M'_x$ bridge. This hinge angle is defined as the M−(μ−SR)−M' angle in B) and the dihedral angle between the $M(N_2S_2)$ and S_2M' planes in C). It leads to a serious bifurcation of steric hindrance at the M' site and provides a challenge for establishing steric hierarchy. However the numerous solid state structures offer a rich backdrop for analysis. Here we describe using X-ray crystallographic data in Tolman cone angle analysis as well as the $\%V_{bur}$.

3.3.1 Cone Angles (for Monodentate MN_2S_2 Ligands) and Wedge Angles (for Bidentate MN_2S_2 Ligands)

In order to measure the ligand cone angle for each of the systems, both monodentate and bidentate cases, each X−ray crystal structure was examined for the atom(s) that exhibit steric encumbrance and/or pressure on the reporter unit $Ni(CO)_3$, $W(CO)_x$, and $Fe(CO)_4$. Thus each cone angle is not necessarily the largest possible for the metalloligand but rather the "effective" cone angle for the specific system. In each case the van der Waals radius of the sulfur and/or hydrogen was taken as the limiting

surface restriction to define the cone angle as shown in Figure 3-3. First the L−M−H angle, θ_1, was measured using crystallographic coordinates. Second the M−H distance was used with the van der Waals radius of hydrogen to form a right triangle as shown in Figure 3-3. Third from this right triangle the second angle, θ_2, could be calculated and added to θ_1 to find the half cone angle of the ligand.

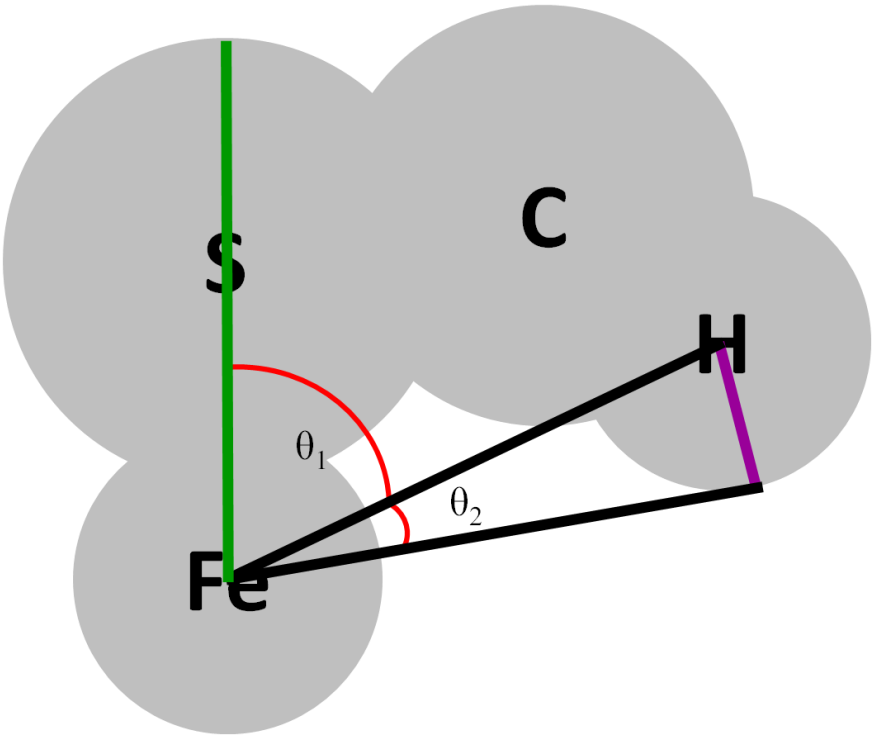

Figure 3-3. Space filling model based on van der Waals radius of atoms showing the vertical in green, Fe−H distance in black, and the radius of hydrogen in green. Angle 1, θ_1, can be measured using crystallographic coordinates and angle 2, θ_2, can be found using the van der Waals radius of hydrogen and the right triangle rules from geometry. Together the two angles equal the half cone angle of the ligand.

First, let us examine a case in which the MN_2S_2 metalloligand is monodentate rather than bidentate, i.e. complex **16** (Figure 3-4C) The ligand cone angle is roughly 140^o, which is most analogous to PPh_3 [~146^o in $(PPh_3)W(CO)_5$], assuming free rotation about the M'−S bond. This is shown in Figure 3-4 where the two structures are overlaid and a single hydrogen from each complex is found to overlap with each other above the carbonyl ligands highlighting the similar steric requirements of the NiN_2S_2 and PPh_3 ligands in complexes **16** and **15**, respectively.

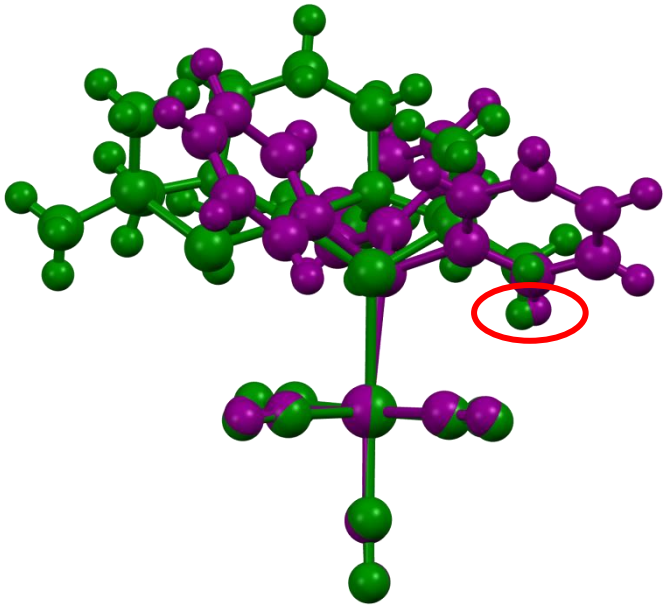

Figure 3-4. X−ray structure overlays of complexes **15**, $(PPh_3)W(CO)_5$, (purple) and **16**, Ni(bme*−daco)$W(CO)_5$, (green) showing the similar steric requirements of the NiN_2S_2 metalloligand and the PPh_3 assuming free rotation about the W−L bond.

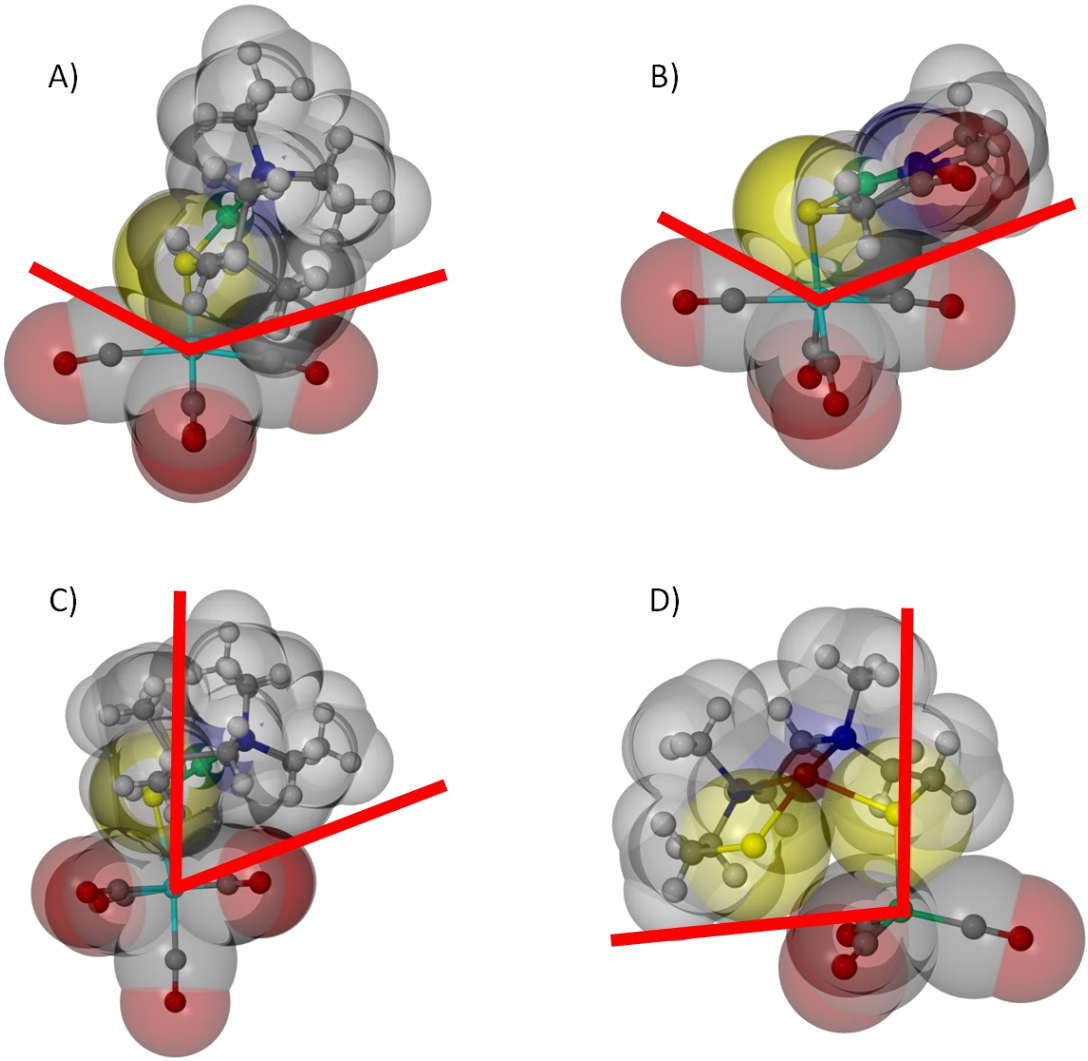

Figure 3-5. Solid state structures of complexes A) **18**, B) **22**, C) **11**, and D) **3** shown in ball and stick representations with transparent space−filling model. A) and B) show complexes **18** and **22** which are bidentate to a $W(CO)_4$ reporter unit. Note the sulfurs (yellow) and nitrogens (blue) are eclipsed. C) and D) show complexes **11** and **3** binding in a monodentate fashion to $W(CO)_5$ and $Ni(CO)_3$, respectively.

The Ni(bme−daco) metalloligand binds to $Fe(CO)_4$, complex **22**, in an axial position, as does PPh_3. The ligand cone angle swept out by a freely rotating NiN_2S_2 is found to be 150°, which is only slightly smaller than PPh_3 in complex **18**, $Fe(CO)_4PPh_3$, with a ligand cone angle of 160°. Complexes **17**, $Fe(CO)_4(\eta_1-dppe)$, and **19**, $Fe(CO)_4P^tBu_3$, exhibit more steric bulk and encumbrance on the $Fe(CO)_4$ unit with cone angles of 166° and 172°, respectively. The small pyridine ligand in complex **20**, $Fe(CO)_4Py$, has a cone angle of 130°, while the NHC derivative, **21**, $Fe(CO)_4IMes$, has the largest cone angle, 172°, equal to P^tBu_3 in complex **19**. The only example of a $M(N_2S_2)Ni(CO)_3$ compound is complex **3** in Figure 3-5 which has the FeN_2S_2 binding to a $Ni(CO)_3$ unit has a Tolman Cone Angle of 188°; for comparison that of $P(C_6F_5)_3$ is 184° as measured in $P(C_6F_5)_3Ni(CO)_3$.[218]

Bidentate cases can be examined using the $W(CO)_4$ scaffold. For example $[Ni(ema)]^{2-}$ is a "planar" metalloligand with very little steric interaction with an adjacent metal center. For example in complex **14** the NiS_2 and WS_2 planes intersect at an angle of ~110°. In contrast, Ni(bme*−daco) is more sterically encumbered in three dimensions which can be seen in complex **10** whose NiS_2 and WS_2 planes intersect at an angle of ~130°, which is 20° degrees larger than complex **14**. In addition, upon comparing the ligand cone angle of the NiN_2S_2 metalloligands in complexes **10** and **14** two cases can be considered; a static conformation of the metalloligand or one in which the metalloligand undergoes a flipping process (~15−16 kcal/mol).[226] Thus, a static scenario is used to measure the ligand cone angles of **10** and **14** which are 135° and 128°, respectively, Figure 3-4A, B. This steric pressure from the metalloligand can be seen in the deviation

of linearity between the two CO ligands cis to the metalloligand (trans to each other); C−W−C 168^{o} and 177^{o}, respectively.

3.3.2 Percent Buried Volume Calculations

However, a better measure of the steric requirements of MN_2S_2 complexes might be the percent buried volume ($\%V_{bur}$) calculation that Nolan and others have recently used for phosphines and NHC's.[222] By using the online SambVca software,[309] the $\%V_{bur}$ for all these complexes were measured and are displayed in Table 3-1 with additional information shown in Figures 3-6, 3-7, 3-8, 3-9, and 3-10 and Tables 3-2 and 3-3. In Figure 3-6 three different views are shown for complex **9** showing the metalloligand in stick, stick with transparent van der Waal's, and space filling forms. Each is shown using three different sphere sizes around the secondary metal center (tungsten in this case). Alternative views of complex **9** from Figure 3-6 are shown from the top and bottow perspective in Figure 3-7. When the calculated $\%V_{bur}$ using the three different sphere radii sizes is graphed, Figure 3-8, it shows the trend in measure steric bulk for the ligands is maintained for the most part. Thus, we calculations reported are based on a sphere of radius 3.5 Å as in Nolan's recent studies. Note from Table 3-2 the trend is also not affected by the inclusion of hydrogen atoms; numbers reported are thus based on hydrogen exclusion.

Table 3-1. Table of monodentate and bidentate complexes showing the electron donating properties of the ligand as measured by IR. Steric bulk is measured using ligand cone or wedge angles, solid angles, and percent buried volume calculations all based on using solid state structures.

No	Ligand	Complex	IR: ν(CO) cm^{-1}	Media	Ligand Cone Angle or Wedge[j]	Solid Angle Ω[n]	Percent Buried Volume[o]
1	PPh_3	$Ni(CO)_3L$	2069, 1990	CH_2Cl_2	145[k]	4.39	28.7
2	IMes[a]	$Ni(CO)_3L$	2051, 1970	CH_2Cl_2	168	5.63	34.0
3	Fe(dsdm)[b]	$Ni(CO)_3L$	2048, 1968, 1949[i]	KBr	188	6.72	26.3
4	dppe[c]	$Fe(CO)_4L$	2052, 1980, 1947, 1939[i]	hexanes	166	5.52	29.4
5	PPh_3	$Fe(CO)_4L$	2050, 1977, 1945	hexanes	160	5.19	28.7
6	P^tBu_3	$Fe(CO)_4L$	2040, 1960, 1920	CH_2Cl_2	172	5.84	35.1
7	pyridine	$Fe(CO)_4L$	2042, 1970, 1943	hexanes	130	3.63	20.6
8	IMes[a]	$Fe(CO)_4L$	2041, 1960, 1935, 1921[i]	hexanes	172	5.84	34.0
9	Ni(bme-daco)[d]	$Fe(CO)_4L$	2030, 1945, 1926, 1907[i]	THF	150	4.66	24.2
10	PPh_3	$W(CO)_5L$	2074, 1981, 1943	$CHCl_3$	146	4.44	23.5
11	Ni(bme*-daco)[e]	$W(CO)_5L$	2061, 1971, 1920, 1874[i]	DMF	140	4.13	22.3
12	dppm[f]	$W(CO)_4(LL)$	2016, 1906, 1906, 1870	DMF	150/190/202/230[l]	4.66/6.83/7.48/8.94[l]	37.9
13	bipyridine	$W(CO)_4(LL)$	2006, 1886, 1870, 1830	DMF	102/191[m]	2.33/6.89[m]	30.0
14	piperidine	$W(CO)_4L_2$	2000, 1863, 1852, 1809	DMF	148	4.55	----------
15	Co(NO)(bme-dach)[g]	$W(CO)_4(LL)$	1998, 1880, 1854, 1827	DMF	131	3.68	33.0
16	Fe(NO)(bme-dach)[g]	$W(CO)_4(LL)$	1997, 1878, 1851, 1824	DMF	136	3.93	33.8
17	Ni(bme-dach)[g]	$W(CO)_4(LL)$	1996, 1873, 1852, 1817	DMF	138	4.03	32.5
18	Ni(bme*-daco)[e]	$W(CO)_4(LL)$	1996, 1871, 1857, 1816	DMF	136	3.93	35.6
19	Ni(bme-daco)[d]	$W(CO)_4(LL)$	1995, 1871, 1853, 1819	DMF	128	3.53	31.6
20	VO(ema)[h]	$W(CO)_4(LL)$	1996, 1872, 1848, 1802	DMF	137	3.98	36.1
21	ZnCl(bme-dach)[g]	$W(CO)_4(LL)$	1988, 1861, 1836, 1801	DMF	143	4.29	33.8
22	Ni(ema)[h]	$W(CO)_4(LL)$	1986, 1853, 1837, 1791	DMF	128	3.53	33.1

Table 3-1. Continued.

[a]1,3-bis(2,4,6-trimethylphenyl)-imidazolium
[b]N,N'-dimethyl-N,N'-bis(2-sulfanyl-ethyl)ethylenediamine)
[c]1,2-bis(diphenylphosphino)ethane
[d]N,N'-bis-mercaptoethylene-1,5-diazacyclooctane
[e]N,N'-bis(2-mercapto-2-methylpropylene-1,5-diazacyclooctane
[f]1,1-bis(diphenylphosphino)methane
[g]N,N'-bis-mercaptoethylene-1,4-diazacycloheptane
[h]N,N'-ethylene-bis(2-mercaptoacetamide)
[i]E band of the ν(CO) IR spectrum is observed as two separate peaks
[j]Ligand cone angles all measured in this work using hydrogen atoms that present the greatest steric encumbrance in the solid state structures
[k]Reported from Tolman Chem. Rev. 1977
[l]Different cone angles based on which proton is selected
[m]Two cone angles reflect the two-dimensions of the bipyridine ligand
[n]Solid Angle, Ω, calculated using ligand cone angle, θ,derived herein; $\Omega = 2\pi(1-\cos(\theta/2))$
[o]Measured using the online SambVca software, see text

Table 3-2. Percent buried volume calculations for monodentate ligands with and without hydrogen atoms as well as at sphere sizes of r = 3.5, 4.0, and 4.5 Å.

			w/o Hydrogens			w/ Hydrogens		
No	**Compound**	**M-L**	**3.5 A**	**4.0 A**	**4.5 A**	**3.5 A**	**4.0 A**	**4.5 A**
1	$(PPh_3)Ni(CO)_3$	2.28	28.7	28.6	27.9	29.5	29.3	28.5
2	$(IMes)Ni(CO)_3$	2.00	34.0	35.4	36.3	34.7	36.0	36.7
3	$[Fe(dsdm)Ni(CO)_3]_2$	2.317	26.3	27.0	27.0	26.9	27.7	27.7
3b	$[Fe(dsdm)Ni(CO)_3]_2$	2.28	26.9	27.5	27.4	27.5	28.2	28.1
4	$(dppe)Fe(CO)_4$	2.247	29.9	29.7	29.0	30.7	30.5	29.7
4b	$(dppe)Fe(CO)_4$	2.28	29.4	29.2	28.6	30.2	30.1	29.3
5	$(PPh_3)Fe(CO)_4$	2.243	29.4	29.1	28.4	30.2	29.9	28.9
5b	$(PPh_3)Fe(CO)_4$	2.28	28.7	28.6	27.9	29.5	29.3	28.5
6	$(P^tBu_3)Fe(CO)_4$	2.363	33.4	34.2	33.9	34.7	35.4	34.9
6b	$(P^tBu_3)Fe(CO)_4$	2.28	35.1	35.6	35.1	36.4	36.8	36.1
7	$(py)Fe(CO)_4$	2.00	20.6	18.3	15.8	21.1	18.8	16.2
9	$Ni(bme\text{-}daco)Fe(CO)_4$	2.331	24.2	23.2	21.8	24.3	23.3	21.9
9b	$Ni(bme\text{-}dach)Fe(CO)_4$	2.324	23.8	22.9	21.5	24.1	23.3	22
10	$(PPh_3)W(CO)_5$	2.544	23.5	24.1	24.1	23.7	24.4	24.3
11	$Ni(bme^*\text{-}daco)W(CO)_5$	2.576	22.3	23.1	23.4	22.9	23.7	24.0
11b	$Ni(bme^*\text{-}daco)W(CO)_5$	2.544	22.8	23.5	23.7	23.4	24.1	24.3

Table 3-3. Percent buried volume calculations for bidentate ligands with and without hydrogen atoms as well as at sphere sizes, r = 3.5, 4.0, and 4.5 Å. The entry for **10-CO** is added to show the calculation for percent volume buried on a single carbon monoxide ligand.

			w/o Hydrogens			w/ Hydrogens		
No	**Compound**	**M-L**	**3.5 A**	**4.0 A**	**4.5 A**	**3.5 A**	**4.0 A**	**4.5 A**
12	(dppm)$W(CO)_4$	1.86	37.9	38.3	37.8	38.6	39.0	38.4
13	(bipy)$W(CO)_4$	1.657	30.0	27.7	25.0	30.3	28.1	25.2
15	(NO)Co(bme-dach)$W(CO)_4$	1.86	33.0	32.0	30.4	33.5	32.6	31.0
16	(NO)Fe(bme-dach)$W(CO)_4$	1.86	33.8	32.6	30.7	34.4	33.3	31.3
17	Ni(bme-dach)$W(CO)_4$	1.86	32.5	30.8	28.2	32.9	31.3	28.8
18	Ni(bme*-daco)$W(CO)_4$	1.86	35.6	34.9	33.2	36.3	35.8	34.2
19	Ni(bme-daco)$W(CO)_4$	1.86	31.6	30.1	27.7	32.1	30.6	28.2
20	VO(ema)$W(CO)_4$	1.772	36.1	34.6	32.4	36.3	35.0	32.8
20b	VO(ema)$W(CO)_4$	1.86	34.6	33.5	31.6	34.9	33.9	32.0
21	(Cl)Zn(bme-dach)$W(CO)_4$	1.756	33.8	32.4	30.3	34.3	33.0	31.0
21b	(Cl)Zn(bme-dach)$W(CO)_4$	1.86	32.2	31.0	29.3	32.7	31.6	29.9
22	Ni(ema)$W(CO)_4$	1.86	33.1	31.6	29.0	33.4	31.9	29.3
10-CO	$(PPh_3)W(CO)_5$	2.03	16.8	13.2	10.4	-----	-----	-----

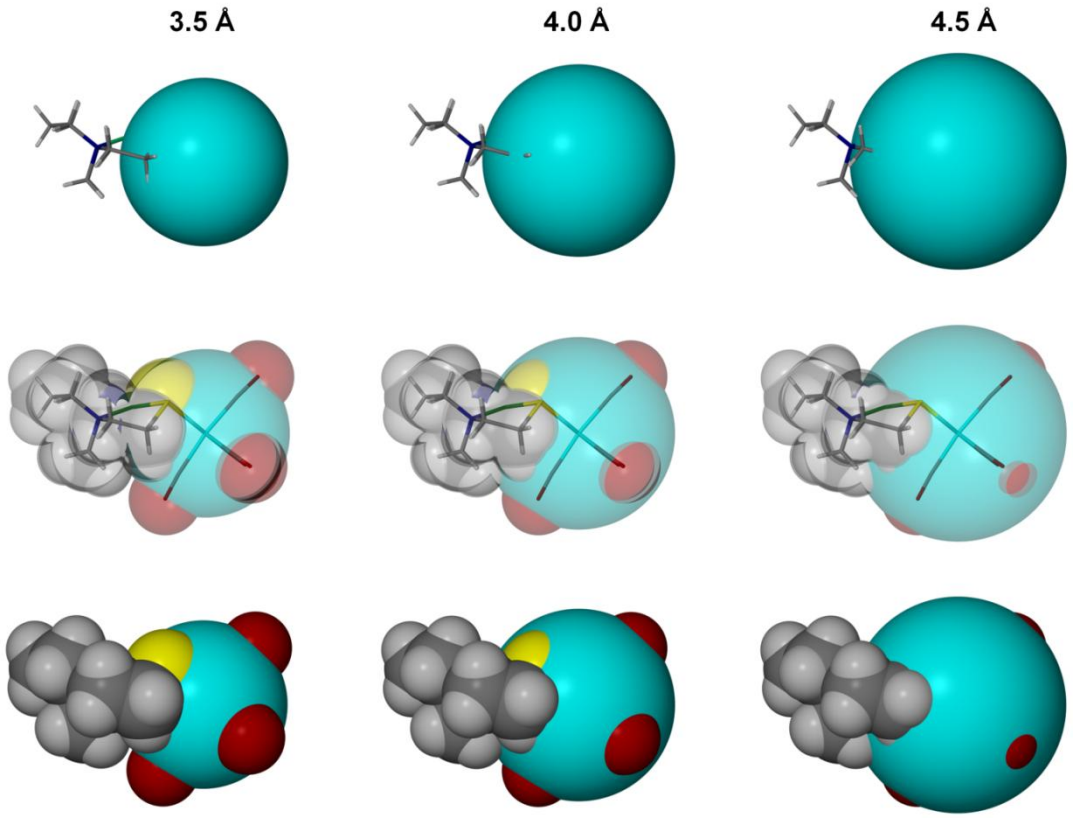

Figure 3-4. Renderings of **9**, Ni(bme−dach)$W(CO)_4$, showing percent volume buried based on the tungsten sitting at the center of a sphere with a radius of 3.5, 4.0, or 4.5 Å.

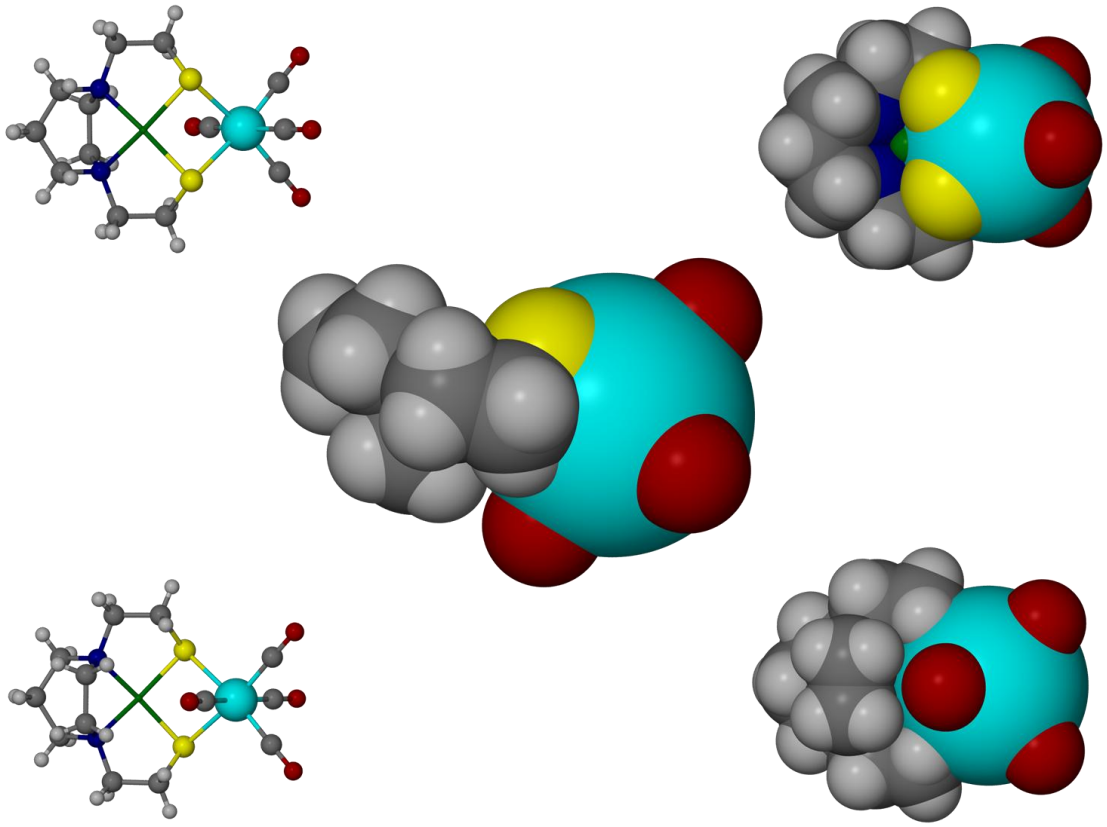

Figure 3-5. Alternative views of the space filling model of complex **9**, Ni(bme-dach)W(CO)4, with sphere of radius 3.5 Å. The middle image is the same as in Figure 3-6 but views from the top and bottom of the complex are also offered in ball and stick and space filling forms.

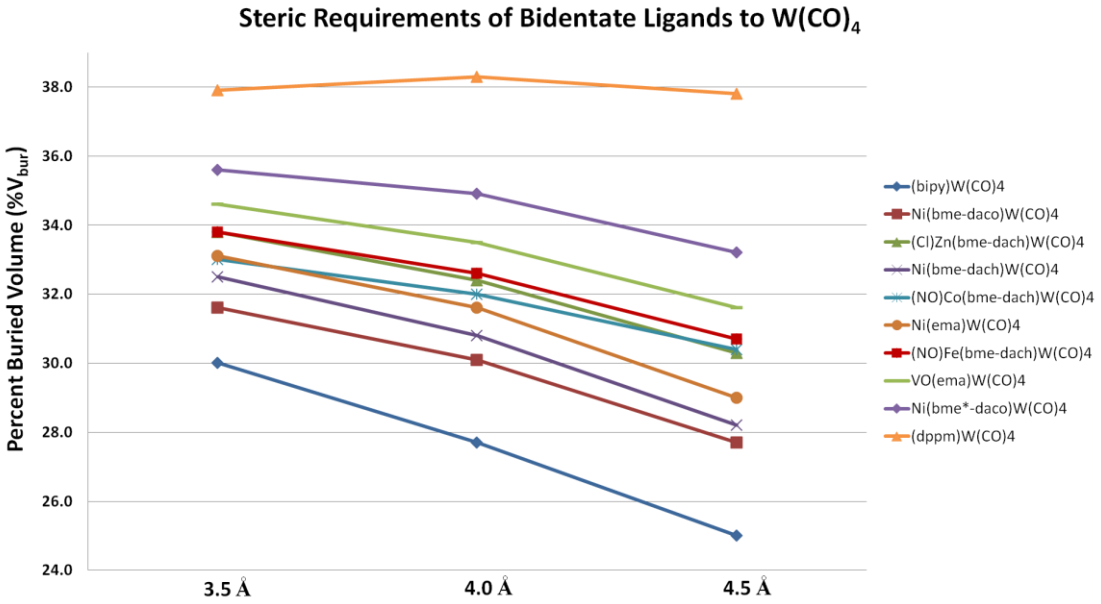

Figure 3-6. Graph of percent buried volume calculated for a range of (κ^2-L)W(CO)4 complexes using different setting for the radius of the main sphere that the volume calculation is based on. A diphosphine ligand (top orange) is the largest, bipyridine (bottom blue) the smallest, and in the middle are eight complexes with MN_2S_2 metalloligands.

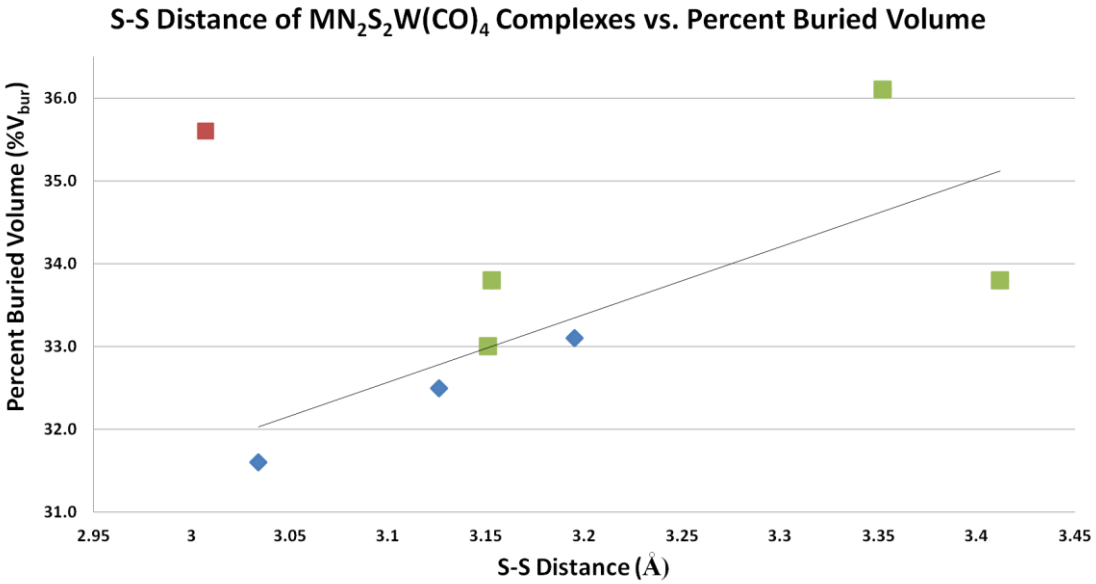

Figure 3-7. Graph showing a correlation between the S to S distance and the calculation $\%V_{bur}$ among $M(N_2S_2)W(CO)_4$ complexes. In blue are the NiN_2S_2 complexes, $M(L)N_2S_2$ in green, and the outliner in red is Ni(bme*-daco) complex **10** which has gem-dimethyl groups. Trend line excludes complex **10**.

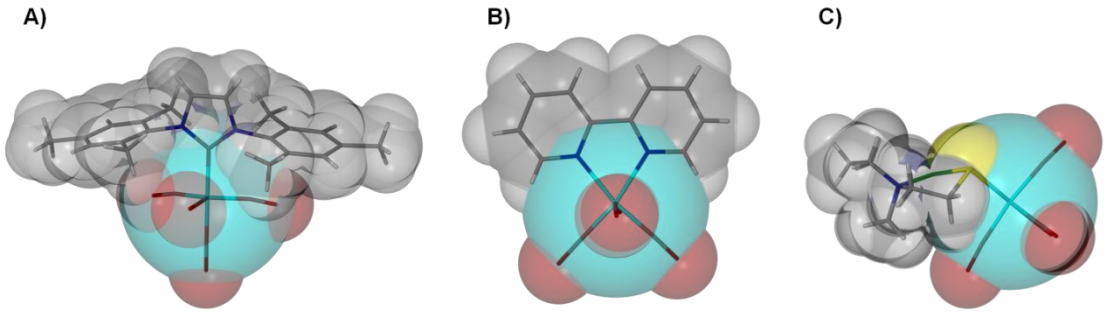

Figure 3-8. Percent buried volume ($\%V_{bur}$) using a sphere of 3.5 Å radius for A) $(IMes)Fe(CO)_4$, 34.0%; B) $(bipy)W(CO)_4$, 30.0%; and, C) $Ni(bme{-}dach)W(CO)_4$, 32.5%.

From these values we conclude that bipyridine, **5**, is the smallest ligand in its 3−dimensional special requirements; and dppm, **4**, the largest. Intermediate between these two are 8 MN_2S_2 complexes which exhibit $\%V_{bur}$ between 32 and 36%. This narrow range is to be expected since these metalloligands are structurally very similar. The small differences between them are explained as follows: the $Ni(ema)^{2-}$, **14**, would be expected to be among the smaller complexes in this category and its V≡O analogue, **12**, would be larger due to the larger S−S distance, Figure 3-9, and the other distortions in the metalloligand resulting from the square pyramidal geometry about the vanadium center.

The three neutral NiN_2S_2 complexes **9** – **11** can be arranged by first assigning complex **10** with the gem−dimethyl groups to be the largest of the three. Despite the fewer atoms within Ni(bme−dach), it occupies a larger percentage of space as compared to Ni(bme−daco) complexes **9** and **11**, respectively,. The reason for this is two−fold; first the S−S distance is greater in the Ni(bme−dach) case and second, the N_2S_2 binding pocket is below the metal rather than being in a plane with the nickel [as in Ni(bme−daco)]. This results in the carbon alpha to the sulfur occupying a larger space around the tungsten center. Both of these result from the smaller, more constricted, diazacyclo−backbone found in Ni(bme−dach), **9**, Figure 3-11.

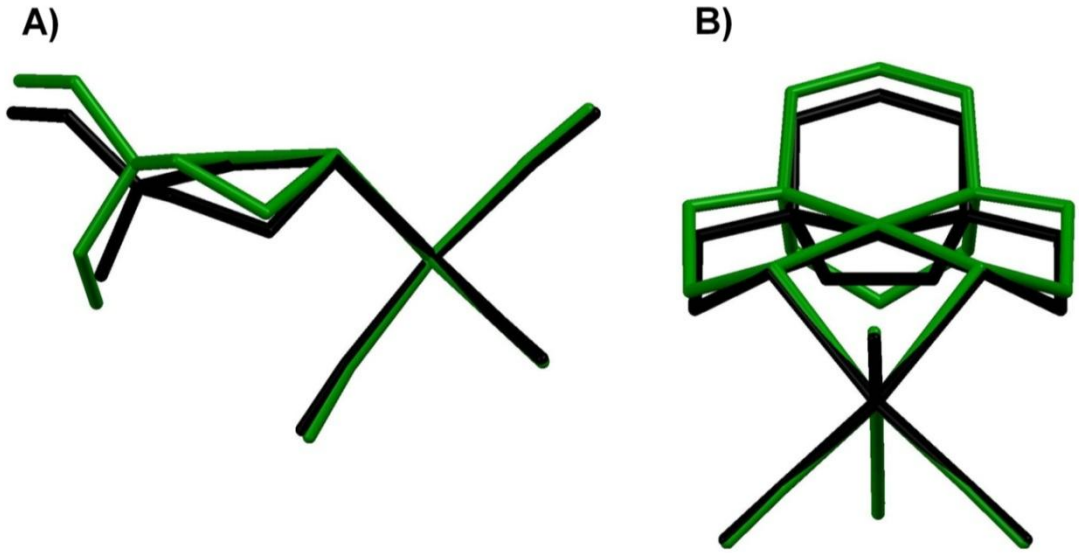

Figure 3-9. Structural overlay of Ni(bme−dach)W(CO)$_4$ (**9**), black, and Ni(bme−daco)W(CO)$_4$ (**11**), green, shown from a A) side view and B) head−on view looking from the tungsten to the nickel. Note that the ethylene sulfide arms of **9** are closer to the tungsten center due to the torsion angles enforced by the more constricted diazacycle.

The final three complexes in this category utilize 5−coordinate metal centers in the bme−dach framework. The square pyramidality wherein the N_2S_2 plane sits lower in comparison to their nickel analogue (greater displacement of the metal center from the N_2S_2 plane); in addition to the extra ligand Cl^- in **13** or NO in **7** and **8** resulting in these three metalloligands having greater spacial requirements, Figure 3-12. The Zn(Cl) metalloligand in **13** can be considered the largest of these three due to the much greater S−S distance (3.412 Å) found in the structure, Figure 3-9. The Fe(NO) metalloligand is slightly larger than its Co(NO) analogue due to the ethylene sulfide arms in the Fe(NO)

complex sitting lower (closer to the tungsten center), which can also be seen in the metal displacement from the N_2S_2 plane 0.552 and 0.385 Å, respectively.

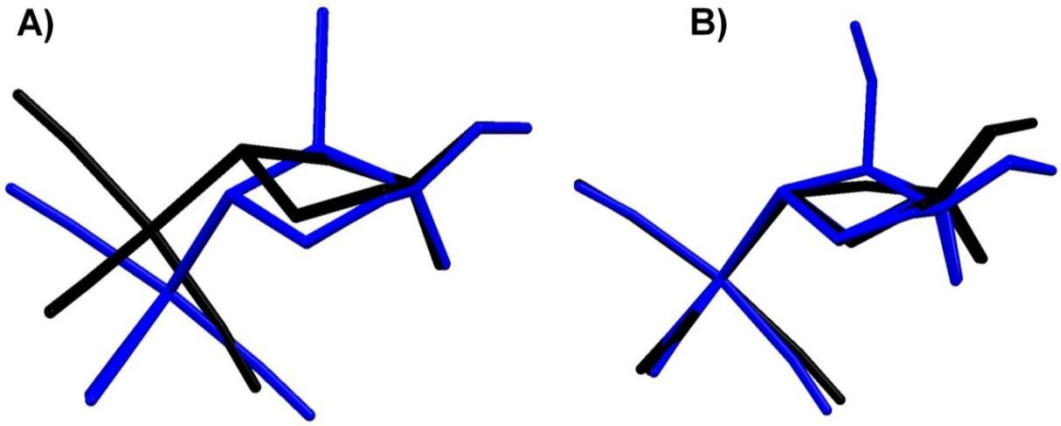

Figure 3-10. Structural overlays of Ni(bme−dach)$W(CO)_4$ (**9**), black, and A) Zn(Cl)(bme−dach)$W(CO)_4$ (**13**), blue; or B) Fe(NO)(bme−dach)$W(CO)_4$ (**8**), blue. Note in A) that when the diazacycle backbone is overlaid how the pentacoordination of the zinc changes the lone pair orientation of the sulfurs causing the ethylene sulfide arms and the $W(CO)_4$ unit to be lower than in the nickel analogue. In B) the $W(CO)_4$ unit was overlaid highlighting the difference in torsion angles of the ethylene sulfide arms causing the hydrogen atoms of the metalloligand to exert a greater steric repulsion with the $W(CO)_4$ unit which is most clearly seen in the bending of the CO that sits under the metalloligand.

Thus, the steric and electronic properties of the MN_2S_2 metalloligand can be tuned through modification of the metal center, the organic linkers between donor atoms, and the denticity of the metalloligand. The examples described herein show that the

steric pressure can come from not only from the mercapto−arms but the N−to−N linker of the backbone as well. The donor strength can be modulated by changing the metal center or changing the charge of the metalloligand. The metalloligands have been shown to be stronger donors than phosphine or imine ligands while still maintaining tunability in the donor strength as well as the steric bulk of the metalloligand. The high degree of customization possible in the MN_2S_2 metalloligands opens the door to countless possibilities for these metalloligands in various catalytic reactions.

4. COMPARISONS OF HEXACOORDINATE $N_2S_2O_2$ METAL COORDINATION COMPLEXES AND THEIR M/M' EXCHANGE REACTIONS

4.1 Introduction

For the chemist, there are in general, no "free" metal ions. In solution, all synthetic procedures entail the transfer of metal ions from one binding site to another, usually involving intricate mechanisms of stepwise and cascading de- and re-ligation. An analogue of this process of particular interest lies in the construction of biocatalytic sites of metalloenzymes concerning nitrogen and sulfur donor atoms from protein-bound histidine imidazoles, cysteine thiolates, methionine thioethers, and tripeptide motifs with deprotonated amido nitrogens. In the form of a protein-Cys-X-Cys-protein chain, such a motif results in a contiguous, largely square planar S-N-N-S tight binding site, displayed in the distal nickel site of acetyl-CoA-synthase (ACS),[310] thiocyanate hydratase,[103] and in the iron and cobalt forms of nitrile hydratase (NHase),[104] Figure 4-1. The sulfurs of the Cys-Ser-Cys tripeptide binding motif found in Co- and Fe-NHase are "post-translationally modified" with oxygen, yielding metallo sulfonyl (R-S=O) and a metallosulfinato ($R\text{-}S(=O)_2$) units.[311] Similar sulfur reactivity is characteristic of synthetic N_2S_2 complexes of nickel, where the N_2S_2 binding is maintained throughout a variety of nickel-bound S-modifications; including metallation, oxygenation, and alkylation, Figure 4-2.[106,128-129,300,312]

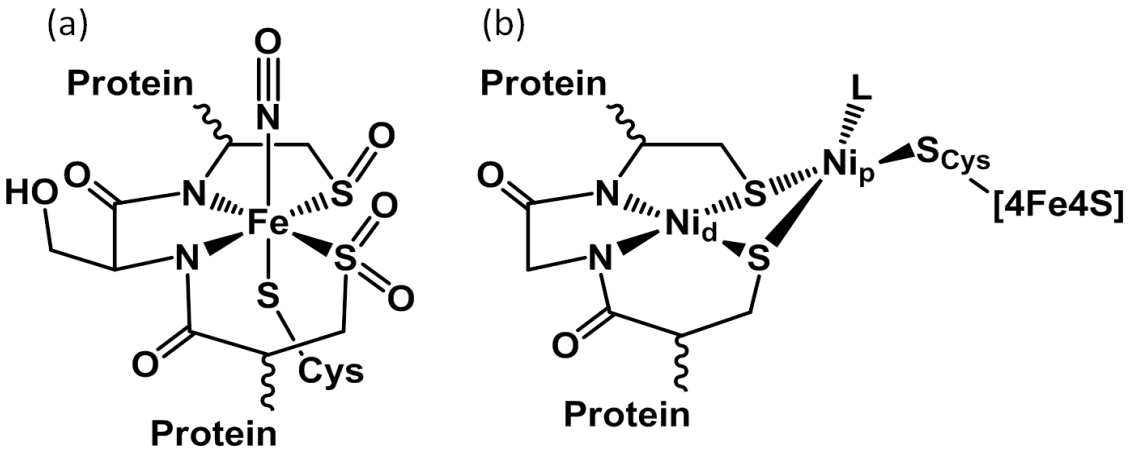

Figure 4-1. Active sites of enzymes with S-modification: a) nitrile hydratase and b) acetyl-CoA synthase.

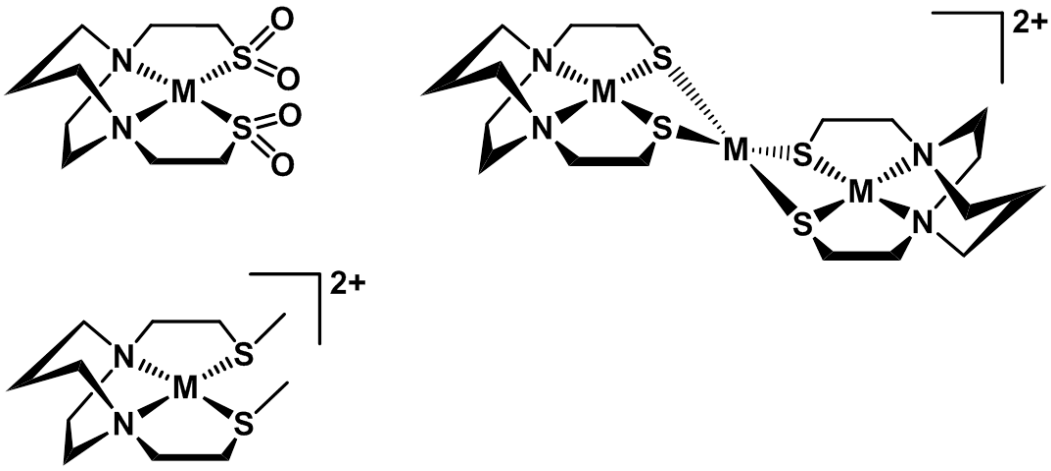

Figure 4-2. Synthetic MN_2S_2 complexes showing modification of thiolates by oxygenation, alkylation, or metallation.

The reactivity of cysteinyl sulfur in proteins with acetylating agents, such as iodoacetamide and iodoacetate, has found application for cysteine protection and as an

analytical tool for protein sequencing/mass spectrometry experiments. The latter is used to monitor the increased mass of the cysteine residues and protein as a whole, and as well to prevent the formation of disulfide bonds in the tertiary structure of the protein.[313] While thioethers are typically poorer binding ligands, the carboxylate or carboxamido terminus is a potential donor, and expansion of the coordination number may occur. Typically it is expected that alkylation of cysteines in an active site can prevent the metal(s) from coordinating to the active site residues, or alternatively, alkylation on sulfurs of metal-bound cysteines will deactivate the enzyme.[314-315] It should be mentioned that alkylating and acetylating agents are known carcinogens. Hence, knowledge of potential sites of reactivity in biomolecules is of even greater significance.

Zinc is the second most abundant transition metal in the human body with 2 - 4 g found in the average human. It is most commonly found as a structural element in zinc fingers and in enzymes such as carbonic anhydrase, carboxypeptidase, and metallothionein.[316] As a kinetically labile metal, zinc may act as a place-holder in an enzyme active site. In the study of zinc containing proteins, the zinc can undergo transmetallation with exogenous metal ions with more spectroscopic features;[317] or it may become the active form of an enzyme active site, for example HypB.[60,62]

For the above reason, metal exchange processes with metal binding sites are of importance to the overall understanding of the generation of enzyme active sites and other metalloproteins. The transmetallation of $Ni(EDTA)^{2-}$ with Cu^{2+} has been extensively studied by Margerum, *et al.* in order to obtain kinetic information as basis for development of a proposed mechanism for the replacement of Ni^{2+} by Cu^{2+}.[318]

Escudero-Adan *et al.* have used transmetallation of Zn-salphen complexes as a synthetic method for a library of transition metal salphen complexes.[319] The exchange of Zn^{2+} by Pt^{2+} in zinc finger sites on transcription factors is theorized to be part of the mechanism by which Cisplatin can interrupt DNA replication in cells.[320]

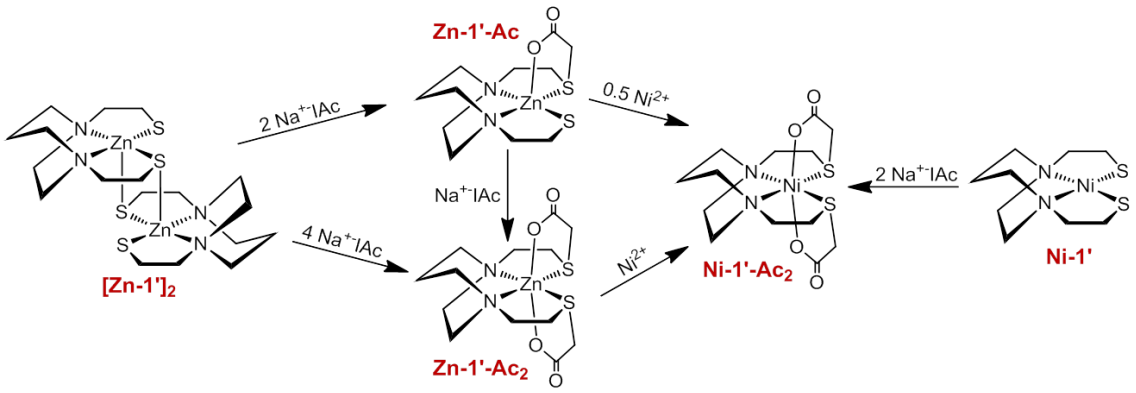

Figure 4-3. Scheme for the synthesis of **Ni-1'-Ac$_2$** and **Zn-1'-Ac$_{1/2}$**, adapted from reference 321.[321]

In this work, we demonstrate, through synthesis and reactivity studies, that metal-bound thiolates in N_2S_2 complexes can be acetylated forming thioethers from the thiolates with expansion of ligand denticity through the carboxylate groups. The thus derived thioethers maintain binding to the metal with notable differences in chemical properties between the unmodified **M-1'** complexes and their modified counterparts, **M-1'-Ac$_2$**, Figure 4-3. Through S-modification, a series of six-coordinate complexes has been directly synthesized and characterized for comparison to the products of metal exchange reactions between **M-1'-Ac$_2$** complexes and exogenous metal ions. Additional

nickel exchange reactions are presented in Appendix B. Even though the complexes are coordinatively saturated, they are still able to undergo transmetallation reactions through a ligand unwrapping/wrapping mechanism similar to what has been shown for metal exchange in the EDTA complexes by Margerum and others.[318]

4.2 Experimental Details

4.2.1 Materials and Methods

Solvents were dried and degassed using a Bruker solvent system. The products are air stable; however, as a precautionary measure, all reactions were carried out under an inert atmosphere of argon using standard Schlenk procedures unless otherwise noted. The acetylated products can be extremely hygroscopic, necessitating exclusion of moisture. Separations used silica gel chromatography both for thin layer and column purifications. Reagents were used as acquired from standard vendors. The bis(2-mercaptoethyl)-1,4-diazacycloheptane (H_2bme-dach),[128] *N*,*N*′-Bis(2-mercaptoethyl)-1,4-diazacycloheptanezinc(II) dimer **[Zn-1']$_2$**,[162] *N*,*N*′-Bis(2-mercaptoethyl)-1,4-diazacycloheptaneiron(II) dimer **[Fe-1']$_2$**,[169] *N*,*N*′-Bis(2-mercaptoethyl)-1,4-diazacycloheptanecobalt(II) dimer **[Co-1']$_2$**,[169] *N*,*N*′-Bis(2-mercaptoethyl)-1,4-diazacycloheptanenickel(II) **Ni-1'**,[128] 1,4-diazacycloheptane-1,4-diylbis(3-thiapentanoato) zinc(II) **Zn-1'-Ac$_2$**,[321] and 1,4-diazacycloheptane-1,4-diylbis(3-thiapentanoato) nickel(II) **Ni-1'-Ac$_2$**,[321] were synthesized according to published procedures.

4.2.2 Physical Measurements

Elemental analyses were performed by Atlantic Microlab, Inc. Norcross, GA, USA. Electrospray ionization mass spectrometry (ESI-MS) was performed by the Laboratory for Biological Mass Spectrometry at Texas A&M University. Solution infrared spectra were recorded on a Bruker Tensor 37 Fourier Transform – IR spectrometer, using a CaF_2 cell with 0.2 mm path length. UV-Visible spectra were obtained using a Shimadzu UV-2450 spectrophotometer with 1.0 cm path length quartz cells. Cyclic voltammograms were recorded on a BAS-100A electrochemical analyzer. All experiments were performed at room temperature under an Ar blanket in MeCN solution containing 0.1 M [t-Bu_4N][BF_4] as the electrolyte, with a 3.0 mm glassy carbon working electrode, an $Ag/AgNO_3$ reference electrode, and a Pt coil counter electrode. All values have been internally referenced to Fc/Fc^+.

4.2.3 Synthesis and Characterization

1,4-diazacycloheptane-1,4-diylbis(3-thiapentanamide) nickel(II) Iodide, [Ni-1'-AA_2][I]$_2$.

NiN_2S_2 Templated Synthesis. A portion of **Ni-1'** (0.25 g, 0.90 mmol) was placed in a 100 mL Schlenk flask and degassed prior to addition of 30 mL MeCN. Iodoacetamide, AA, (0.35 g, 1.90 mmol) in 20 mL MeCN was cannulated into the stirring **Ni-1'** solution. The reaction mixture was stirred at room temperature for two days yielding a blue precipitate. The mixture was filtered anaerobically and the solid was washed with 3x5 mL MeCN and 3x10 mL Et_2O and dried in vacuo to yield 0.48 g (0.74

mmol, 82%) of **Ni-1'-AA$_2$** solid. ESI-mass spectrum in CH_3OH: $[NiN_4S_2O_2C_{13}H_{26}]^{2+}$ m/z = 196.0 (100 %) $[NiN_4S_2O_2C_{13}H_{26} + H^+]^+$ m/z = 391.0 (44 %). UV-Vis (CH_3OH): λ_{max}, nm (ε, $M^{-1}cm^{-1}$) = 831 (37), 573 (38), 358 (56), 255 (6580) nm. IR (in MeOH, cm^{-1}): 1673 (vs, sharp). Magnetic moment, Guoy Balance: 2.93 B.M. Elem. Anal. Calc'd for $[NiN_4S_2O_2C_{13}H_{26}]I_2$•2MeOH (found): C: 25.34 (25.24), H: 4.82 (4.72), N: 7.88 (7.62).

1,4-diazacycloheptane-1,4-diylbis(3-thiapentanoic) cobalt(II), (Co-1'-Ac$_2$).

1) Cobalt N_2S_2 Templated Synthesis. A sample of **[Co-1']$_2$** (0.50 g, 0.90 mmol) within a 250 mL Schlenk flask, was degassed prior to the addition of 50 mL of dry MeOH, producing a green solution. Sodium iodoacetate, Na^+IAc^-, (0.84 g, 4.0 mmol) in 40 mL dry MeOH, was added via cannula to the stirring **[Co-1']$_2$** solution. The solution became a dark red/brown and stirring was continued for 24 h; the solvent was reduced in vacuo and the mixture was filtered to remove any NaI formed. The filtrate was chromatographed on a silica gel column (3 x 20 cm) using a 1:1 MeOH:MeCN solvent mixture as eluent. An initial band of yellow material was discarded and the magenta product, with an R_f value of 0.45, was collected as the desired product. The solvent was removed in vacuo, and precipitation of a powder forced with addition of ether. The product was collected by filtration, washed 3x with ether, and dried in vacuo yielding 0.40 g (0.88 mmol, 98%) of **Co-1'-Ac$_2$•2MeOH** solid. ESI-mass spectrum in CH_3OH: $[CoN_2S_2O_4C_{13}H_{22} + Na^+]^+$ m/z = 416 (27%). UV-Vis (CH_3OH): λ_{max}, nm (ε, $M^{-1}cm^{-1}$) = 570 (29), 537 (28), 487 (30), 279 (408) nm. IR (in CH_2Cl_2, cm^{-1}): 1627 (vs, sharp), 1348 (m), 1329 (m). Cyclic Voltammetry: $E_{1/2}$ = -240 mV vs. Fc/Fc^+ in MeCN assigned to the

Co^{III}/Co^{II} couple. Magnetic moment, Guoy Balance: 4.79 B.M. Elem. Anal. Calc'd for $CoN_2S_2O_4C_{13}H_{22}$•2MeOH (found): C: 39.69 (39.09), H: 5.64 (5.96), N: 7.12 (6.53).

2) Cobalt Ion Exchange into Zn-1'-Ac_2. To a 0.20 g, 0.51 mmol, sample of Zn-1'-Ac_2, 75 mL of dry degassed MeOH was added, producing a clear colorless solution to which was added 0.15 g, 0.51 mmol of $Co(NO_3)_2$ as light pink solution in 25 mL dry MeOH. The mixture was stirred for 24 h. The solid magenta product was isolated as above to yield 0.14 g (0.37 mmol, 72%) and characterization matched above results.

3) Hexadentate $N_2S_2O_2$ Ligand Synthesis Followed by Addition of $Co(NO_3)_2$. The H_2bme-dach ligand (0.50 g, 2.3 mmol) was placed in a 500 mL Schlenk flask under Ar along with 50 mL of dry MeOH. To this flask Na^+IAc^- (1.0 g, 5.0 mmol) in 50 mL dry MeOH was added. The pale yellow solution was magnetically stirred for 18 h before it was used *in situ*. To the stirring acetylated bme-dach ligand solution, $Co(NO_3)_2$ (0.66 g, 2.3 mmol) was added as a clear pink solution in 50 mL of dry MeOH whereupon a magenta color developed. The solution volume was partially reduced in vacuo before filtering to remove Na^+ salts formed during the reaction. Addition of Et_2O resulted in precipitation of a magenta solid, which was isolated by filtration. This powder was redissolved in MeOH and chromatographed through a silica gel column with MeOH as the eluent yielding 0.36 g (0.92 mmol, 40%). The properties of this product matched those from the templated synthetic route 1.

1,4-diazacycloheptane-1,4-diylbis(3-thiapentanoic) copper(II), (Cu-1'-Ac_2).

1) Copper N_2S_2 Templated Synthesis. A monomeric complex Cu-1' is not known and has not been previously synthesized; thus, a templated synthesis similar to that used with Ni-1' or $[Co\text{-}1']_2$ was not attempted.

2) Copper Ion Exchange into Zn-1'-Ac_2. A 100 mL Schlenk flask was charged with a sample of **Zn-1'-Ac_2** (0.10 g, 0.25 mmol) and degassed prior to the addition of 25 mL of dry MeOH, producing a clear colorless solution. Copper nitrate, $Cu(NO_3)_2$, (0.059 g, 0.25 mmol) in 25 mL dry MeOH was added via cannula to the stirring **Zn-1'-Ac_2** solution. The solution developed a very intense blue color and stirring was continued for 24 h. The solvent was reduced in vacuo, and then Et_2O was added to force precipitation of a blue powder which was collected by filtration. Under moisture-excluding conditions the product, washed 3x with Et_2O, was redissolved in MeOH and chromatographed through a silica gel column (3 x 20 cm) using MeOH as the eluent. The material with an R_f value of 0.25 was collected as the desired product, the solvent was reduced in vacuo, and precipitation forced with addition of Et_2O. The sticky blue product was collected by anerobic filtration, redissolved, precipitated, and washed until a blue powder could be isolated. This powder was further dried in vacuo yielding 0.030 g (0.076 mmol, 30%) of **$[Cu\text{-}1'\text{-}Ac_2]_2$** solid. ESI-mass spectrum in CH_3OH: $[CuN_2S_2O_4C_{13}H_{22} + H^+]^+$ m/z = 398. UV-Vis (CH_3OH): λ_{max}, nm (ε, $M^{-1}cm^{-1}$) = 607 (202), 348 (2660), 287 (1560) nm. IR (in CH_2Cl_2, cm^{-1}): 1631 (vs, sharp), 1347 (m), 1329 (m). $E_{1/2}$ = -360 mV vs. Fc/Fc^+ in CH_2Cl_2 for the Cu^{II}/Cu^{I} couple. Magnetic

moment, Evans Method: 1.46 B.M. Elem. Anal. Calc'd for $CuN_2S_2O_4C_{13}H_{22}•H_2O$ (found): C: 37.53 (37.04), H: 5.81 (5.76), N: 6.73 (6.64).

3) Hexadentate $N_2S_2O_2$ Ligand Synthesis Followed by Addition of $Cu(NO_3)_2$. The H_2bme-dach ligand (0.23 g, 1.0 mmol) was placed in a 100 mL Schlenk flask and 10 mL of dry MeOH was added. To this flask, Na^+IAc^- (0.45 g, 2.2 mmol) in 15 mL dry MeOH was added. The pale yellow solution was magnetically stirred for 18 h prior to the addition of $Cu(NO_3)_2$ (0.25 g, 1.0 mmol) in 20 mL of a degassed 50/50 MeOH/H_2O mixture was added to the ligand solution, whereupon a rich blue solution developed along with an unknown green/brown precipitate. After stirring overnight, the solution was filtered anerobically through Celite. The filtrate volume was partially reduced in vacuo before Et_2O addition precipitated a blue powder. The powder was redissolved in MeOH and chromatographed through a silica gel column (3 x 20 cm) with MeOH as the eluent. The blue fractions were combined and the solvent was reduced, followed by precipitation with Et_2O to yield a blue powder. The powder was washed with Et_2O and dried in vacuo to yield 0.096 g (0.24 mmol, 24%) **[Cu-1'-Ac_2]$_2$** solid. The product had identical properties as described above.

1,4-diazacycloheptane-1,4-diylbis(3-thiapentanoic) iron(II), (Fe-1'-Ac_2).

1) Iron N_2S_2 Templated Synthesis. A sample of **[Fe-1']$_2$** (0.250 g, 0.456 mmol) within a 250 mL Schlenk flask, was degassed prior to the addition of 75 mL of dry MeOH, producing a brown solution. Sodium iodoacetate, Na^+IAc^-, (0.475 g, 2.28 mmol) in 30 mL dry MeOH was added via cannula to the stirring **[Fe-1']$_2$** solution. The solution

became a cloudy yellow/brown and was allowed to react overnight; solvent was reduced in vacuo, and then filtered to remove NaI formed. The solution was purified by silica column chromatography using MeOH as the eluent, the second yellow band was collected. The volume was reduced and product precipitated upon ether addition. The powder was collected by anerobic filtration, washed 3x with ether, and dried in vacuo to yield 0.259 g (0.659 mmol 72%) **Fe-1'-Ac_2** solid. ESI-mass spectrum in CH_3OH: $[M + H^+]^+$ m/z = 391. UV-Vis (CH_3OH): λ_{max}, nm (ε, $M^{-1}cm^{-1}$) = 346 (2660), 280 (1560) nm. IR (in CH_2Cl_2, cm^{-1}): 1631 (vs, sharp), 1348 (m), 1327 (m).

2) Iron Ion Exchange into Zn-1'-Ac_2. Transmetallation between Fe^{2+} and **Zn-1'-Ac_2** doesn't appear to occur.

3) Ligand Synthesis Followed by Addition of $FeSO_4$. The H_2bme-dach (0.250 g, 1.13 mmol) was placed in a 250 mL Schlenk flask and 20 mL of dry MeOH was added. To this flask, Na^+IAc^- (0.520 g, 2.50 mmol) in 20 mL dry MeOH was added. The pale yellow solution was magnetically stirred for 18 h before it was used *in situ*. Then $FeSO_4$ (0.317 g, 1.13 mmol), in 25 mL of dry MeOH, was added to the ligand solution, whereupon a yellow solution and an off-white precipitate developed. After overnight stirring the solution was anerobically filtered and solvent was reduced in vacuo. The solution was purified as above in the templated synthesis to yield 0.294 g (0.753 mmol 66%) **Fe-1'-Ac_2** solid. The product had identical characterization as above.

4.2.4 Control Reactions: Metal Exchange between N_2S_2 Bound and Nitrate Salts

1) $[Co\text{-}1']_2$ + $Ni(NO_3)_2$. The cobalt dimer **$[Co\text{-}1']_2$** (0.050 g, 0.18 mmol) and $Ni(NO_3)_2$ (0.052 g, 0.18 mmol) were added to a 30 mL vial and degassed followed by addition of 20 mL of MeOH. The solution was stirred overnight both at 22 ^oC (trial 1) and 70 ^oC (trial 2), no changes in UV-Vis spectra were observed.

2) $[Co\text{-}1']_2$ + $Ni(NO_3)_2$ + Na^+ CH_3COO^-. A 30 mL vial was charged with the cobalt dimer **$[Co\text{-}1']_2$** (0.050 g, 0.18 mmol), $Ni(NO_3)_2$ (0.052 g, 0.18 mmol), and 2/5 equiv. of NaOAc (0.0060 g, 0.073 mmol) and degassed before the addition of 20 mL of MeOH. The resulting mixture was stirred overnight at 22 ^oC. No change was observed in the UV-Vis when compared to control reactions in 1, so an additional 8/5 equiv. of NaOAc (0.023 g, 0.29 mmol) in 5 mL MeOH was added and the mixture stirred overnight. Again, no change was observed so 18 equiv. of NaOAc (0.27 g, 3.3 mmol) in 10 mL MeOH was added and stirred overnight. No changes were observed.

3) $[Co\text{-}1']_2$ + $Ni(NO_3)_2$ + Na^+ CH_3COO^- with heating. The above reaction conditions were repeated with the reaction stirring at 70 ^oC overnight. No changes observed.

4) $[Co\text{-}1']_2$ + $Ni(NO_3)_2$ + Na^+ ICH_2COO^-. The cobalt dimer **$[Co\text{-}1']_2$** (0.050 g, 0.18 mmol), $Ni(NO_3)_2$ (0.052 g, 0.18 mmol), and 2/5 equiv. of Na^+ ICH_2COO^- (0.015 g, 0.072 mmol) were added to a 30 mL vial and degassed. Then 20 mL of MeOH was added and the solution stirred overnight at 22 °C. As no change was observed when compared to control reaction 1, an additional 8/5 equiv. of Na^+ ICH_2COO^- (0.060 g, 0.29 mmol) in 5 mL MeOH was added and stirred overnight. Again, no change was observed

a further 18 equiv. of Na^+ ICH_2COO^- (0.68 g, 3.25 mmol) in 10 mL MeOH was added and the solution was stirred overnight. The reaction mixture was then purified by silica gel column chromatography. The blue band was collected and reduced in vacuo. Et_2O was added and the mixture left overnight at 22 ^oC to isolate 0.041 g (0.10 mmol, 58 %) of **Ni-1'-Ac_2**.

5) Co-1' + Ni^{2+} + $NaO_2C_2H_2I$ with heating. The above reaction conditions were repeated with the reaction stirring at 70 ^oC and purified by the same means to yield 0.043 g (0.11 mmol, 59 %) of **Ni-1'-Ac_2**.

6) Ni-1'-Ac_2 + $Co(NO_3)_2$. Ni-1'-Ac_2 (0.050 g, 0.13 mmol) and $Co(NO_3)_2$ (0.037 g, 0.13 mmol) were added to a 100 mL Schlenk flask which was degassed prior to the addition of 25 mL MeOH. No exchange product was observed by UV-Vis spectroscopy so an additional 9 equiv. of $Co(NO_3)_2$ (0.33 g, 1.14 mmol) in 10 mL MeOH was added and stirred for 6 h. No product formation was observed by UV-Vis analysis so a further 90 equiv. of $Co(NO_3)_2$ (3.33 g, 11.44 mmol) in 15 mL was added. The reaction volume was reduced in vacuo and purified by silica gel column chromatography using MeOH as an eluent. The $M(NO_3)_2$ salts elute first and a blue/purple band eluted second. The blue/purple band was collected and volume reduced in vacuo. UV-Vis and mass spec analysis was used to quantify the amount of **Co-1'-Ac_2** (18 - 19 %) formed since the **M-1'-Ac_2** species cannot be separated from one another.

7) Ni-1' + Zn-1'-Ac_2. Ni-1' (0.050 g, 0.18 mmol) and **Zn-1'-Ac_2** (0.072 g, 0.18 mmol) were added to a 100 mL Schlenk flask, degassed, and 50 mL of MeOH was added yielding a brown solution. After stirring overnight at room temperature no **Ni-1'-**

Ac_2 formation was observed by UV-Vis spectroscopy. The solution was then stirred overnight at 70 ^oC and still no **Ni-1'-Ac_2** was observable by UV-Vis spectroscopy.

4.2.5 X-ray Diffraction Analysis.

The X-ray data for **Ni-1'-AA_2**, **Co-1'-Ac_2**, **Fe-1'-Ac_2**, and **[Cu-1'-Ac_2]$_2$** were obtained on a single-crystal APEX2 CCD diffractometer (Mo Kα radiation, λ = 0.71073 Å) in the X-ray Diffraction Laboratory at Texas A&M University. Crystal samples were coated in mineral oil, affixed to a Nylon loop, and placed under streaming N_2 (110/150 K). The structures were solved by direct methods. H atoms were placed at idealized positions and refined with fixed isotropic displacement parameters, and anisotropic displacement parameters were employed for all non-hydrogen atoms. The following programs were used: data collection and reduction, APEX2;[322] absorption correction SADABS;[323] cell refinement SHELXTL;[324] structure solutions, SHELXS-97;[324] and structure refinement, SHELXL-97.[324] The final data presentation and structure plots were generated in X-Seed Version 2.0.[325] CIF files were prepared for publication using WinGX and its included programs.[326] Data acquisition and refinement data are in Supporting Information.

4.3 Results and Discussion

4.3.1 Molecular Structure X-ray Diffraction Analysis

The **Co-1'-Ac_2**, **Fe-1'-Ac_2**, and **[Cu-1'-Ac_2]$_2$** crystals were obtained from layering a methanol solution with diethyl ether with product from the template, ligand synthesis, or ligand synthesis routes, respectively; crystallizing as racemic mixtures in the P-1 (triclinic), P-1 (triclinic), and C 2/c (monoclinic) space groups, respectively. The former two co-crystallize with two MeOH molecules that are H-bonded to the free carboxylate oxygens, vide infra.

Figures 4-4 shows the thermal ellipsoid renderings for the **Fe-1'-Ac_2** and **Co-1'-Ac_2** structures. The distorted octahedral **Co-1'-Ac_2** molecule contains a near perfect N(1)N(2)S(1)S(2) plane with a mean atom deviation of 0.013 Å (without Co). The cobalt center is displaced from the best N_2S_2 plane by 0.004 Å. The Fe analog contains an average deviation of 0.0105 Å from the N_2S_2 plane and the Fe displacement is 0.012 Å. Note that the O—M—O angles are $\neq 180^o$ and are bent toward the M—S side of the molecule as observed in the previously reported Zn and Ni analogs.

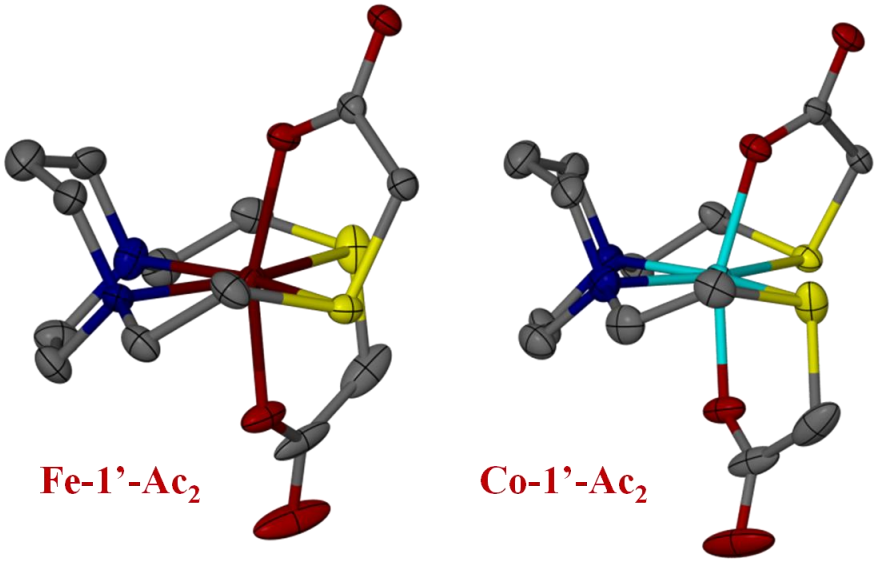

Figure 4-4. Thermal ellipsoid plots shown at 50% for the **Fe-1'-Ac_2** and **Co-1'-Ac_2** molecular structures.

a)

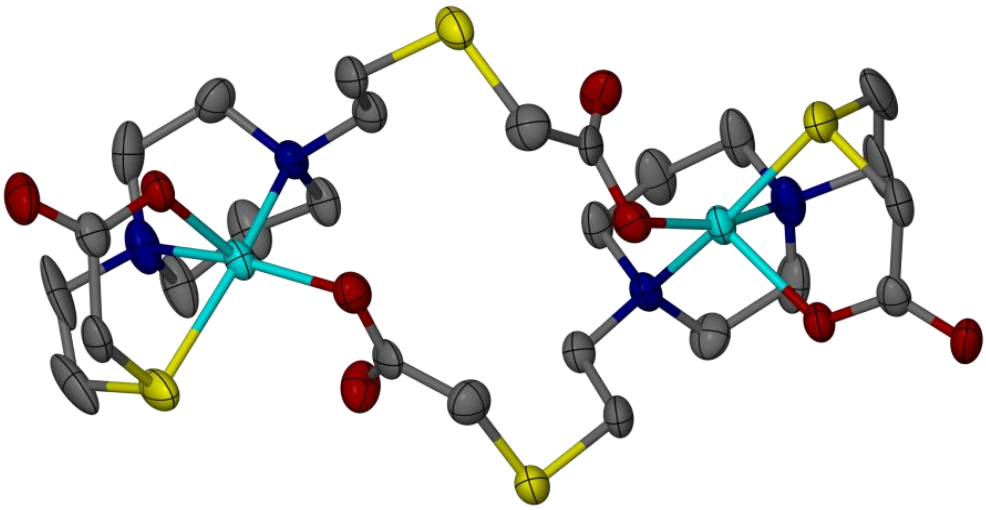

b)

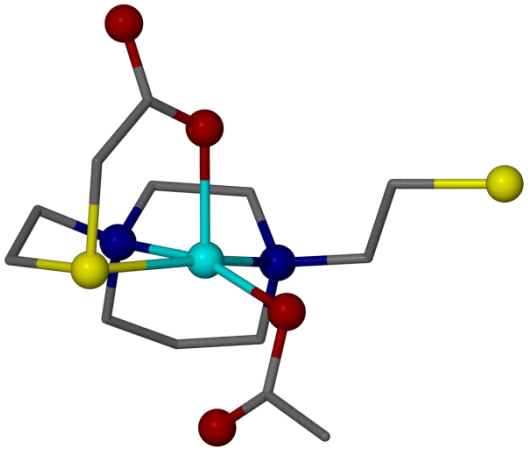

Figure 4-5. Thermal ellipsoid plots of **[Cu-1'-Ac_2]$_2$** molecular structure showing a) the carboxylate bridged dimer and b) one unit of the dimer.

The [**Cu-1'-Ac$_2$]$_2$** complex exists as a dimer resulting from dissociation of one of the thioether arms which allows the carboxylate oxygen to bridge to a second copper center, Figure 4-5. The copper center shows a distorted square pyramidal structure, CuN_2SO_2, with a τ value of 0.022 and contains an almost ideal N(1)N(2)O(1)S(2) plane with a mean atom deviation of 0.0548 Å. The Cu metal center is displaced from this N_2OS best plane by 0.211 Å and the Cu—Cu distance is 7.191 Å. Also of note are the two N_2OS planes present in the **[Cu-1'-Ac$_2$]$_2$** dimer intersect at an angle of 64.56^o. Table 4-1 lists selected bond distances and angles of the **M-1'-Ac$_2$** complexes.

Trends in the molecular structures from Fe → Zn are as follows. Table 4-1 compares selected crystallographic data and metric parameters for the three new complexes of this study with **Ni-1'-Ac$_2$** and **Zn-1'-Ac$_2$**.[321] Note that the **Zn-1'-Ac$_2$** is completely analogous to the Co and Fe analogues. The M-S distances from Fe to Cu are found to shrink and then increase at the end with the **Zn-1'-Ac$_2$** complex, which tracks with the periodic trend observed for their ionic radii and as noted by the Irving-Williams Series.[327] The same trend can be seen with the M-N distances; however, the M-O bond distances actually increase across the row as the radii decrease. This is probably a result of the more drastic decrease in M-S distances coupled into the torsion angles through the acetate arm; thus, the oxygen donors are prohibited from moving toward the metal center, but rather shift away as the metal ion gets smaller. Overall, the metric parameters for the **Zn-l'-Ac$_2$** complex fall between those of the **Fe-1'-Ac$_2$** and **Co-1'-Ac$_2$** complexes.

Table 4-1. Selected crystallographic data, bond distances, and angles of **Fe-1'-Ac$_2$**, **Co-1'-Ac$_2$**, **Ni-1'-Ac$_2$**, **[Cu-1'-Ac$_2$]$_2$**, and **Zn-1'-Ac$_2$**.

	Fe-1'-Ac$_2$	**Co-1'-Ac$_2$**	**Ni-1'-Ac$_2$**	**Cu-1'-Ac$_2$**	**Zn-1'-Ac$_2$**
System	Triclinic	Triclinic	Monoclinic	Monoclinic	Triclinic
Point Group	P-1	P-1	P 2_1	C 2/c	P-1
Solvation	2 MeOH	2 MeOH	3 H_2O	1 MeOH	2 MeOH
Z	2	2	4	4	2
R-Factor	5.63 %	4.42 %	5.72 %	4.25 %	3.68 %
M—S$_{avg}$	2.530(2)	2.495(1)	2.399(3)	2.382(2)	2.577(1)
M—N$_{avg}$	2.177(4)	2.135(3)	2.094(7)	2.023(6)	2.165(3)
M—O$_{avg}$	2.023(3)	2.030(2)	2.056(6)	1.962(5)	2.042(3)
∠S—M—S	116.43(4)	112.99(3)	106.02(8)	92.60(1)*	114.80(3)
∠N—M—N	74.5(1)	75.8(1)	77.8(3)	80.1(2)	75.6(1)
∠O—M—O	162.3(1)	160.6(1)	169.2(2)	102.5(2)**	159.1(1)

*∠S—M—O from the N_2SO plane in the **[Cu-1'-Ac$_2$]$_2$** complex.
The oxygen atoms are cis in the [Cu-1'-Ac$_2$]$_2$** structure rather than trans as observed in the other **M-1'-Ac$_2$** structures.

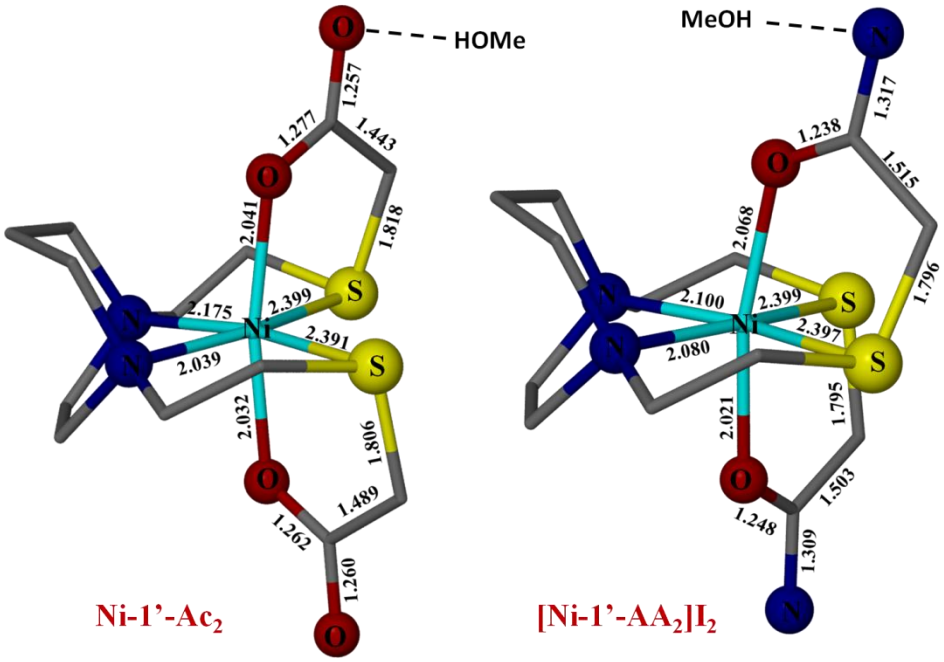

Figure 4-6. Comparison of the metric parameters in **Ni-1'-Ac$_2$** (left) and **[Ni-1'-AA$_2$]I$_2$** (right). Hydrogen atoms, counter ions, and solvent molecules have been removed for clarity.

For comparison of the analogous NiN_2S_2 that is S-modified by acetoamide, AA, the structure of **[Ni-1'-AA$_2$]I$_2$** is shown in Figure 4-6, along with **Ni-1'-Ac$_2$**, and features two I^- counter ions and two methanol solvates in each unit cell. The metric parameters of **[Ni-1'-AA$_2$]I$_2$** largely track with the **Ni-1'-Ac$_2$** structure, the only notable difference being the C—O and C—NH_2 distances. In the **M-1'-Ac$_2$** structures, the C—O bonds are within 0.02 Å of each other; however, in the structure of **Ni-1'-AA$_2$**, a distinction can be seen between the C—O and C—N bonds which differ by almost 0.1 Å. As expected, this

shows the greater extent of delocalization of the π-electrons in the RCO_2^- versus the $RCONH_2$ analog.

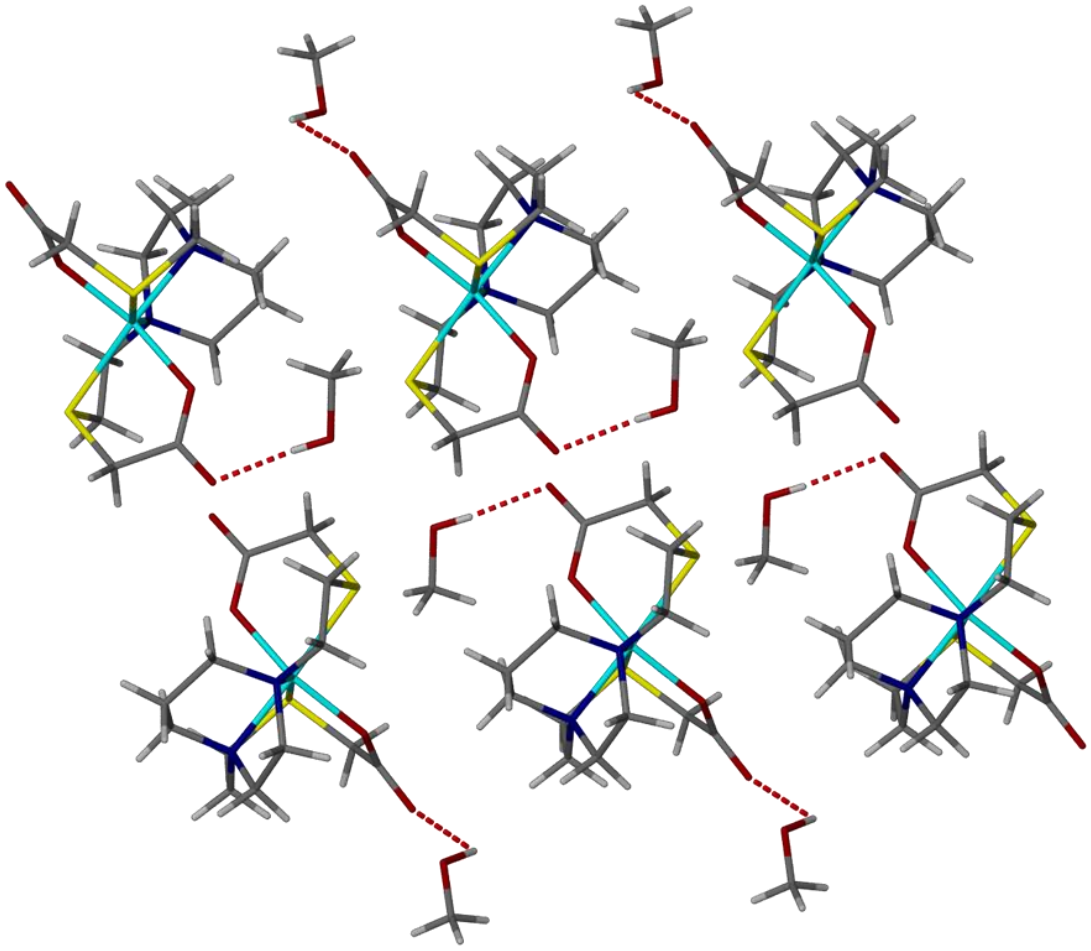

Figure 4-7. Packing diagram of **Co-1'-Ac$_2$** highlighting the typical hydrogen bonding network observed for these complexes in the solid state between the complex and co-crystallized solvent molecules.

All the compounds in the **M-1'-Ac$_2$** and **Ni-1'-AA$_2$** series co-crystallize with MeOH or H_2O in a hydrogen-bonded network. The hydrogen bonding links the solvent molecules and the =O or $–NH_2$ groups that are directed into the interstitial space between molecules. Figure 4-7 shows an example of this hydrogen bonding network in **Co-1'-Ac$_2$**.

4.3.2 Direct Synthesis of M-1'-Ac$_2$ via Reaction of Na^+IAc^- with [M-1']$_2$

The direct synthesis of the **M-1'-Ac$_2$** complexes was performed through acetylation of the thiolate donors of the parent **[M-1']$_2$** complex for comparison to the isolated product from the Zn^{2+}/M^{2+} transmetallation reactions. As shown in Figure 4-8 and similar to the previously reported synthesis of **Ni-1-Ac$_2$**, diacetylated Ni(bme-daco),[328] an excess of $Na^+[ICH_2CO_2]^-$ was reacted with the **[M-1']$_2$** complex in a methanolic solution to yield the **Co-1'-Ac$_2$** and **Fe-1'-Ac$_2$** complexes in 98% and 72% yields respectfully. The ESI-MS, IR acetate stretches, and UV-Vis of the transmetallation products matched the directly synthesized **M-1'-Ac$_2$** complexes.

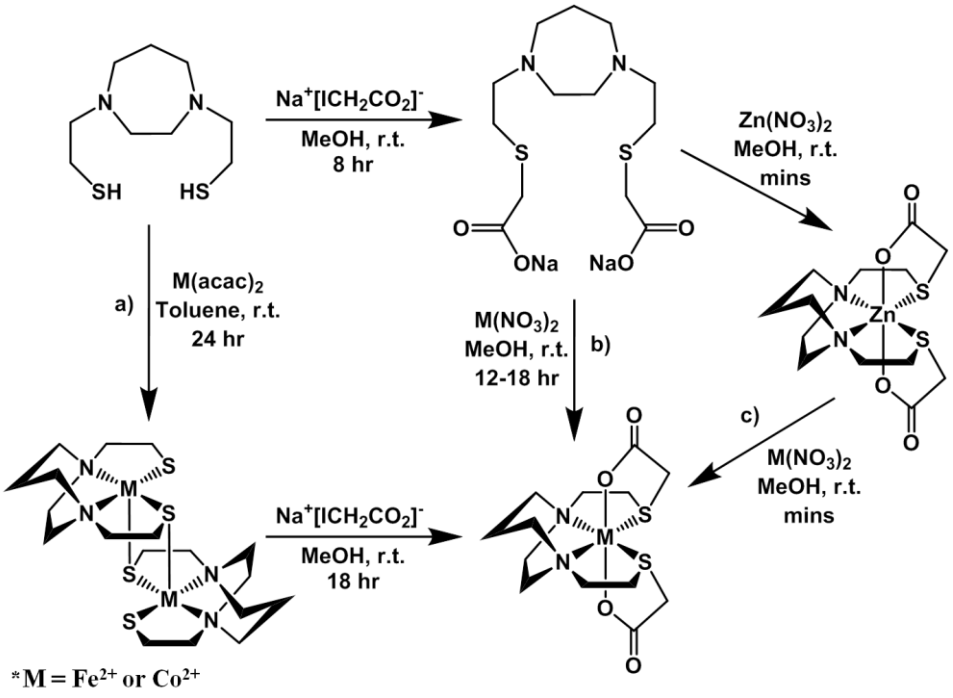

Figure 4-8. Synthetic routes yielding **M-1'-Ac$_2$** complexes: a) templated synthesis from $[MN_2S_2]_2$ precursors; b) direct addition to $N_2S_2O_2^{2-}$ ligand; c) metal exchange with **Zn-1'-Ac$_2$**.

4.3.3 Metallation of Hexadentate Ligand Na$_2$-1'-Ac$_2$ to Form M-1'-Ac$_2$

The hexadentate ligand **Na$_2$-1'-Ac$_2$** was synthesized as previously reported through the reaction of a slight excess of $Na^+[ICH_2CO_2]^-$ with the free H_2bme-dach ligand.[167] A methanolic solution of $M(NO_3)_2$ was added to the ligand solution to form the hexadentate metal complex **M-1'-Ac$_2$**. The products isolated from the $Co(NO_3)_2$ and $Fe(NO_3)_2$ reactions had physical properties matching the directly synthesized **M-1'-Ac$_2$** complexes from the acetylation of the parent **[M-1']$_2$** complex. The product obtained from the reaction of $Cu(NO_3)_2$ with the disodium salt of the hexadentate ligand was

characterized and compared to the product isolated from the Zn/Cu transmetallation reaction mixture. The two synthetic routes to **[Cu-1'-Ac_2]$_2$** yielded identical physical properties.

4.3.4 Zinc/Metal Transmetallation

In a previous study, nickel was shown to rapidly replace zinc in the hexadentate $N_2S_2O_2$ ligand 1'-Ac_2 as shown in Figure 4-3.[321] The addition of a light pink solution of $Co(NO_3)_2$ to a colorless methanolic solution of **Zn-1'-Ac_2** resulted in an immediate color change to a deep magenta color eventually yielding 72 % **Co-1'-Ac_2**. In a similar manner $Cu(NO_3)_2$ was reacted with **Zn-1'-Ac_2** to ultimately yield 30 % **[Cu-1'-Ac_2]$_2$** (deep blue). The characterization of **Co-1'-Ac_2** and **[Cu-1'-Ac_2]$_2$** match the properties of the direct synthesis products. Thus, a transmetallation reaction between the kinetically labile zinc center in **Zn-1'-Ac_2** and an exogenous secondary metal ion occurs with the aid of the acetate arms, similarly to the exchange processes Margerum observed with M(EDTA) complexes.[318]

4.3.5 Control Reactions for Cobalt/Nickel Transmetallation

Previous results[321] combined with the metal exchange work presented here, highlighted the need for control reactions to elucidate the metal exchange process that is occurring. The addition of $Ni(NO_3)_2$ in the presence and absence of sodium acetate to a stirring solution of **[Co-1']$_2$**, both at 22 °C and 70 °C, resulted in the formation of metallo-aggregates rather than a quantitative exchange of metals, Figure 4-9. However,

if $Ni(NO_3)_2$ and $Na^+[ICH_2CO_2]^-$ are added simultaneously to a solution of **[Co-1']$_2$**, pure **Ni-1'-Ac$_2$** could be isolated from the reaction in a 59% yield illustrating that the modification of the thiolate sulfurs through acetylation is necessary to facilitate a clean metal exchange process to occur between the $N_2S_2O_2$ ligand frameworks.

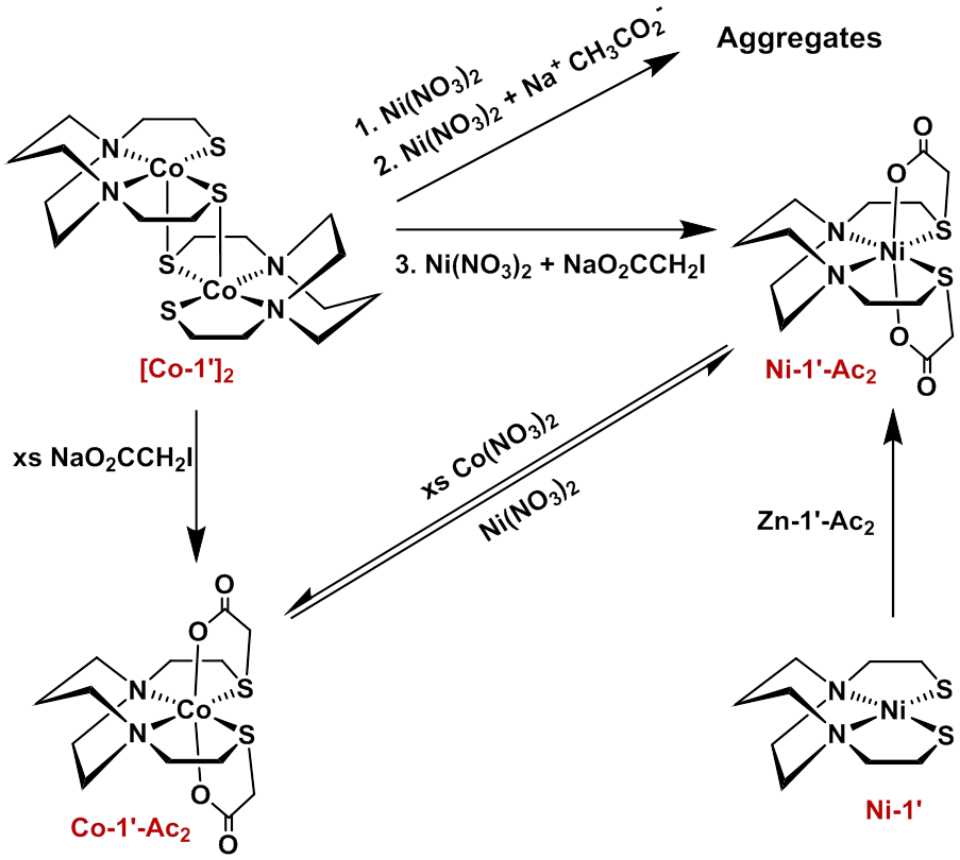

Figure 4-9. Reaction scheme illustrating control reactions that were carried out during the investigation of metal exchange reactions.

The Irving-Williams stability series,[327] determined for octahedral homoleptic complexes with hard N-donors, prescribes that more stable complexes are formed as the ionic radius of the metal decreases. Thus, Ni^{2+} should replace the cobalt center in **Co-1'-Ac$_2$** to yield **Ni-1'-Ac$_2$**; near quantitative yields were observed experimentally. The reverse process of Co^{2+} replacing the nickel in the complex, required a large excess (100x) of added $Co(NO_3)_2$ in order to observe by UV-Vis spectroscopy any formation of **Co-1'-Ac$_2$** in the reaction mixture, Figure 4-9. Upon purification by silica gel chromatography the **M-1'-Ac$_2$** complexes could be separated from the other species present in the reaction mixture. However, due to the extremely similar properties of **Co-1'-Ac$_2$** and **Ni-1'-Ac$_2$** the two could not be separated from each other, thus UV-Vis and mass spectral analyses were used to elucidate the ratio of the two present in the isolated **M-1'-Ac$_2$** band. From the peak intensities of the isotopic bundle observed in the mass spectrum, assuming the ionizability of the two complexes under the mass spectroscopy conditions are equal; and the concentrations calculated from the absorbance bands detected in the UV-Vis, both methods indicate the formation of about 18% **Co-1'-Ac$_2$** leaving 82% **Ni-1'-Ac$_2$** remaining. From this data, equilibrium constants were estimated for the forward (Ni^{2+} replacement of Co^{2+}) and reverse (Co^{2+} replacement of Ni^{2+}) reactions to be 2×10^3 and 1×10^{-8}, respectively. The equilibrium constants measured below were performed in aqueous media.

The exchange properties between two different metallated ligands were also investigated. In the first reaction **Ni-1'** and **Zn-1'-Ac$_2$** were stirred in a methanol solution for 7 days over which time there was no indication of any metal exchange

occurring through MS and UV-Vis analysis. Then, the opposite conditions of a mixture of **Ni-1'-Ac_2** and **[Zn-1']$_2$** were examined. Once again MS and UV-Vis indicated no metal exchange occurring between the two complexes ever after stirring for 7 days.

4.3.6 Properties of M-1'-Ac_2 Complexes

The IR stretches observed for the **M-1'-Ac_2** complexes in CH_2Cl_2 solutions are listed in Table 4-2. All the complexes exhibit a very strong solution IR stretch at ca. 1630 cm^{-1} corresponding to the acetate group. The identity of the bands in the 1300's region are not known with certainty but are presumed to correspond to M-O or C-O stretches.

Table 4-2. IR stretching frequencies of **M-1'-Ac_2** complexes in CH_2Cl_2.

Assignment / Complex	C=O	M-O/C-O	M-O/C-O
Zn-1'-Ac_2	1630	1350	1331
Cu-1'-Ac_2	1631	1347	1329
Ni-1'-Ac_2	1625	1349	1333
Co-1'-Ac_2	1626	1348	1327
Fe-1'-Ac_2	1631	1348	1327
Cd-1'-Ac_2[a]	1710	1359	1221

[a] The identity of these bands is not known for certain but presumed to correspond to either M-O or C-O stretches.

As described in the experimental section, Gouy balance and Evans method magnetic studies established that the octahedral complexes of Cu^{2+}, Ni^{2+}, Co^{2+}, and high-

spin Fe^{2+} are paramagnetic with experimental magnetic moments largely matching the expected $\mu_{s.o.}$ values; the Zn^{2+} derivative is diamagnetic, d^{10}. The cyclic voltammograms for **Ni-1'-Ac$_2$** and **Co-1'-Ac$_2$** are shown in Figures 4-10 and 4-11, respectively. Both complexes show a reversible oxidation event which is assigned as the Ni^{2+}/Ni^{3+} (0.69 V) and Co^{2+}/Co^{3+} (-0.24 V) couple. An irreversible event is seen at -2.33 V and -2.31 V for **Ni-1'-Ac$_2$** and **Co-1'-Ac$_2$**, respectively. Data relating to reversibility are as follows: For the **Ni-1'-Ac$_2$**, E_{pa}, E_{pc}, ΔE, and i_{pc}/i_{pa} are 0.656 V, 0.716 V, 60 mV, and 0.41, respectively; and for **Co-1'-Ac$_2$**, -0.390 V, -0.090 V, 300 mV, and 0.74, respectively.

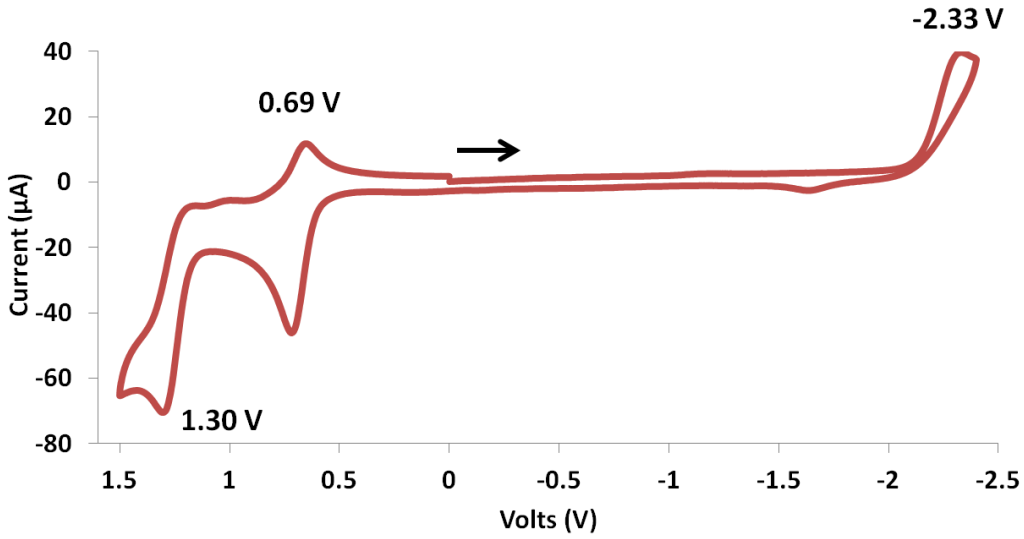

Figure 4-10. Cyclic voltammagram of **Ni-1'-Ac$_2$** in MeCN at a scan rate of 100 mV/s. $E_{1/2}$ is given in the Figure as 0.686 V.

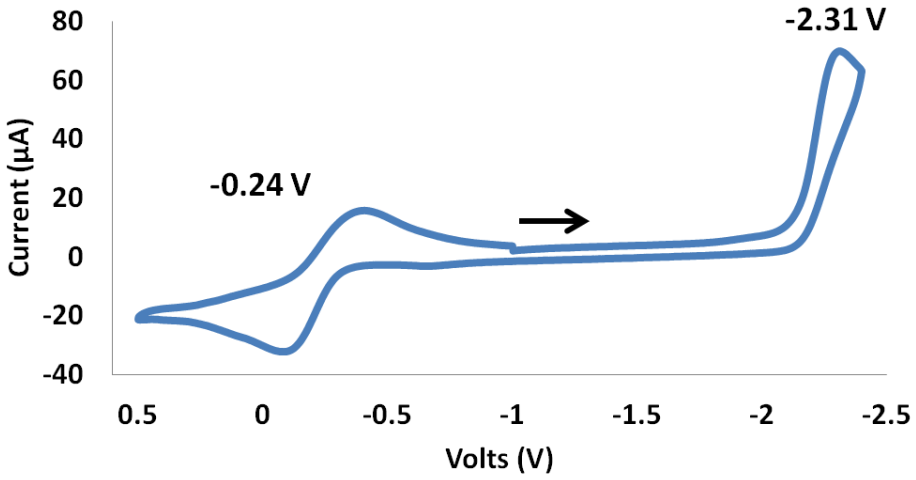

Figure 4-11. Cyclic voltammagram of **Co-1'-Ac$_2$** in MeCN at a scan rate of 100 mV/s. $E_{1/2}$ is given in the Figure as -0.240 V.

4.3.7 Equilibrium Constants

Attempts were made to measure equilibrium constants of the metal exchange reactions in aqueous solutions using UV-Vis spectroscopy. Metal salts, see Table 4-3, and **M-1'-Ac$_2$** complexes, dissolved in water, were combined in a 1:1 ratio at 0.007-0.008 M concentrations and allowed to equilibrate for 3 hrs at room temperature. The UV-Vis spectra were then recorded and, in combination with molar absorptivity values at selected wavelengths, Appendix C, the concentrations of the species in solution at equilibrium were calculated. An assumption was made that all exchange reactions were a simple conversion according to the equation:

$$\mathbf{M\text{-}1'\text{-}Ac_2 + M'(H_2O)_x^{2+} \rightleftharpoons M'\text{-}1'\text{-}Ac_2 + M(H_2O)_x^{2+}}$$

$$K_{eq} = \frac{[M'1'Ac_2][M^{2+}]}{[M1'Ac_2][M'^{2+}]}$$

Thus, the equilibrium constants shown in Table 4-3 assumed that each metal is contained in one of the two forms shown above and not as any aggregates or mixed metal complexes, see Appendix D for equations used. In the following discussion, the exchange pairs are expressed as M-1'-Ac_2/M'^{2+} → M'-1'-Ac_2/M^{2+} and shortened to M/M' and M'/M, respectively.

Table 4-3. Equilibrium constants measured in water by UV-Vis spectroscopy at 0.007-0.008 M concentrations and 22 °C for metal exchange reactions. Each reaction was performed three times and the average of the trials along with standard deviation is reported.

	$Zn(BF_4)_2$	**$CoSO_4$**	**$NiSO_4$**
Zn-1'-Ac_2		5.48 ± 0.80	220 ± 40
Co-1'-Ac_2	0.20 ± 0.03		210 ± 120
Ni-1'-Ac_2	0.01 ± 0.009	0.0002 ± 0.0004	

The fundamentals of equilibria require that the forward reaction and reverse reaction should have equilibrium constants that are mathematical inverses of each other. In my experiments this is realized for the Zn/Co and Co/Zn exchange pairs and within the error of measurement for the Zn/Ni and Ni/Zn exchange pairs. However the Co/Ni

(210) and Ni/Co (0.0002) exchange pairs are not consistent with this expectation. Should the former value be accurate, the expected Ni/Co equilibrium constant would be 0.005 and if the latter is accurate then the Co/Ni would be 5000. In my opinion, the experimental errors correspond to problems of measuring molar absorptivity values and with accurately measuring out small volumes. Such errors limited accurate measurement for the small Ni/Co equilibrium value. The presence of four UV-Vis active species in solution further complicates accurate measurements of the equilibrium constants using the available techniques. For example, the molar absorptivity used for the **Ni-1'-Ac$_2$** complex at 575 nm is 23.0 $M^{-1}cm^{-1}$ but if this value was changed to 23.4 $M^{-1}cm^{-1}$ which is a very small change and within the errors of measuring molar absorptivities, the equilibrium constant for the Ni/Co exchange would indeed be 0.005.

Overall, the values are not precise but serve to highlight the exchange hierarchy observed, which is consistent with the Irving-Williams series $Zn^{2+} < Co^{2+} < Ni^{2+}$.[327] More accurate measurements might be made by performing a greater number of trials for molar absorptivity values and equilibrium constants to minimize the possible errors in measurements throughout the experiment.

4.3.8 Kinetic Studies

A monitor for the addition of $Cu(NO_3)_2$ to a MeOH solution of **Zn-1'-Ac$_2$** is shown in Figure 4-12. The reaction is complete at the time of mixing and thus is too fast to obtain rates by our available techniques. This is also the case with the other Zn/M transmetallation reactions. Thus, the displacement of **Co-1'-Ac$_2$** by Ni^{2+} in MeOH was

chosen as a reaction slow enough for kinetic monitoring since these two metals are closer together in the Irving-Williams series. Figures 4-13 and 4-14 display full UV-Vis scans for this metal exchange reaction, changing which reactant was under pseudo first order conditions. Figure 4-13 includes an inset showing the UV-Vis spectra of pure **Co-1'-Ac$_2$** and **Ni-1'-Ac$_2$**. A ten-fold excess of **Co-1'-Ac$_2$** reacted with Ni^{2+} in MeOH show UV-Vis absorptions at 362 and 845 nm increase while a peak at 487 nm decreases in absorbance, Figure 4-13. If the opposite molar ratio is used (1 **Co-1'-Ac$_2$**: 10 Ni^{2+}) then the peaks at 362, 580, and 845 nm increase corresponding to the formation of **Ni-1'-Ac$_2$**; the peak at 487 nm decreases as **Co-1'-Ac$_2$** undergoes metal exchange, Figure 4-14.

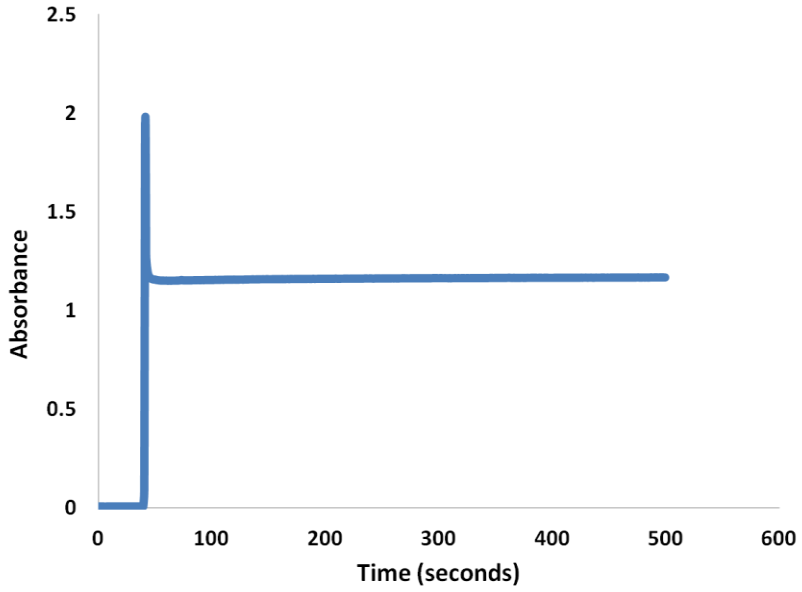

Figure 4-12. UV-Vis monitoring in MeOH of the Cu/Zn transmetallation reaction with the molar ratio of reactants 50:1, respectively. Reaction followed the band at 607 nm corresponding to **[Cu-1'-Ac$_2$]$_2$**. Time of injection corresponds to the spike in the spectra from the baseline where only spectroscopically silent Zn was present.

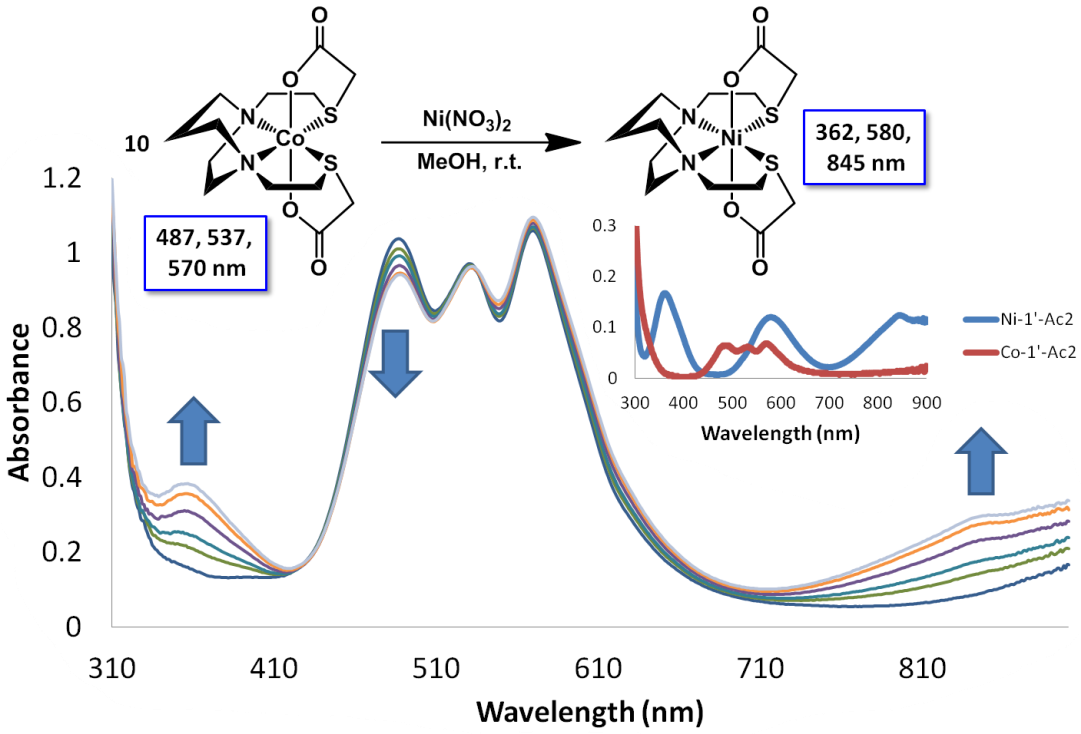

Figure 4-13. UV-Vis traces in MeOH for the reaction of Ni^{2+} with a ten-fold excess of **Co-1'-Ac$_2$**. An inset shows the UV-Vis spectra for the pure **Ni-1'-Ac$_2$** and **Co-1'-Ac$_2$**. The peaks at 362 and 845 nm increase as a result of **Ni-1'-Ac$_2$** formation and a decrease at 487 nm as **Co-1'-Ac$_2$** undergoes transmetallation. Reaction was monitored until no further change in the UV-Vis was observed, requiring approximately 20 mins at room temperature.

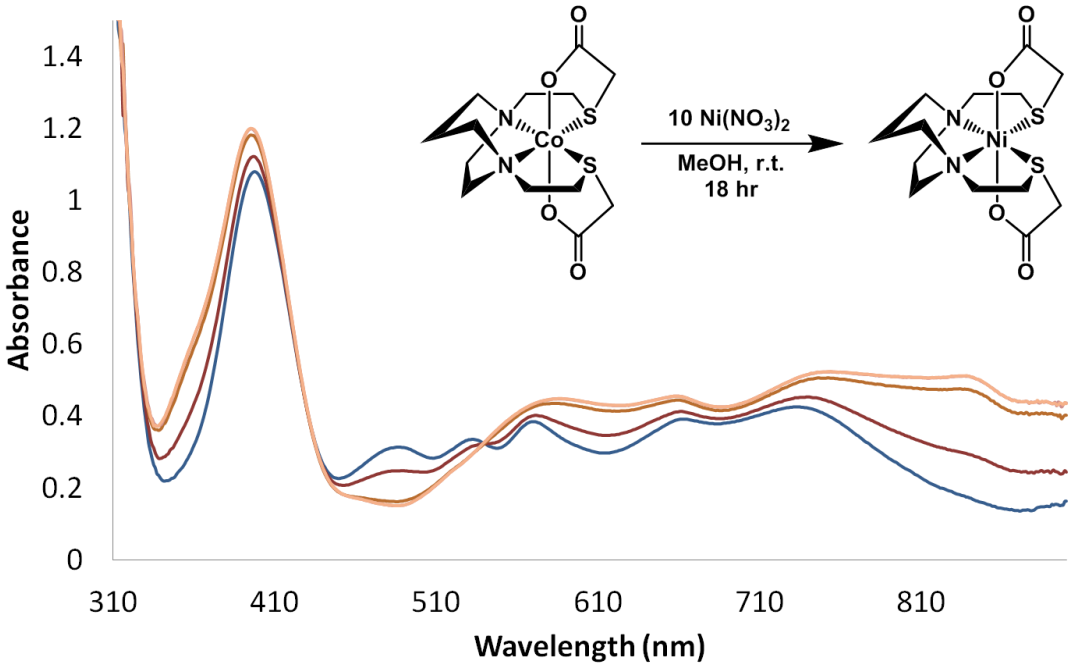

Figure 4-14. UV-Vis traces in MeOH for the reaction of a ten-fold excess of Ni^{2+} with **Co-1'-Ac$_2$** at ambient temperature, ca. 22 °C. The blue line corresponds to the spectra at the time of mixing and the orange line at completion, over the course of approximately 20 mins following which no further changes were observed.

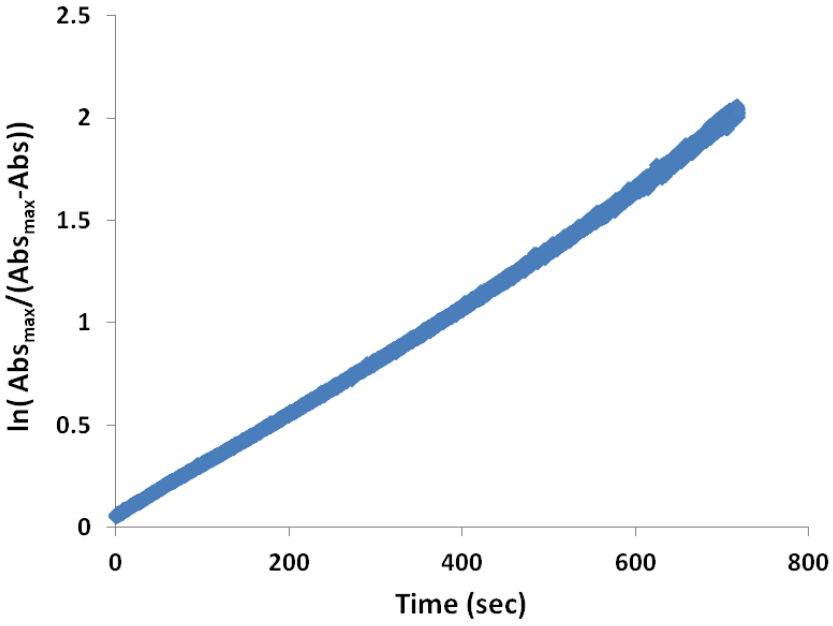

Figure 4-15. Plot of the natural log of the absorbance at 845 nm versus time for the reaction of a 25-fold excess of $Ni(NO_3)_2$ with **Co-1'-Ac$_2$** at room temperature. A linear trend consistent with a first-order dependence on **Co-1'-Ac$_2$**, gives a k_{obs} value of 2.65 x 10^{-3} s^{-1} calculated from the slope.

In a typical experiment the **Co-1'-Ac$_2$** concentration was 0.005 M and the $Ni(NO_3)_2$ was at concentrations of 12.5, 25, or 50 times higher. The reactions were monitored at ambient temperature by a UV-Vis band appearing at 845 nm with data collection started as soon as the two solutions were injected into the cuvette, and followed until completion. The natural log plot of the absorbance, which is indicated by the value at 845 nm, versus time, Figure 4-15, indicates that the reaction is first order in complex when the Co/Ni ratio is 1:25.

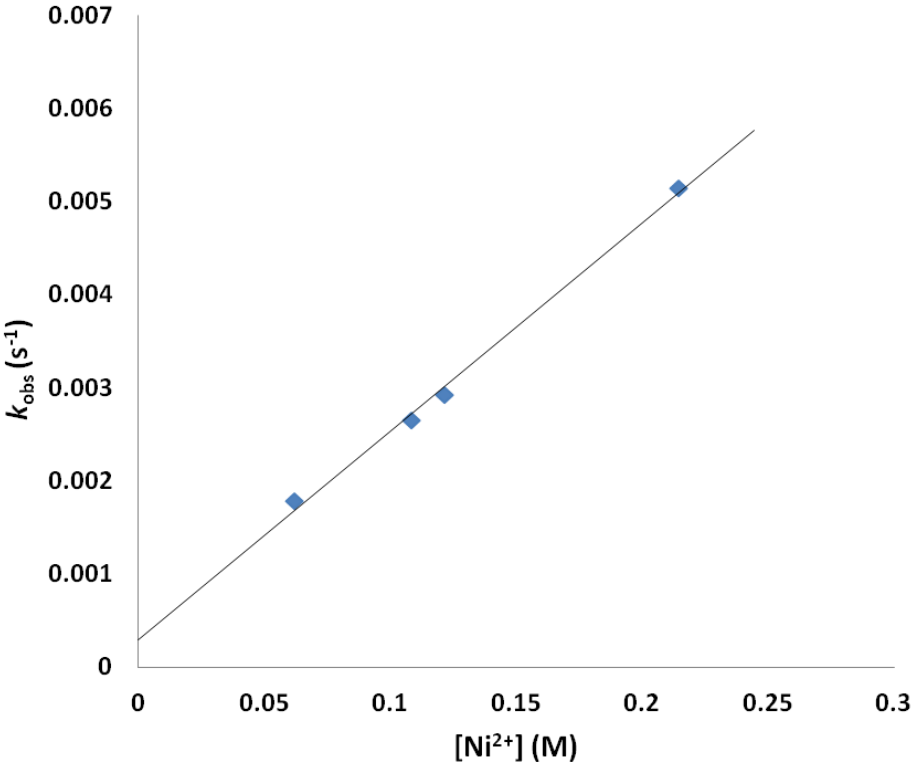

Figure 4-16. Plot of k_{obs} vs [Ni^{2+}] at 298 K for the formation of **Ni-1'-Ac$_2$**. The R^2 value is 0.996.

The order of reaction dependence of Ni^{2+} was determined by monitoring the exchange at multiple concentrations of excess Ni^{2+}. A plot of k_{obs} vs [Ni^{2+}], Figure 4-16, is linear with a y-intercept of nearly zero indicating a first-order dependence for Ni^{2+}. Thus, the complete bimolecular rate law is shown below with a first order dependence of both **Co-1'-Ac$_2$** and Ni^{2+}.

$$\boldsymbol{rate = k_{obs}[Co1'Ac_2]^1}$$

$$\boldsymbol{k_{obs} = k[Ni^{2+}]^n}$$

$$\boldsymbol{rate = k[Co1'Ac_2]^1[Ni^{2+}]^1}$$

The temperature dependence of the rate constant, k, was measured over a 37.5 K range (286-313 K), Figure 4-17, for the conversion of **Co-1'-Ac$_2$** to **Ni-1'-Ac$_2$** when reacted with a large excess of Ni^{2+} (1:25). During these experiments the **Co-1'-Ac$_2$** solution was allowed to come to temperature in the temperature-controlled cuvette holder before injection of the $Ni(NO_3)_2$ solution. Prior to injection, the $Ni(NO_3)_2$ solution was adjusted to the proper temperature using a water bath. The resulting temperatures, k_{obs}, and k values are shown in Table 4-4.

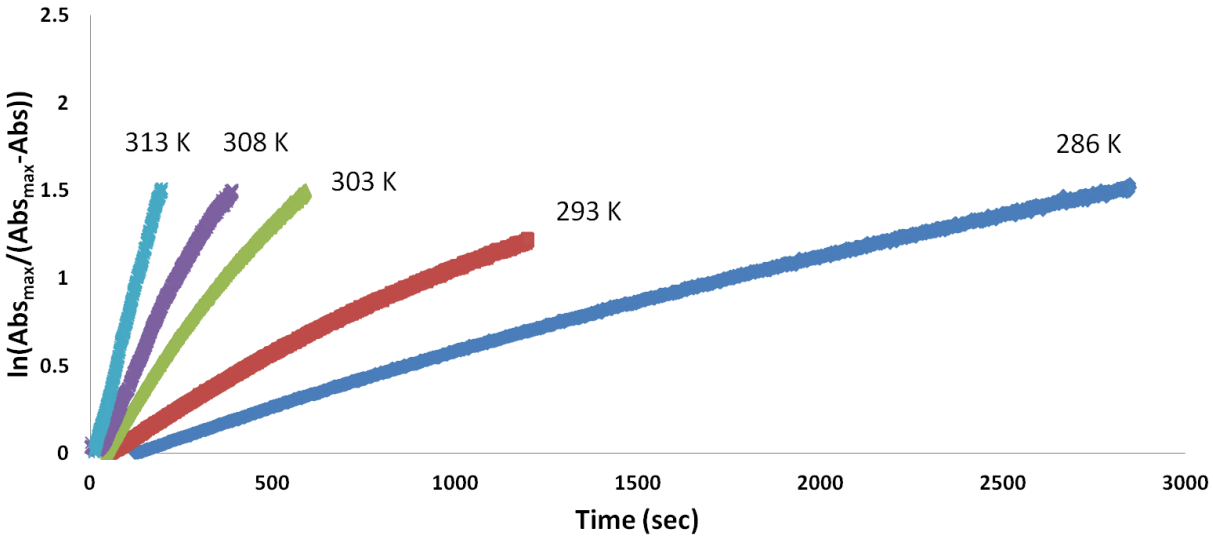

Figure 4-17. Natural log plots of absorbance data vs. time for the formation of **Ni-1'-Ac$_2$** at various temperatures from the reaction of **Co-1'-Ac$_2$** and excess $Ni(NO_3)_2$.

Table 4-4. Kinetic parameters obtained from the natural log plots from varying temperature for the reaction of **Co-1'-Ac_2** with excess $Ni(NO_3)_2$. The concentration of **Co-1'-Ac_2** was 4.75 x 10^{-3} M and $Ni(NO_3)_2$ was 0.119 M.

T (K)	k_{obs} (s^{-1})	k (M^{-1} s^{-1})
285.65	7.32 x 10^{-3}	4.65 x 10^{-3}
293.15	3.93 x 10^{-3}	9.04 x 10^{-3}
303.15	2.54 x 10^{-3}	2.14 x 10^{-2}
308.15	1.07 x 10^{-3}	3.31 x 10^{-2}
313.15	5.51 x 10^{-4}	6.17 x 10^{-2}

The activation parameters for the formation of **Ni-1'-Ac$_2$** were determined by an Eyring analysis which found $\Delta H^{\ddagger}$ of 15.7 ± 0.7 kcal/mol and a $\Delta S^{\ddagger}$ of -14.3 ± 2.3 e.u., Figure 4-18. The $\Delta G^{\ddagger}$ can be calculated as 19.9 ± 0.7. The small $\Delta H^{\ddagger}$ and negative $\Delta S^{\ddagger}$ values are indicative of an associative mechanism for the Co/Ni transmetallation reaction, consistent with the bimolecular rate law above.

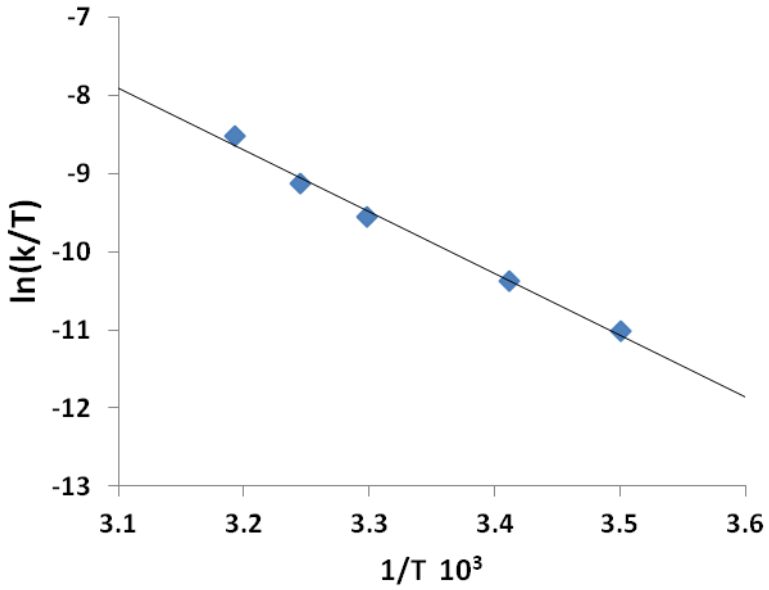

Figure 4-18. Eyring plot obtained from the dependence of *k* on temperature. The equation for the best-fit line is y = -7.8938x + 16.557 with an R^2 value of 0.993.

4.4 Conclusions

The N_2S_2 ligand binding site has been found to be largely inert to metal exchanges rather yielding metal aggregation products of various structural types. The tight binding characteristic of the tetradentate N_2S_2 ligands are lessened on S-alkylation.

For example, S-methylation of $[Zn(bme\text{-}dach)]_2$ with MeI results in deligation of the newly formed thioethers and coordination of the iodide ions yielding a tetrahedral ZnN_2I_2, Figure 4-19. However, if the alkylation agent has additional donor atoms within the ligand framework as in the iodoacetamide and iodoacetate agents, the chelate effect will keep the poor thioether donors bound to the Zn in a hexacoordinate, octahedral $ZnN_2S_2O_2$ site. This S-modification with sodium iodoacetate can render the metal center labile and replaceable by exogenous metal ions through interaction with the available carboxylate oxygen atom. This interaction can cause a ligand unwrapping/rewrapping process to occur leading to facile metal exchange rather than aggregation products.

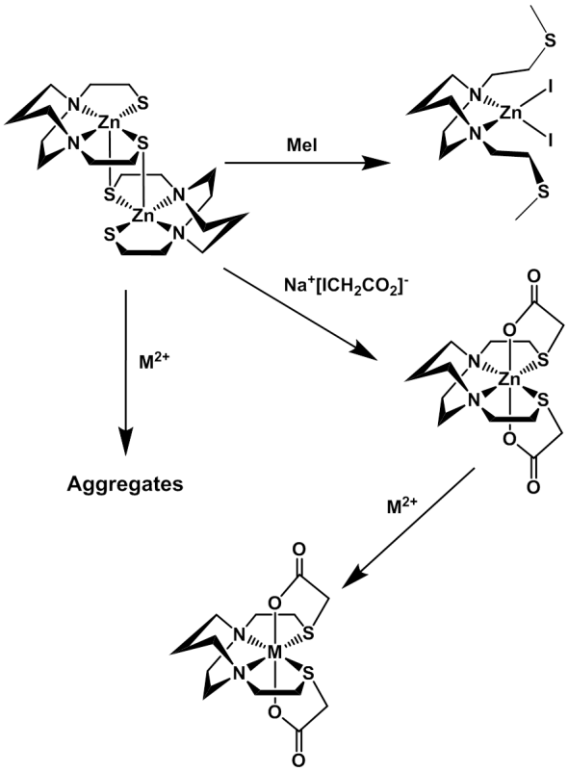

Figure 4-19. Reactivity of $[Zn(bme\text{-}dach)]_2$ toward alkylation or metallation.

Three new **M-1'-Ac$_2$** complexes were synthesized and characterized with M = Co^{2+}, Fe^{2+}, and Cu^{2+}. The cobalt and iron complexes were isostructual with the previously reported nickel and zinc complexes. However, the copper complex forms a unique dimeric structure. The series of **M-1'-Ac$_2$** complexes was shown to undergo metal exchange reaction in a hierarchy prescribed by the Irving-William series of stability: $Fe^{2+} < Co^{2+} < Ni^{2+} < Cu^{2+} > Zn^{2+}$. Nevertheless, there appears to be an equilibrium established during metal exchange reactions that prevents a quantitative conversion. A mechanistic hypothesis for the metal exchange reactions involves the exogenous metal ion first interacting with the unbound oxygen of the acetate group. The ligand will then undergo an unwrapping and re-wrapping process from the initial metal center to the new exogenous metal similar to the mechanism shown in Figure 4-20. The rate-limiting step should be the breaking of the M-N bonds. An important feature of these systems that allows such facile metal exchange to occur is the "taming" of the thiolates in the parent **M-1'** complex by conversion into thioethers, which decreases their nucleophilicity and metal savaging ability.

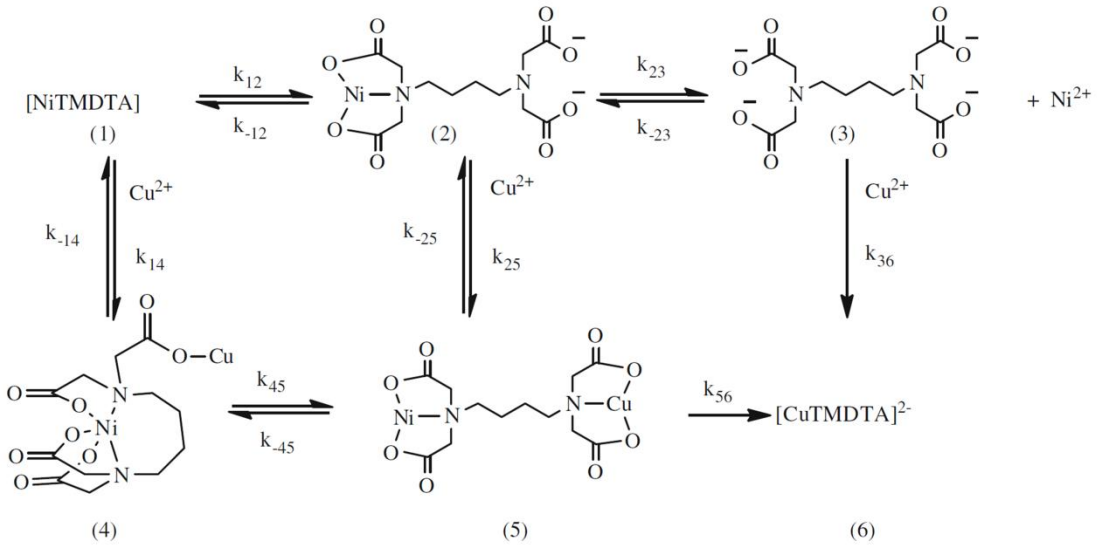

Figure 4-20. Mechanistic scheme proposed for the exchange of Ni^{2+} for Cu^{2+} in tetramethylenediaminetetraacetato-nickel.[350]

5. X-RAY DIFFRACTION MEASUREMENTS ON BIOMIMETIC COMPLEXES

5.1 Introduction

X-ray diffraction (XRD) studies were performed on a series of biomimetic complexes and other compounds isolated and crystallized as side products. The XRD studies were carried out using three different diffractometers available at Texas A&M University during my PhD work: Bruker Smart 1000 using MoKα radiation (0.71073 Å), Bruker APEX2 using MoKα radiation (0.71073 Å), and Bruker GADDS using CuKα (1.54059 Å) radiation. All crystals were coated in paraffin oil, mounted on a nylon loop, and placed under streaming N_2 (110/150 K). The space groups were determined by systematic absences and intensity statistics, and structures were solved by direct methods and refined by full-matrix least-squares on F^2. Anisotropic displacement parameters were employed for all non-hydrogen atoms; H atoms were placed at idealized positions and refined with fixed isotropic displacement parameters. The following programs were used: cell refinement, data collection, data reduction, APEX2;[322] absorption correction, SADABS;[323] structure solutions, SHELXS-97;[324] and structure refinement, SHELXL-97.[324] The final data presentation and structure plots were generated in X-Seed Version 2.0.[325] CIF files were prepared for publication using WinGX and its included programs.[326]

The structures within this section are organized into subcategories which include [FeFe]-H_2ase active site model compounds, MN_2S_2 complexes and derivatives, nitrosyl-containing iron and cobalt compounds, other inorganic compounds, salts, and organic

ligands. The [FeFe] category is further organized into carbon and nitrogen based μ-SCH_2XCH_2S-μ dithiolate bridges with increasing CO substitution on the iron. The MN_2S_2 compounds are sorted by the free MN_2S_2 metalloligands, S-metallated poly-metallics, and thiolate S-alkylation. The nitrosyl complexes are sorted by reduced and oxidized DNIC's followed by cobalt compounds.

All structures are presented as thermal ellipsoids shown at 50% probability with counter-ions and solvent molecules shown, Figures 5-1 to 5-86. Select hydrogen atoms are also shown to clarify certain structures. The structures are a compilation of the finalized structures solved by the author during his time as the primary crystallographer in the MYD group. They are the results from synthetic efforts of Dr. Leo Liu, Dr. Ben Li, Dr. Mike Singleton, Dr. Roxanne Jenkins, Dr. Tiffany Pinder, Dr. Chung-Hung Hsieh, Dr. Ryan Bethel, Dr. Ning Wang, Danielle Crouthers, Randara Pulukkody, Allen Lunsford, Rachel Chupik, Pokhraj Ghosh, and the author. Attempts have been made to credit the experimental synthesis and crystal growth to the respective group members. The author acknowledges assistance from Dr. Nattami Bhuvanesh and Dr. Joe Reibenspies on certain structures as indicated in the figure caption. Additionally, some structures were already known in the literature or have subsequently been published; these are indicated in each respective figure caption and CCDC reference codes included either as a 6-letter code or a numerical one.[329]

The structures that are unpublished are largely intended for use in future publications or dissertations by group members. Thus, all finalized/publishable data is

contained in cif files in a crystallographic database organized by the author and available to all current and future group members.

5.2 FeFe Hydrogenase Models

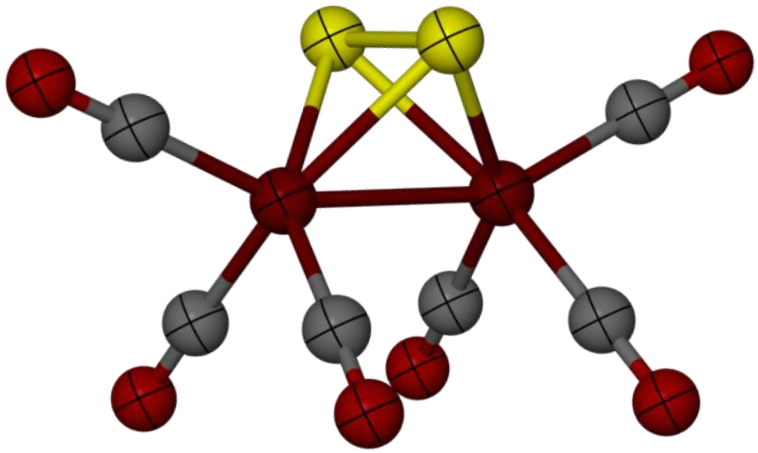

Figure 5-1. The XRD study of the $(\mu_2\text{-}S_2)[Fe(CO)_3]_2$ complex was performed by the author. This structure was previously published: FOKCOX.[330]

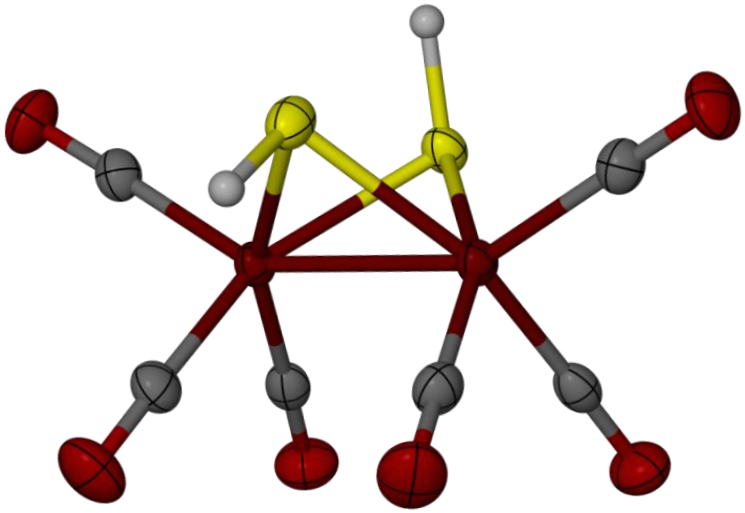

Figure 5-2. The $(\mu\text{-SH})_2[Fe(CO)_3]_2$ complex was synthesized by Danielle Crouthers and described in her dissertation.[331] The crystal structure was solved by the author.

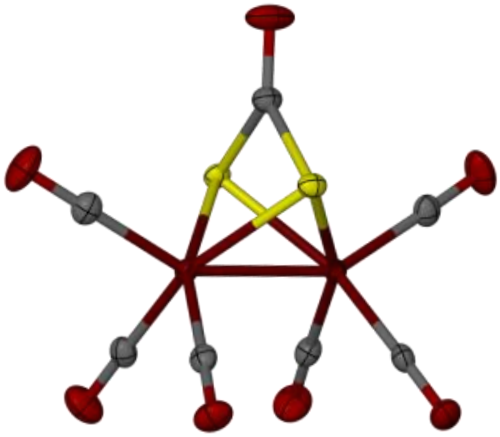

Figure 5-3. The $(\mu\text{-SCOS-}\mu)_2[Fe(CO)_3]_2$ complex was isolated as a by-product in the synthesis of the disulfide model (Figure 5-1). The author analyzed the crystals by XRD; the structure had previously been reported, FUJMOM.[332]

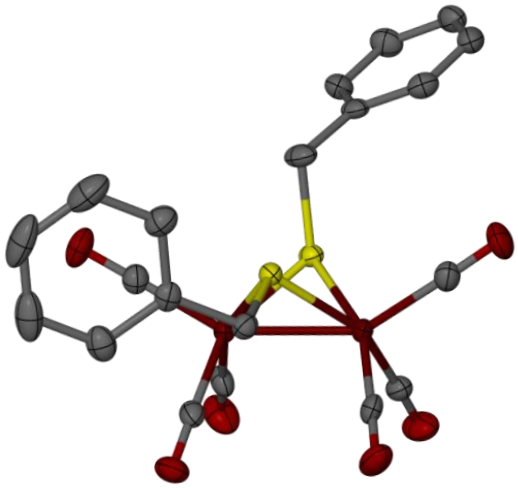

Figure 5-4. The structure of the $(\mu\text{-}SCH_2Ph)_2[Fe(CO)_3]_2$ complex was solved by the author. The complex was synthesized and isolated by Pokhraj Ghosh. Note the benzylic substituents are in the up-down orientation.

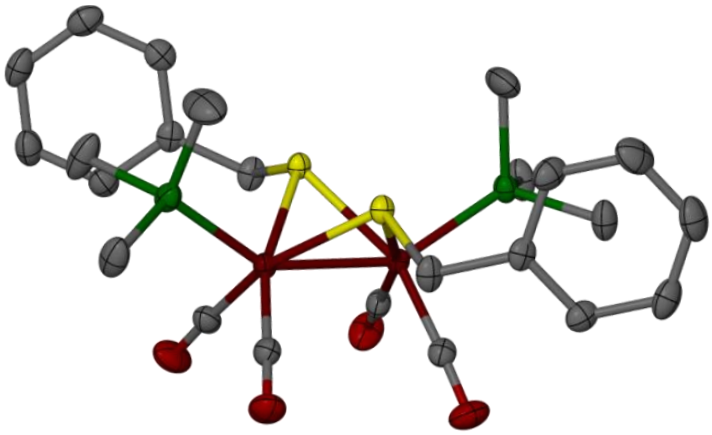

Figure 5-5. The $(\mu\text{-}SCH_2Ph)_2[Fe(CO)_2(PMe_3)]_2$ complex was synthesized by Dr. Chung-Hung Hsieh and structure solved by the author. The PMe_3 ligands are both in the apical position, and the benzylic substituents are in the down-down orientation.

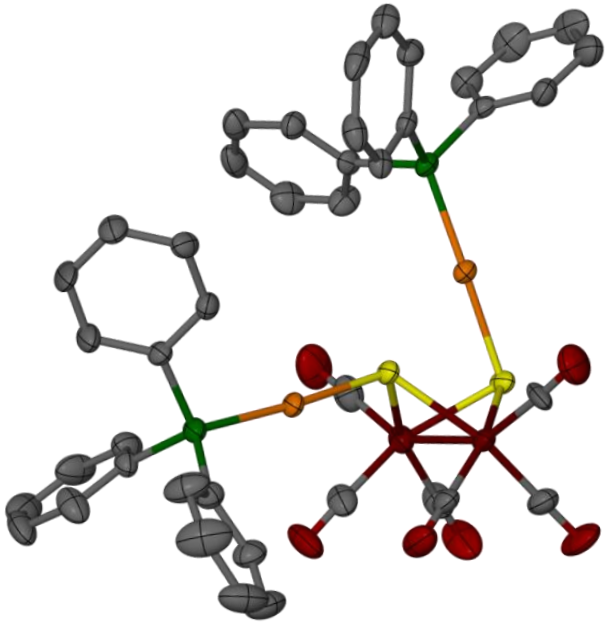

Figure 5-6. The $(\mu\text{-SAuPPh}_3)_2[\text{Fe(CO)}_3]_2$ complex was synthesized by Danielle Crouthers and described in her dissertation;[331] the structure was solved by the author.

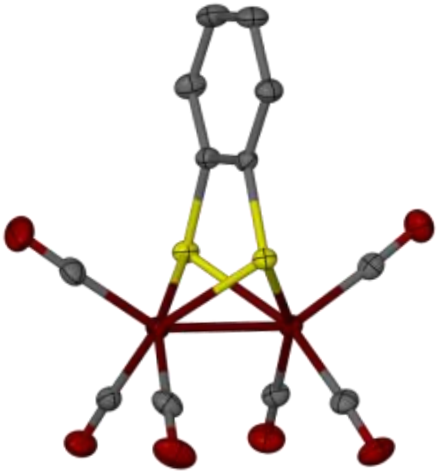

Figure 5-7. The $(\mu\text{-S-C}_6\text{H}_4\text{-S-}\mu)[\text{Fe(CO)}_3]_2$ complex was synthesized and analyzed by XRD by the author; the structure had previously been reported: SIHXIQ.[333]

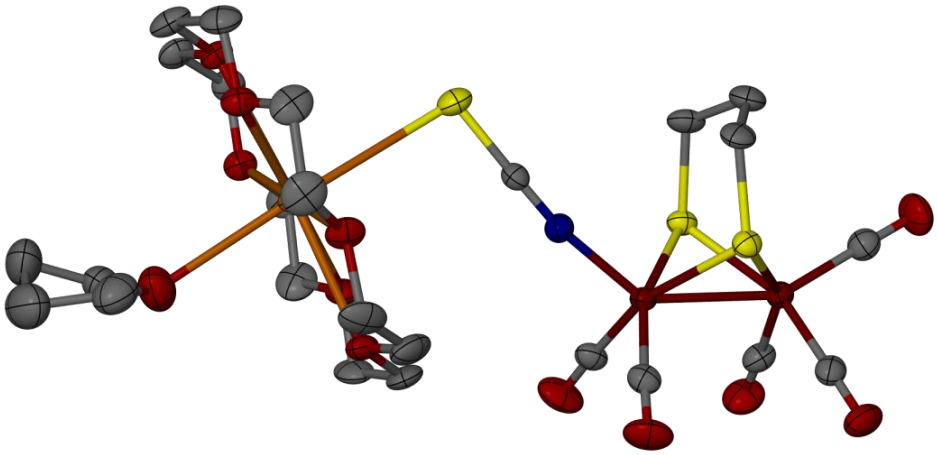

Figure 5-8. The (THF)K(18-crown-6)(μ-S(CH_2)$_3$S-μ)[Fe(CO)$_3$][Fe(CO)$_2$(NCS)] complex was synthesized and diffraction data collected by Dr. Chung-Hung Hsieh, and solved by the author; Dr. Nattami Bhuvanesh refined the disorder in the THF molecule.

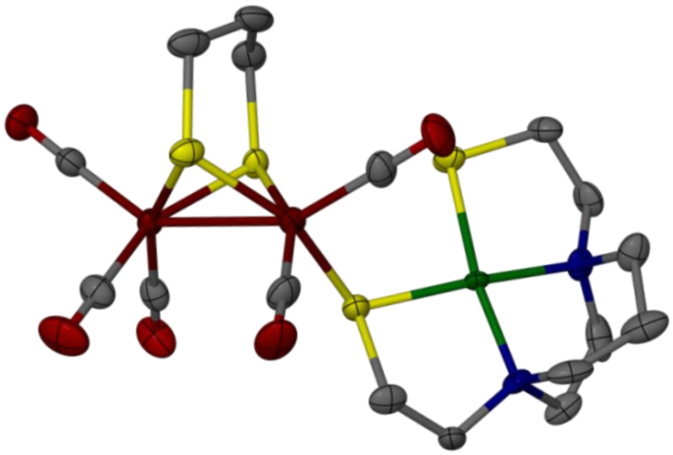

Figure 5-9. The (μ-S(CH_2)$_3$S-μ)[Fe(CO)$_3$][Fe(CO)$_2$Ni(bme-dach)] complex was synthesized by Pokhraj Ghosh, XRD collection by Dr. Chung Hsieh, and solved by the author. The NiN_2S_2 serves as a monodentate, S-bound ligand in the basal position.

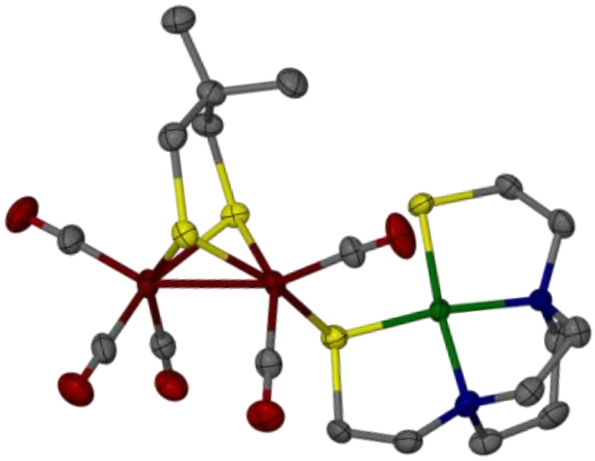

Figure 5-10. The (μ-$SCH_2C(CH_3)_2CH_2S$-μ)[$Fe(CO)_3$][$Fe(CO)_2$Ni(bme-dach)] complex was synthesized by Pokhraj Ghosh, XRD collection by Dr. Chung Hsieh, and the structure was solved by the author. The NiN_2S_2 is in the basal position.

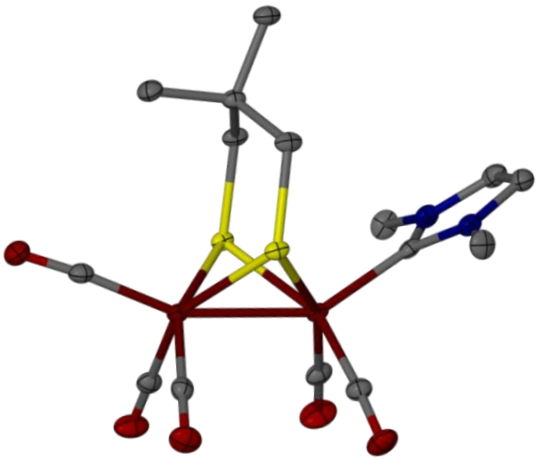

Figure 5-11. The (μ-$SCH_2C(CH_3)_2CH_2S$-μ)[$Fe(CO)_3$][$Fe(CO)_2$(IMe)] complex was solved by the author. Note the carbene is in the apical position as reported in similar complexes.[334] IMe = 1,3-bis(methyl)imidazolate.

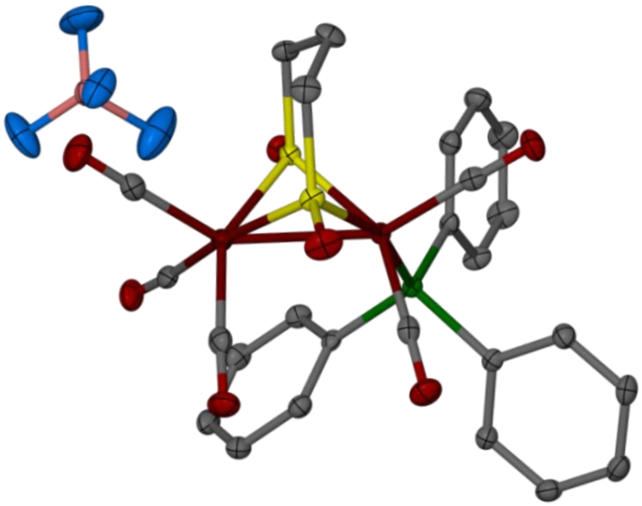

Figure 5-12. The (μ-S(O)$(CH_2)_3$(O)S-μ)[Fe$(CO)_3$][Fe$(CO)_2(PPh_3)$][BF_4] complex was solved by the author. Whether the cationic charge on the complex is a result of external oxidation or oxidation by protonation of the Fe-Fe bond is unknown.[335]

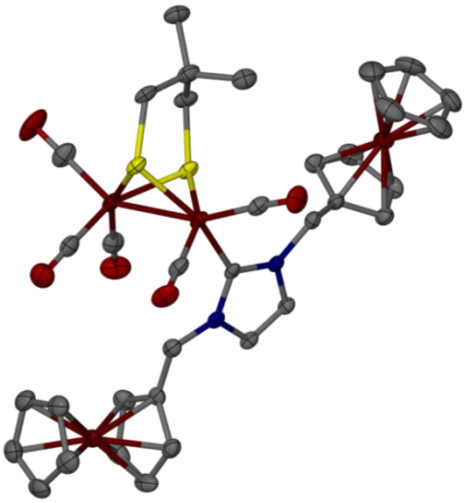

Figure 5-13. The (μ-S$CH_2C(CH_3)_2CH_2$S-μ)[Fe$(CO)_3$][Fe$(CO)_2$(2Fc)] complex was synthesized and diffraction data collected by Allen Lunsford; the structure was solved by the author. Note the carbene is in the basal position. 2Fc = diferrocenyl NHC.

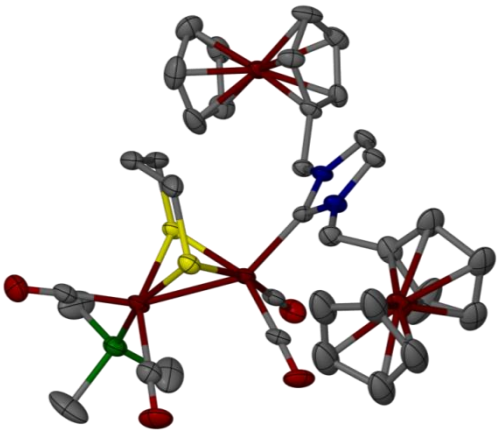

Figure 5-14. The (μ-S$(CH_2)_3$S-μ)[Fe$(CO)_2$(PMe_3)][Fe$(CO)_2$(2Fc)] complex was synthesized and XRD collection by Allen Lunsford and solved by the author. Note the carbene is in the apical position and the phosphine basal. 2Fc = diferrocenyl NHC.

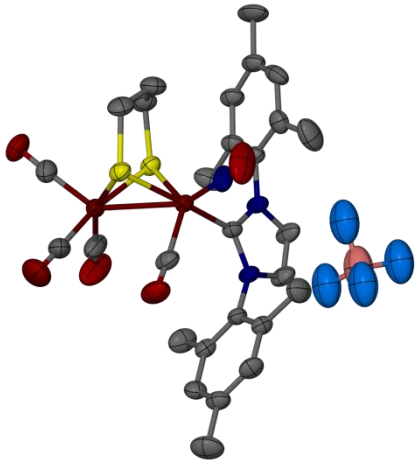

Figure 5-15. The (μ-S$(CH_2)_3$S-μ)[Fe$(CO)_3$][Fe(CO)(NO)(IMes)][BF_4] complex was synthesized by Dr. Ryan Bethel, data collection and structure solved by the author. The structure was subsequently published.[336]

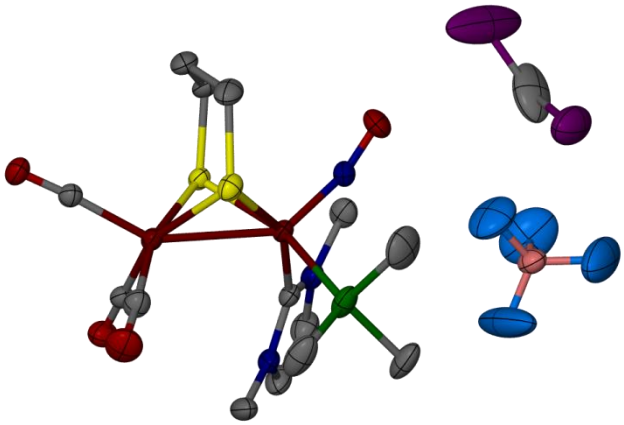

Figure 5-16. The (μ-S$(CH_2)_3$S-μ)[Fe$(CO)_3$][Fe(NO)(IMe)(PMe_3)][BF_4] complex was synthesized by Dr. Ryan Bethel, data collection and structure solved by the author. The structure has one molecule of DCM per unit cell and was subsequently published.[336]

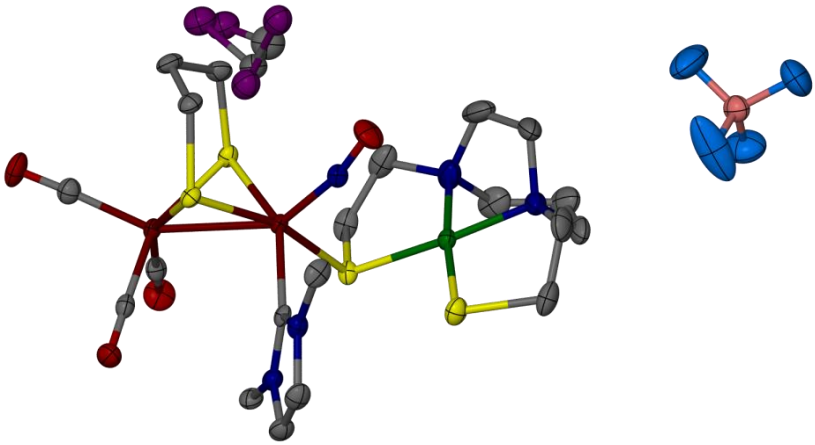

Figure 5-17. The (μ-S$(CH_2)_3$S-μ)[Fe$(CO)_3$][Fe(NO)(IMe)Ni(bme-dach)][BF_4] complex was synthesized by Pokhraj Ghosh, data collection by Dr. Chung Hsieh, and solved by the author. A single molecule of DCM co-crystallizes but is disordered over two positions. Such asymmetric substitution has been previously reported.[336-337]

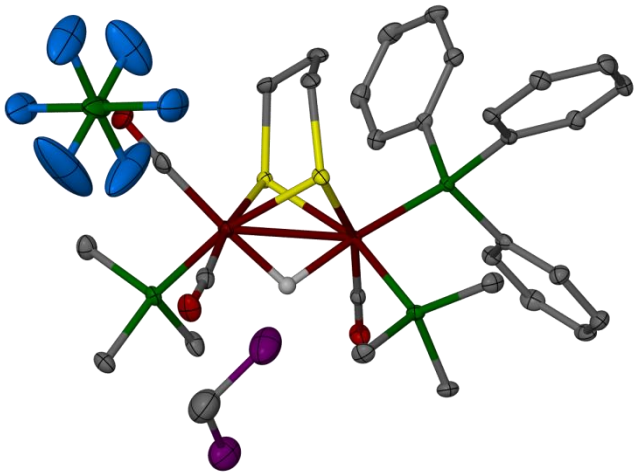

Figure 5-18. The (μ-S$(CH_2)_3$S-μ)[Fe$(CO)_2(PMe_3)$][Fe$(CO)(PMe_3)(PPh_3)$](μ-H)PF_6 complex was synthesized by Pokhraj Ghosh and XRD study performed by the author. Note the PMe_3 ligands are trans-basal and the PPh_3 is apical

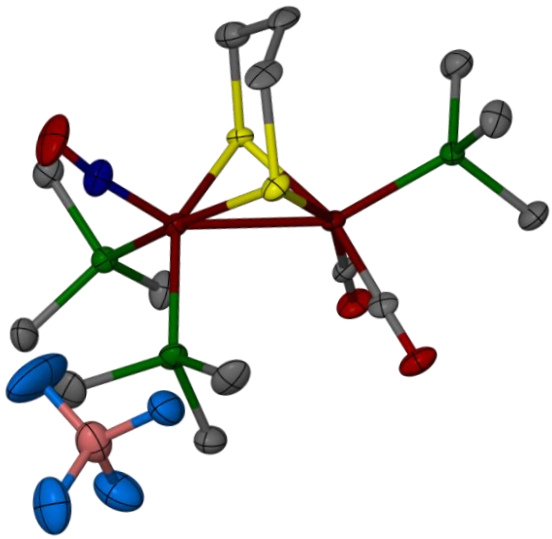

Figure 5-19. The (μ-S$(CH_2)_3$S-μ)[Fe$(CO)_2(PMe_3)$][Fe$(NO)(PMe_3)_2$][BF_4] complex was synthesized by Dr. Chung-Hung Hsieh and structure solved by the author. The structure was previously published: NOJWAL.[338]

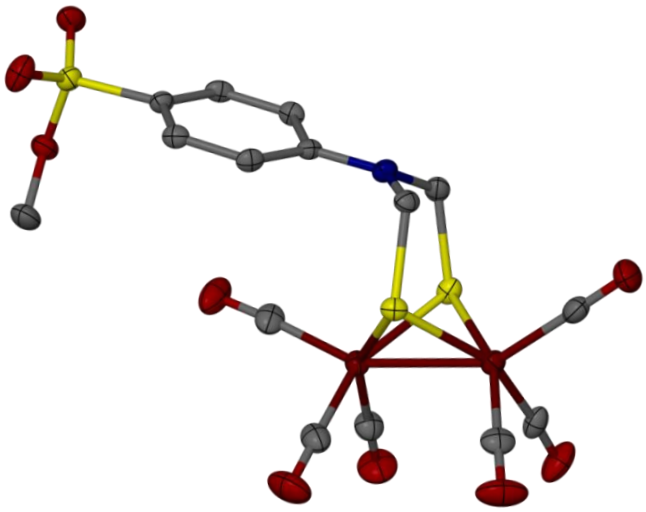

Figure 5-20. The (μ-$SCH_2N(PhSO_3Me)CH_2S$-μ)$[Fe(CO)_3]_2$ complex was synthesized and diffraction collection by Dr. Mike Singleton; the structure solved by the author.[339]

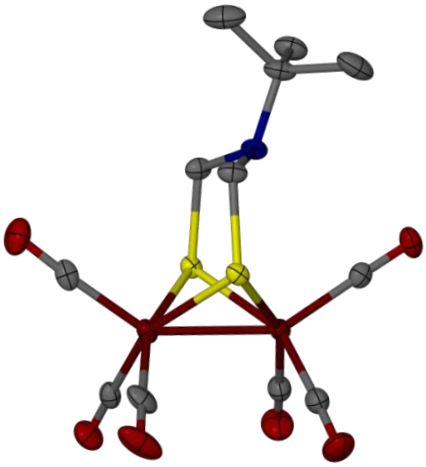

Figure 5-21. The (μ-$SCH_2N(tBu)CH_2S$-μ)$[Fe(CO)_3]_2$ complex was synthesized by Danielle Crouthers and the XRD study performed by the author. The complex has been published by Crouthers, Denny, Darensbourg, *et. al.*: ZORDUH.[340]

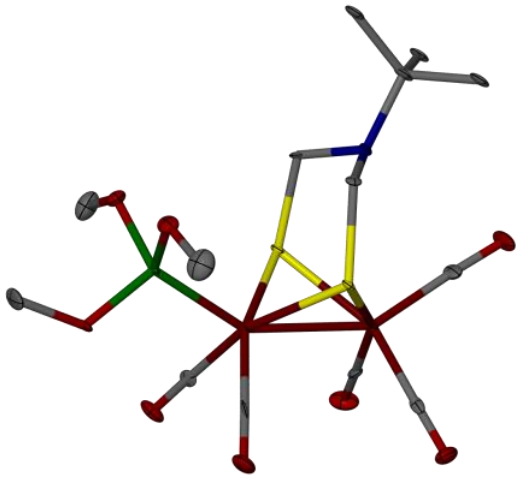

Figure 5-22. The (μ-$SCH_2N(tBu)CH_2S$-μ)[$Fe(CO)_3$][$Fe(CO)_2(P(OMe)_3)$] complex was synthesized by Danielle Crouthers and described in her dissertation.[331] The crystal study was performed by the author. The phosphite is in the apical position.

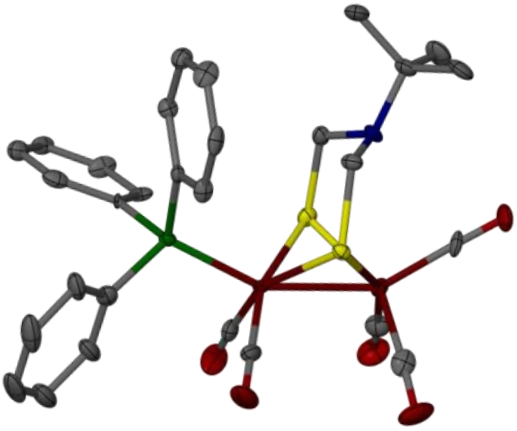

Figure 5-23. The (μ-$SCH_2N(tBu)CH_2S$-μ)[$Fe(CO)_3$][$Fe(CO)_2(PPh_3)$] complex was synthesized by Danielle Crouthers and described in her dissertation.[331] The crystal study was performed by the author. The phosphine is in the apical position.

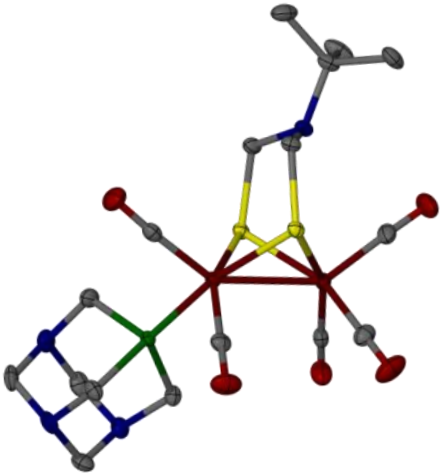

Figure 5-24. The (μ-$SCH_2N(tBu)CH_2S$-μ)[$Fe(CO)_3$][$Fe(CO)_2$(PTA)] complex was synthesized by Danielle Crouthers and described in her dissertation.[331] The crystal study was performed by the author. The phosphine is in the basal position.

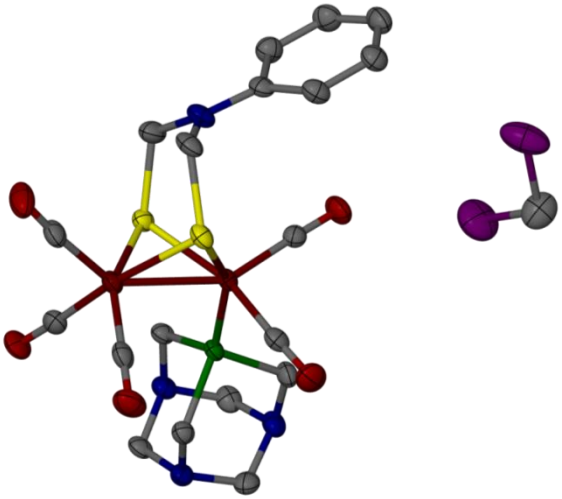

Figure 5-25. The (μ-$SCH_2N(Ph)CH_2S$-μ)[$Fe(CO)_3$][$Fe(CO)_2$(PTA)] complex was synthesized by Danielle Crouthers and described in her dissertation.[331] The crystal study was performed by the author. The phosphine is in the basal position and a molecule of DCM is found co-crystallized in the unit cell. The nitrogen is nearly planar.

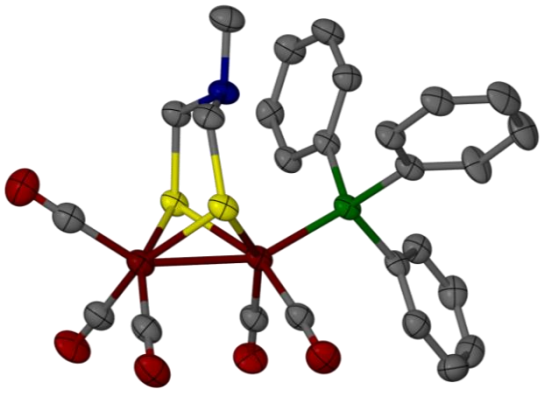

Figure 5-26. The (μ-$SCH_2N(Me)CH_2S$-μ)[$Fe(CO)_3$][$Fe(CO)_2(PPh_3)$] complex was synthesized by Danielle Crouthers and described in her dissertation.[331] The crystal study was performed by the author. The phosphine is in the apical position.

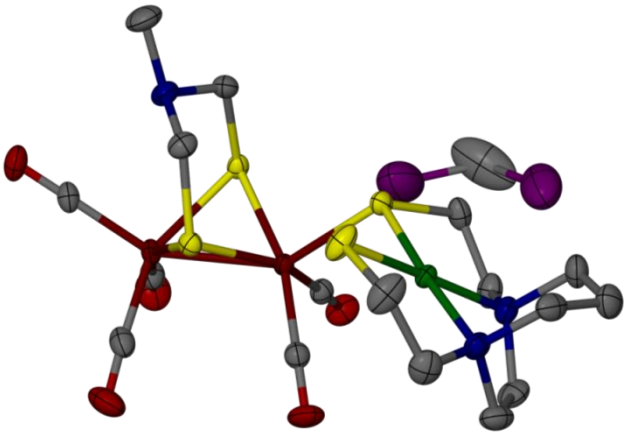

Figure 5-27. The (μ-$SCH_2N(Me)CH_2S$-μ)[$Fe(CO)_3$][$Fe(CO)_2$Ni(bme-dach)] complex was synthesized by Pokhraj Ghosh, XRD collection by Dr. Chung-Hung Hsieh, and the structure was solved by the author. A co-crystallized molecule of DCM is found in each unit cell.

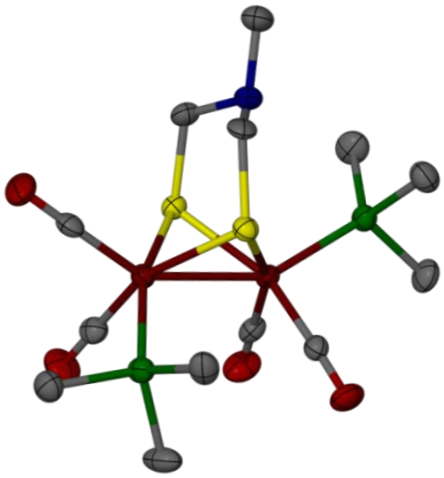

Figure 5-28. The (μ-$SCH_2N(Me)CH_2S$-μ)$[Fe(CO)_2(PMe_3)]_2$ complex was synthesized by Danielle Crouthers and described in her dissertation.[331] The crystal study was performed by the author. The phosphines are in the trans-apical/basal positions.

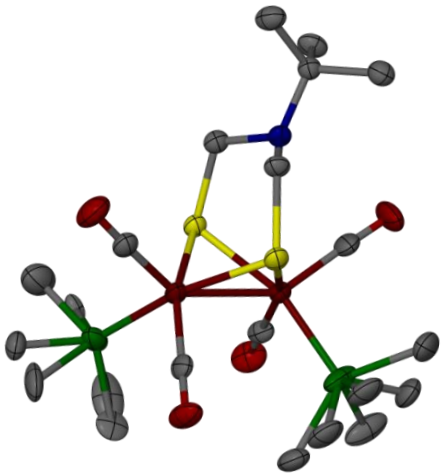

Figure 5-29. The (μ-$SCH_2N(tBu)CH_2S$-μ)$[Fe(CO)_2(PMe_3)]_2$ complex was synthesized by Danielle Crouthers and described in her dissertation.[331] The crystal study was performed by the author. The phosphines are in the trans-basal positions and are disordered and modeled over two positions.

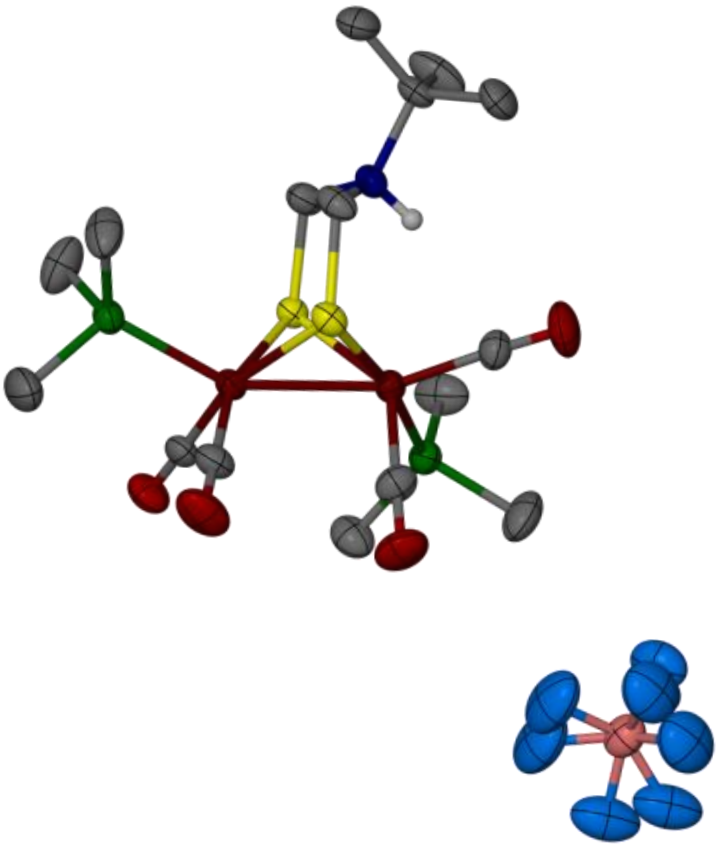

Figure 5-30. The (μ-$SCH_2NH(tBu)CH_2S$-μ)$[Fe(CO)_2(PMe_3)]_2BF_4$ complex was synthesized by Danielle Crouthers and described in her dissertation.[331] The crystal study was performed by the author. Note the phosphines are in the trans-apical/basal positions and the counter-ion is disordered over two positions. From the Fe-Fe distance as well as the Fe-L distances the oxidation states of the irons remain 1+. Additionally, there is a substantial distortion in the $Fe(CO)_2(PMe_3)$ rotor that the proton is directed toward as compared to the unprotonated structure (Figure 5-26).

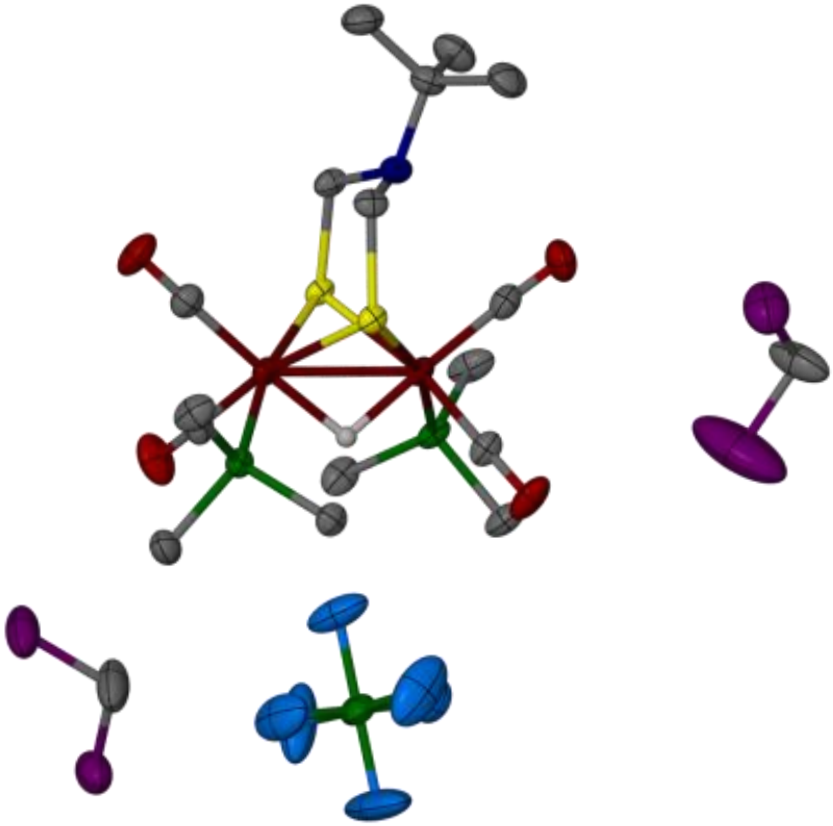

Figure 5-31. The (μ-$SCH_2N(tBu)CH_2S$-μ)[$Fe(CO)_2(PMe_3)]_2$(μ-H)PF_6 complex was synthesized by Danielle Crouthers and described in her dissertation.[331] The crystal study was performed by the author. The phosphines are in the trans-basal positions and two molecules of DCM are found co-crystallized in the unit cell. This product results from DCM as the reaction media as compared to MeCN for the previous complex (Figure 5-28).

5.3 MN_2S_2 Complexes

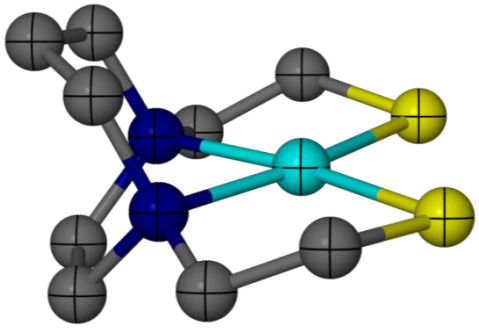

Figure 5-32. The Pd(bme-dach) complex was synthesized and data collected by the author and solved by Dr. Nattami Bhuvanesh. Hence, the structure was published by the author: OJAVIF.[161]

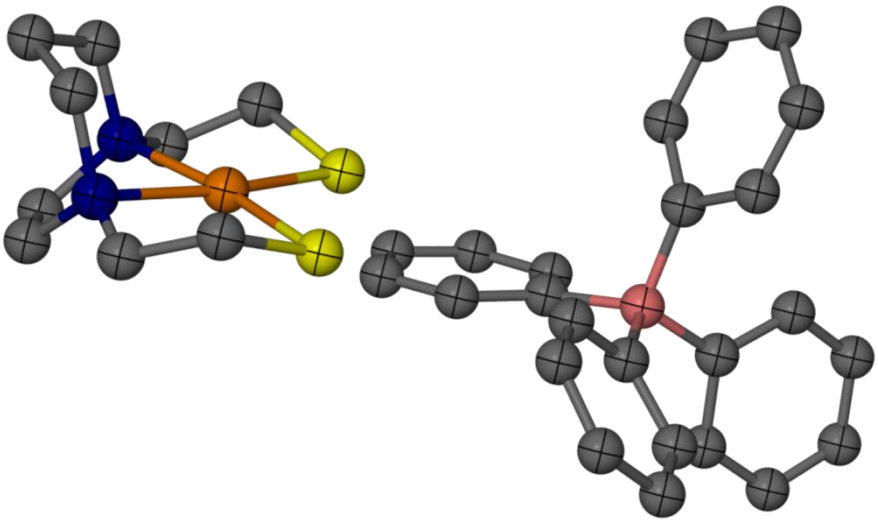

Figure 5-33. The [Au(bme-dach)][BPh_4] complex was synthesized and data collected by the author and solved by Dr. Nattami Bhuvanesh. The structure has been published by the author: OJAVEB.[161]

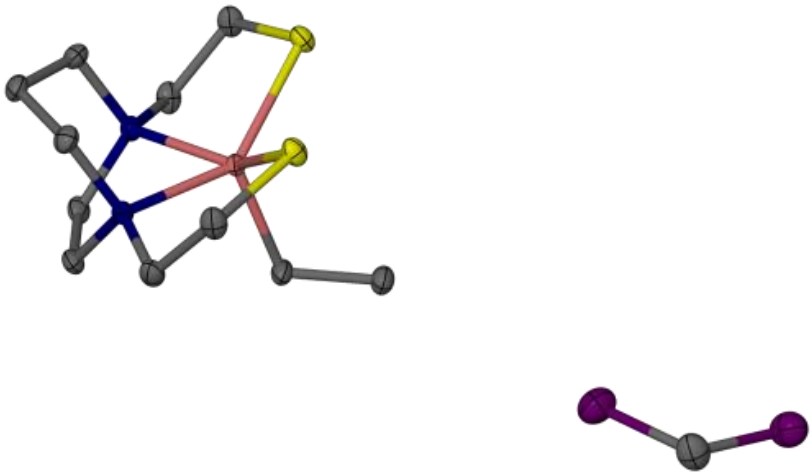

Figure 5-34. The Al(Et)(bmedach) complex was synthesized and XRD data collected by Allen Lunsford and structure solved by the author. A single molecule of DCM is found co-crystallized in the unit cell: CCDC# 1044541.

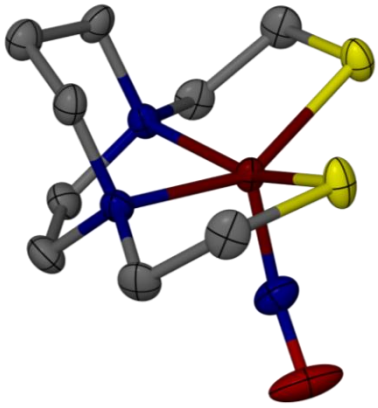

Figure 5-35. The Fe(NO)(bme-dach) complex analyzed by XRD and structure solved by the author. The structure had previously been published however the author was able to refine disorder in the structure that explained the previous observation of the NO conformations: RAWHED.[169]

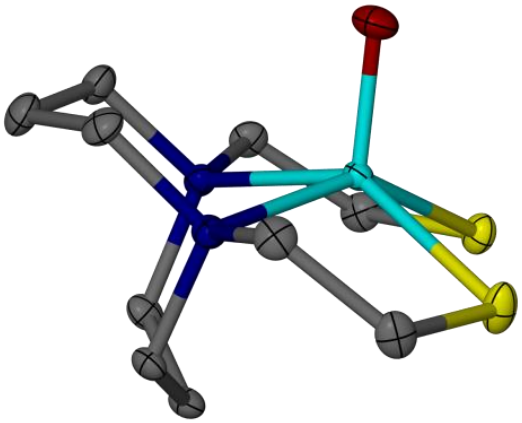

Figure 5-36. The V(O)(bme-daco) complex was synthesized and diffraction data collected by Allen Lunsford. The structure was solved by the author and was already known: IXEJEB.[225]

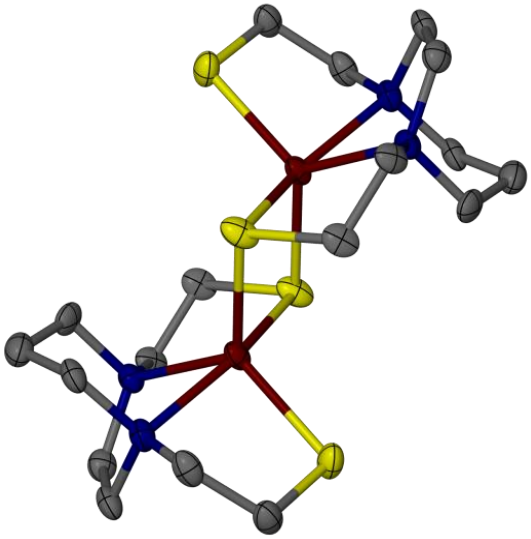

Figure 5-37. The $[Fe(bme\text{-}dach)]_2$ complex was synthesized and structure solved by XRD by the author. Nattami Bhuvanesh modeled disorder in the diazacycloheptane ring. The structure was submitted as a crystallographic paper.[165]

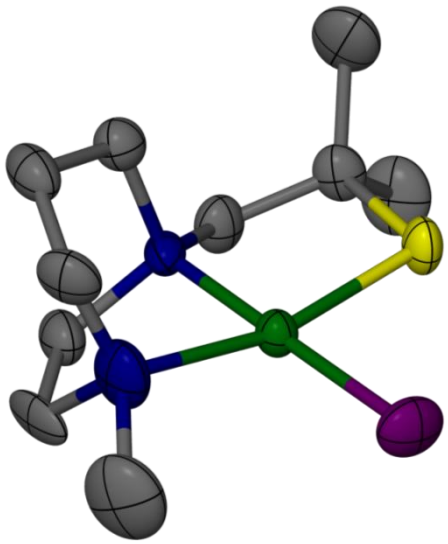

Figure 5-38. The structure of the Ni(mme*-dach)Cl complex was solved by the author.

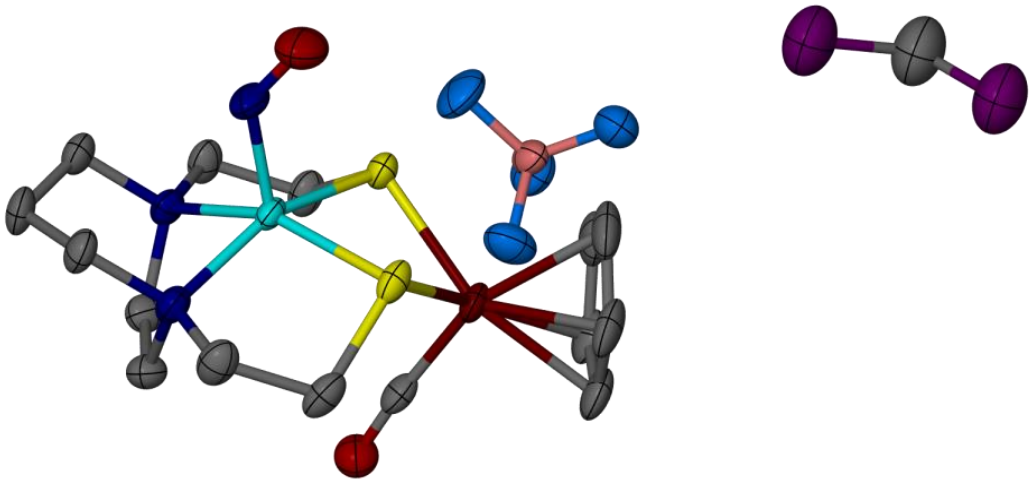

Figure 5-39. The Co(NO)(bme-dach)FeCp(CO)BF_4 complex was synthesized and XRD data collected by Ning Wang and solved by Nattami Bhuvanesh. Figures were generated and structural analysis by the author. A molecule of DCM is found co-crystallized in the unit cell.

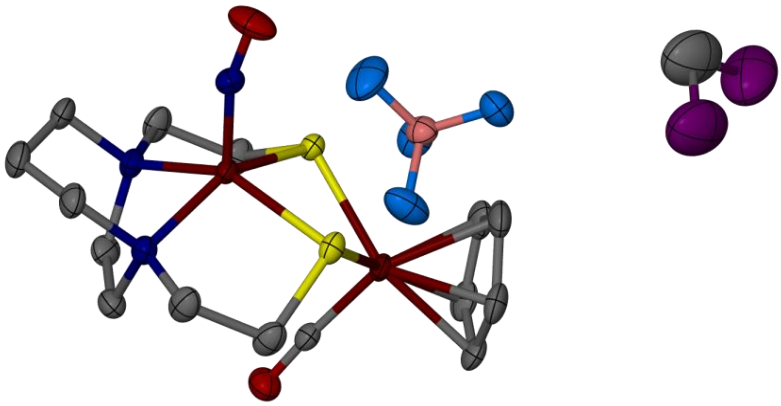

Figure 5-40. The Fe(NO)(bme-dach)FeCp(CO)BF_4 complex was synthesized and XRD collection by Ning Wang and solved by Nattami Bhuvanesh. Figures were generated and structural analysis by the author. A molecule of DCM is found co-crystallized in the unit cell.

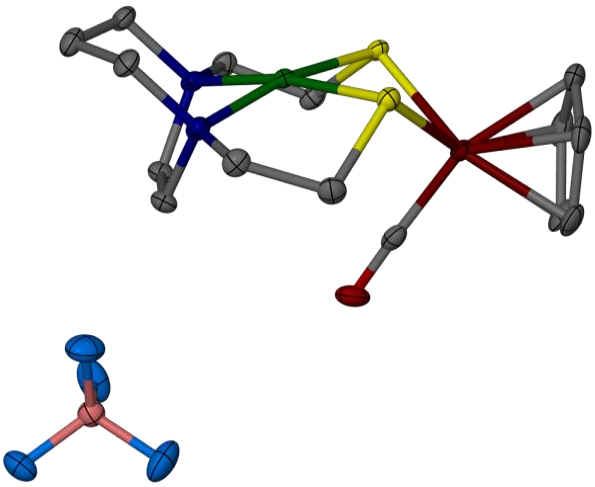

Figure 5-41. The Ni(bme-dach)FeCp(CO)BF_4 complex was synthesized and XRD collection by Ning Wang and solved by Nattami Bhuvanesh. Figures were generated and structural analysis by the author.

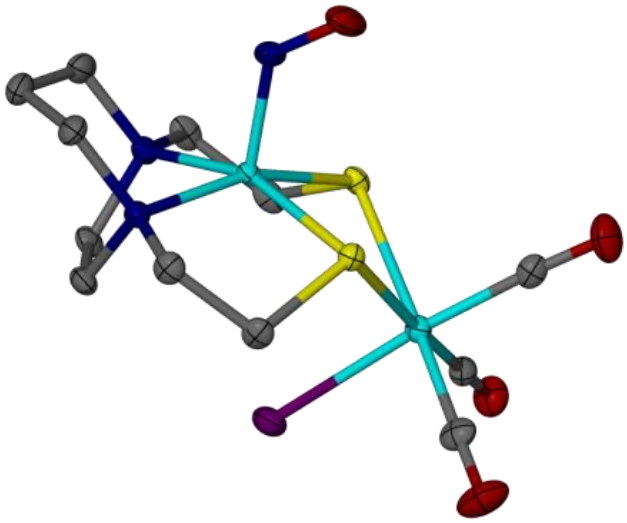

Figure 5-42. The Co(NO)(bme-dach)Mn(CO)$_3$Br complex was synthesized and XRD data collected by Allen Lunsford. The structure was solved by the author.

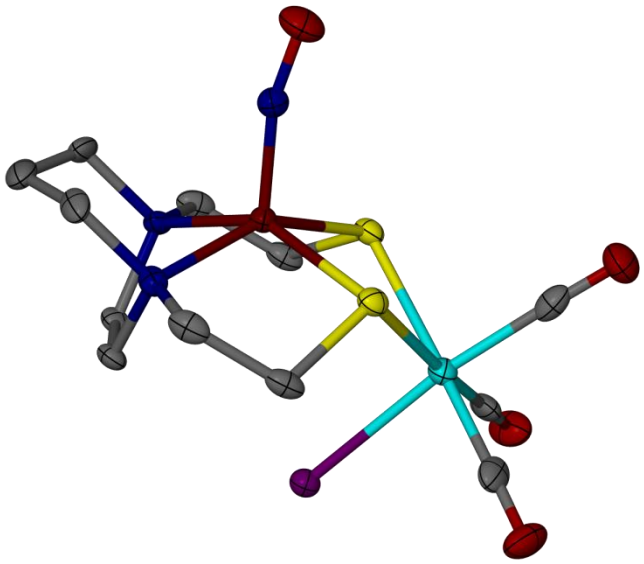

Figure 5-43. The Fe(NO)(bme-dach)Mn(CO)$_3$Br complex was synthesized by Allen Lunsford and XRD performed by Nattami Bhuvanesh.

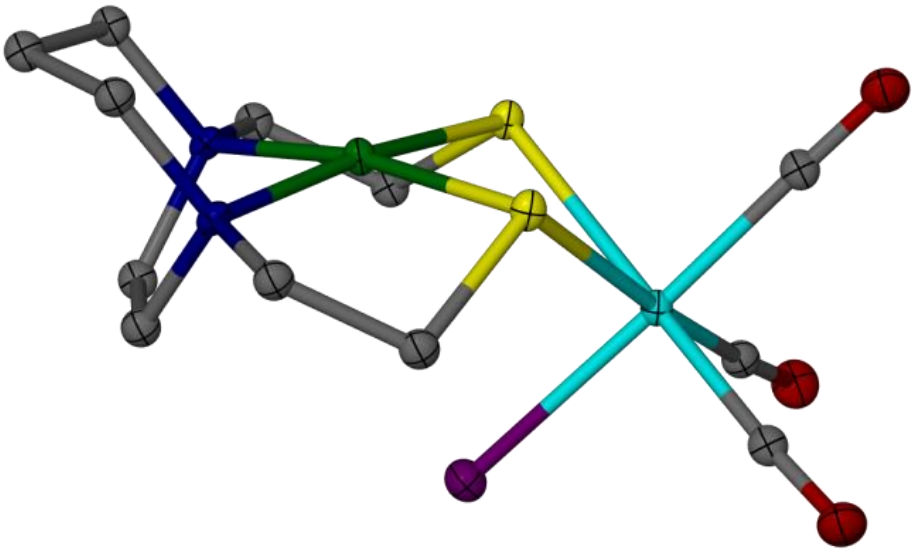

Figure 5-44. The Ni(bme-dach)Re(CO)$_3$Cl complex was synthesized by Allen Lunsford and XRD analysis performed by the author.

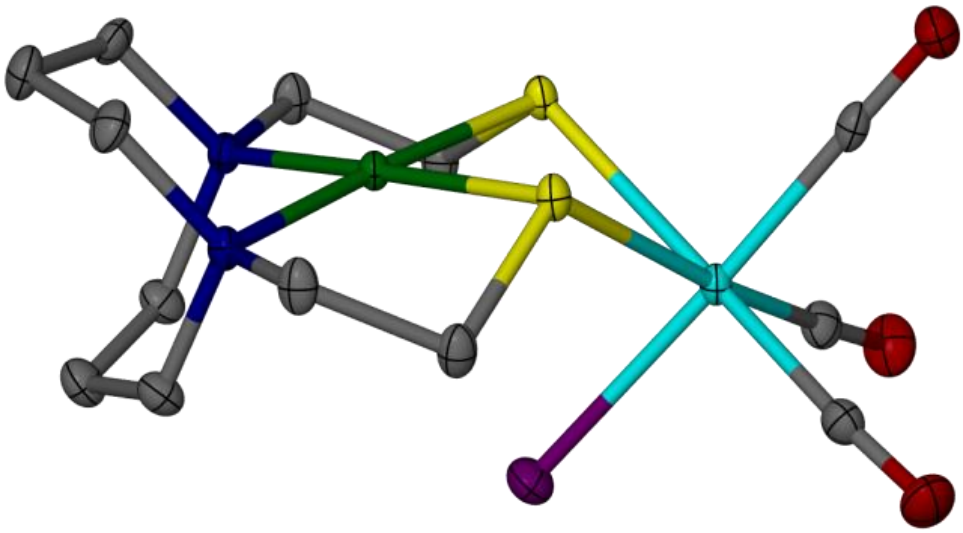

Figure 5-45. The Ni(bme-daco)Re(CO)$_3$Cl complex was synthesized by Allen Lunsford and XRD analysis performed by the author.

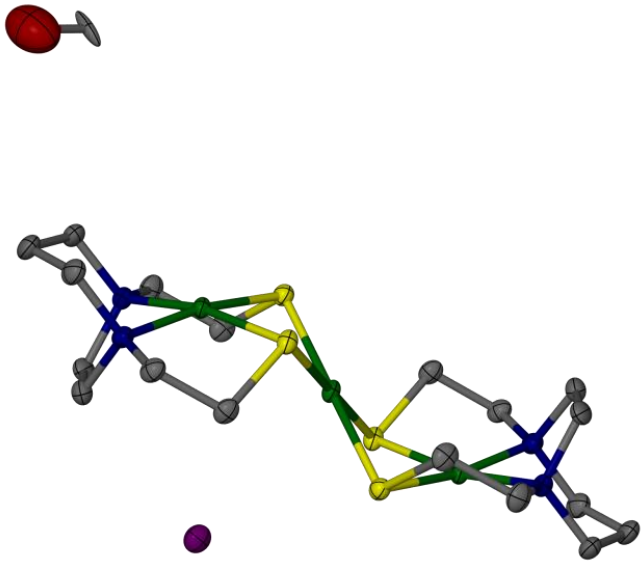

Figure 5-46. The structure of the $[Ni(bme\text{-}dach)]_2NiCl_2$ complex was solved by XRD by the author. One molecule of MeOH is found in the unit cell. The second Cl^- ion is symmetry derived and not shown. The structure was previously published: EROPIK.[258]

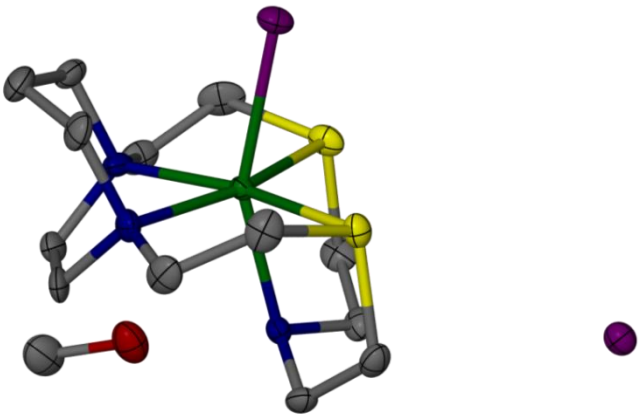

Figure 5-47. The $[Ni(Cl)(bme\text{-}dach)CH_2CH_2NHCH_2CH_2][Cl]$ complex was synthesized and XRD data collected by Allen Lunsford. The structure was solved by the author. One molecule of MeOH co-crystallizes per unit cell.

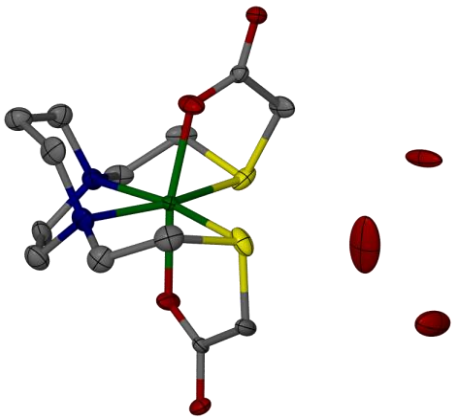

Figure 5-48. The Ni(bme-dach)($CH_2COO)_2$ complex was synthesized and crystallized by the author and XRD structure solved by Dr. Joe Reibenspies. Three molecules of water are found per unit cell. Previously published by the author: OHABAB.[321]

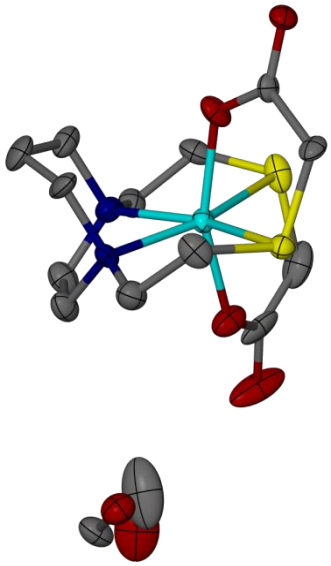

Figure 5-49. The Zn(bme-dach)($CH_2COO)_2$ complex was synthesized and crystallized by the author. The XRD structure was solved by Dr. Nattami Bhuvanesh. Two molecules of MeOH are found per unit cell. Previously published by the author: OGUZUM.[321]

5.4 Nitrosyl Iron and Cobalt Complexes

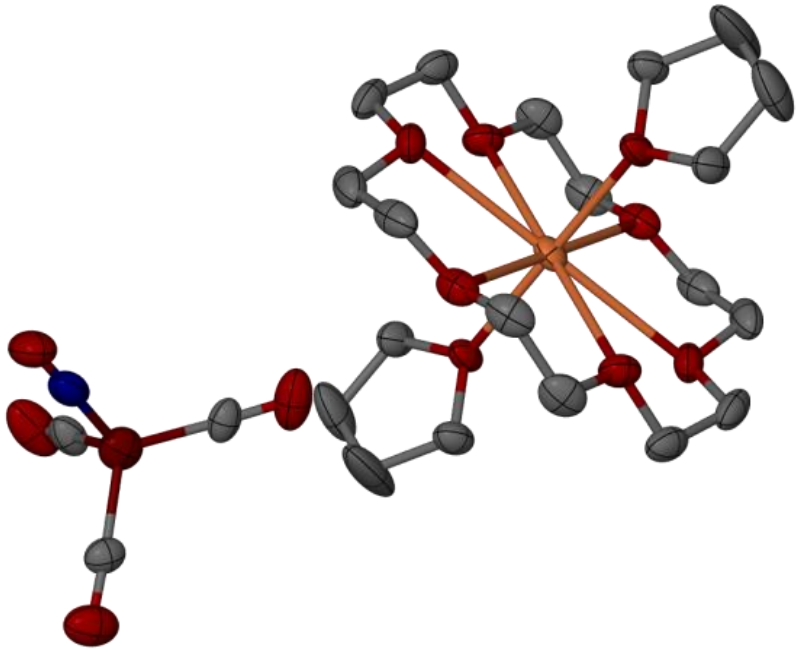

Figure 5-50. The structure of the $(THF)_2Na(18\text{-crown-}6)Fe(CO)_3(NO)$ complex was solved by the author using XRD.

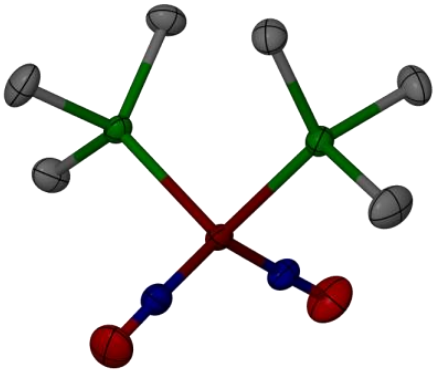

Figure 5-51. The $Fe(NO)_2(PMe_3)_2$ complex was synthesized by Randara Pulukkody discussed in her dissertation (2015) and the structure solved by the author.

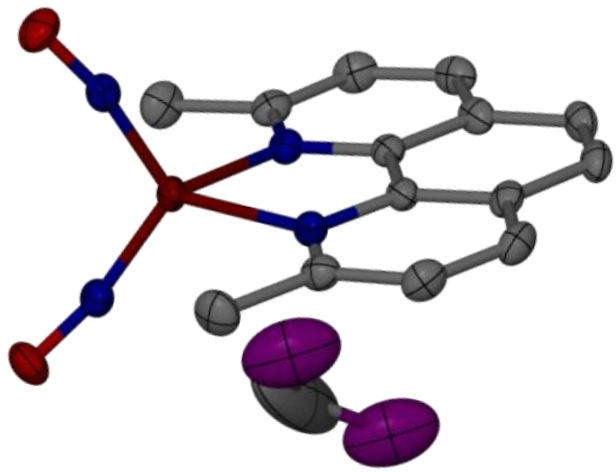

Figure 5-52. The $Fe(NO)_2$(neocup) complex was synthesized by Rachel Chupik and structure solved by the author. There is one molecule of DCM found per unit cell. neocup = 2,9-dimethyl-1,10-phenanthroline.

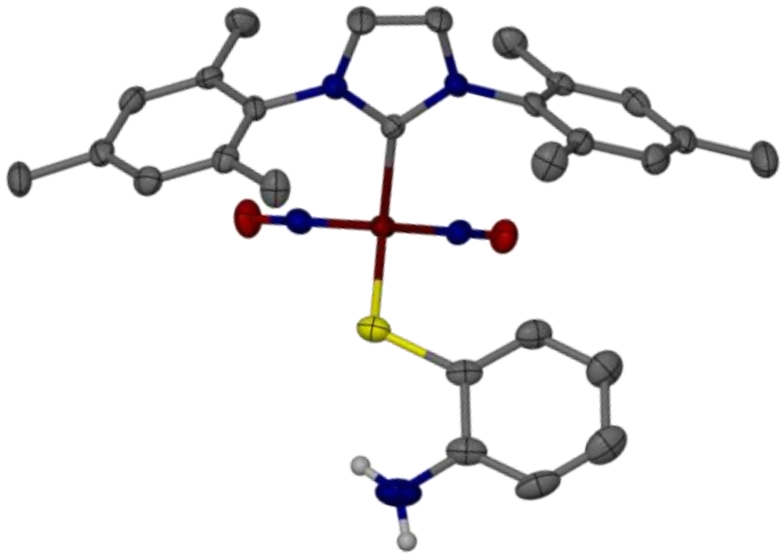

Figure 5-53. The $Fe(NO)_2(IMes)(SC_6H_4NH_2)$ complex was synthesized and XRD collection performed by Dr. Chung-Hung Hsieh and structure solved by the author.

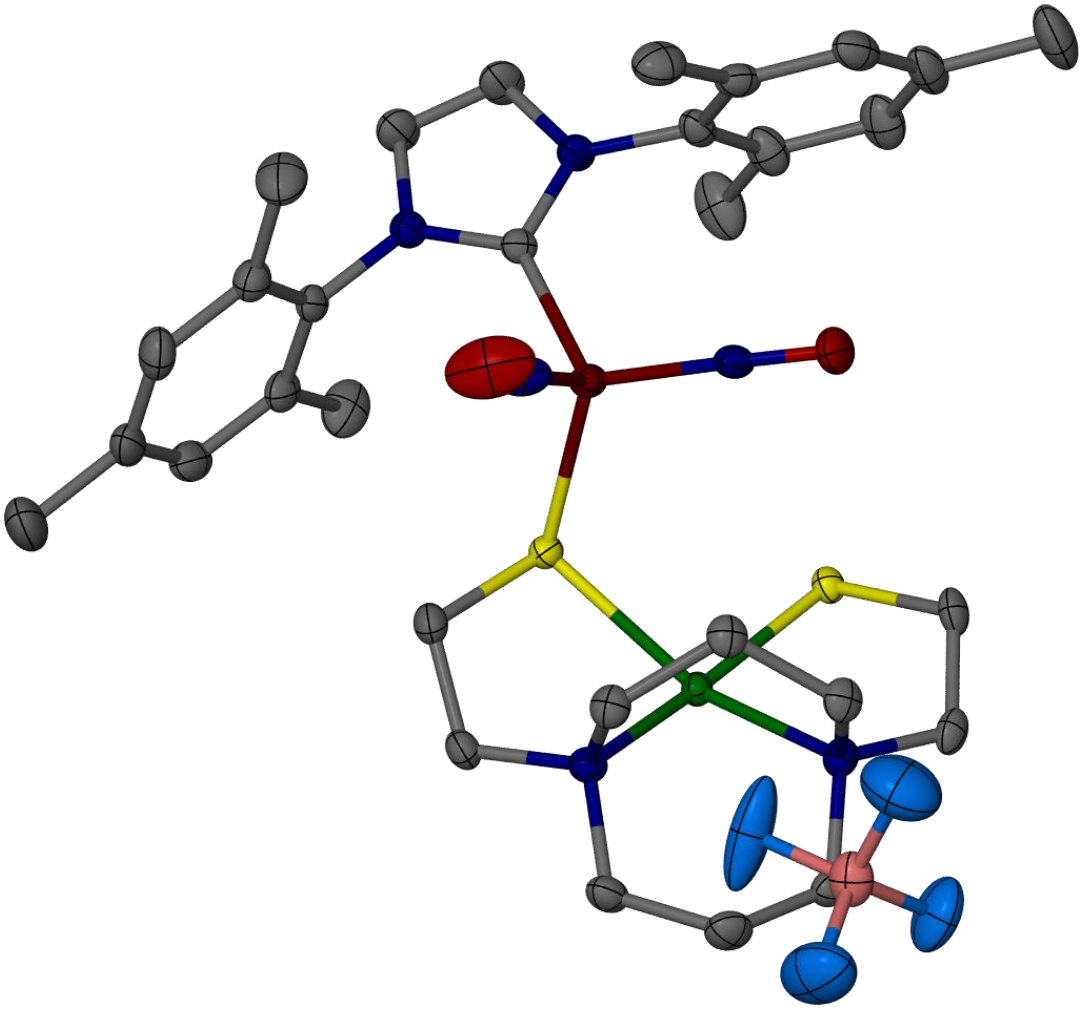

Figure 5-54. The $[Fe(NO)_2(IMes)Ni(bme\text{-}daco)]_2[BF_4]_2$ dimeric complex was synthesized by Rachel Chupik and structure solved by the author. Note the structure dimerizes through the available thiolate but only one unit is shown for clarity. CCDC #1045460.

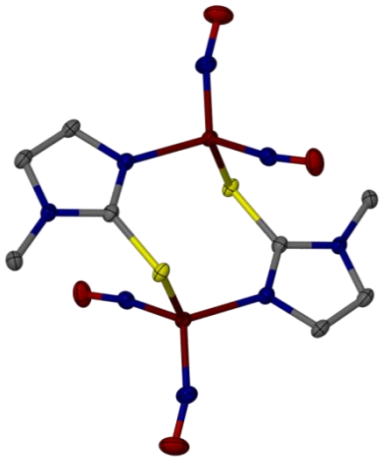

Figure 5-55. The structure of the $[Fe(NO)_2(SMeImid)]_2$ dimeric complex was solved by the author. SMeImid = $SCN(CH_3)CHCHN$.

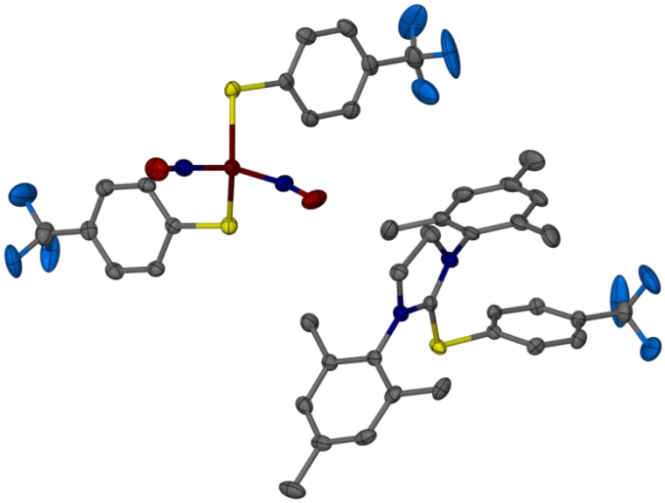

Figure 5-56. The $[IMesSPhCF_3][Fe(NO)_2(SPhCF_3)_2]$ complex was synthesized by Randara Pulukkody, XRD data collected by Dr. Chung Hsieh, and structure solved by the author. The counter-ion charge is on the sulfur atom and stabilized by resonance between the two aromatic rings.

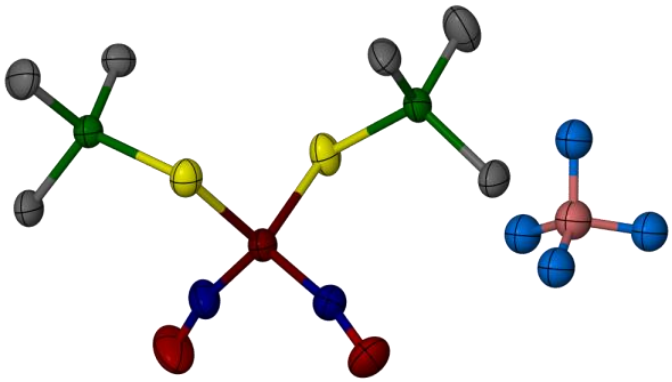

Figure 5-57. The $Fe(NO)_2(SPMe_3)_2BF_4$ complex was isolated by Danielle Crouthers as a decomposition product of nitrosylation of the [FeFe] model compound shown in Figure 5-28. The XRD study was performed by the author.

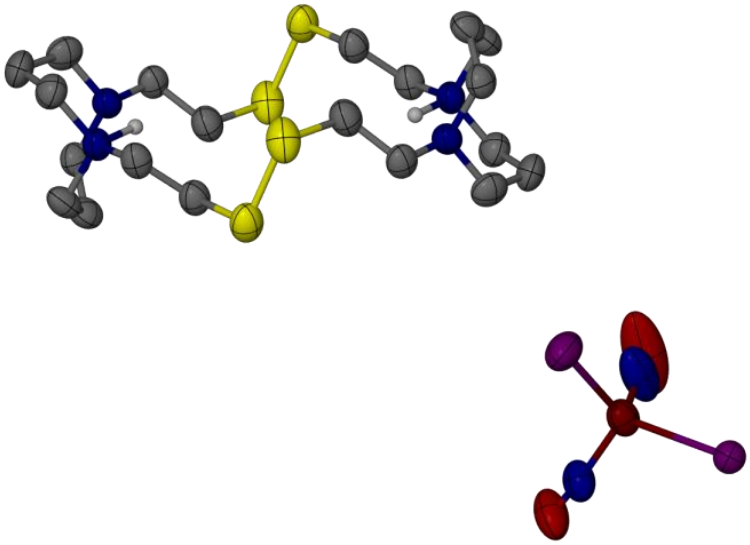

Figure 5-58. The $[Hbmedaco]_2[Fe(NO)_2(I)_2]_2$ complex was isolated by Dr. Tiffany Pinder and structure solved by the author. Note the charge of the counter-ion is from a proton bridging between the nitrogen atoms. The dication has been observed before.[341]

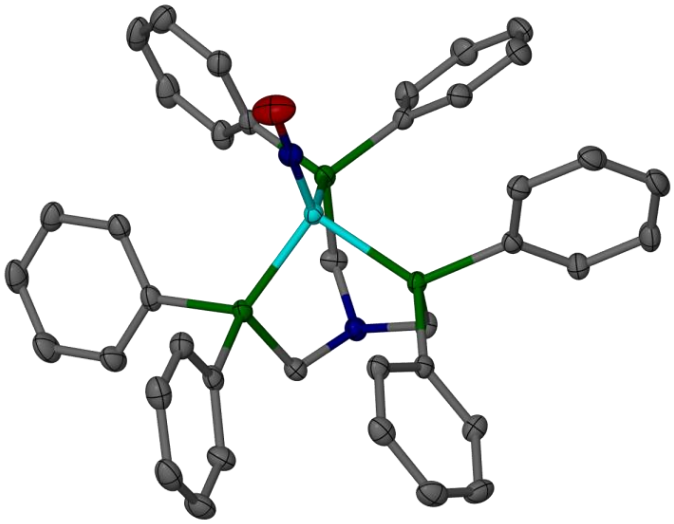

Figure 5-59. The $Co(NO)N(CH_2PPh_2)_3$ complex was synthesized by Dr. Ning Wang and XRD data collected and solved by the author. Formally this is a $\{Co(NO)\}^{10}$ neutral species.

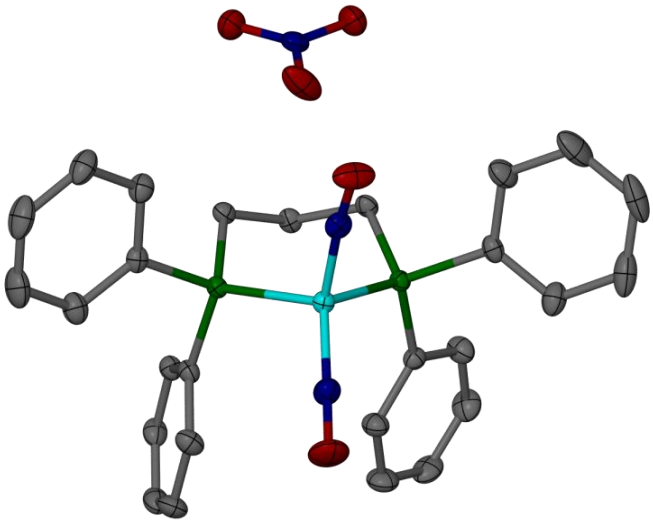

Figure 5-60. The $[Co(NO)_2(dppp)][NO_3]$ complex was synthesized by Pokhraj Ghosh and structure solved by the author using XRD.

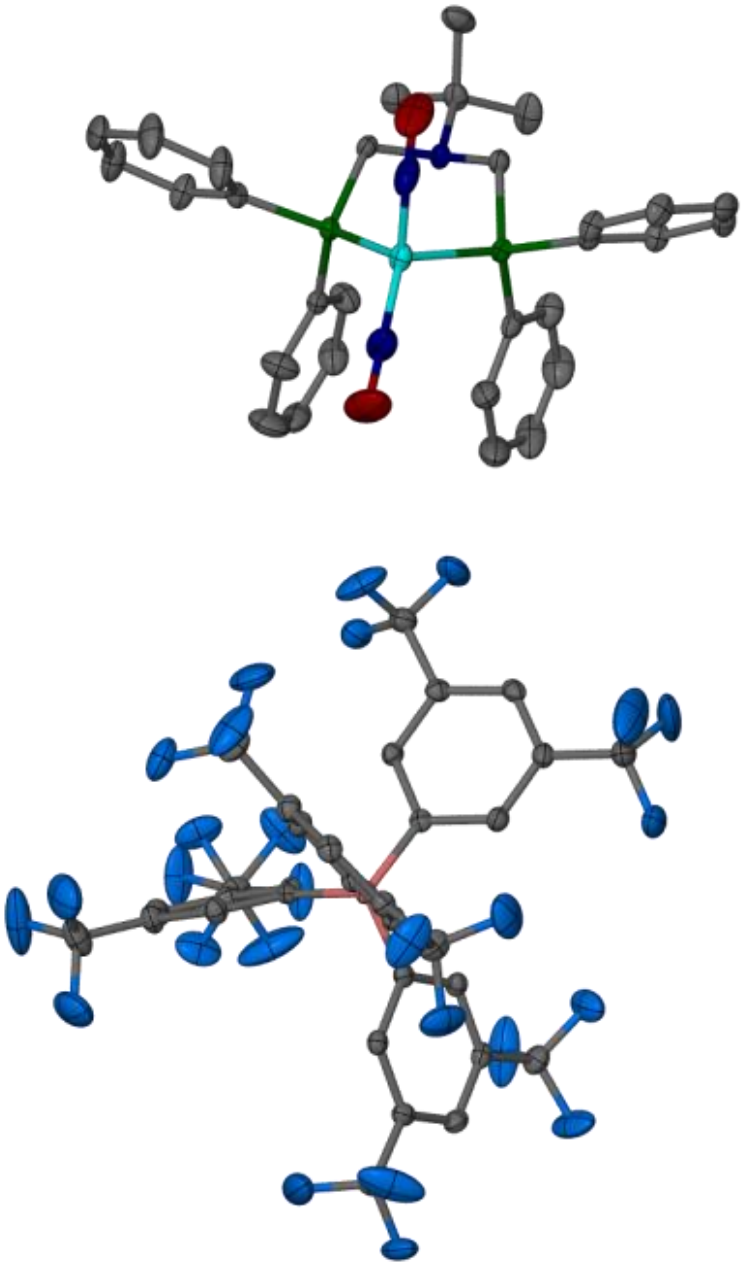

Figure 5-61. The $[Co(NO)_2N(CH_2PPh_2)_2tBu][BArF]$ was synthesized by Dr. Ning Wang and Pokhraj Ghosh and XRD data collected and structure solved by the author. Note the high degree of disorder in the CF_3 groups of the BArF counter-ion.

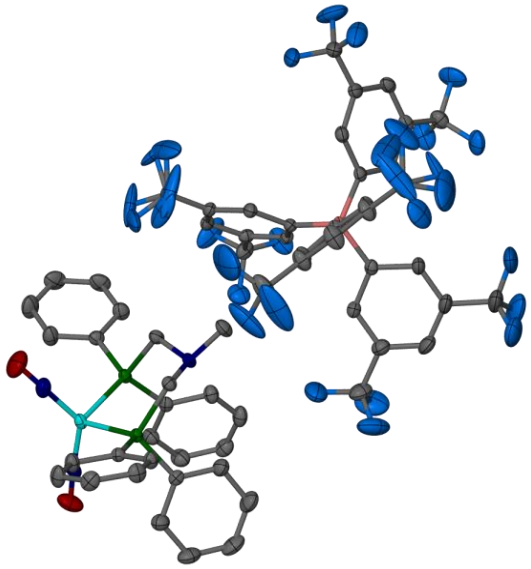

Figure 5-62. The $[Co(NO)_2N(CH_2PPh_2)_2Me][BArF]$ was synthesized by Dr. Ning Wang and Pokhraj Ghosh and structure solved by the author. Note the high degree of disorder in the CF_3 groups of the BArF counter-ion.

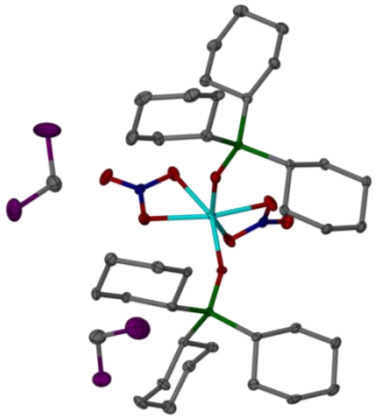

Figure 5-63. The $Co(NO_3)_2(OPCy_3)_2$ was isolated during experiments by Pokhraj Ghosh and the author solved the structure. Two molecules of DCM are found in the unit cell. The product results from unintentional oxygenation.

5.5 Other Inorganic Complexes

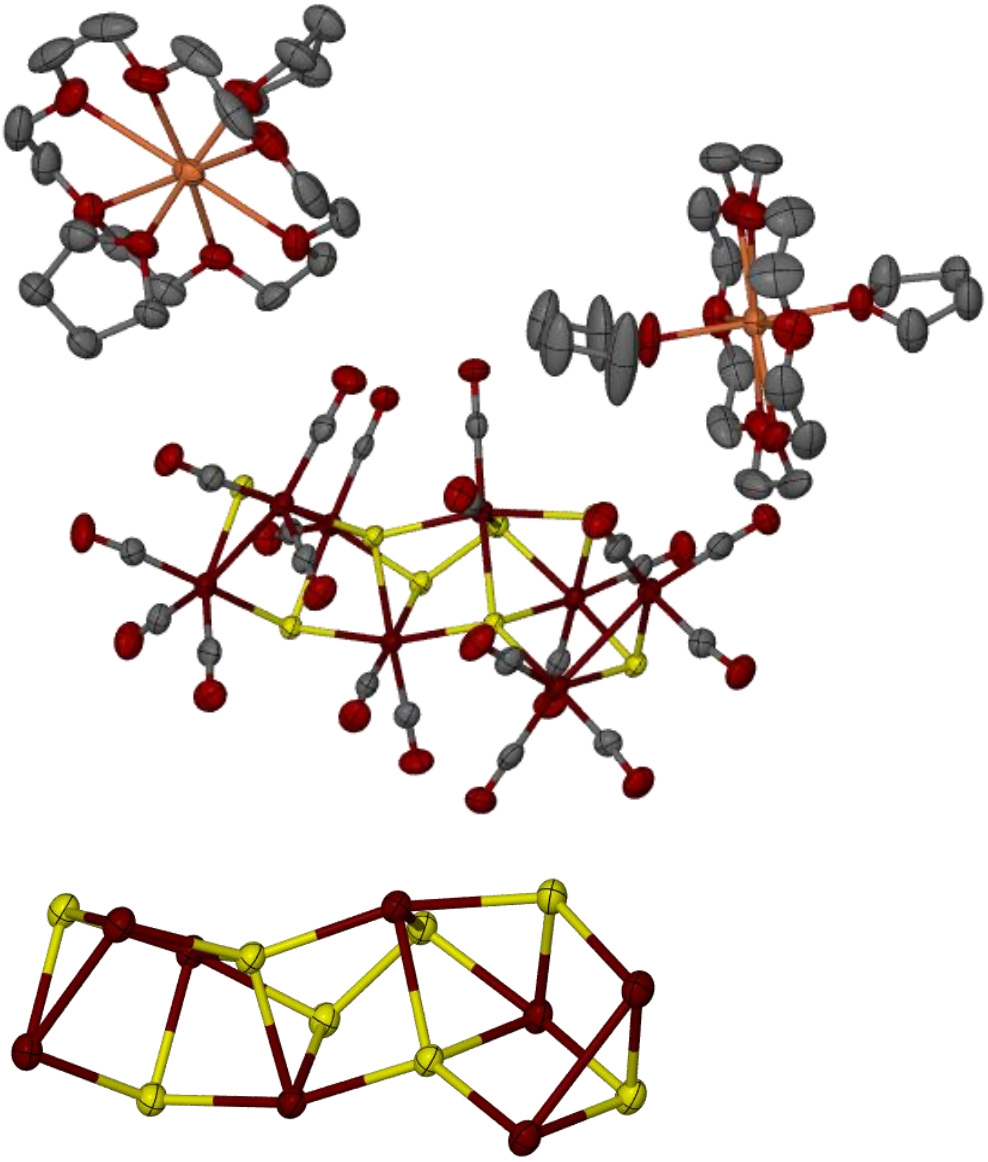

Figure 5-64. The $[(THF)_2K(18\text{-crown-}6)]_2[Fe_8S_8(CO)_{24}]$ complex was synthesized and XRD collection by Scott Harman and structure solved by the author. Disorder in THF was modeled by Dr. Nattami Bhuvanesh. Note the iron sulfur cluster is a dication. A second view highlights the 8Fe8S core.

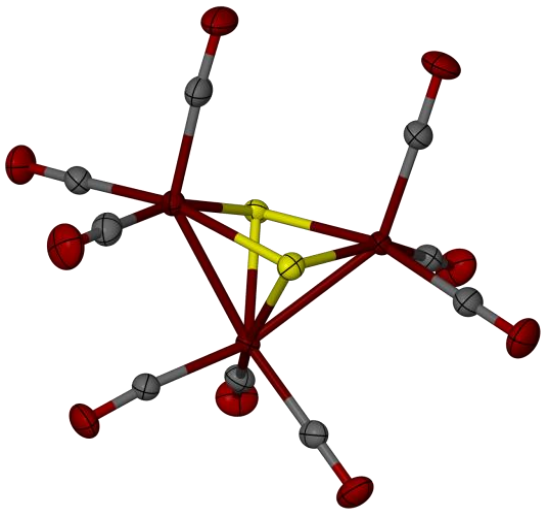

Figure 5-65. The $Fe_3S_2(CO)_9$ cluster was synthesized by Pokhraj Ghosh and structure solved by the author through XRD analysis. This structure had previously been published: TOJHAB.[342]

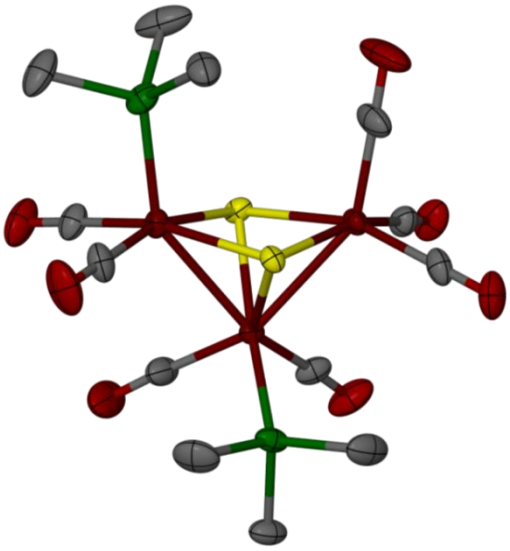

Figure 5-66. The $Fe_3S_2(CO)_7(PMe_3)_2$ complex was synthesized and XRD performed by Scott Harman. The structure was solved by the author.

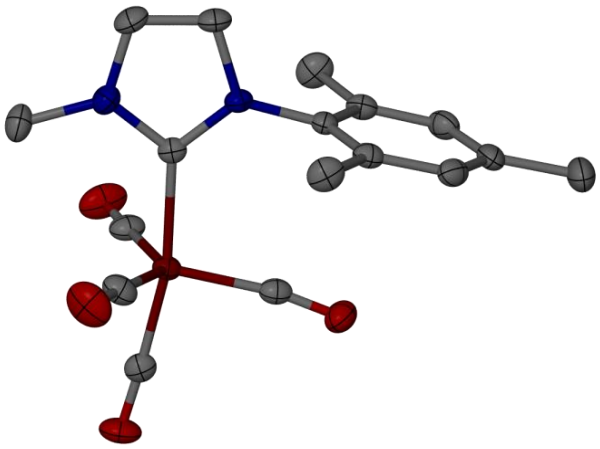

Figure 5-67. The structure of the $Fe(CO)_4$(IMeMes) complex was solved by the author.

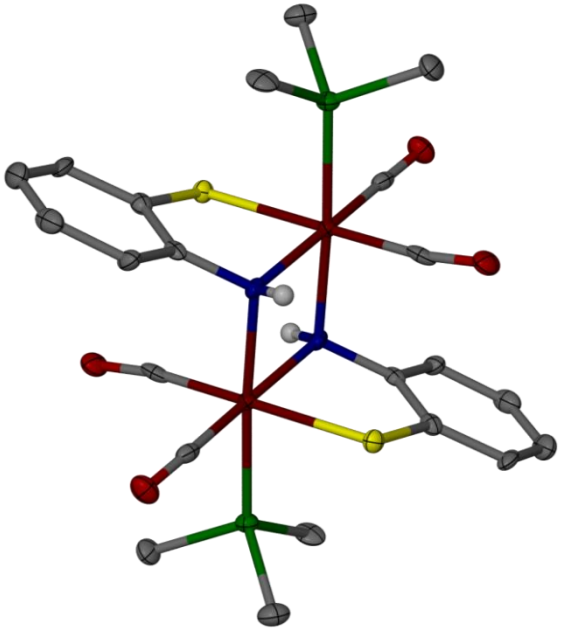

Figure 5-68. The $[Fe(CO)_2(PMe_3)(\mu\text{-}NHPhS)]_2$ complex was synthesized and analyzed by XRD by Dr. Leo Liu and the structure was solved by the author. This complex relates to other published mono-iron hydrogenase model complexes.[343]

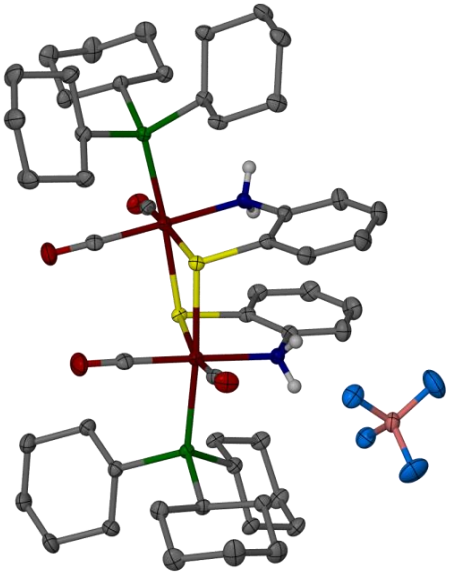

Figure 5-69. The $[Fe(CO)_2(PCy_3)(\mu\text{-}SPhNH_2)]_2[BF_4]_2$ complex was synthesized and XRD data collected by Dr. Leo Liu and structure solved by the author. This complex relates to other published mono-iron hydrogenase model complexes.[343]

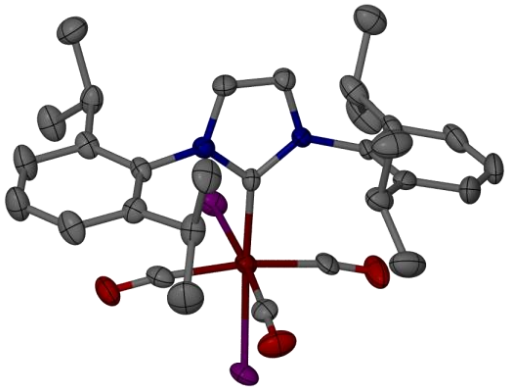

Figure 5-70. The $Fe(CO)_3I_2$(IMesiPr) complex was synthesized and analyzed by XRD by Dr. Leo Liu and structure was solved by the author. IMesiPr = 1,3-bis-(2,6-isopropylphenyl)imidazolate. This complex relates to other published mono-iron hydrogenase model complexes.[343]

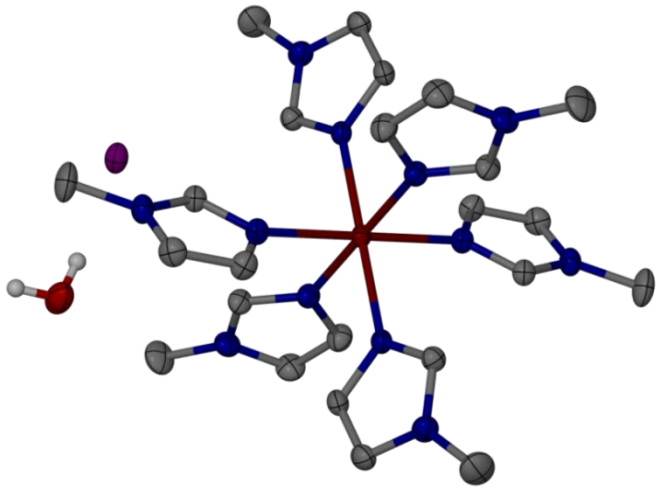

Figure 5-71. The structure of the $[Fe(MeImid)_6][I]_2$ complex was solved by the author with solvent and counterion identified by Dr. Nattami Bhuvanesh. There is one molecule of water per unit cell.

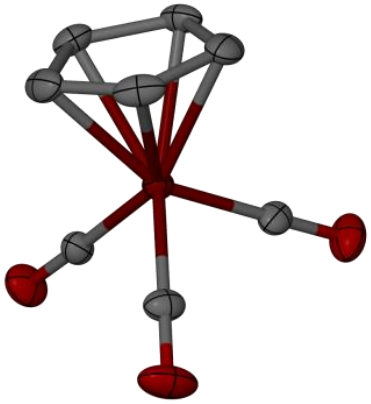

Figure 5-72. The structure of the neutral $(\eta_4\text{-}C_5H_6)Fe(CO)_3$ complex was solved by the author. Note this is a neutral diene bound to an Fe^0. Disorder in the CH_2 position gives the illusion of an $\eta_5\text{-}C_5H_5$ complex.

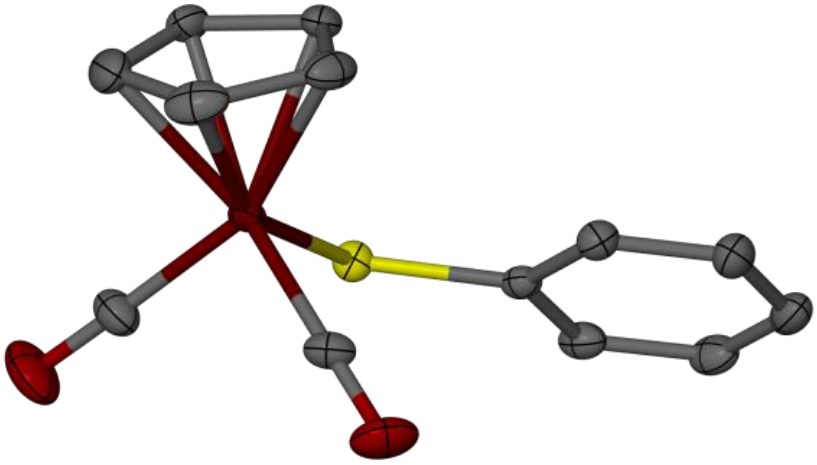

Figure 5-73. The $CpFe(CO)_2SPh$ was synthesized and XRD performed by Allen Lunsford. The structure was solved by the author. The structure was previously published: XOYBES.[344]

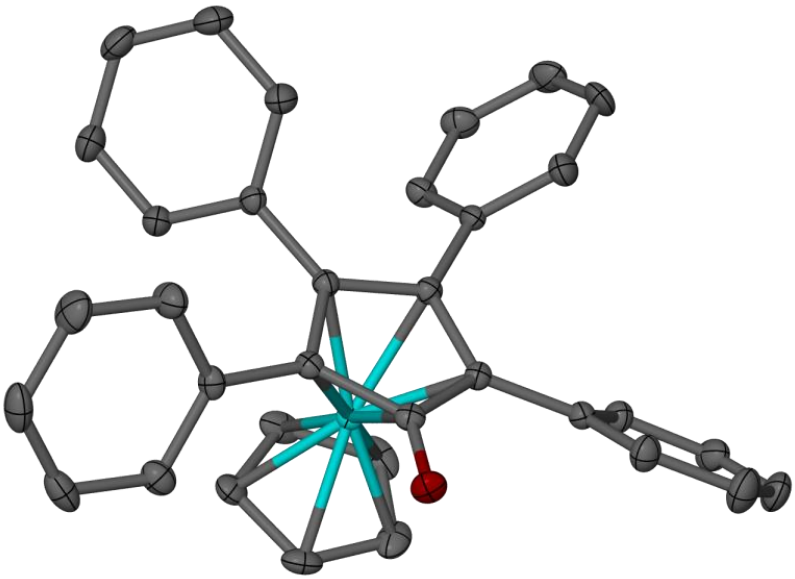

Figure 5-74. The $CpCo(\eta_4\text{-}Ph_4C_5O)$ complex was synthesized and data collected by Allen Lunsford. The structure was solved by the author.

5.6 Salts

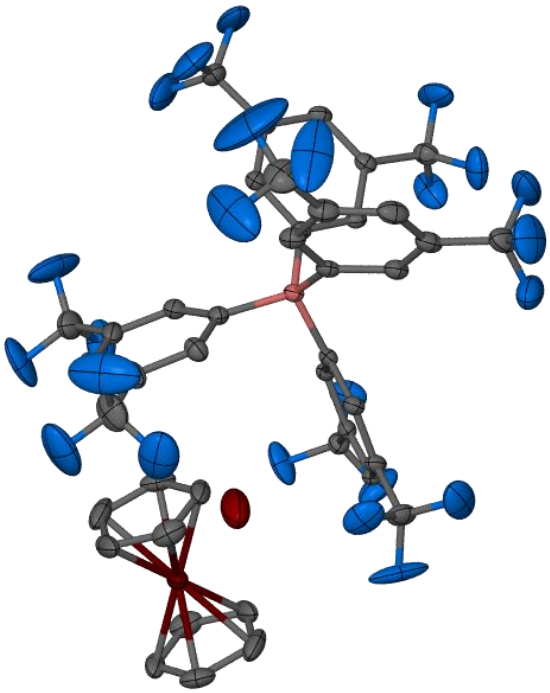

Figure 5-75. The $[Cp_2Fe][BArF]$ salt was isolated by Allen Lunsford and structure solved by the author. A molecule of H_2O is found in the unit cell; and the structure was previously published, FOZXUN.[345]

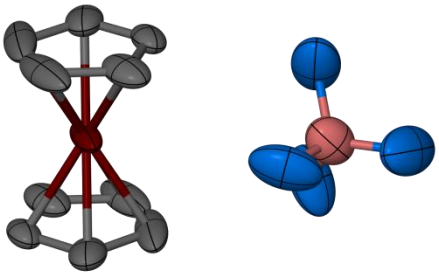

Figure 5-76. The $[Cp_2Fe][BF_4]$ salt was isolated by Rachel Chupik and structure solved by the author. The structure was previously reported: AFALID.[346]

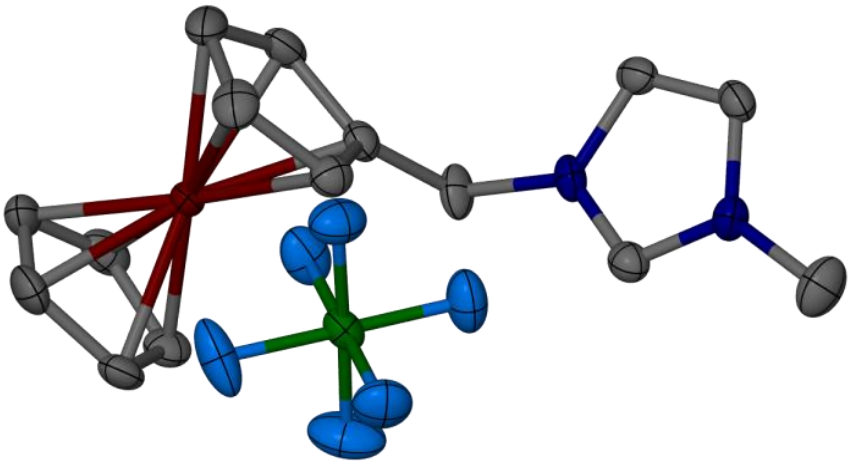

Figure 5-77. The [1Fc][PF_6] ligand was synthesized and XRD collection performed by Allen Lunsford and data solved by the author. 1Fc = 1-methyl-3-methyleneferrocene-imidazolium. The structure was previously reported: YATLEM.[347]

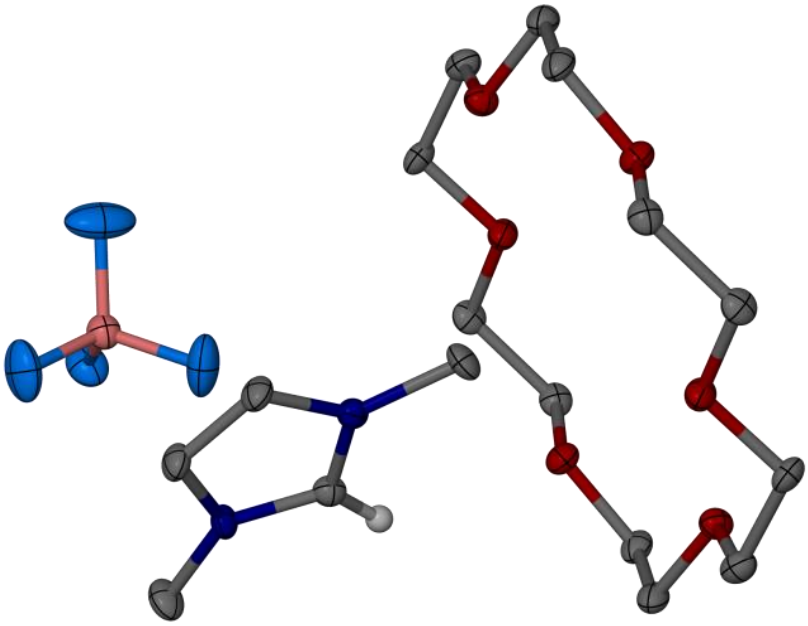

Figure 5-78. The structure of the [IMe][18-crown-6][BF_4] salt was solved by the author.

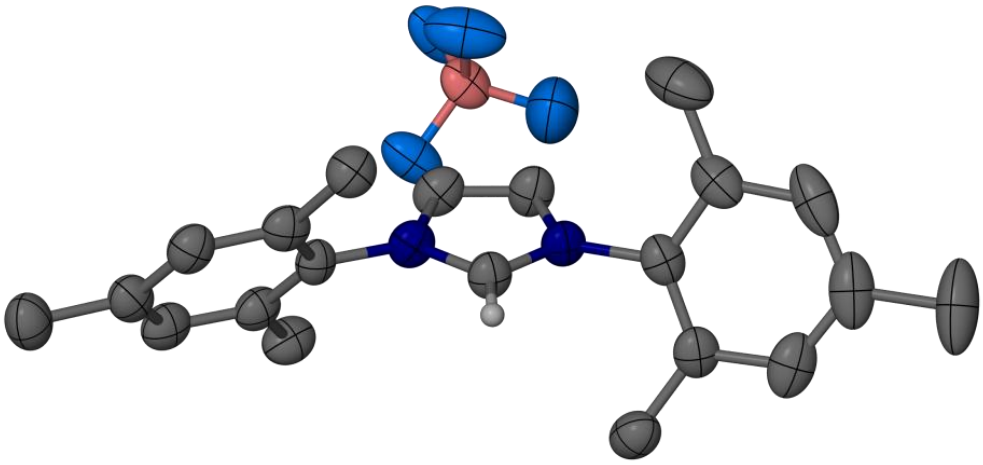

Figure 5-79. The [IMes][BF_4] salt was isolated as single crystals by Ryan Bethel and XRD analysis was performed by the author.

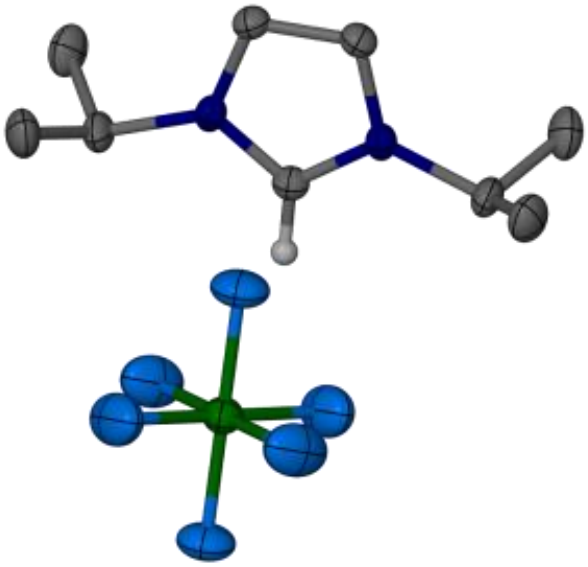

Figure 5-80. The [IPr][PF_6] salt was isolated and XRD data collected by Dr. Jen Hess and structure solved by the author. The structure had previously been reported: ODOLID.[348]

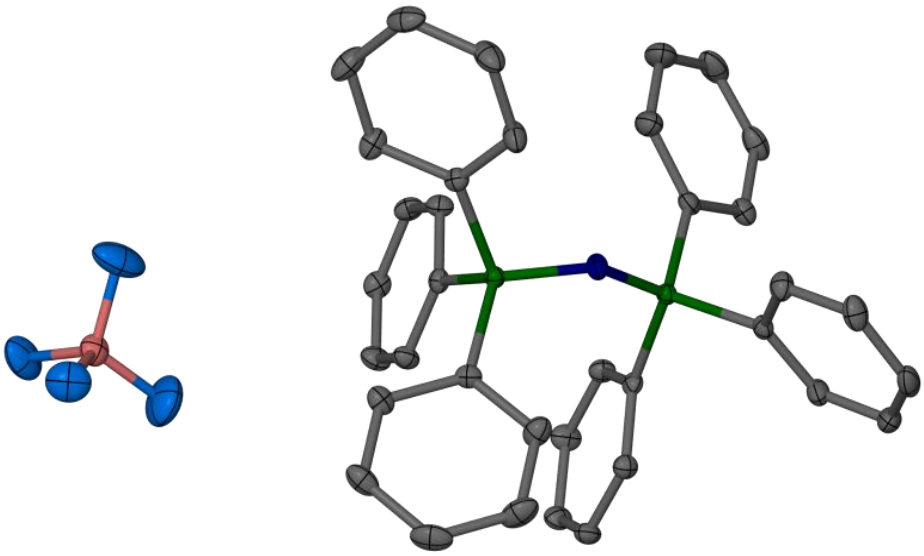

Figure 5-81. The structure of the [PPN][BF_4] salt was solved by the author.

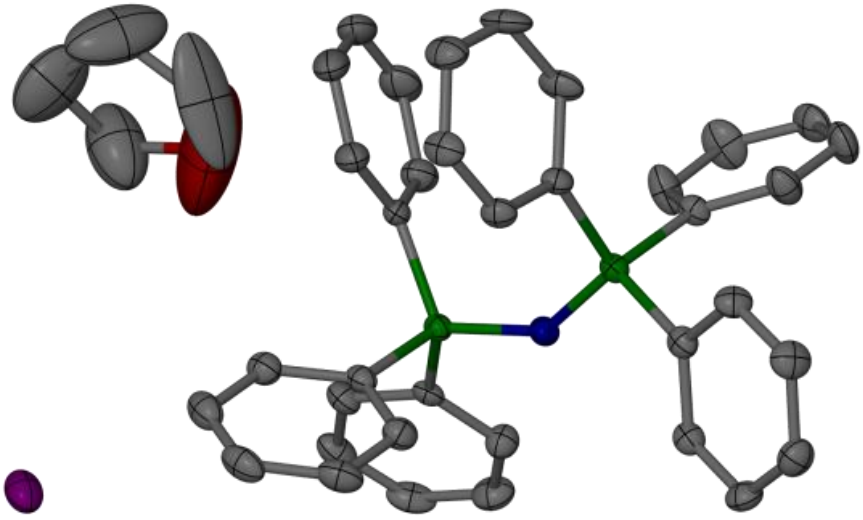

Figure 5-82. The [PPN][I] structure was solved by the author and shows a single THF molecule co-crystallized per unit cell.

5.7 Organic Molecules

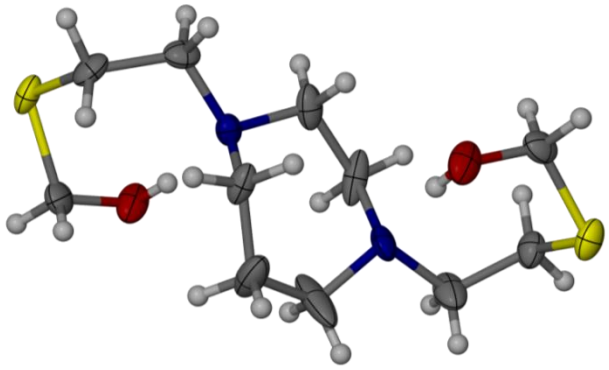

Figure 5-83. The (bme-dach)$(CH_2OH)_2$ ligand was synthesized by condensation of paraformaldehyde and bme-dach. XRD data was collected by Allen Lunsford and structure solved by the author. Note the hydrogen bonding interactions between the hydroxyl groups and the amines.

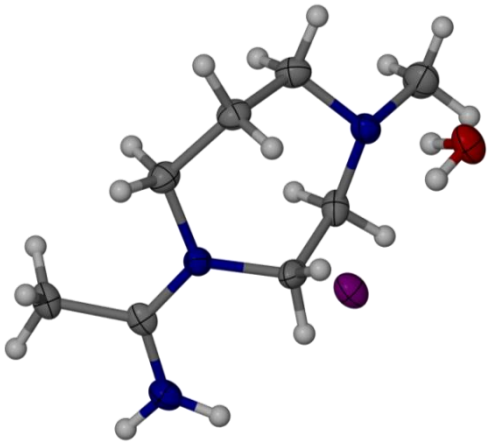

Figure 5-84. The 1-(1-aminoethane)-4-methyl-1,4-diazacycloheptane ligand was isolated and XRD performed by the author. The compound is presumed to arise from the activation of MeCN by an amine or amide during the synthesis of the mme-dach ligand.

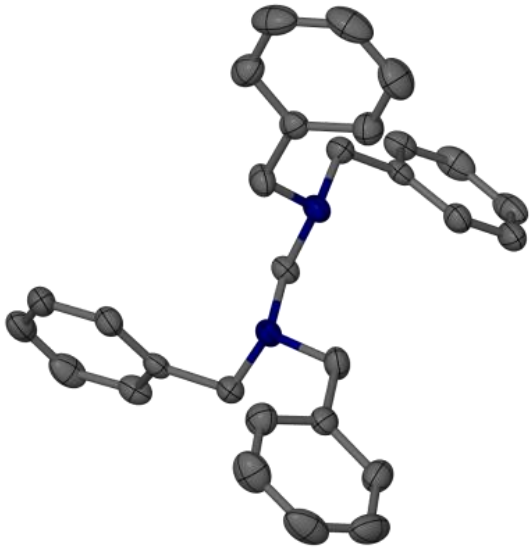

Figure 5-85. The $CH_2(NBz_2)_2$ molecule was isolated by Pokhraj Ghosh and the structure solved by the author. The structure was previously published; MIKQON.[349]

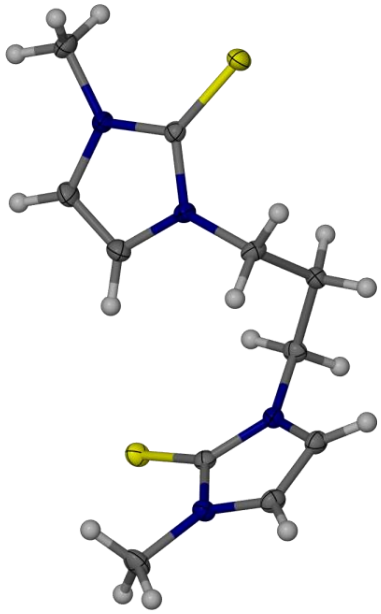

Figure 5-86. The $(SIMe)_2(CH_2)_3$ was synthesized by Dr. Tiffany Pinder and the structure was solved by the author using XRD.

6. SUMMARY

The work presented in this dissertation has investigated the modeling of biological nickel binding sites and other N_2S_2 sites such as those found in the active sites of nitrile hydratase and thiocyanate reductase. The modeling of such biological sites with N_2S_2 ligands offers opportunities to explore a rich area of chemistry, including metal effects, sulfur reactivity, structural diversity, etc. Presented in Section 2 is the summation of a large subset of such complexes which was written as an article for the journal, Chemical Reviews, with a focus on MN_2S_2 complexes acting as metalloligands.[300] The article categorized a variety of supported metal aggregation modes with the available lone pairs of the dithiolate ligands, Figure 6-1. The study found that MN_2S_2 ligands are able to support M'-M' distances ranging from 2.1 Å in Mo-Mo paddlewheels to over 4.3 Å in zinc bridged species with near constant S-S distances.

The goal of work recorded in Section 3 was the investigation into various methods for classifying the electronic and steric properties of a small subset of MN_2S_2 complexes as metalloligands to organometallic fragments such as $W(CO)_4$, $Ni(CO)_3$, and $Fe(CO)_4$ containing diatomic ligand reporters. The ν(CO) IR study found that the metallodithiolate ligands are better donors than phosphines, imines, or N-heterocyclic carbene ligands; but they aren't as strong as anionic RS^- ligands. Due to the extreme asymmetry in such dithiolate ligands conventional ligand cone angles didn't yield a discernible trend. Instead, the percent buried volume concept derived by Nolan *et al.* for the investigation of NHC ligands[222] followed the expected trends in steric encumbrance

seen for the MN_2S_2 ligand in both monodentate and bidentate binding modes, as established by XRD.

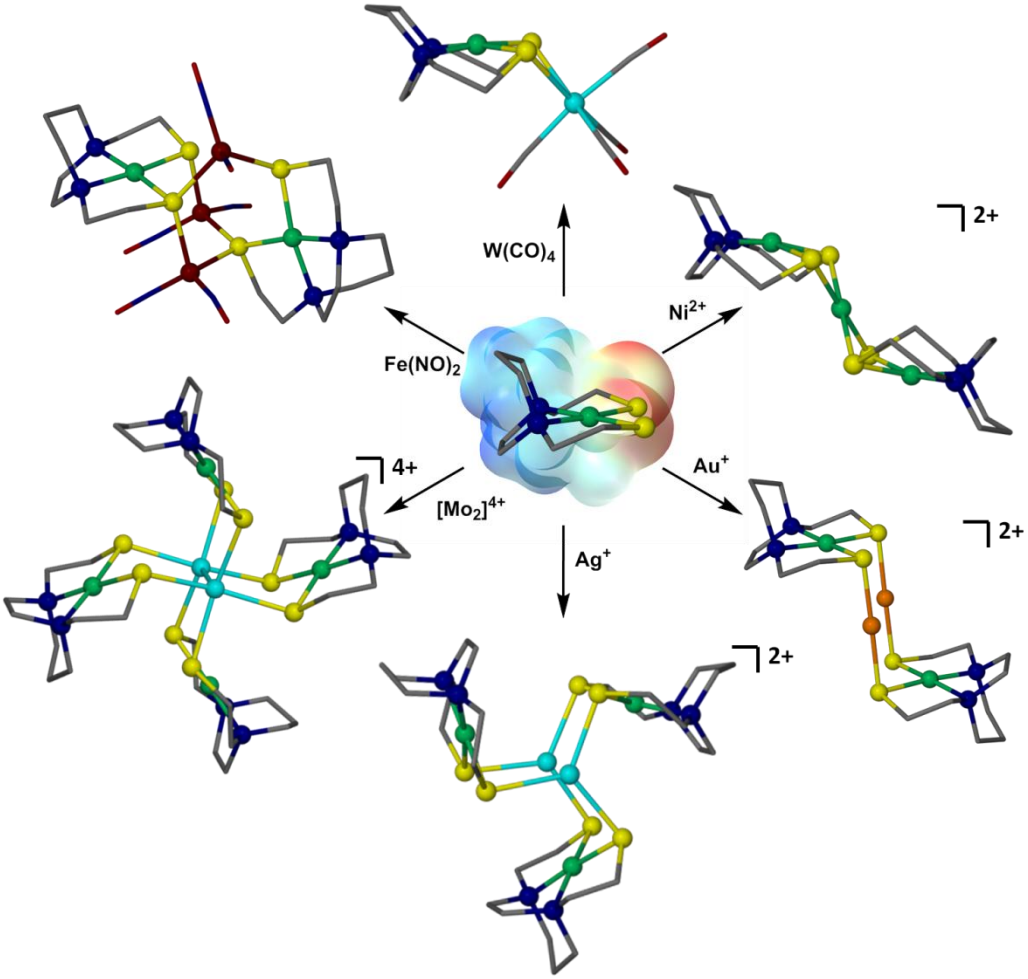

Figure 6-1. Summation of the structural types observed using MN_2S_2 metalloligands as donors to a secondary metal(s). Starting at the top (12 O'clock) position and moving clockwise: bimetallic, stair-step, C_2 propeller, C_3 paddlewheel, C_4 paddlewheel, and adamantane-like clusters.

Section 4 was an experimental investigation into the methods of simple metal-exchange of the metal in the N_2S_2 binding pocket with exogenous metal ions under mild conditions without aggregate formation. This study found upon modification of the parent MN_2S_2 complex with sodium iodoacetate to form the octahedral M-1'-Ac_2, $MN_2(S_{thioether})_2(O_{acetate})_2$, series clean metal exchange reactions could be observed. These products were fully characterized by mass spectroscopy, infrared spectroscopy, UV-Vis, elemental analysis, X-ray diffraction, Guoy balance or Evan's method magnetic studies, and cyclic voltammetry. The hierarchy of metal exchange reactions follows the Irving-Williams series, $Fe^{2+} < Co^{2+} < Ni^{2+} < Cu^{2+} > Zn^{2+}$. From synthetic procedures and analysis of solid-state structures, the Zn-1'-Ac_2 complex would fit in between Fe-1'-Ac_2 and Co-1'-Ac_2 in the exchange series. Measurements of equilibrium constants and kinetic data were performed using UV-Vis methods and are presented within the section. Reactions appear to be first order in M-1'-Ac_2 complex but undergo a change in reaction order as the reactions progressed, which follows the previous observations with EDTA systems.[318,350] This observation indicates the reaction mechanism proceeds via different routes depending on the concentration of the reactants in solution.

Additional exchange reactions which model the biological trafficking of nickel into the cell to storage proteins, metallochaperones, and enzyme active sites are presented in Appendix B. These studies show the exchange of nickel between ligands to mimic the transfer in biology from N_4 to N_2S_2 to S_4 ligation modes.

Section 5 is a presentation of a collection of crystal structure which I have solved during my Ph.D. work. These complexes were synthesized by past and current student

for their dissertation work, as well as myself. These complexes range from [FeFe]-hydrogenase models, to N_2S_2 complexes, to nitrosyl-containing iron and cobalt complexes. Also presented are other (frequently untargeted) inorganic complexes and various salts. Some of the crystal structures were previously known but the majority have already been or are to be published by the MYD group.

The biomimetics of metal binding sites in biological systems have provided a rich source of inspiration for fundamental studies. In particular our group has worked with N_2S_2 complexes for 25 years. Such systems could provide the basis for biomimetics and/or organometallic reactions through utilization of MN_2S_2 complexes as metalloligands. The studies presented herein have raised the question to which metal the bridging thiolate serves as an X-donor or as an L-donor toward. This dichotomy is expressed in Figure 6-2. Additionally, there is the possibility of a reversal of donor type of the thiolate during a catalytic cycle. Such a reversal could prove beneficial in stabilizing higher oxidation states during oxidative addition in activation of substrates. Another bonding scenario could be an intermediate case in which the $M(\mu\text{-}S)_2M'$ unit is fully delocalized and each thiolate serves as an ½ X-donor and ½ L-donor. Such flexibility in electronic structure has not yet been exploited in catalyst design, but should be an interesting and profitable endeavor.

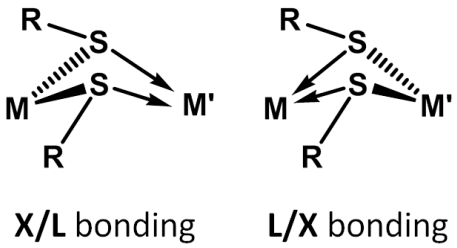

Figure 6-2. ChemDraw representation of bridging thiolates and their respective donor type. In the first example the thiolate is an X-donor to M and an L-donor to M'; the second example shows a reversal of donor type and the system is now L/X to M and M', respectively.

REFERENCES

(1) Jaun, B.; Thauer, R. K.; Sigel, A.; Sigel, H.; Sigel, R. K. O. *Metal Ions in Life Sciences*, 2007.

(2) Denkhaus, E.; Salnikow, K. *Crit. Rev. Oncol. Hematol.* **2002**, *42*, 35.

(3) Harford, C.; Sarkar, B. *Acc. Chem. Res.* **1997**, *30*, 123.

(4) Phipps, T.; Tank, S. L.; Wirtz, J.; Brewer, L.; Coyner, A.; Ortego, L. S.; Fairbrother, A. *Environmental Reviews* **2002**, *10*, 209.

(5) Li, Y.; Zamble, D. B. *Chem. Rev.* **2009**, *109*, 4617.

(6) Shima, S.; Thauer, R. K. *Curr. Opin. Microbiol.* **2005**, *8*, 643.

(7) Färber, G.; Keller, W.; Kratky, C.; Jaun, B.; Pfaltz, A.; Spinner, C.; Kobelt, A.; Eschenmoser, A. *Helv. Chim. Acta* **1991**, *74*, 697.

(8) Friedmann, H. C.; Klein, A.; Thauer, R. K. *FEMS Microbiol. Rev.* **1990**, *7*, 339.

(9) Mulrooney, S. B.; Hausinger, R. P. *FEMS Microbiol. Rev.* **2003**, *27*, 239.

(10) Al-Mjeni, F.; Ju, T.; Pochapsky, T. C.; Maroney, M. J. *Biochemistry* **2002**, *41*, 6761.

(11) Chai, S. C.; Ju, T.; Dang, M.; Goldsmith, R. B.; Maroney, M. J.; Pochapsky, T. C. *Biochemistry* **2008**, *47*, 2428.

(12) Pochapsky, T. C.; Pochapsky, S. S.; Ju, T.; Hoefler, C.; Liang, J. *J. Biomol. NMR* **2006**, *34*, 117.

(13) Pochapsky, T. C.; Pochapsky, S. S.; Ju, T.; Mo, H.; Al-Mjeni, F.; Maroney, M. J. *Nat. Struct. Biol.* **2002**, *9*, 966.

(14) Thornalley, P. J. *Biochem. Soc. Trans.* **2003**, *31*, 1343.

(15) He, M. M.; Clugston, S. L.; Honek, J. F.; Matthews, B. W. *Biochemistry* **2000**, *39*, 8719.

(16) Davidson, G.; Clugston, S. L.; Honek, J. F.; Maroney, M. J. *Inorg. Chem.* **2000**, *39*, 2962.

(17) Sumner, J. B. *J. Biol. Chem.* **1926**, *69*, 435.

(18) Follmer, C. *Phytochemistry* **2008**, *69*, 18.

(19) Jabri, E.; Carr, M. B.; Hausinger, R. P.; Karplus, P. A. *Science* **1995**, *268*, 998.

(20) Kuchar, J.; Hausinger, R. P. *Chem. Rev.* **2004**, *104*, 509.

(21) Brayman, T. G.; Hausinger, R. P. *J. Bacteriol.* **1996**, *178*, 5410.

(22) Colpas, G. J.; Brayman, T. G.; McCracken, J.; Pressler, M. A.; Babcock, G. T.; Ming, L.-J.; Colangelo, C. M.; Scott, R. A.; Hausinger, R. P. *JBIC* **1998**, *3*, 150.

(23) Lee, M. H.; Pankratz, H. S.; Wang, S.; Scott, R. A.; Finnegan, M. G.; Johnson, M. K.; Ippolito, J. A.; Christianson, D. W.; Hausinger, R. P. *Protein Sci.* **1993**, *2*, 1042.

(24) Stola, M.; Musiani, F.; Mangani, S.; Turano, P.; Safarov, N.; Zambelli, B.; Ciurli, S. *Biochemistry* **2006**, *45*, 6495.

(25) Benoit, S. L.; Mehta, N.; Weinberg, M. V.; Maier, C.; Maier, R. J. *Microbiology* **2007**, *153*, 1474.

(26) Stingl, K.; Schauer, K.; Ecobichon, C.; Labigne, A.; Lenormand, P.; Rousselle, J. C.; Namane, A.; De Reuse, H. *Mol. Cell. Proteomics* **2008**, *7*, 2429.

(27) Suerbaum, S.; Thiberge, J. M.; Kansau, I.; Ferrero, R. L.; Labigne, A. *Mol. Microbiol.* **1994**, *14*, 959.

(28) Gilbert, J. V.; Ramakrishna, J.; Sunderman, F. W.; Wright, A.; Plaut, A. G. *Infect. Immun.* **1995**, *63*, 2682.

(29) Ge, R.; Watt, R. M.; Sun, X.; Tanner, J. A.; He, Q. Y.; Huang, J. D.; Sun, H. *Biochem. J.* **2006**, *393*, 285.

(30) Zeng, Y. B.; Zhang, D. M.; Li, H.; Sun, H. *J. Biol. Inorg. Chem.* **2008**, *13*, 1121.

(31) Vignais, P. M.; Billoud, B. *Chem. Rev.* **2007**, *107*, 4206.

(32) Vignais, P. M.; Billoud, B.; Meyer, J. *FEMS Microbiol. Rev.* **2001**, *25*, 455.

(33) Wu, L. F.; Mandrand, M. A. *FEMS Microbiol. Rev.* **1993**, *10*, 243.

(34) Fontecilla-Camps, J. C.; Volbeda, A.; Cavazza, C.; Nicolet, Y. *Chem. Rev.* **2007**, *107*, 4273.

(35) Blokesch, M.; Paschos, A.; Bauer, A.; Reissmann, S.; Drapal, N.; Böck, A. *Eur. J. Biochem.* **2004**, *271*, 3428.

(36) Blokesch, M.; Albracht, S. P. J.; Matzanke, B. F.; Drapal, N. M.; Jacobi, A.; Böck, A. *J. Mol. Biol.* **2004**, *344*, 155.

(37) Blokesch, M.; Böck, A. *J. Mol. Biol.* **2002**, *324*, 287.

(38) Ludwig, M.; Schubert, T.; Zebger, I.; Wisitruangsakul, N.; Saggu, M.; Strack, A.; Lenz, O.; Hildebrandt, P.; Friedrich, B. *J. Biol. Chem.* **2009**, *284*, 2159.

(39) Magalon, A.; Böck, A. *FEBS Lett.* **2000**, *473*, 254.

(40) Du, L.; Tibelius, K. *Current Microbiology* **1994**, *28*, 21.

(41) Hoffmann, D.; Gutekunst, K.; Klissenbauer, M.; Schulz-Friedrich, R.; Appel, J. *FEBS J.* **2006**, *273*, 4516.

(42) Hube, M.; Blokesch, M.; Böck, A. *J. Bacteriol.* **2002**, *184*, 3879.

(43) Jacobi, A.; Rossmann, R.; Böck, A. *Arch. Microbiol.* **1992**, *158*, 444.

(44) Maier, T.; Lottspeich, F.; Böck, A. *Eur. J. Biochem.* **1995**, *230*, 133.

(45) Olson, J. W.; Fu, C.; Maier, R. J. *Mol. Microbiol.* **1997**, *24*, 119.

(46) Olson, J. W.; Mehta, N. S.; Maier, R. J. *Mol. Microbiol.* **2001**, *39*, 176.

(47) Rey, L.; Imperial, J.; Palacios, J. M.; Ruiz-Argüeso, T. *J. Bacteriol.* **1994**, *176*, 6066.

(48) Waugh, R.; Boxer, D. H. *Biochimie* **1986**, *68*, 157.

(49) Böck, A.; King, P. W.; Blokesch, M.; Posewitz, M. C. In *Advances in Microbial Physiology*; Robert, K. P., Ed.; Academic Press, 2006; Vol. Volume 51.

(50) Hottenrott, S.; Schumann, T.; Plückthun, A.; Fischer, G.; Rahfeld, J. U. *J. Biol. Chem.* **1997**, *272*, 15697.

(51) Wülfing, C.; Lombardero, J.; Plückthun, A. *J. Biol. Chem.* **1994**, *269*, 2895.

(52) Leach, M. R.; Zhang, J. W.; Zamble, D. B. *J. Biol. Chem.* **2007**, *282*, 16177.

(53) Zhang, J. W.; Butland, G.; Greenblatt, J. F.; Emili, A.; Zamble, D. B. *J. Biol. Chem.* **2005**, *280*, 4360.

(54) Fu, C.; Olson, J. W.; Maier, R. J. *Proc. Natl. Acad. Sci. U.S.A.* **1995**, *92*, 2333.

(55) Atanassova, A.; Zamble, D. B. *J. Bacteriol.* **2005**, *187*, 4689.

(56) Borden, K. L. B. *J. Mol. Biol.* **2000**, *295*, 1103.

(57) Dawid, I. B.; Breen, J. J.; Toyama, R. *Trends Genet.* **1998**, *14*, 156.

(58) Mackay, J. P.; Crossley, M. *Trends Biochem. Sci* **1998**, *23*, 1.

(59) Mehta, N.; Olson, J. W.; Maier, R. J. *J. Bacteriol.* **2003**, *185*, 726.

(60) Leach, M. R.; Sandal, S.; Sun, H.; Zamble, D. B. *Biochemistry* **2005**, *44*, 12229.

(61) Robson, R.; Cammack, R.; Frey, M.; Robson, R. *Hydrogen as a fuel: Learning from nature*, 2001.

(62) Gasper, R.; Scrima, A.; Wittinghofer, A. *J. Biol. Chem.* **2006**, *281*, 27492.

(63) Magalon, A.; Blokesch, M.; Zehelein, E.; Böck, A. *FEBS Lett.* **2001**, *499*, 73.

(64) Menon, A. L.; Robson, R. L. *J. Bacteriol.* **1994**, *176*, 291.

(65) Rodrigue, A.; Boxer, D. H.; Mandrand-Berthelot, M. A.; Wu, L. F. *FEBS Lett.* **1996**, *392*, 81.

(66) Rossmann, R.; Sauter, M.; Lottspeich, F.; Böck, A. *Eur. J. Biochem.* **1994**, *220*, 377.

(67) Theodoratou, E.; Paschos, A.; Magalon, A.; Fritsche, E.; Huber, R.; Böck, A. *Eur. J. Biochem.* **2000**, *267*, 1995.

(68) Cabiscol, E.; Tamarit, J.; Ros, J. *Int. Microbiol.* **2000**, *3*, 3.

(69) Barondeau, D. P.; Kassmann, C. J.; Bruns, C. K.; Tainer, J. A.; Getzoff, E. D. *Biochemistry* **2004**, *43*, 8038.

(70) Wuerges, J.; Lee, J. W.; Yim, Y. I.; Yim, H. S.; Kang, S. O.; Carugo, K. D. *Proc. Natl. Acad. Sci. U.S.A.* **2004**, *101*, 8569.

(71) Bryngelson, P. A.; Arobo, S. E.; Pinkham, J. L.; Cabelli, D. E.; Maroney, M. J. *J. Am. Chem. Soc.* **2004**, *126*, 460.

(72) Choudhury, S. B.; Lee, J. W.; Davidson, G.; Yim, Y. I.; Bose, K.; Sharma, M. L.; Kang, S. O.; Cabelli, D. E.; Maroney, M. J. *Biochemistry* **1999**, *38*, 3744.

(73) Neupane, K. P.; Gearty, K.; Francis, A.; Shearer, J. *J. Am. Chem. Soc.* **2007**, *129*, 14605.

(74) Szilagyi, R. K.; Bryngelson, P. A.; Maroney, M. J.; Hedman, B.; Hodgson, K. O.; Solomon, E. I. *J. Am. Chem. Soc.* **2004**, *126*, 3018.

(75) Darnault, C.; Volbeda, A.; Kim, E. J.; Legrand, P.; Vernede, X.; Lindahl, P. A.; Fontecilla-Camps, J. C. *Nat. Struct. Biol.* **2003**, *10*, 271.

(76) Dobbek, H.; Svetlitchnyi, V.; Gremer, L.; Huber, R.; Meyer, O. *Science* **2001**, *293*, 1281.

(77) Doukov, T. I.; Iverson, T. M.; Seravalli, J.; Ragsdale, S. W.; Drennan, C. L. *Science* **2002**, *298*, 567.

(78) Drennan, C. L.; Heo, J.; Sintchak, M. D.; Schreiter, E.; Ludden, P. W. *Proc. Natl. Acad. Sci. U.S.A.* **2001**, *98*, 11973.

(79) Gong, W.; Hao, B.; Wei, Z.; Ferguson, D. J.; Tallant, T.; Krzycki, J. A.; Chan, M. K. *Proc. Natl. Acad. Sci. U.S.A.* **2008**, *105*, 9558.

(80) Jeoung, J. H.; Dobbek, H. *Science* **2007**, *318*, 1461.

(81) Drennan, C. L.; Doukov, T. I.; Ragsdale, S. W. *J. Biol. Inorg. Chem.* **2004**, *9*, 511.

(82) Svetlitchnyi, V.; Dobbek, H.; Meyer-Klaucke, W.; Meins, T.; Thiele, B.; Römer, P.; Huber, R.; Meyer, O. *Proc. Natl. Acad. Sci. U. S. A.* **2004**, *101*, 446.

(83) Davidson, G.; Clugston, S. L.; Honek, J. F.; Maroney, M. J. *Biochemistry* **2001**, *40*, 4569.

(84) Higgins, C. F. *Res. Microbiol.* **2001**, *152*, 205.

(85) Allan, C. B.; Wu, L.-F.; Gu, Z.; Choudhury, S. B.; Al-Mjeni, F.; Sharma, M. L.; Mandrand-Berthelot, M.-A.; Maroney, M. J. *Inorg. Chem.* **1998**, *37*, 5952.

(86) Addy, C.; Ohara, M.; Kawai, F.; Kidera, A.; Ikeguchi, M.; Fuchigami, S.; Osawa, M.; Shimada, I.; Park, S.-Y.; Tame, J. R. H.; Heddle, J. G. *Acta Crystallographica Section D* **2007**, *63*, 221.

(87) Navarro, C.; Wu, L. F.; Mandrand-Berthelot, M. A. *Mol. Microbiol.* **1993**, *9*, 1181.

(88) Grass, G.; Fricke, B.; Nies, D. H. *Biometals* **2005**, *18*, 437.

(89) Nies, D. H. *FEMS Microbiol. Rev.* **2003**, *27*, 313.

(90) Chivers, P. T.; Sauer, R. T. *Protein Sci.* **1999**, *8*, 2494.

(91) Chivers, P. T.; Tahirov, T. H. *J. Mol. Biol.* **2005**, *348*, 597.

(92) Dosanjh, N. S.; Michel, S. L. *Curr. Opin. Chem. Biol.* **2006**, *10*, 123.

(93) Schreiter, E. R.; Sintchak, M. D.; Guo, Y.; Chivers, P. T.; Sauer, R. T.; Drennan, C. L. *Nat. Struct. Biol.* **2003**, *10*, 794.

(94) Schreiter, E. R.; Wang, S. C.; Zamble, D. B.; Drennan, C. L. *Proc. Natl. Acad. Sci. U.S.A.* **2006**, *103*, 13676.

(95) Bloom, S. L.; Zamble, D. B. *Biochemistry* **2004**, *43*, 10029.

(96) Chivers, P. T.; Sauer, R. T. *J. Biol. Chem.* **2000**, *275*, 19735.

(97) Zambelli, B.; Bellucci, M.; Danielli, A.; Scarlato, V.; Ciurli, S. *Chem. Commun.* **2007**, *35*, 3649.

(98) Leitch, S.; Bradley, M. J.; Rowe, J. L.; Chivers, P. T.; Maroney, M. J. *J. Am. Chem. Soc.* **2007**, *129*, 5085.

(99) Iwig, J. S.; Leitch, S.; Herbst, R. W.; Maroney, M. J.; Chivers, P. T. *J. Am. Chem. Soc.* **2008**, *130*, 7592.

(100) Cavet, J. S.; Meng, W.; Pennella, M. A.; Appelhoff, R. J.; Giedroc, D. P.; Robinson, N. J. *J. Biol. Chem.* **2002**, *277*, 38441.

(101) Pennella, M. A.; Shokes, J. E.; Cosper, N. J.; Scott, R. A.; Giedroc, D. P. *Proc. Natl. Acad. Sci. U.S.A.* **2003**, *100*, 3713.

(102) Campbell, D. R.; Chapman, K. E.; Waldron, K. J.; Tottey, S.; Kendall, S.; Cavallaro, G.; Andreini, C.; Hinds, J.; Stoker, N. G.; Robinson, N. J.; Cavet, J. S. *J. Biol. Chem.* **2007**, *282*, 32298.

(103) Arakawa, T.; Kawano, Y.; Kataoka, S.; Katayama, Y.; Kamiya, N.; Yohda, M.; Odaka, M. *J. Mol. Biol.* **2007**, *366*, 1497.

(104) Nagashima, S.; Nakasako, M.; Dohmae, N.; Tsujimura, M.; Takio, K.; Odaka, M.; Yohda, M.; Kamiya, N.; Endo, I. *Nat. Struct. Mol. Biol.* **1998**, *5*, 347.

(105) Miyanaga, A.; Fushinobu, S.; Ito, K.; Wakagi, T. *Biochem. Biophys. Res. Commun.* **2001**, *288*, 1169.

(106) Farmer, P. J.; Solouki, T.; Mills, D. K.; Soma, T.; Russell, D. H.; Reibenspies, J. H.; Darensbourg, M. Y. *J. Am. Chem. Soc.* **1992**, *114*, 4601.

(107) Jicha, D. C.; Busch, D. H. *Inorg. Chem.* **1962**, *1*, 872.

(108) Busch, D. H.; Jicha, D. C.; Thompson, M. C.; Wrathall, J. W.; Blinn, E. *J. Am. Chem. Soc.* **1964**, *86*, 3642.

(109) Busch, D. H.; Stephenson, N. A. *Coord. Chem. Rev.* **1990**, *100*, 119.

(110) Hubin, T. J.; Busch, D. H. *Coord. Chem. Rev.* **2000**, *200–202*, 5.

(111) Wei, C. H.; Dahl, L. F. *Inorg. Chem.* **1970**, *9*, 1878.

(112) Doukov, T. I.; Blasiak, L. C.; Seravalli, J.; Ragsdale, S. W.; Drennan, C. L. *Biochemistry* **2008**, *47*, 3474.

(113) Webster, C. E.; Darensbourg, M. Y.; Lindahl, P. A.; Hall, M. B. *J. Am. Chem. Soc.* **2004**, *126*, 3410.

(114) Darnault, C.; Volbeda, A.; Kim, E. J.; Legrand, P.; Vernede, X.; Lindahl, P. A.; Fontecilla-Camps, J. C. *Nat. Struct. Mol. Biol.* **2003**, *10*, 271.

(115) Harrop, T. C.; Mascharak, P. K. *Coord. Chem. Rev.* **2005**, *249*, 3007.

(116) Rampersad, M. V.; Zuidema, E.; Ernsting, J. M.; van Leeuwen, P. W. N. M.; Darensbourg, M. Y. *Organometallics* **2007**, *26*, 783.

(117) Ittel, S. D.; Johnson, L. K.; Brookhart, M. *Chem. Rev.* **2000**, *100*, 1169.

(118) Ogo, S.; Kabe, R.; Uehara, K.; Kure, B.; Nishimura, T.; Menon, S. C.; Harada, R.; Fukuzumi, S.; Higuchi, Y.; Ohhara, T.; Tamada, T.; Kuroki, R. *Science* **2007**, *316*, 585.

(119) Ogo, S.; Ichikawa, K.; Kishima, T.; Matsumoto, T.; Nakai, H.; Kusaka, K.; Ohhara, T. *Science* **2013**, *339*, 682.

(120) Thomas, I. R.; Bruno, I. J.; Cole, J. C.; Macrae, C. F.; Pidcock, E.; Wood, P. A. *J. Appl. Crystallogr.* **2010**, *43*, 362.

(121) Rao, P. V.; Bhaduri, S.; Jiang, J.; Holm, R. H. *Inorg. Chem.* **2004**, *43*, 5833.

(122) Bouwman, E.; Reedijk, J. *Coord. Chem. Rev.* **2005**, *249*, 1555.

(123) Ohki, Y.; Tatsumi, K. *Eur. J. Inorg. Chem.* **2011**, *2011*, 973.

(124) Volbeda, A.; Charon, M.-H.; Piras, C.; Hatchikian, E. C.; Frey, M.; Fontecilla-Camps, J. C. *Nature* **1995**, *373*, 580.

(125) Volbeda, A.; Martin, L.; Cavazza, C.; Matho, M.; Faber, B.; Roseboom, W.; Albracht, S. J.; Garcin, E.; Rousset, M.; Fontecilla-Camps, J. *J. Biol. Inorg. Chem.* **2005**, *10*, 239.

(126) Kawamoto, T.; Takeda, K.; Nishiwaki, M.; Aridomi, T.; Konno, T. *Inorg. Chem.* **2007**, *46*, 4239.

(127) Kawamoto, T.; Suzuki, N.; Ono, T.; Gong, D.; Konno, T. *Chem. Commun.* **2013**, *49*, 668.

(128) Smee, J. J.; Miller, M. L.; Grapperhaus, C. A.; Reibenspies, J. H.; Darensbourg, M. Y. *Inorg. Chem.* **2001**, *40*, 3601.

(129) Mills, D. K.; Reibenspies, J. H.; Darensbourg, M. Y. *Inorg. Chem.* **1990**, *29*, 4364.

(130) Mills, D. K.; Font, I.; Farmer, P. J.; Hsiao, Y.-M.; Tuntulani, T.; Buonomo, R. M.; Goodman, D. C.; Musie, G.; Grapperhaus, C. A.; Maguire, M. J.; Lai, C.-H.; Hatley, M. L.; Smee, J. J.; Bellefeuille, J. A.; Darensbourg, M. Y.; Hancock, R. D.; Eng, S.; Martell, A. E. In *Inorg. Synth.*; John Wiley & Sons, Inc., 1998.

(131) Darensbourg, M. Y.; Font, I.; Pala, M.; Reibenspies, J. H. *J. Coord. Chem.* **1994**, *32*, 39.

(132) Buonomo, R. M.; Font, I.; Maguire, M. J.; Reibenspies, J. H.; Tuntulani, T.; Darensbourg, M. Y. *J. Am. Chem. Soc.* **1995**, *117*, 963.

(133) Kure, B.; Taniguchi, A.; Nakajima, T.; Tanase, T. *Organometallics* **2012**, *31*, 4791.

(134) Hosler, E. R.; Herbst, R. W.; Maroney, M. J.; Chohan, B. S. *Dalton Trans.* **2012**, *41*, 804.

(135) Crouse, H. F.; Potoma, J.; Nejrabi, F.; Snyder, D. L.; Chohan, B. S.; Basu, S. *Dalton Trans.* **2012**, *41*, 2720.

(136) Grapperhaus, C. A.; Mullins, C. S.; Kozlowski, P. M.; Mashuta, M. S. *Inorg. Chem.* **2004**, *43*, 2859.

(137) Mathrubootham, V.; Thomas, J.; Staples, R.; McCraken, J.; Shearer, J.; Hegg, E. L. *Inorg. Chem.* **2010**, *49*, 5393.

(138) Gale, E. M.; Cowart, D. M.; Scott, R. A.; Harrop, T. C. *Inorg. Chem.* **2011**, *50*, 10460.

(139) Shearer, J.; Zhao, N. *Inorg. Chem.* **2006**, *45*, 9637.

(140) Hanss, J.; Krüger, H.-J. *Angew. Chem. Int. Ed.* **1998**, *37*, 360.

(141) Hatlevik, O.; Blanksma, M. C.; Mathrubootham, V.; Arif, A. M.; Hegg, E. L. *J. Biol. Inorg. Chem.* **2004**, *9*, 238.

(142) Kruger, H. J.; Peng, G.; Holm, R. H. *Inorg. Chem.* **1991**, *30*, 734.

(143) Schneider, J.; Hauptmann, R.; Osterloh, F.; Henkel, G. *Acta Crystallogr. Sect. C: Cryst. Struct. Commun.* **1999**, *55*, 328.

(144) Colpas, G. J.; Kumar, M.; Day, R. O.; Maroney, M. J. *Inorg. Chem.* **1990**, *29*, 4779.

(145) Stibrany, R. T.; Fox, S.; Bharadwaj, P. K.; Schugar, H. J.; Potenza, J. A. *Inorg. Chem.* **2005**, *44*, 8234.

(146) Grapperhaus, C. A.; O'Toole, M. G.; Mashuta, M. S. *Acta Crystallogr. Sect. Sect. E: Struct. Rep. Online* **2007**, *63*, m2281.

(147) Linck, R. C.; Spahn, C. W.; Rauchfuss, T. B.; Wilson, S. R. *J. Am. Chem. Soc.* **2003**, *125*, 8700.

(148) Fernando, Q.; Wheatley, P. J. *Inorg. Chem.* **1965**, *4*, 1726.

(149) Sellmann, D.; Prechtel, W.; Knoch, F.; Moll, M. *Z. Naturforsch., B: Chem. Sci.* **1992**, *47*, 1411.

(150) Dori, Z.; Eisenberg, R.; Stiefel, E. I.; Gray, H. B. *J. Am. Chem. Soc.* **1970**, *92*, 1506.

(151) Sellmann, D.; Ruf, R.; Knoch, F.; Moll, M. *Z. Naturforsch., B: Chem. Sci.* **1995**, *50*, 791.

(152) Kawamoto, T.; Kushi, Y. *Bull. Chem. Soc. Jpn.* **2004**, *77*, 289.

(153) Goswami, N.; Eichhorn, D. M. *Inorg. Chim. Acta* **2000**, *303*, 271.

(154) Yamamura, T.; Tadokoro, M.; Hamaguchi, M.; Kuroda, R. *Chem. Lett.* **1989**, 1245.

(155) Smeets, W. J. J.; Spek, A. L.; Henderson, R. K.; Bouwman, E.; Reedijk, J. *Acta Crystallogr. Sect. C: Cryst. Struct. Commun.* **1997**, *53*, 1564.

(156) Stenson, P. A.; Board, A.; Marin-Becerra, A.; Blake, A. J.; Davies, E. S.; Wilson, C.; McMaster, J.; Schröder, M. *Chem. Eur. J.* **2008**, *14*, 2564.

(157) Henderson, R. K.; Bouwman, E.; Reedijk, J.; Powell, A. K. *Acta Crystallogr. Sect. C: Cryst. Struct. Commun.* **1996**, *52*, 2696.

(158) Fierro, C. M.; Murphy, B. P.; Smith, P. D.; Coles, S. J.; Hursthouse, M. B. *Inorg. Chim. Acta* **2006**, *359*, 2321.

(159) Addison, A. W.; Rao, T. N.; Reedijk, J.; van Rijn, J.; Verschoor, G. C. *J. Chem. Soc., Dalton Trans.* **1984**, 1349.

(160) O'Toole, M. G.; Kreso, M.; Kozlowski, P. M.; Mashuta, M. S.; Grapperhaus, C. A. *J. Biol. Inorg. Chem.* **2008**, *13*, 1219.

(161) de Paula, Q. A.; Liu, Q.; Almaraz, E.; Denny, J. A.; Mangrum, J. B.; Bhuvanesh, N.; Darensbourg, M. Y.; Farrell, N. P. *Dalton Trans.* **2009**, 10896.

(162) Almaraz, E.; de Paula, Q. A.; Liu, Q.; Reibenspies, J. H.; Darensbourg, M. Y.; Farrell, N. P. *J. Am. Chem. Soc.* **2008**, *130*, 6272.

(163) Darensbourg, M. Y.; Tuntulani, T.; Reibenspies, J. H. *Inorg. Chem.* **1995**, *34*, 6287.

(164) Tuntulani, T.; Reibenspies, J. H.; Farmer, P. J.; Darensbourg, M. Y. *Inorg. Chem.* **1992**, *31*, 3497.

(165) CCDC-1046569 *Submitted* **2014**.

(166) Mills, D. K.; Hsiao, Y. M.; Farmer, P. J.; Atnip, E. V.; Reibenspies, J. H.; Darensbourg, M. Y. *J. Am. Chem. Soc.* **1991**, *113*, 1421.

(167) Denny, J. A.; Foley, W. S.; Almaraz, E.; Reibenspies, J. H.; Bhuvanesh, N.; Darensbourg, M. Y. *Dalton Trans.* **2012**, *41*, 143.

(168) Golden, M. L.; Reibenspies, J. H.; Darensbourg, M. Y. *Inorg. Chem.* **2004**, *43*, 5798.

(169) Chiang, C.-Y.; Lee, J.; Dalrymple, C.; Sarahan, M. C.; Reibenspies, J. H.; Darensbourg, M. Y. *Inorg. Chem.* **2005**, *44*, 9007.

(170) Chiang, C.-Y.; Miller, M. L.; Reibenspies, J. H.; Darensbourg, M. Y. *J. Am. Chem. Soc.* **2004**, *126*, 10867.

(171) Hess, J. L.; Conder, H. L.; Green, K. N.; Darensbourg, M. Y. *Inorg. Chem.* **2008**, *47*, 2056.

(172) Enemark, J. H.; Feltham, R. D. *Coord. Chem. Rev.* **1974**, *13*, 339.

(173) CCDC-1044541 *Submitted* **2014**.

(174) Musie, G.; Lai, C.-H.; Reibenspies, J. H.; Sumner, L. W.; Darensbourg, M. Y. *Inorg. Chem.* **1998**, *37*, 4086.

(175) Baltusis, L. M.; Karlin, K. D.; Rabinowitz, H. N.; Dewan, J. C.; Lippard, S. J. *Inorg. Chem.* **1980**, *19*, 2627.

(176) Karlin, K. D.; Rabinowitz, H. N.; Lewis, D. L.; Lippard, S. J. *Inorg. Chem.* **1977**, *16*, 3262.

(177) Hu, W.-J.; Lippard, S. J. *J. Am. Chem. Soc.* **1974**, *96*, 2366.

(178) Karlin, K. D.; Lewis, D. L.; Rabinowitz, H. N.; Lippard, S. J. *J. Am. Chem. Soc.* **1974**, *96*, 6519.

(179) Rabinowitz, H. N.; Karlin, K. D.; Lippard, S. J. *J. Am. Chem. Soc.* **1977**, *99*, 1420.

(180) Emig, S.; Sellmann, D.; Heinemann, F. W., Private Communication.

(181) Bonnet, D.; Leduc, P.; Bill, E.; Chottard, G.; Mansuy, D.; Artaud, I. *Eur. J. Inorg. Chem.* **2001**, *2001*, 1449.

(182) Herebian, D.; Bothe, E.; Bill, E.; Weyhermüller, T.; Wieghardt, K. *J. Am. Chem. Soc.* **2001**, *123*, 10012.

(183) Sproules, S.; Kapre, R. R.; Roy, N.; Weyhermüller, T.; Wieghardt, K. *Inorg. Chim. Acta* **2010**, *363*, 2702.

(184) Presow, S. R.; Ghosh, M.; Bill, E.; Weyhermüller, T.; Wieghardt, K. *Inorg. Chim. Acta* **2011**, *374*, 226.

(185) Schneider, J.; Schnautz, B.; Hauptmann, R.; Henkel, G. *Acta Crystallogr. Sect. C: Cryst. Struct. Commun.* **1999**, *55*, 489.

(186) Sellmann, D.; Käppler, O.; Knoch, F. *J. Organomet. Chem.* **1989**, *367*, 161.

(187) Sellmann, D.; Ruf, R.; Knoch, F.; Moll, M. *Inorg. Chem.* **1995**, *34*, 4745.

(188) Sellmann, D.; Emig, S.; Heinemann, F. W.; Knoch, F. *Angew. Chem. Int. Ed.* **1997**, *36*, 1201.

(189) Sellmann, D.; Emig, S.; Heinemann, F. W. *Angew. Chem. Int. Ed.* **1997**, *36*, 1734.

(190) Heinrich, L.; Li, Y.; Vaissermann, J.; Chottard, G.; Chottard, J.-C. *Angew. Chem. Int. Ed.* **1999**, *38*, 3526.

(191) Kawamoto, T.; Kuma, H.; Kushi, Y. *Bull. Chem. Soc. Jpn.* **1997**, *70*, 1599.

(192) Kawamoto, T.; Nagasawa, I.; Kuma, H.; Kushi, Y. *Inorg. Chim. Acta* **1997**, *265*, 163.

(193) Tsagkalidis, W.; Rehder, D. *J. Biol. Inorg. Chem.* **1996**, *1*, 507.

(194) Yano, T.; Arii, H.; Yamaguchi, S.; Funahashi, Y.; Jitsukawa, K.; Ozawa, T.; Masuda, H. *Eur. J. Inorg. Chem.* **2006**, *2006*, 3753.

(195) Heinrich, L.; Li, Y.; Provost, K.; Michalowicz, A.; Vaissermann, J.; Chottard, J.-C. *Inorg. Chim. Acta* **2001**, *318*, 117.

(196) Yano, T.; Wasada-Tsutsui, Y.; Kajita, Y.; Shibayama, T.; Funahasi, Y.; Ozawa, T.; Masuda, H. *Chem. Lett.* **2008**, *37*, 66.

(197) Li, Y.; Lai, Y.-H.; Mok, K. F.; Drew, M. G. B. *Inorg. Chim. Acta* **1999**, *285*, 31.

(198) Li, Y.; Martell, A. E.; Hancock, R. D.; Reibenspies, J. H.; Anderson, C. J.; Welch, M. J. *Inorg. Chem.* **1996**, *35*, 404.

(199) Zheng, Y. Y.; Saluja, S.; Yap, G. P. A.; Blumenstein, M.; Rheingold, A. L.; Francesconi, L. C. *Inorg. Chem.* **1996**, *35*, 6656.

(200) Francesconi, L. C.; Liu, B.-L.; Billings, J. J.; Carroll, P. J.; Graczyk, G.; Kung, H. F. *J. Chem. Soc., Chem. Commun.* **1991**, 94.

(201) Grapperhaus, C. A.; Li, M.; Patra, A. K.; Poturovic, S.; Kozlowski, P. M.; Zgierski, M. Z.; Mashuta, M. S. *Inorg. Chem.* **2003**, *42*, 4382.

(202) Bharadwaj, P. K.; Potenza, J. A.; Schugar, H. J. *J. Am. Chem. Soc.* **1986**, *108*, 1351.

(203) Marsh, R. E.; Clemente, D. A. *Inorg. Chim. Acta* **2007**, *360*, 4017.

(204) Desbenoit, N.; Galardon, E.; Roussel, P.; Artaud, I.; Tomas, A. *J. Coord. Chem.* **2009**, *62*, 2472.

(205) Shaban, S. Y. *Inorg. Chim. Acta* **2011**, *367*, 212.

(206) Hanss, J.; Krüger, H.-J. *Angew. Chem. Int. Ed.* **1996**, *35*, 2827.

(207) Chatel, S.; Chauvin, A.-S.; Tuchagues, J.-P.; Leduc, P.; Bill, E.; Chottard, J.-C.; Mansuy, D.; Artaud, I. *Inorg. Chim. Acta* **2002**, *336*, 19.

(208) Grapperhaus, C. A.; Patra, A. K.; Mashuta, M. S. *Inorg. Chem.* **2002**, *41*, 1039.

(209) Stibrany, R. T.; Fikar, R.; Brader, M.; Potenza, M. N.; Potenza, J. A.; Schugar, H. J. *Inorg. Chem.* **2002**, *41*, 5203.

(210) Potenza, M. N.; Stibrany, R. T.; Potenza, J. A.; Schugar, H. J. *Acta Crystallogr. Sect. C: Cryst. Struct. Commun.* **1992**, *48*, 454.

(211) Alves de Sousa, R.; Galardon, E.; Rat, M.; Giorgi, M.; Artaud, I. *J. Inorg. Biochem.* **2005**, *99*, 690.

(212) Fallon, G. D.; Gatehouse, B. M. *Acta Crystallogr. Sect. B: Struct. Sci.* **1976**, *32*, 97.

(213) Fallon, G. D.; Gatehouse, B. M.; Marini, P. J.; Murray, K. S.; West, B. O. *J. Chem. Soc., Dalton Trans.* **1984**, 2733.

(214) Karsten, P.; Strahle, J. *Acta Crystallogr. Sect. C: Cryst. Struct. Commun.* **1999**, *55*, 488.

(215) Fallon, G. D.; Gatehouse, B. M. *Cryst. Struct. Commun.* **1982**, *11*, 1759.

(216) Martell, A. E.; Hancock, R. D. *Metal Complexes in Aqueous Solutions*; Plenum: New York, 1996.

(217) Constable, E. C.; Housecroft, C. E. *Chem. Soc. Rev.* **2013**, *42*, 1429.

(218) Tolman, C. A. *Chem. Rev.* **1977**, *77*, 313.

(219) Smith, J. M.; Taverner, B. C.; Coville, N. J. *J. Organomet. Chem.* **1997**, *530*, 131.

(220) Guzei, I. A.; Wendt, M. *Dalton Trans.* **2006**, 3991.

(221) Immirzi, A.; Musco, A. *Inorg. Chim. Acta* **1977**, *25*, L41.

(222) Clavier, H.; Nolan, S. P. *Chem. Commun.* **2010**, *46*, 841.

(223) Balboa, S.; Carballo, R.; Castiñeiras, A.; González-Pérez, J. M.; Niclós-Gutiérrez, J. *Polyhedron* **2013**, *50*, 512.

(224) Braunstein, P.; Taquet, J.-p.; Siri, O.; Welter, R. *Angew. Chem. Int. Ed.* **2004**, *43*, 5922.

(225) Jenkins, R. M.; Pinder, T. A.; Hatley, M. L.; Reibenspies, J. H.; Darensbourg, M. Y. *Inorg. Chem.* **2011**, *50*, 1849.

(226) Rampersad, M. V.; Jeffery, S. P.; Golden, M. L.; Lee, J.; Reibenspies, J. H.; Darensbourg, D. J.; Darensbourg, M. Y. *J. Am. Chem. Soc.* **2005**, *127*, 17323.

(227) Rampersad, M. V.; Jeffery, S. P.; Reibenspies, J. H.; Ortiz, C. G.; Darensbourg, D. J.; Darensbourg, M. Y. *Angew. Chem. Int. Ed.* **2005**, *44*, 1217.

(228) Pinder, T. A.; Montalvo, S. K.; Hsieh, C.-H.; Lunsford, A. M.; Bethel, R. D.; Pierce, B. S.; Darensbourg, M. Y. *Inorg. Chem.* **2014**, *53*, 9095.

(229) Almaraz, E.; Foley, W. S.; Denny, J. A.; Reibenspies, J. H.; Golden, M. L.; Darensbourg, M. Y. *Inorg. Chem.* **2009**, *48*, 5288.

(230) Ye, Q.; Wu, Q.; Zhao, H.; Song, Y.-M.; Xue, X.; Xiong, R.-G.; Pang, S.-M.; Lee, G.-H. *J. Organomet. Chem.* **2005**, *690*, 286.

(231) Cotton, F. A.; Kraihanzel, C. S. *J. Am. Chem. Soc.* **1962**, *84*, 4432.

(232) Phelps, A. L.; Rampersad, M. V.; Fitch, S. B.; Darensbourg, M. Y.; Darensbourg, D. J. *Inorg. Chem.* **2005**, *45*, 119.

(233) Jeffery, S. P.; Singleton, M. L.; Reibenspies, J. H.; Darensbourg, M. Y. *Inorg. Chem.* **2006**, *46*, 179.

(234) Aroney, M. J.; Buys, I. E.; Davies, M. S.; Hambley, T. W. *J. Chem. Soc., Dalton Trans.* **1994**, 2827.

(235) Lai, C.-H.; Reibenspies, J. H.; Darensbourg, M. Y. *Angew. Chem. Int. Ed.* **1996**, *35*, 2390.

(236) CCDC-1045847 *Submitted* **2014**.

(237) Chalbot, M.-C.; Mills, Allison M.; Spek, Anthony L.; Long, Gary J.; Bouwman, E. *Eur. J. Inorg. Chem.* **2003**, *2003*, 453.

(238) Green, K. N.; Jeffery, S. P.; Reibenspies, J. H.; Darensbourg, M. Y. *J. Am. Chem. Soc.* **2006**, *128*, 6493.

(239) Ito, M.; Kotera, M.; Matsumoto, T.; Tatsumi, K. *Proc. Natl. Acad. Sci. U. S. A.* **2009**, *106*, 11862.

(240) Bouwman, E.; Henderson, R. K.; Spek, A. L.; Reedijk, J. *Eur. J. Inorg. Chem.* **1999**, *1999*, 217.

(241) Peleg, A.; Lo, W.; Jiang, J. *Acta Crystallogr. Sect. Sect. E: Struct. Rep. Online* **2011**, *67*, m766.

(242) Ye, S.; Neese, F. *J. Am. Chem. Soc.* **2010**, *132*, 3646.

(243) Brothers, S. M.; Darensbourg, M. Y.; Hall, M. B. *Inorg. Chem.* **2011**, *50*, 8532.

(244) Hsieh, C.-H.; Darensbourg, M. Y. *J. Am. Chem. Soc.* **2010**, *132*, 14118.

(245) Hsieh, C.-H.; Ding, S.; Erdem, O. F.; Crouthers, D. J.; Liu, T.; McCrory, C. C. L.; Lubitz, W.; Popescu, C. V.; Reibenspies, J. H.; Hall, M. B.; Darensbourg, M. Y. *Nat. Commun.* **2014**, *5*, 3684.

(246) CCDC-1044624 *Submitted* **2014**.

(247) CCDC-1044522 *Submitted* **2014**.

(248) CCDC-1044611 *Submitted* **2014**.

(249) CCDC-1045461; CCDC-1045460; CCDC-1044794 *Submitted* **2014**.

(250) Osterloh, F.; Saak, W.; Haase, D.; Pohl, S. *Chem. Commun.* **1997**, 979.

(251) CCDC-1044523 *Submitted* **2014**.

(252) Hsieh, C. H.; Chupik, R. B.; Brothers, S. M.; Hall, M. B.; Darensbourg, M. Y. *Dalton Trans.* **2011**, *40*, 6047.

(253) Hsieh, C.-H.; Chupik, R. B.; Pinder, T. A.; Darensbourg, M. Y. *Polyhedron* **2013**, *58*, 151.

(254) Ito, M.; Kotera, M.; Song, Y.; Matsumoto, T.; Tatsumi, K. *Inorg. Chem.* **2009**, *48*, 1250.

(255) Rao, P. V.; Bhaduri, S.; Jiang, J.; Hong, D.; Holm, R. H. *J. Am. Chem. Soc.* **2005**, *127*, 1933.

(256) Gibson, D.; Lippard, S. J. *Inorg. Chem.* **1986**, *25*, 219.

(257) Turner, M. A.; Driessen, W. L.; Reedijk, J. *Inorg. Chem.* **1990**, *29*, 3331.

(258) Golden, Melissa L.; Jeffery, Stephen P.; Miller, Matthew L.; Reibenspies, Joseph H.; Darensbourg, Marcetta Y. *Eur. J. Inorg. Chem.* **2004**, *2004*, 231.

(259) Braga, D.; Grepioni, F.; Tedesco, E.; Biradha, K.; Desiraju, G. R. *Organometallics* **1997**, *16*, 1846.

(260) Brookhart, M.; Green, M. L. H.; Parkin, G. *Proc. Natl. Acad. Sci. U. S. A.* **2007**, *104*, 6908.

(261) Hirotsu, M.; Kuwamura, N.; Kinoshita, I.; Kojima, M.; Yoshikawa, Y. *Acta Crystallogr. Sect. Sect. E: Struct. Rep. Online* **2012**, *68*, m307.

(262) Barrera, H.; Suades, J.; Perucaud, M. C.; Briansó, J. L. *Polyhedron* **1984**, *3*, 839.

(263) Duff, S. E.; Barclay, J. E.; Davies, S. C.; Evans, D. J. *Inorg. Chem. Commun.* **2005**, *8*, 170.

(264) Musie, G.; Farmer, P. J.; Tuntulani, T.; Reibenspies, J. H.; Darensbourg, M. Y. *Inorg. Chem.* **1996**, *35*, 2176.

(265) Drew, M. G. B.; Rice, D. A.; Richards, K. M. *J. Chem. Soc., Dalton Trans.* **1980**, 2075.

(266) Stordal, B.; Davey, M. *IUBMB Life* **2007**, *59*, 696.

(267) Fox, S.; Stibrany, R. T.; Potenza, J. A.; Schugar, H. J. *Inorg. Chim. Acta* **2001**, *316*, 122.

(268) Jeffery, S. P.; Green, K. N.; Rampersad, M. V.; Reibenspies, J. H.; Darensbourg, M. Y. *Dalton Trans.* **2006**, 4244.

(269) Colpas, G. J.; Day, R. O.; Maroney, M. J. *Inorg. Chem.* **1992**, *31*, 5053.

(270) Golden, M. L.; Whaley, C. M.; Rampersad, M. V.; Reibenspies, J. H.; Hancock, R. D.; Darensbourg, M. Y. *Inorg. Chem.* **2005**, *44*, 875.

(271) Pinder, T. A.; Montalvo, S. K.; Lunsford, A. M.; Hsieh, C. H.; Reibenspies, J. H.; Darensbourg, M. Y. *Dalton Trans.* **2014**, *43*, 138.

(272) Konno, T.; Usami, M.; Toyota, A.; Hirotsu, M.; Kawamoto, T. *Chem. Lett.* **2005**, *34*, 1146.

(273) Krishnan, R.; Voo, J. K.; Riordan, C. G.; Zahkarov, L.; Rheingold, A. L. *J. Am. Chem. Soc.* **2003**, *125*, 4422.

(274) Birker, P. J. M. W. L.; Verschoor, G. C. *Inorg. Chem.* **1982**, *21*, 990.

(275) Taguchi, M.; Igashira-Kamiyama, A.; Kajiwara, T.; Konno, T. *Angew. Chem. Int. Ed.* **2007**, *46*, 2422.

(276) Taguchi, M.; Sameshima, Y.; Igashira-Kamiyama, A.; Akine, S.; Nabeshima, T.; Konno, T. *Chem. Lett.* **2008**, *37*, 244.

(277) Schneider, J.; Köckerling, M.; Kopitzky, R.; Henkel, G. *Eur. J. Inorg. Chem.* **2003**, *2003*, 1727.

(278) Hu, W. J.; Barton, D.; Lippard, S. J. *J. Am. Chem. Soc.* **1973**, *95*, 1170.

(279) Hess, J. L.; Young, M. D.; Murillo, C. A.; Darensbourg, M. Y. *J. Mol. Struct.* **2008**, *890*, 70.

(280) Konno, T.; Usami, M.; Hirotsu, M.; Yoshimura, T.; Kawamoto, T. *Chem. Commun.* **2004**, 2296.

(281) Bharadwaj, P. K.; John, E.; Xie, C. L.; Zhang, D.; Hendrickson, D. N.; Potenza, J. A.; Schugar, H. J. *Inorg. Chem.* **1986**, *25*, 4541.

(282) Golden, M. L.; Rampersad, M. V.; Reibenspies, J. H.; Darensbourg, M. Y. *Chem. Commun.* **2003**, 1824.

(283) Jeffery, S. P.; Lee, J.; Darensbourg, M. Y. *Chem. Commun.* **2005**, 1122.

(284) Amoroso, A. J.; Chung, S. S. M.; Spencer, D. J. E.; Danks, J. P.; Glenny, M. W.; Blake, A. J.; Cooke, P. A.; Wilson, C.; Schröder, M. *Chem. Commun.* **2003**, 2020.

(285) Miller, M. L.; Ibrahim, S. A.; Golden, M. L.; Darensbourg, M. Y. *Inorg. Chem.* **2003**, *42*, 2999.

(286) Amoureux, J. P.; Foulon, M. *Acta Crystallogr. Sect. B: Struct. Sci.* **1987**, *43*, 470.

(287) Fox, S.; Stibrany, R. T.; Potenza, J. A.; Schugar, H. J. *Acta Crystallogr. Sect. C: Cryst. Struct. Commun.* **1996**, *52*, 2731.

(288) Stibrany, R. T.; Schugar, H. J.; Potenza, J. A. *Acta Crystallogr. Sect. Sect. E: Struct. Rep. Online* **2003**, *59*, m630.

(289) Sukal, S.; Bradshaw, J. E.; He, J.; Yap, G. P. a.; Rheingold, A. L.; Kung, H. F.; Francesconi, L. C. *Polyhedron* **1998**, *18*, 7.

(290) Xu, H.-W.; Chen, Z.-N.; Ishizaka, S.; Kitamura, N.; Wu, J.-G. *Chem. Commun.* **2002**, 1934.

(291) Zhou, J.; Hu, Z.; Münck, E.; Holm, R. H. *J. Am. Chem. Soc.* **1996**, *118*, 1966.

(292) Osterloh, F.; Saak, W.; Haase, D.; Pohl, S. *Chem. Commun.* **1996**, 777.

(293) Osterloh, F.; Saak, W.; Pohl, S. *J. Am. Chem. Soc.* **1997**, *119*, 5648.

(294) Osterloh, F.; Saak, W.; Pohl, S.; Kroeckel, M.; Meier, C.; Trautwein, A. X. *Inorg. Chem.* **1998**, *37*, 3581.

(295) Spatzal, T.; Aksoyoglu, M.; Zhang, L.; Andrade, S. L. A.; Schleicher, E.; Weber, S.; Rees, D. C.; Einsle, O. *Science* **2011**, *334*, 940.

(296) Li, B.; Liu, T.; Singleton, M. L.; Darensbourg, M. Y. *Inorg. Chem.* **2009**, *48*, 8393.

(297) McGlynn, S. E.; Mulder, D. W.; Shepard, E. M.; Broderick, J. B.; Peters, J. W. *Dalton Trans.* **2009**, 4274.

(298) Rees, D. C.; Howard, J. B. *Science* **2003**, *300*, 929.

(299) Wächtershäuser, G. *Philos. Trans. R. Soc., B* **2006**, *361*, 1787.

(300) Denny, J. A.; Darensbourg, M. Y. *Chem. Rev.* **2015**, Accepted.

(301) Liaw, W. F.; Kim, C.; Darensbourg, M. Y.; Rheingold, A. L. *J. Am. Chem. Soc.* **1989**, *111*, 3591.

(302) Dorta, R.; Stevens, E. D.; Scott, N. M.; Costabile, C.; Cavallo, L.; Hoff, C. D.; Nolan, S. P. *J. Am. Chem. Soc.* **2005**, *127*, 2485.

(303) Cotton, F. A.; Troup, J. M. *J. Am. Chem. Soc.* **1974**, *96*, 3438.

(304) Keiter, R. L.; Rheingold, A. L.; Hamerski, J. J.; Castle, C. K. *Organometallics* **1983**, *2*, 1635.

(305) Pickardt, J.; Rösch, L.; Schumann, H. *J. Organomet. Chem.* **1976**, *107*, 241.

(306) Riley, P. E.; Davis, R. E. *Inorg. Chem.* **1980**, *19*, 159.

(307) Warratz, S.; Postigo, L.; Royo, B. *Organometallics* **2013**, *32*, 893.

(308) Wong, G. W.; Harkreader, J. L.; Mebi, C. A.; Frost, B. J. *Inorg. Chem.* **2006**, *45*, 6748.

(309) Poater, A.; Cosenza, B.; Correa, A.; Giudice, S.; Ragone, F.; Scarano, V.; Cavallo, L. *Eur. J. Inorg. Chem.* **2009**, *2009*, 1759.

(310) Doukov, T. I.; Blasiak, L. C.; Seravalli, J.; Ragsdale, S. W.; Drennan, C. L. *Biochemistry* **2008**, *47*, 3474.

(311) Song, L.; Wang, M.; Shi, J.; Xue, Z.; Wang, M.-X.; Qian, S. *Biochem. Biophys. Res. Commun.* **2007**, *362*, 319.

(312) Grapperhaus, C. A.; Tuntulani, T.; Reibenspies, J. H.; Darensbourg, M. Y. *Inorg. Chem.* **1998**, *37*, 4052.

(313) Lundblad, R. L. In *Chemical Reagents for Protein Modification, Fourth Edition*; CRC Press, 2014.

(314) Reynolds, C. H.; McKinley-McKee, J. S. *Eur. J. Biochem.* **1969**, *10*, 474.

(315) Dahl, K. H.; McKinley-McKee, J. S. *Eur. J. Biochem.* **1981**, *118*, 507.

(316) *Nature's Building Blocks: An A-Z Guide to the Elements*; Emsley, J., Ed.; Oxford University Press: Oxford, U.K., 2003.

(317) Berg, J. M.; Godwin, H. A. *Annu. Rev. Biophys. Biomol. Struct.* **1997**, *26*, 357.

(318) Bydalek, T. J.; Margerum, D. W. *J. Am. Chem. Soc.* **1961**, *83*, 4326.

(319) Escudero-Adán, E. C.; Benet-Buchholz, J.; Kleij, A. W. *Inorg. Chem.* **2007**, *46*, 7265.

(320) Anzellotti, A. I.; Liu, Q.; Bloemink, M. J.; Scarsdale, J. N.; Farrell, N. *Chemistry & Biology* **2006**, *13*, 539.

(321) Almaraz, E.; Denny, J. A.; Foley, W. S.; Reibenspies, J. H.; Bhuvanesh, N.; Darensbourg, M. Y. *Dalton Trans.* **2009**, 9496.

(322) Bruker In *APEX2*; Bruker AXS Inc.: Madison, Wisconsin, USA., 2007.

(323) Bruker In *SADABS*; Bruker AXS Inc.: Madison, Wisconsin, USA, 2001.

(324) Sheldrick, G. *Acta Crystallographica Section A* **2008**, *64*, 112.

(325) Barbour, L. J. *Journal of Supramolecular Chemistry* **2001**, *1*, 189.

(326) Farrugia, L. *J. Appl. Crystallogr.* **1999**, *32*, 837.

(327) Irving, H.; Williams, R. J. P. *Journal of the Chemical Society (Resumed)* **1953**, 3192.

(328) Goodman, D. C.; Tuntulani, T.; Farmer, P. J.; Darensbourg, M. Y.; Reibenspies, J. H. *Angewandte Chemie International Edition in English* **1993**, *32*, 116.

(329) Allen, F. *Acta Crystallographica Section B* **2002**, *58*, 380.

(330) Wei, C. H.; Dahl, L. F. *Inorg. Chem.* **1965**, *4*, 1.

(331) Crouthers, D. J. *Dissertation* **2015**.

(332) Nametkin, N. S.; Kolobkov, B. I.; Tyurin, V. D.; Muratov, A. N.; Nekhaev, A. I.; Mavlonov, M.; Sideridu, A. Y.; Aleksandrov, G. G.; Lebedev, A. V.; Tashev, M. T.; Dustov, H. B. *J. Organomet. Chem.* **1984**, *276*, 393.

(333) Cabeza, J. A.; Martínez-García, M. A.; Riera, V.; Ardura, D.; García-Granda, S. *Organometallics* **1998**, *17*, 1471.

(334) Tye, J. W.; Lee, J.; Wang, H.-W.; Mejia-Rodriguez, R.; Reibenspies, J. H.; Hall, M. B.; Darensbourg, M. Y. *Inorg. Chem.* **2005**, *44*, 5550.

(335) Liu, T.; Li, B.; Singleton, M. L.; Hall, M. B.; Darensbourg, M. Y. *J. Am. Chem. Soc.* **2009**, *131*, 8296.

(336) Bethel, R. D.; Crouthers, D. J.; Hsieh, C.-H.; Denny, J. A.; Hall, M. B.; Darensbourg, M. Y. *Inorg. Chem.* **2015**, ASAP.

(337) Olsen, M. T.; Justice, A. K.; Gloaguen, F.; Rauchfuss, T. B.; Wilson, S. R. *Inorg. Chem.* **2008**, *47*, 11816.

(338) Olsen, M. T.; Bruschi, M.; De Gioia, L.; Rauchfuss, T. B.; Wilson, S. R. *J. Am. Chem. Soc.* **2008**, *130*, 12021.

(339) Singleton, M. L.; Crouthers, D. J.; Duttweiler, R. P.; Reibenspies, J. H.; Darensbourg, M. Y. *Inorg. Chem.* **2011**, *50*, 5015.

(340) Crouthers, D. J.; Denny, J. A.; Bethel, R. D.; Munoz, D. G.; Darensbourg, M. Y. *Organometallics* **2014**, *33*, 4747.

(341) Lai, C.-H.; H. Reibenspies, J.; Y. Darensbourg, M. *Chem. Commun.* **1999**, 2473.

(342) Seidel, R.; Schnautz, B.; Henkel, G. *Angewandte Chemie International Edition in English* **1996**, *35*, 1710.

(343) Liu, T.; Li, B.; Popescu, C. V.; Bilko, A.; Pérez, L. M.; Hall, M. B.; Darensbourg, M. Y. *Chemistry – A European Journal* **2010**, *16*, 3083.

(344) McGuire, D. G.; Khan, M. A.; Ashby, M. T. *Inorg. Chem.* **2002**, *41*, 2202.

(345) Chávez, I.; Alvarez-Carena, A.; Molins*, E.; Roig, A.; Maniukiewicz, W.; Arancibia, A.; Arancibia, V.; Brand, H.; Manuel Manríquez*, J. *J. Organomet. Chem.* **2000**, *601*, 126.

(346) Scholz, S.; Scheibitz, M.; Schödel, F.; Bolte, M.; Wagner, M.; Lerner, H.-W. *Inorg. Chim. Acta* **2007**, *360*, 3323.

(347) Nyamori, V. O.; Zulu, S. M.; Omondi, B. *Acta Crystallogr., Sect. E: Struct. Rep. Online* **2012**, *68*, m353.

(348) Reichert, W. M.; Holbrey, J. D.; Swatloski, R. P.; Gutowski, K. E.; Visser, A. E.; Nieuwenhuyzen, M.; Seddon, K. R.; Rogers, R. D. *Crystal Growth & Design* **2007**, *7*, 1106.

(349) Castillo, J. C.; Abonia, R.; Cobo, J.; Glidewell, C. *Acta Crystallographica Section C* **2013**, *69*, 798.

(350) Naik, R. M.; Asthana, A.; Rastogi, R. *Transition Met. Chem.* **2011**, *37*, 163.

APPENDIX A

TABLES OF IR AND METRIC DATA FOR SECTION 2

Table A-1. ν(CO) IR data and related force constants for complexes **121** − **130**. Complexes are ranked by donating strength of the bidentate ligand as indicated by k_1 force constant, Figure 2-26.

CCDC Code	Compound	Solvent	A_1	B_1	A_1	B_2	NO	Avg	k_1	k_2	k_i	Rank (k_1)
FIXYUH	**126**	DMF	1986	1853	1837	1791	-----	1866.75	13.41	14.77	0.46	1
RULXEC	**128**	DMF	1988	1861	1836	1801	-----	1871.5	13.64	14.69	0.54	2
-----	**127**	DMF	1996	1872	1848	1802	-----	1879.5	13.67	14.90	0.56	3
FATNOE	**pip**	DMF	2000	1863	1852	1809	-----	1881	13.68	14.94	0.46	4
ACUWIF	**121**	DMF	1996	1873	1852	1817	-----	1884.5	13.74	14.98	0.41	5
FIXZAO	**123**	DMF	1996	1871	1857	1816	-----	1885	13.74	14.99	0.43	6
ACUWAX	**122**	DMF	1995	1871	1853	1819	-----	1884.5	13.77	14.95	0.41	7
ACUWEB	**125**	DMF	1998	1878	1854	1821	-----	1887.75	13.77	15.00	0.38	8
FIXZES	**124**	DMF	1993	1876	1843	1826	-----	1884.5	13.81	14.91	0.35	9
VIZZEK	**129**	DMF	1997	1878	1851	1824	1638	1887.5	13.94	14.86	0.51	10
FOHXUW	**bipy**	DMF	2006	1886	1870	1830	-----	1898	13.94	15.19	0.41	11
VIZZIO	**130**	DMF	1998	1880	1854	1827	1697	1889.75	13.99	14.89	0.51	12
-----	**dppe**	DMF	2015	1900	1900	1870	-----	1921.25	14.50	15.34	0.38	13
CEMSAP	**dppm**	DMF	2016	1906	1906	1870	-----	1924.5	14.50	15.43	0.38	14

Table A-2. ν(NO) IR data for complexes **144** – **157**. Complexes are sorted by donating strength of the MN_2S_2 metalloligand and the redox level of the DNIC unit.

CCDC Code	Compound	Solvent	$Fe(NO)_2^{9/10}$	Symmetric	Asymmetric	NO	CO	Avg
-----	**157**	DCM	9	1789	1728	-----	-----	1758.5
-----	**152**	THF	9	1793	1731	-----	-----	1762
-----	**153**	THF	9	1796	1733	-----	-----	1764.5
CIFTIW	**155**	DCM	9	1794	1735	1622	-----	1764.5
ARUTAJ	**145**	DCM	9	1795	1740	1763	-----	1767.5
-----	**147**	DCM	9	1806	1745	1759	-----	1775.5
-----	**144**	DCM	9	1810	1743	1779	-----	1776.5
-----	**156**	DCM	9	1805	1749	-----	-----	1777
-----	**154**	DCM	9	-----	-----	-----	-----	-----
RUFSAM	**150**	KBr	10	1663	1624	-----	-----	1643.5
-----	**149**	DCM	10	1677	1630	-----	-----	1653.5
-----	**148**	DCM	10	1687	1633	1624	-----	1660
SOBKIF	**146**	DCM	10	1690	1640	1662	-----	1665
ISIZOA	**151**	THF	10	1732	1689	-----	2007	1710.5

Table A-3. Metric parameters, Å and deg, for NiN_2S_2 complexes **1** − **21** of Figure 2-7.

Complex	Ni-N	Ni-S	N-N	S-S	Ni-Nc[a]	Ni-Sc[a]	N-Ni-N	S-Ni-S	N-Ni-S	Ni-Displacement[b]	Td Twist[c]	Code
1	1.9393(7)	2.1645(7)	2.557(5)	3.202(2)	1.458	1.457	82.5(1)	95.40(5)	91.04(4)	0.026	2.03	XISKAL
2	1.980(4)	2.158(2)	2.784(7)	3.036(3)	1.408	1.534	89.3(2)	89.4(1)	91.40(6)	0.000	13.32	VIGBES
3	1.9946(7)	2.1521(7)	2.831(2)	3.011(2)	1.405	1.538	90.42(9)	88.79(5)	90.38(4)	0.019	1.52	YOCGEC
4	1.969(4)	2.167(1)	2.728(5)	3.157(2)	1.420	1.484	87.7(1)	93.54(4)	89.4(1)	0.083	9.09	CEPXIG
5	1.937(5)	2.170(2)	2.698(6)	3.173(2)	1.389	1.480	88.3(2)	93.99(6)	89.6(1)	0.003	12.54	FANWEY
6	1.939(3)	2.168(2)	2.683(4)	3.227(3)	1.400	1.448	87.6(1)	96.18(4)	90.26(3)	0.000	21.92	WAPHEC
7	1.940(3)	2.155(1)	2.698(4)	3.181(1)	1.394	1.453	88.1(1)	95.16(4)	89.25(9)	0.005	14.15	AYIDOB
8	1.9226(7)	2.1576(7)	2.634(6)	3.161(2)	1.400	1.469	86.5(3)	94.2(1)	89.57(7)	0.053	4.27	LAHDUU
9	1.953(7) 1.862(2)	2.1691(8)	2.590(7)	3.2104(9)	1.402	1.459	85.5(2)	95.47(3)	89.5(1)	0.028 0.176	4.96 19.08	BABPEB
10	1.857(2) 1.954(2)	2.1771(9)	2.574(3)	3.210(1)	1.406	1.472	85.0(1)	94.96(3)	89.99(8)	0.055	5.04	UCAMOC
11	1.858(8) 1.989(7)	2.157(2)	2.621(9)	3.244(3)	1.409	1.422	85.8(3)	97.52(9)	89.1(2)	0.007	13.22	QETKIK
12	1.856(7)	2.114(3)	2.54(1)	3.070(3)	1.353	1.454	86.4(3)	93.1(1)	90.4(2)	0.007	3.29	NIFSEA
13	1.879(2)	2.1706(9)	2.558(4)	3.229(1)	1.377	1.451	85.79(9)	96.10(3)	89.06(7)	0.019	1.69	NIFSAW
14	1.866(3)	2.1848(9)	2.519(4)	3.313(1)	1.376	1.424	84.9(1)	98.62(4)	88.23(9)	0.004	1.74	BABPAX
15	1.874(1)	2.1791(5)	2.491(2)	3.3222(7)	1.400	1.410	83.32(7)	99.33(2)	88.71(5)	0.012	3.29	WARJOP
16	1.8619(2)	2.1831(2)	2.527(1)	3.2761(5)	1.367	1.443	85.49(4)	97.24(2)	88.60(3)	0.038	3.07	VIPJOT
17	1.858(2)	2.1807(8)	2.526(3)	3.319(1)	1.362	1.415	85.67(9)	99.10(3)	87.66(7)	0.003	3.20	LAHDAA
18	2.019(2)	2.1741(7)	3.047(2)	2.9151(9)	1.324	1.613	98.00(6)	84.20(2)	89.11(4)	0.013	6.94	GODHEM
19	2.002(3)	2.175(1)	3.006(4)	2.949(1)	1.323	1.599	97.3(1)	85.36(4)	88.79(8)	0.029	5.91	KIGYEE
20	1.987(1)	2.1649(5)	2.947(2)	2.9817(7)	1.332	1.570	95.77(4)	87.05(2)	88.65(3)	0.001	3.56	WAPGIF
21	1.972(2)	2.159(1)	2.855(3)	3.007(1)	1.361	1.549	92.7(1)	88.29(3)	89.72(7)	0.019	7.51	XAYSAS

a. Distance from nickel to a centroid placed midway between the two nitrogens or sulfurs.
b. Displacement of nickel from the best N_2S_2 plane.
c. Dihedral angle of NiN_2 and NiS_2 planes.

Table A-4. Metric parameters, Å and deg, for NiN_2S_2 complexes **22** − **33** of Figure 2-9.

Complex	Ni-N	Ni-S	N-N	S-S	Ni-Nc[a]	Ni-Sc[a]	N-Ni-N	S-Ni-S	N-Ni-S	Ni-Displacement[b]	Td Twist[c]	Code
22	2.006(1)	2.1868(6)	2.770(2)	2.8971(7)	1.451	1.638	87.34(5)	82.97(2)	94.90(4)	0.018	4.04	AFEGAU
23	1.9363(5)	2.1918(7)	2.628(1)	2.9161(9)	1.422	1.637	85.48(4)	83.40(1)	96.09(1)	0.000	11.59	IKEPIX
24	1.936(2)	2.1902(8)	2.606(3)	2.955(1)	1.432	1.617	84.6(1)	84.85(3)	95.45(7)	0.003	6.68	WARJUV
25	1.83(1) 1.93(1)	2.160(4) 2.187(4)	2.53(2)	3.049(5)	1.392	1.549	84.6(6)	89.1(1)	84.3(5) 102.1(4)	0.000	0.00	LAHJAG
26	1.930(6)	2.153(2)	2.679(8)	3.150(2)	1.390	1.468	87.9(2)	94.02(6)	89.3(2)	0.005	6.68	XAYRUL
27	1.8538	2.1572	2.4543	3.2385	1.390	1.425	82.9	97.28	90.93	0.004	2.02	BAEINI
28	1.84(3)	2.16(1)	2.41(3)	3.20(1)	1.379	1.439	82.0(10)	96.1(4)	90.9(8)	0.013	5.51	KUXRIE
29	1.823(6)	2.145(6)	2.538(4)	3.182(5)	1.309	1.438	88.19	95.8	87.76	0.092	7.84	EASANI
30	1.947(4)	2.161(2)	2.741(5)	3.233(2)	1.384	1.434	89.4(1)	96.86(5)	89.0(1)	0.008	21.61	YUMBAJ
31	1.809(7)	2.119(3)	2.470(9)	3.097(4)	1.322	1.445	86.1(3)	94.0(1)	90.0(2)	0.013	2.38	TEPGIG
32	1.810(2)	2.130(1)	2.485(3)	3.145(2)	1.316	1.437	86.7(1)	95.17(4)	89.15(8)	0.009	4.54	TEPGOM
33	1.815(4)	2.129(2)	2.481(5)	3.129(3)	1.325	1.444	86.2(2)	94.61(6)	89.6(1)	0.007	1.12	AXEHEQ

a. Distance from nickel to a centroid placed midway between the two nitrogens or sulfurs.
b. Displacement of nickel from the best N_2S_2 plane.
c. Dihedral angle of NiN_2 and NiS_2 planes.

Table A-5. Metric parameters, Å and deg, for NiN_2S_2 complexes **34 − 44** of Figures 2-11 and 2-12.

Complex	Ni-N	Ni-S	N-N	S-S	Ni-Nc[a]	Ni-Sc[a]	N-Ni-N	S-Ni-S	N-Ni-S	Ni-Displacement[b]	Td Twist[c]	Code
34	1.800(5)	2.113(2)	2.471(6)	3.118(3)	1.309	1.426	86.7(2)	95.11(5)	89.1(1)	0.009	0.78	UDOQAG
35	1.82(1)	2.13(1)	2.47(1)	3.14(1)	1.333	1.440	85.6(3)	94.9(1)	89.7(2)	0.034	2.96	UDOQEK
36	1.804(3)	2.112(2)	2.457(5)	3.076(2)	1.321	1.447	85.8(1)	93.50(5)	90.4(1)	0.001	1.89	UDOPOT
37	1.884(5)	2.152(2)	2.579(7)	2.843(3)	1.374	1.616	86.4(2)	82.69(6)	95.6(2)	0.011	0.87 8.93	MELHUG
38	1.86(1)	2.157(5)	2.53(2)	2.882(8)	1.356	1.605	86.0(5)	83.8(2)	95.0(4)	0.008	2.77	SEDZEG
39	1.903(1)	2.1577(4)	2.603(2)	2.8286(5)	1.388	1.630	86.30(5)	81.91(2)	96.89(4)	0.001	15.93	ROKGUT
40	1.921(3)	2.174(2)	2.595(2)	2.760(1)	1.417	1.679	84.96(9)	78.83(5)	98.37(5)	0.000	8.47	TELBER
41	1.881(2)	2.1441(6)	2.596(2)	2.8505(8)	1.361	1.602	87.28(7)	83.33(2)	96.47(5)	0.005	21.14	TIXQEX
42	1.912(3)	2.169(2)	2.748(4)	2.878(4)	1.330	1.623	91.88(9)	83.13(2)	92.96(7)	0.004	10.55	TEDPUO
43	2.178(9)	2.368(5)	2.91(1)	3.551(6)	1.622	1.568	83.7(3)	97.1(1)	87.6(2)	0.428	-----	CEPXEC
44	1.970(2)	2.1850(7)	2.716(3)	3.2231(8)	1.427	1.475	87.16(9)	95.05(3)	88.55(7)	0.116	-----	YUJZAF

a. Distance from nickel to a centroid placed midway between the two nitrogens or sulfurs.
b. Displacement of nickel from the best N_2S_2 plane.
c. Dihedral angle of NiN_2 and NiS_2 planes.

Table A-6. Metric parameters, Å and deg, for M(bme-dach) complexes **45 − 53** of Figure 2-13.

Complex	M-N	M-S	N-N	S-S	M-Nc[a]	M-Sc[a]	N-M-N	S-M-S	N-M-S	M-Displacement[b]	Td Twist[c]	Code
45	2.0744(9)	2.2825(9)	2.637(8)	3.540(2)	1.601	1.441	78.9(2)	101.71(5)	89.67(3)	(Pd) 0.018	1.34	OJAVIF
46	2.0886(7)	2.2974(8)	2.70(2)	3.582(3)	1.593	1.439	80.6(3)	102.45(7)	88.48(2)	(Pt) 0.000	0.02	IFEGAC
47	2.16(2)	2.291(7)	2.75(4)	3.50(1)	1.658	1.481	79.2(8)	99.5(2)	90.7(6)	(Au) 0.001	1.62	OJAVEB
48[d]	2.2270(2)	2.3077(2) 2.4960(2)	2.617(2)	3.8950(3)	1.803	1.409	71.9(2)	108.29(6)	85.0(2)	(Zn) 0.582	-----	IFEFUV
49[d]	2.278(9)	2.378(3) 2.409(2)	2.65(2)	3.849(4)	1.850	1.397	71.3(4)	108.07(9)	82.9(3)	(Fe) 0.688	-----	-----
50	2.4958(6)	2.5621(6) 2.8418(8)	2.680(5)	4.690(2)	2.106	1.032	64.94(9)	132.50(3)	81.48(1)	(Cd) 0.000	-----	RANYEM
51	2.013(3)	2.2314(8)	2.561(3)	3.288(1)	1.553	1.509	79.02(9)	94.91(3)	86.99(7)	(Fe) 0.490	-----	RAWHED
52	1.965(8)	2.221(3)	2.54(1)	3.311(4)	1.499	1.480	80.6(3)	96.4(1)	88.6(2)	(Co) 0.334	-----	VIZZAG
53	2.0926(1)	2.3188(1)	2.550(1)	3.4409(2)	1.659	1.555	75.09	95.8	84.55	(Al) 0.650	-----	-----

a. Distance from M to a centroid placed midway between the two nitrogens or sulfurs.
b. Displacement of M from the best N_2S_2 plane.
c. Dihedral angle of MN_2 and MS_2 planes.
d. See text for discussion of distortion between square pyramidal and TBP.

Table A-7. Metric parameters, Å and deg, of M(bme-daco) complexes **54** − **63** of Figures 2-14 and 2-15.

Complex	M-N	M-S	N-N	S-S	M-Nc[a]	M-Sc[a]	N-M-N	S-M-S	N-M-S	M-Displacement[b]	Td Twist[c]	Code
54	2.0906(5)	2.2823(6)	2.882(3)	3.354(2)	1.515	1.548	87.15(9)	94.56(4)	89.06(2)	(Pd) 0.060	4.50	ZIQZOO
55[d]	2.2429(3)	2.3270(3) 2.4929(3)	2.9103(6)	3.6292(7)	1.707	1.588	80.90(9)	97.64(5)	84.64(8)	(Zn) 0.567	-----	KULXUK
56[d]	2.8006(3)	2.6191(2) 2.7315(3)	2.9689(2)	3.7682(2)	2.375	1.900	64.0(5)	89.5(1)	73.0(4)	(Pb) 1.393	-----	ACAVIK
57[d]	2.249(4)	2.3462(4) 2.4195(4)	2.9311(6)	3.5936(8)	1.714	1.565	81.1(1)	97.88(5)	83.73(8)	(Fe) 0.588	-----	KINRUU
58	2.074(6)	2.244(3)	2.852(8)	3.120(4)	1.506	1.612	86.9(2)	88.11(9)	87.1(2)	(Fe) 0.480	-----	ABIJEB
59	2.039(5)	2.225(2)	2.831(6)	3.108(2)	1.468	1.592	87.9(2)	88.63(6)	88.6(1)	(Co) 0.372	-----	RAWHIH
60	2.071(2)	2.2257(8)	2.868(3)	3.045(1)	1.494	1.624	87.64(7)	86.32(3)	87.31(5)	(Fe) 0.479	-----	RAWHAZ
61[d]	2.2925(4)	2.3129(4) 2.4439(4)	2.9331(6)	3.6210(8)	1.762	1.544	79.5(2)	99.1(1)	83.9(2)	(Fe) 0.578	-----	GITFOE
62	2.2203(6)	2.3309(4)	2.8877(6)	3.3405(7)	1.687	1.626	81.1(2)	91.5(1)	84.4(2)	(Fe) 0.649	-----	GITGAR
63	2.2004(6)	2.3358(8)	2.856(1)	3.361(1)	1.674	1.623	80.9(3)	92.0(1)	84.9(2)	(Fe) 0.624	-----	GITGEV

a. Distance from M to a centroid placed midway between the two nitrogens or sulfurs.
b. Displacement of M from the best N_2S_2 plane.
c. Dihedral angle of MN_2 and MS_2 planes.
d. See text for discussion of distortion between square pyramidal and TBP.

Table A-8. Metric parameters, Å and deg, for MN_2S_2 complexes **64 − 73** of Figure 2-16.

Complex	M-N	M-S	N-N	S-S	M-Nc[a]	M-Sc[a]	N-M-N	S-M-S	N-M-S	M-Displacement[b]	Code
64	2.045(1)	2.2147(5)	3.034(2)	3.0137(7)	1.371	1.623	95.80(5)	85.75(2)	86.86(4)	(Co) 0.308	RAWHON
65	2.0878(9)	2.2242(9)	3.056(2)	3.044(2)	1.423	1.622	94.1	86.34	85.53	(Fe) 0.414	MCPFEB
66	2.0773(2)	2.2367(3)	2.8012(4)	3.1113(5)	1.534	1.607	84.79	88.14	86.72	(Fe) 0.548	MECECO
67[c]	2.2075(2) 2.3371(2)	2.3245(3) 2.4896(2)	3.2226(4)	3.5637(5)	1.604	1.620	90.28	95.45	83.64	(Fe) 0.605	MCPRDE
68[c]	2.197(4) 2.316(4)	2.304(2) 2.471(8)	2.88(1)	3.58(1)	1.738	1.583	79.28	97.01	83.58	(Fe) 0.671	MCENDI
69	2.0958(9)	2.2866(8)	2.8197(9)	4.569(2)	1.550	0.094	84.56	175.34	84.55	(Fe) -----	MENTFE
70	2.052(1)	2.246(1) 2.314(1)	2.833(2)	4.546(3)	1.485	0.181	87.29	171.1	86.77	(Co) -----	MEENCO
71[c]	1.876(5)	2.248(2)	2.501(7)	3.352(2)	1.398	1.498	83.7(2)	96.42(7)	85.8(2)	(Fe) 0.399	BECKAX
72[c]	1.846(5)	2.173(2)	2.4782(8)	3.186(2)	1.369	1.477	84.3(2)	94.32(6)	87.8(2)	(Co) 0.317	OBODAK
73[c]	2.2508(3) 2.3699(3)	2.4084(5) 2.6132(4)	3.3007(7)	3.764(1)	1.618	1.665	91.14(6)	97.02(2)	81.83(4)	(Mn) 0.639	HIPYOU

a. Distance from M to a centroid placed midway between the two nitrogens or sulfurs.
b. Displacement of M from the best N_2S_2 plane.
c. See text for discussion of distortion between square pyramidal and TBP.

Table A-9. Metric parameters, Å and deg, for MN_2S_2 complexes **74 − 81** of Figures 2-17.

Complex	M-N	M-S	N-N	S-S	M-Nc[a]	M-Sc[a]	N-M-N	S-M-S	N-M-S	M-Displacement[b]	Code
74[c]	1.9520(6)	2.265(1)	2.5708(6)	3.460(1)	1.469	1.462	82.4(3)	99.6(1)	83.1(2)	(Ru) 0.494	VAKYOV
75	1.972(5)	2.290(2)	2.615(8)	2.612(3)	1.476	1.408	83.1(2)	104.13(7)	82.8(2)	(Ru) 0.385	ZEQKIP
76	1.843(5)	2.204(2)	2.512(6)	3.380(2)	1.349	1.414	85.9(2)	100.18(8)	84.9(2)	(Fe) 0.270	ETINIF
77	1.8405(9)	2.1856(8)	2.511(6)	3.254(2)	1.346	1.459	86.0(2)	96.24(6)	86.51(4)	(Fe) 0.288	RETCIC
78	1.854(5)	2.193(2)	2.489(7)	3.263(2)	1.374	1.464	84.3(2)	96.19(7)	86.7(2)	(Fe) 0.331	RETCOI
79	1.847(5)	2.184(2)	2.486(6)	3.222(2)	1.365	1.475	84.6(2)	95.03(6)	86.7(1)	(Fe) 0.355	RIRXUL
80	1.8338(5)	2.1804(5)	2.4722(6)	3.2719(8)	1.355	1.442	84.8(2)	97.24(5)	86.7(1)	(Fe) 0.282	BECJOK
81	1.952(7)	2.219(3)	2.80(1)	3.067(4)	1.360	1.603	91.7(3)	87.5(1)	86.4(2)	(Fe) 0.393	LAQKOD

a. Distance from M to a centroid placed midway between the two nitrogens or sulfurs.
b. Displacement of M from the best N_2S_2 plane.
c. See text for discussion of distortion between square pyramidal and TBP.

Table A-10. Metric parameters, Å and deg, for MN_2S_2 complexes **82** − **92** of Figures 2-18, 2-19, and 2-20.

Complex	M-N	M-S	N-N	S-S	M-Nc[a]	M-Sc[a]	N-M-N	S-M-S	N-M-S	M-Displacement[b]	Td Twist[c]	Code
82	1.816(2)	2.1387(6)	2.473(2)	3.1841(8)	1.329	1.428	85.87(8)	96.22(2)	89.22(6)	(Co) 0.035	8.71	POQLOW
83	1.825(4)	2.171(2)	2.492(5)	3.228(2)	1.333	1.451	86.1(2)	96.10(6)	88.9(1)	(Co) 0.015	2.24	GADFOI
84	1.96(2)	2.233(6)	2.58(2)	3.517(8)	1.467	1.375	82.7(6)	103.9(2)	86.8(5)	(Pt) 0.020	6.07	NUCTOU
85[d]	1.901(8) 2.154(8)	2.334(7)	2.67(1)	3.277(9)	1.534	1.661	81.9(2)	89.26(8)	82.1(1)	(V) 0.748 0.866	-----	ALACOF
86	1.899(3)	2.141(1)	2.854(3)	2.934(1)	1.253	1.559	97.4(1)	86.50(4)	88.22(9)	(Co) 0.035	7.36	PENBEQ
87	1.919(3)	2.142(1)	2.897(3)	2.924(1)	1.258	1.565	98.1(1)	86.13(3)	87.90(8)	(Co) 0.016	1.27	PENBUG
88	1.9735(3)	2.2491(3)	3.018(2)	3.1562(8)	1.272	1.602	99.77(6)	89.12(2)	85.55(4)	(Co) 0.000	-----	PENBOA
89	1.882(7)	2.130(3)	2.73(1)	2.956(5)	1.292	1.534	93.2(3)	87.9(1)	89.4(2)	(Co) 0.047	3.88	VIWQEX
90	1.897(4)	2.143(1)	2.566(5)	2.972(2)	1.397	1.544	85.1(2)	87.81(5)	86.7(1) 100.4(1)	(Co) 0.003	3.72	QIVJIP
91	2.1512(3)	2.3320(4)	3.386(2)	3.822(1)	1.327	1.336	103.83(6)	110.07(2)	73.04(4)	(Rh) 0.016	-----	GOSJON
92	2.0701(4)	2.2770(5)	3.221(6)	3.594(3)	1.300	1.399	102.1(1)	104.21(7)	76.63(2)	(Pd) 0.085	7.22	GOSJED

a. Distance from M to a centroid placed midway between the two nitrogens or sulfurs.
b. Displacement of M from the best N_2S_2 plane.
c. Dihedral angle of MN_2 and MS_2 planes.
d. See text for discussion of distortion between square pyramidal and TBP.

Table A-11. Metric parameters, Å and deg, for MN_2S_2 complexes **93 − 99** of Figure 2-21.

Complex	M-N	M-S	N-N	S-S	M-Nc[a]	M-Sc[a]	N-M-N	S-M-S	N-M-S	M-Displacement[b]	Code
93	2.115(1)	2.309(3)	2.77(1)	3.659(4)	1.600	1.409	81.7(3)	104.8(1)	86.81(5)	(In) 0.000	ZOQBAI
94	2.1471(9)	2.2836(9)	2.732(6)	3.45(2)	1.656	1.496	79.0(2)	98.1(2)	85.64(4)	(Ga) 0.496	TUNZUX
95	2.142(3)	2.252(1)	2.707(3)	3.923(2)	1.661	1.104	78.3(1)	121.25(4)	88.33(8)	(Ga) 0.623	VIKKIJ
96	2.282(4)	2.4517(9)	2.844(7)	4.157(4)	1.784	1.301	77.1(2)	115.9(1)	83.49(5)	(In) 0.000	ZOPZUZ
97	2.327(5)	2.448(3)	2.836(9)	3.896(5)	1.845	1.482	75.1(2)	105.47(8)	82.32(3)	(In) 0.601	TUPBAH
98	2.307(6)	2.422(2)	2.809(9)	3.901(3)	1.831	1.436	75.0(2)	107.28(8)	83.2(2)	(In) 0.542	TUPBEL
99	2.333(4)	2.466(4)	2.887(5)	3.973(4)	1.832	1.460	76.5(1)	107.4(1)	81.1(1)	(In) 0.787	TUPBIP

a. Distance from M to a centroid placed midway between the two nitrogens or sulfurs.
b. Displacement of M from the best N_2S_2 plane.

Table A-12. Metric parameters, Å and deg, for MN_2S_2 complexes **100 − 106** of Figure 2-22.

Complex	M-N	M-S	N-N	S-S	M-Nc[a]	M-Sc[a]	N-M-N	S-M-S	N-M-S	M-Displacement[b]	Td Twist[c]	Code
100	2.255(1)	2.3670(5)	2.870(2)	3.6897(6)	1.742	1.415	78.91(5)	110.94(2)	85.43(4)	(Zn) 0.449	-----	IJUGOJ
101	2.1299(6)	2.2366(6)	2.931(3)	4.257(2)	1.546	0.687	86.94(7)	144.25(4)	91.42(5)	(Zn) -----	72.40	AYIFAP
102	2.0163(8)	2.2308(7)	2.75(1)	3.408(5)	1.475	1.440	86.0(4)	99.6(1)	89.25(2)	(Cu) 0.000	21.22	DOMKIZ
103	1.845(3)	2.152(1)	2.541(4)	3.169(2)	1.339	1.456	87.0(2)	94.85(4)	89.1(1)	(Cu) 0.016	3.42	UGASUR
104[d]	2.1734(1)	2.2938(4) 2.5692(4)	2.8184(2)	3.7810(4)	1.656	1.535	80.79(5)	101.92(1)	78.19(3) 84.35(3)	(Zn) 0.745	-----	UMEVIS
105	2.086(6)	2.256(2)	2.890(7)	4.255(3)	1.504	0.750	87.7(2)	141.15(7)	89.7(2)	(Zn) -----	68.00	ALACUL
106	2.121(2)	2.2389(9)	2.885(3)	4.184(1)	1.555	0.799	85.71(9)	138.20(3)	90.92(7)	(Zn) -----	67.37	UMEVOY

a. Distance from M to a centroid placed midway between the two nitrogens or sulfurs.
b. Displacement of M from the best N_2S_2 plane.
c. Dihedral angle of MN_2 and MS_2 planes.
d. See text for discussion of distortion between square pyramidal and TBP.

Table A-13. Metric parameters, Å and deg, for MN_2S_2 complexes **107 − 114** of Figure 2-23.

Complex	M-N	M-S	N-N	S-S	M-Nc[a]	M-Sc[a]	N-M-N	S-M-S	N-M-S	M-Displacement[b]	Td Twist[c]	Code
107	1.962(2)	2.241(1)	2.625(3)	3.439(2)	1.459	1.436	84.0(1)	100.26(3)	87.89(7)	(Cu) 0.018	2.07	TIQPOY
108	1.864(3)	2.148(1)	2.578(3)	3.092(1)	1.346	1.490	87.5(1)	92.11(4)	90.31(8)	(Cu) 0.013	5.41	TIQPUE
109	1.8620(2)	2.1451(5)	2.562(1)	3.0886(6)	1.351	1.489	86.93(5)	92.10(2)	90.54(5)	(Cu) 0.000	3.63	UGASOL
110	1.945(5)	2.202(2)	2.575(5)	3.166(2)	1.458	1.530	82.9(1)	91.96(5)	86.4(1)	(Fe) 0.481	-----	WUCBUR
111	1.925(9)	2.194(4)	2.51(1)	3.119(4)	1.459	1.543	81.4(4)	90.6(1)	86.9(3)	(Fe) 0.513	-----	WUCCAY
112	2.046(2)	2.2316(8)	2.752(3)	3.579(1)	1.513	1.333	84.57(8)	106.62(3)	89.30(6)	(Cu) 0.024	32.76	UGUWAU
113	2.1016(4)	2.2534(6)	2.855(2)	4.240(1)	1.542	0.764	85.58(6)	140.36(2)	92.33(4)	(Zn) -----	70.98	KOPYOD
114	2.033(6)	2.311(2)	2.672(9)	3.973(3)	1.532	1.181	82.2(3)	118.55(8)	99.9(2)	(Zn) -----	67.72	FILGEN

a. Distance from M to a centroid placed midway between the two nitrogens or sulfurs.
b. Displacement of M from the best N_2S_2 plane.
c. Dihedral angle of MN_2 and MS_2 planes.

Table A-14. Metric parameters, Å and deg, for MN_2S_2 complexes **115 − 120** of Figure 2-24.

Complex	M-N	M-S	N-N	S-S	M-Nc[a]	M-Sc[a]	N-M-N	S-M-S	N-M-S	M-Displacement[b]	Td Twist[c]	Code
115	1.976(4)	2.223(2)	2.671(5)	3.134(2)	1.457	1.577	85.0(2)	89.63(5)	95.2(1)	(Cu) 0.004	24.94	MELJAO
116[d]	1.917(1)	2.201(2)	2.618(2)	2.951(2)	1.400	1.633	86.18	84.21	94.28	(Co) 0.181	-----	TSALCO
117	1.97(4)	2.21(1)	2.61(5)	2.90(2)	1.474	1.666	83(1)	82.0(5)	94(1)	(Fe) 0.398	-----	DABMUO
118	2.154(5)	2.339(2)	2.699(7)	3.329(3)	1.679	1.643	77.6(2)	90.77(6)	86.6(1)	(Fe) 0.689	-----	HIPYIO
119	1.9677(8)	2.2738(9)	2.693(1)	3.107(1)	1.435	1.660	86.37	86.21	93.71	(Fe) 0.010	-----	BUHKUK
120[d]	2.121(2)	2.2989(6) 2.4085(6)	2.675(3)	3.720(1)	1.646	1.442	78.18(6)	103.65(2)	89.14(5)	(Zn) 0.473	-----	TIXQUN

a. Distance from M to a centroid placed midway between the two nitrogens or sulfurs.
b. Displacement of M from the best N_2S_2 plane.
c. Dihedral angle of MN_2 and MS_2 planes.
d. See text for discussion of distortion between square pyramidal and TBP.

Table A-15. Metric parameters, Å and deg, for $MN_2S_2W(CO)_{4/5}$ complexes **121 − 133** of Figures 2-26 and 2-30.

Complex	M-N	M-S	N-N	S-S	M-Nc[a]	M-Sc[a]	M-W	N-M-N	S-M-S	N-M-S	M-Displacement[b]	Hinge Angle[c]	Code
121	1.933(3)	2.167(1)	2.571(5)	3.126(2)	1.444	1.502	3.249(2)	83.4(1)	92.29(6)	91.65(5)	(Ni) 0.139	132	ACUWIF
122	1.9721(7)	2.1899(7)	2.829(4)	3.034(1)	1.374	1.579	3.350(1)	91.7(1)	87.70(5)	90.31(4)	(Ni) 0.024	131	ACUWAX
123	1.978(3)	2.169(1)	2.840(5)	3.007(3)	1.377	1.564	3.388(3)	91.8(1)	87.75(4)	90.24(3)	(Ni) 0.010	134	FIXZAO
124	1.9874(7)	2.1898(8)	3.008(5)	2.926(2)	1.299	1.629	3.033(1)	98.4(1)	83.84(5)	88.89(4)	(Ni) 0.015	106	FIXZES
125	1.944(6)	2.155(2)	2.744(9)	3.087(3)	1.378	1.504	3.021(1)	89.8(3)	91.49(8)	90.6(2)	(Ni) 0.001	112	ACUWEB
126	1.848(9)	2.172(3)	2.53(1)	3.195(3)	1.349	1.472	2.931(1)	86.3(4)	94.7(1)	89.2(3)	(Ni) 0.111	106	FIXYUH
127	1.992(4)	2.586(1)	2.545(7)	3.352(2)	1.533	1.695	3.298(1)	79.4(2)	89.36(6)	82.7(1)	(V) 0.729	103	-----
128	2.207(3)	2.395(1)	2.632(5)	3.412(2)	1.772	1.681	3.5120(6)	73.2(1)	90.84(4)	86.0(1)	(Zn) 0.744	124	RULXEC
129	2.032(7)	2.260(2)	2.61(1)	3.153(3)	1.559	1.619	3.431(1)	79.8(3)	88.48(9)	88.3(2)	(Fe) 0.552	122	VIZZIO
130	2.00(2)	2.223(6)	2.62(2)	3.151(7)	1.508	1.569	3.392(3)	82.0(6)	90.2(2)	90.1(4)	(Co) 0.385	124	VIZZEK
131	2.004(4)	2.165(1)	2.850(6)	3.017(2)	1.408	3.017	3.848(1)	90.7(2)	88.36(5)	90.6(1)	(Ni) 0.025	107.95[d]	NECXUP
132	1.982(9)	2.178(3)	2.83(1)	3.060(2)	1.392	1.550	4.021(2)	90.9(3)	89.3(1)	90.8(3)	(Ni) 0.002	115.44[d]	HEYCAQ
133	2.4008(4)	2.5508(5)	2.601(1)	4.439(1)	2.018	1.257	4.252(2)	65.6(9)	107.3(2)	81.9(6)	(Cd) 0.494	112.66[d]	RANYAI

a. Distance from M to a centroid placed midway between the two nitrogens or sulfurs.
b. Displacement of M from the best N_2S_2 plane.
c. Dihedral angle between best N_2S_2 plane (without M) and best S_2WC_2 plane.
d. Defined as the M-S-W angle.

Table A-16. Metric parameters, Å and deg, for $MN_2S_2M'(CO)_x$ complexes **134 − 143** of Figures 2-33.

Complex	M-N	M-S	N-N	S-S	M-Nc[a]	M-Sc[a]	M-M'	N-M-N	S-M-S	N-M-S	M-Displacement[b]	Hinge Angle[c]	Code
134	1.986(9)	2.164(4)	2.79(1)	3.066(5)	1.410	1.527	3.762(2)	89.5(4)	90.2(1)	90.2(3)	(Ni) 0.036	113.36[d]	TUBFIF
135	1.936(5)	2.158(1)	2.536(6)	3.208(2)	1.462	1.442	3.791(1)	81.9(2)	96.08(5)	91.1(1)	(Ni) 0.017	115.29[d]	-----
136	1.957(6)	2.155(3)	2.780(8)	2.896(3)	1.377	1.596	3.094(4)	90.6(2)	84.5(1)	92.3(2)	(Ni) 0.090	130	TUBFOL
137	2.069(4)	2.166(1)	2.843(6)	4.133(1)	1.504	0.650	2.5096(8)	86.8(1)	145.10(5)	91.3(1)	(Ni) -----	-----	QAFPIX
138	1.861(4)	2.1942(8)	2.534(6)	3.326(2)	1.363	1.432	3.2924(8) 3.5394(8)	85.8(2)	98.55(5)	87.9(1)	(Ni) 0.020	96.39[d]	JEMKUI
139	1.961(3)	2.1699(9)	2.824(4)	2.922(1)	1.361	1.604	2.8709(6)	92.1(1)	84.64(3)	91.08(8)	(Ni) 0.144	112	JEMLAP
140	2.002(2)	2.1911(8)	3.047(3)	2.888(1)	1.300	1.648	2.6598(6)	99.06(8)	82.45(3)	89.26(6)	(Ni) 0.022	98	HUBYIN
141	1.894(6)	2.194(2)	2.528(8)	2.926(2)	1.410	1.635	2.835(2)	83.8(3)	83.64(7)	96.3(2)	(Ni) 0.020	110	IKEPOD
142[e]	2.1681(4) 2.3303(6)	2.3458(5) 2.4435(6)	2.8541(6)	3.6093(8)	1.740	1.575	3.098(1) 3.8985(9)	78.7(1)	97.79(4)	83.28(8)	(Fe) 0.668	113[d]	GOCZIH
143[e]	2.247(1)	2.3347(4) 2.4516(4)	2.861(2)	3.5181(5) 3.6315(5)	1.735	1.543 1.640	3.0945 (4) 2.8505 (3)	79.02(5)	96.66(2)	83.80(4)	(Fe) 0.665	127	ERIDOZ

a. Distance from M to a centroid placed midway between the two nitrogens or sulfurs.
b. Displacement of M from the best N_2S_2 plane.
c. Dihedral angle between best N_2S_2 plane (without M) and $M'S_2$ plane.
d. Defined as the M-S-M' angle
e. See text for discussion of distortion between square pyramidal and TBP.

Table A-17. Metric parameters, Å and deg, for $MN_2S_2Fe'(NO)_2$ complexes **144 − 157** of Figures 2-34 and 2-36.

Complex	M-N	M-S	N-N	S-S	M-Nc[a]	M-Sc[a]	M-Fe'	N-M-N	S-M-S	N-M-S	M-Displacement[b]	Hinge Angle[c]	Code
144	2.0617(2)	2.2415(2)	2.7831(4)	3.1500(5)	1.521	1.595	2.7130(3)	84.9	89.28	89.46	(Fe) 0.518	115	-----
145	2.032(2)	2.2514(8)	2.571(3)	3.253(1)	1.573	1.557	2.7860(8)	78.51(8)	92.52(2)	87.60(6)	(Fe) 0.524	127	ARUTAJ
146	2.0360(7)	2.2456(9)	2.5951(9)	3.132(1)	1.569	1.609	3.006(1)	79.18	88.43	88.59	(Fe) 0.550	129	SOBKIF
147	2.0521(5)	2.2472(4)	2.8014(5)	3.1431(6)	1.500	1.606	2.7606(6)	86.09	88.75	87.64	(Fe) 0.445	118	-----
148	2.0077(5)	2.2164(6)	2.7946(7)	2.9763(7)	1.442	1.642	2.9860(7)	88.21	84.36	90.48	(Co) 0.353	119	-----
149	1.9739(9)	2.1645(9)	2.814(1)	2.938(1)	1.385	1.590	3.001(2)	90.91	85.47	91.54	(Ni) 0.101	121	-----
150	1.9855(9)	2.176(1)	3.063(3)	2.839(1)	1.263	1.649	2.796(2)	101.0(1)	81.45(6)	88.77(5)	(Ni) 0.028	105	RUFSAM
151	1.937(5)	2.166(3)	2.569(5)	3.180(3)	1.449	1.470	3.229(3)	83.1(2)	94.51(5)	91.2(1)	(Ni) 0.016	91.27[d]	ISIZOA
152	1.9728(5)	2.1825(6)	2.7804(6)	3.0925(7)	1.400	1.540	3.4218(7) 3.7396(9)	89.61	90.22	90.04	(Ni) 0.060	105.19[d]	-----
153	2.183(2)	2.421(1) 2.322(2)	2.872(1)	3.304(2)	1.584	1.702	3.731(3)	84.4	88.3	84.14	(V) 0.649	103.71[d]	-----
154	2.0557(6)	2.2418(5) 2.2150(5)	2.8332(7)	3.1088(8)	1.490	1.597	3.9249(9)	87.12	88.46	85.42 88.24	(Fe) 0.478	121.49[d]	-----
155	1.960(6)	2.237(2)	2.548(9)	3.284(3)	1.489	1.520	3.697(2)	81.1(2)	94.42(7)	88.5(2)	(Co) 0.379	107.73[d]	CIFTIW
156	1.980	2.181	2.808	3.053	1.395	1.558	3.714	90.35	88.95	90.16	(Ni) 0.015	-----[d]	-----
157[e]	2.115	2.3583	2.899	3.461	1.541	1.594	3.8387	86.50	94.71	86.56	(Ni) 0.396	-----[d]	-----

a. Distance from M to a centroid placed midway between the two nitrogens or sulfurs.
b. Displacement of M from the best N_2S_2 plane.
c. Dihedral angle between best N_2S_2 plane (without M) and best $Fe'S_2$ plane.
d. Defined as the M-S-Fe' angle
e. See text for discussion of distortion between square pyramidal and TBP.

Table A-18. Metric parameters, Å and deg, for $[NiN_2S_2]_2Ni$' stair-step complexes **158 − 170** of Figure 2-38.

Complex	Charge	Ni-N	Ni-S	Ni'-S	S-S	Ni-Ni	Ni-Ni'	N-Ni-N	S-Ni-S	N-Ni-S	S-Ni'-S	Hinge Angle[a]	Code
158	2+	1.9241(4)	2.1493(4)	2.2112(3)	3.0057(5)	5.694(1)	2.8472(6)	83.6(2)	88.73(7)	92.9(2)	85.64(6) 94.36(4)	122	EROPIK
159	2+	1.9570(3)	2.1521(3)	2.1996(5)	2.8463(4)	5.369(2)	2.6847(6)	92.4(2)	82.80(7)	91.6(1)	80.63(5) 99.37(4)	103	VUHFAF
160	2+	1.9940(2)	2.1736(3)	2.1932(6)	2.7958(4)	5.6636(7)	2.8318(3)	101.84(9)	80.05(3)	88.81(7)	79.19(3) 100.81(2)	112	COPYEM
161	2+	1.9794(1)	2.1703(1)	2.2082(1)	2.8266(1)	5.5536(7)	2.7768(4)	100.4(2)	81.26(6)	89.2(1)	79.59(5) 100.41(3)	112	FIMFUD
162	2+	1.9444(8)	2.1520(9)	2.2179(8)	2.929(1)	5.495(2)	2.747(1)	90.2(2)	85.77(4)	91.2(1)	82.64(4) 97.36(3)	108	DOGTAU
163	2+	1.914(4)	2.155(5)	2.212(5)	2.885(5)	5.47(1)	2.733(7)	96.14	84.02	89.58	81.4 98.60	109	AETHNI
164	2+	1.9810(4)	2.1744(5)	2.1930(6)	2.8598(7)	6.304(1)	3.1518(5)	88.9(1)	82.24(3)	94.51(7)	81.39(2) 98.61(2)	146	LAMWAZ
165	2+	1.970(1)	2.181(3)	2.194(3)	2.839(3)	6.210(3)	3.105(2)	86.5(4)	81.2(1)	96.1(3)	80.7(1) 99.35(8)	139	TAPTRI
166	2-	1.915(2)	2.1735(4)	2.1922(4)	2.7823(5)	5.9894(2)	2.9947(2)	86.82(6)	79.59(2)	96.87(5)	78.78(1) 101.22(1)	125	WARKAC
167	2-	1.8376(6) 2.0161(5)	2.1514(6)	2.2040(9)	2.8680(8)	5.514(2)	2.7568(7)	85.8(5)	83.6(1)	86.6(3) 103.2(4)	81.18(9) 98.82(6)	110	LAHHUY
168	2-	1.844(4)	2.146(1)	2.243(1)	3.037(1)	5.3977(5)	2.6989(5)	85.8(2)	90.10(5)	91.1(1)	85.21(4) 94.79(3)	110	BABNUP
169	2-	1.8413(6)	2.1480(4)	2.2408(3)	3.0280(3)	5.3335(2)	2.6668(2)	86.49(7)	89.64(2)	90.88(5)	85.01(2) 94.99(1)	101	FEPRAU
170	1+	1.9296(7)	2.1547(7)	2.4199(7)	3.060(1)	5.328(1)	2.679(1) 3.053(1)	83.2(1)	90.48(5)	92.62(4)	78.44(4) 96.21(4)	85 139	EROPUW

a. Dihedral angle between best N_2S_2 plane (without M) and best S_4 (without M') plane.

Table A-19. Metric parameters, Å and deg, for $[MN_2S_2]_2M'$ (M = Ni; except for **174** and **175**) trimetallic complexes **171 − 180** of Figures 2-40 and 2-41.

Complex	Charge	Ni-N	Ni-S	M'-S	S-S	Ni-Ni	Ni-M'	N-Ni-N	S-Ni-S	N-Ni-S	S-M'-S	Hinge Angle[a]	Code
171 (M' = Pd)	2+	1.9572(5)	2.1733(5)	2.2950(5)	2.9474(7)	5.646(2)	2.8229(6)	91.3(3)	85.39(9)	91.0(2)	79.90(7) 100.10(5)	109	ZUVLUX
172 (M' = Pd)	2+	1.957(9)	2.190(3)	2.369(3)	3.089(4)	5.972(3)	3.100(2)	83.2(4)	89.7(1)	92.6(3)	81.38(8) 98.12(8)	133	EROPEG
173 (M' = Pd)	2+	1.964(1)	2.182(2)	2.338(2)	2.992(2)	5.888(5)	2.944(3)	91.27	86.59	90.6	79.58 100.42	116	AZNIPD
174[b] (M' = Pd)	0	2.171(2)	2.4296(6)	2.3527(5)	3.2185(1)	6.3221(6)	3.1610(3)	74.76(9)	82.96(3)	84.59(7)	86.32(3) 93.68(2)	98	OJAVAX
175[b] (M' = Pt)	0	2.186(5)	2.430(2)	2.343(1)	3.214(2)	6.399(1)	3.2010(9)	74.7(2)	82.81(6)	84.8(1)	86.62(5) 93.40(5)	99	IFEGIK
176 (M' = Cu)	2-	1.8663(2)	2.1571(2)	2.2368(3)	2.8981(3)	5.496(1)	2.7480(2)	83.3(4)	84.41(8)	89.1(3) 102.6(3)	80.75(7) 99.25(5)	109	LAHJOU
177 (M' = Ag)	3-	1.8457(2) 1.8668(2)	2.1572(3) 2.1908(3)	2.3853(3)	3.2904(5)	6.0125(9)	3.0062(6)	86.1(2)	98.36(6)	87.8(2)	180.00(3)	96	LAHDEE
178 (M' = Co)	1+	1.97(2)	2.162(7)	2.370(7) 2.477(7)	2.95(1)	5.958(8)	2.982(5)	91.2(6)	85.9(2)	91.2(5)	74.9(2) 96.4(2)	112	ZUVMAE
179 (M' = Ni)	1+	1.921(7)	2.161(3)	2.300(3)	3.209(4)	5.967(2)	3.174(2)	86.6(3)	95.9(1)	89.5(2)	123.9(1)	-----	IBOCUX
180 (M' = Ni)	2+	1.92(1)	2.147(4)	2.236(3)	2.877(5) 3.163(5)	5.317(3)	2.870(3) 3.233(2)	88.3(5)	89.5(1)	90.7(4)	79.8(1) 94.4(1)	114	LAHHAE

a. Dihedral angle between best N_2S_2 plane (without M) and best S_4 (without M') plane for **171 – 176**. Ni-S-Ag angle for **177**. Dihedral angle between best N_2S_2 plane (without M) and $M'S_2$ plane for **178** and **180**.
b. $[Zn(Cl)N_2S_2]M'$ stair-step complex

Table A-20. Metric parameters, Å and deg, for tetrametallic complexes **181** − **184** of Figure 2-42.

Complex	Charge	Ni-N	Ni-S	M'-S	S-S	Ni-Ni	Ni-M'	N-Ni-N	S-Ni-S	N-Ni-S	S-M'-S	Hinge Angle[a]	Code
181 (M' = Ni)	2+	1.9133(6)	2.1148(6)	2.222(5)	2.934(6)	7.937(4)	2.8481(9)	87.4(9)	87.9(2)	92.0(6)	81.3(2) 98.3(2)	126	LAHHOS
182 (M' = Rh)	3+	1.9228(2)	2.1520(2)	2.3790(8)	3.0360(3)	5.3831(4)	3.1284(3)	83.5(4)	89.7(1)	92.5(3)	79.30(3)	131	YEQHUY
183 (M' = Pb)	2+	1.92(1)	2.136(5)	2.895(4)	3.099(6)	6.041(4)	3.489(3)	83.0(5)	93.0(2)	91.9(4)	85.5(1)	115	FIYMEG
184 (M' = Fe)	2+	1.98(1)	2.164(6)	2.473(6)	2.881(8)	5.333(3)	3.123(4)	98.9(6)	83.4(3)	88.8(5)	69.5(2)	111	PASHEW

a. Dihedral angle between best N_2S_2 plane (without M) and best S_4 (without M') plane for **181**. Dihedral angle between best N_2S_2 plane (without M) and M'S_2 plane for **182** − **184**.

Table A-21. Metric parameters, Å and deg, for $[MN_2S_2]_2M'_2$ (M = Ni; except for **193**, **196**, **197**, and **200**) C_2 propeller or paddlewheel complexes **185** − **200** of Figures 2-43 and 2-44.

Complex	Charge	Ni-N	Ni-S	M'-S	M'-M'	S-S	Ni-Ni	Ni-M'	N-Ni-N	S-Ni-S	N-Ni-S	S-M'-S	Hinge Angle[a]	Code
185 (M' = Au)	2+	1.977(2)	2.1861(9)	2.3021(9)	3.1273(5)	3.050(1)	5.594(1)	3.2045(7)	90.48(8)	88.47(3)	90.30(7)	177.97(2)	94	TINDEB
186 (M' = Au)	2+	1.923(4)	2.183(2)	2.298(1)	3.1103(4)	3.215(2)	5.754(1)	3.2706(9)	82.6(2)	94.90(5)	91.2(1)	177.35(4)	99	TINDAX
187 (M' = Au)	2-	1.852(4)	2.192(1)	2.293(1)	3.1170(6)	3.302(2)	5.762(1)	3.2754(8)	85.6(1)	97.71(4)	88.4(1)	175.35(4)	99	TINDOL
188 (M' = Au)	2+	1.935(6)	2.185(2)	2.294(2)	3.0045(4)	3.129(2)	6.156(1)	3.4252(6)	91.2(2)	91.46(5)	88.7(2)	175.45(6)	107	TAWZUN
189 (M' = Cu)	2-	1.872(2)	2.1736(5)	2.1761(4)	2.8561(3)	3.2251(7)	5.2322(3)	2.9805(3)	86.14(7)	95.78(2)	89.04(5)	170.26(2)	91	GUZCEJ
190 (M' = Cu)	2+	1.9319(7)	2.1680(8)	2.168(1)	2.866(1)	3.186(1)	5.816(2)	2.940(1) 3.518(1)	88.9(1)	94.56(4)	89.3(1)	165.21(3)	108	IKENUH
191 (M' = Au)	2-	1.902(4)	2.146(4)	2.286(4)	2.966(6)	3.118(6)	6.12(1)	3.258(7) 3.580(8)	90.08	93.18	88.54	175.36	-----	BEPMEO
192 (M' = Au)	2-	1.923(4)	2.180(2)	2.303(1)	2.9836(3)	3.228(2)	6.1489(7)	3.2409(6) 3.6546(6)	86.9(1)	95.67(5)	88.7(1)	174.57(5)	-----	PICKES
193[b] (M' = Au)	2-	2.11(4)	2.285(5)	2.299(5)	2.996(1)	3.397(6)	6.014(2)	3.410(2) 3.752(2)	93.6(7)	96.1(1)	85.2(5)	176.0(2)	-----	NIXWUN
194 (M' = Hg)	3-	1.86(2)	2.1763(5)	2.441(4)	3.772(1)	3.296(6)	4.375(3)	3.250(2) 3.372(2) 3.705(2)	86.0(7)	98.4(2)	87.7(5)	145.7(1) 148.6(1)	-----	LAHDOO
195 (M' = Cu)	2-	1.854(3)	2.182(1)	2.173(2)	2.6434(9)	3.308(2)	4.897(1)	2.7854(9) 3.1241(9)	86.4(1)	98.62(5)	87.5(1)	167.48(5)	-----	LAHDII
196[b] (M' = Cu)	0	2.1955(3)	2.2734(7)	2.1716(3)	2.6747(7)	4.3825(9)	4.5697(5)	2.6475(3)	97.92(5)	149.11(2)	111.71(3)	157.82(2)	-----	EHIFUW
197[b] (M' = Cu)	0	2.201(5)	2.268(2)	2.167(2)	2.7259(9)	4.335(2)	4.6251(9)	2.685(1)	96.2(2)	145.77(6)	89.0(1)	163.17(7)	-----	EHIFOQ
198 (M' = Zn)	2+	1.9197(3)	2.1585(3)	2.3208(3)	4.449(2)	3.1618(5)	5.782(2)	3.6507(9)	86.3(3)	94.18(9)	89.6(2)	111.56(7)	-----	LAHFAC
199 (M' = Zn)	0	1.9343(6)	2.1777(8)	2.3773(8)	4.475(2)	3.284(3)	5.782(2)	3.203(1) 4.056(1)	85.8(2)	97.90(7)	89.9(2)	113.90(6)	-----	LAHFEG
200[b] (M' = Zn)	0	2.0922(5)	2.2854(5)	2.3493(5)	4.9805(9)	4.3947(8)	5.0267(8)	3.5380(7)	87.13	148.09	91.74	106.78	-----	MCECZN

a. Dihedral angle between best N_2S_2 plane (without M) and best S_4 (without M') plane.
b. PdN_2S_2 for **193**, CuN_2S_2 for **196** and **197**, and ZnN_2S_2 for **200**.

Table A-22. Metric parameters, Å and deg, for $[MN_2S_2]_3M'_2$ (M = Ni; except for **202**, **206**, and **208**) C_3 paddlewheel complexes **201** − **212** of Figures 2-46 and 2-47.

Complex	Charge	Ni-N	Ni-S	M'-S	M'-M'	S-S	Ni-Ni	Ni-M'	N-Ni-N	S-Ni-S	S-M'-S	Torsion[a]	M'-Displacement[b]	Code
201	2+	1.9320(1)	2.1703(1)	2.5148(1)	2.998(1)	3.1950(1)	5.2179(1)	3.3650(4)	82.8(2)	94.80(8)	119.67(4)	3.95(4)	0.111	FIYMAC
202[d]	2+	2.0101(6)	2.2371(7)	2.5073(7)	2.866(3)	3.314(3)	6.279(3)	3.900(1)	79.3(5)	95.6(2)	118.57(7)	7.94(7)	0.423	SOJFON
203	2+	1.867(6)	2.148(2)	2.548(2)	3.038(1)	3.219(3)	4.819(1)	3.170(1)	82.9(3)	97.05(8)	119.87(7)	1.23(7)	0.09	WAHNUP
204	2+	1.90(2)	2.161(3)	2.290(4)	3.094(2)	3.228(4)	4.827(2)	3.183(2)	85.7(7)	96.7(1)	119.9(1)	2.9(1)	0.075	LAHFUW
205	2+	2.006(4)	2.194(1)	2.284(2)	2.644(1)	2.993(2)	5.2895(9)	3.3462(9)	97.6(2)	86.02(6)	119.31(5)	28.07(6)	0.175	GUZCAF
206[d]	2+	2.01(1)	2.254(5)	2.262(5)	3.016(4)	3.468(6)	4.973(3)	3.037(4)	84.8(5)	100.6(2)	119.7(2)	45.1(2)	0.125	FASVOK
207	2+	1.864(6)	2.149(2)	2.602(2)	3.1934(9)	3.214(3)	4.850(1)	2.985(1) 3.537(1)	82.6(2)	96.78(7)	116.85(6)	5.41(6)	0.015	WAHPAX
208[d]	1+	2.0437(2)	2.2615(2)	2.247(1) 2.387(1)	3.923(2)	3.597(3)	4.9035(4)	3.557(1) 3.339(1)	83.5(3)	105.4(1)	119.99(8) 107.08(7)	49.96(4)	0.026 0.885	UGUWOI
209	1+	1.928(6)	2.170(2)	2.251(2) 2.355(2)	3.373(1)	3.200(2)	4.987(1)	3.336(1)	82.8(2)	95.05(7)	118.97(7) 115.02(7)	22.88(7)	0.229 0.533	FIYLOP
210	0	1.988(3)	2.164(6)	2.3165(1)	4.052(3)	3.031(8)	5.050(6)	3.552(5)	89.8(8)	88.9(3)	115.3(3)	0.0(2)	0.51	IJOHOE
211	2+	1.917(6)	2.169(2)	2.330(2) 2.382(2)	4.277(1)	3.204(2)	5.086(2)	3.853(1) 3.436(1)	83.0(2)	95.25(6)	114.72(6) 111.28(5)	26.26(5)	0.542 0.719	FIYLUV
212	2+	2.0087(4)	2.1868(4)	2.355(3)	4.354(2)	3.0399(3)	5.1081(7)	3.666(2)	90.0(6)	88.1(2)	112.50(7)	3.02(4)	0.658	KULYAR

a. Defined as the average of the S-M'-M'-S torsion angles.
b. Displacement of M' from the S_3 plane.
c. Dihedral angle between best N_2S_2 plane (without M) and best M'_2S_2 plane.
d. $Fe(NO)N_2S_2$ for **202** and CuN_2S_2 for **206** and **208**.

Table A-23. Metric parameters, Å and deg, for $[MN_2S_2]_4M'_2$ (M = Ni; except for **217**) C_4 paddlewheel complexes **213 − 219** of Figure 2-48.

Complex	Charge	Ni-N	Ni-S	M'-S	M'-M'	S-S	Ni-Ni	Ni-M'	N-Ni-N	S-Ni-S	N-Ni-S	S-M'-S	Torsion[a]	Hinge Angle[b]	Code
213	4+	1.9737(7)	2.162(3)	2.5257(8)	2.142(1)	3.001(3)	5.334(2)	3.9215(2)	90.9(4)	87.89(9)	90.5(3)	88.35(9)	2.08(7)	133	YAPRIR
214	4+	1.9209(5)	2.1420(5)	2.5170(5)	2.1624(7)	3.097(1)	5.049(1)	3.7300(8)	83.3(2)	92.60(5)	92.0(2)	88.03(5)	0.99(3)	129	YAPROX
215	4+	1.9139(4)	2.1243(5)	2.3595(5)	2.8924(6)	3.044(1)	4.935(1)	3.7772(8)	82.9(2)	91.56(3)	92.6(1)	89.94(4)	0.36(3)	130	YEQHOS
216	4+	1.9400(5)	2.1569(7)	2.3339(4)	3.1315(8)	3.198(2)	4.8595(1)	3.7758(8)	82.5(3)	95.67(5)	90.8(2)	89.99(6)	0.79(4)	132	EROPOQ
217[c]	4+	2.1019(7)	2.2786(9)	2.3287(7)	3.095(2)	3.224(8)	4.997(3)	3.855(2)	95.1(6)	90.1(2)	87.2(4)	89.95(2)	0.29(3)	127	UJUYUT
218	4-	1.858(4)	2.1747(7)	2.231(1)	3.2099(5)	3.308(2)	4.726(7)	3.7070(7)	85.3(2)	99.00(5)	87.6(1)	89.97(4)	0.73(4)	136	WARKIK
219	4+	1.9172(3)	2.1649(3)	2.2192(4)	3.024(5)	3.3889(6)	4.6578(9)	3.632(2)	77.3(5)	103.0(1)	89.9(4)	89.9(2)	32.2(2)	-----	UJUYON

a. Defined as the average of the S-M'-M'-S torsion angles.
b. Dihedral angle between best N_2S_2 plane (without M) and best S_4 (without M') plane.
c. PdN_2S_2 for **217**.

APPENDIX B

ADDITIONAL EXCHANGE REACTIONS MODELLING THE BIOLOGICAL TRANSFER OF NICKEL

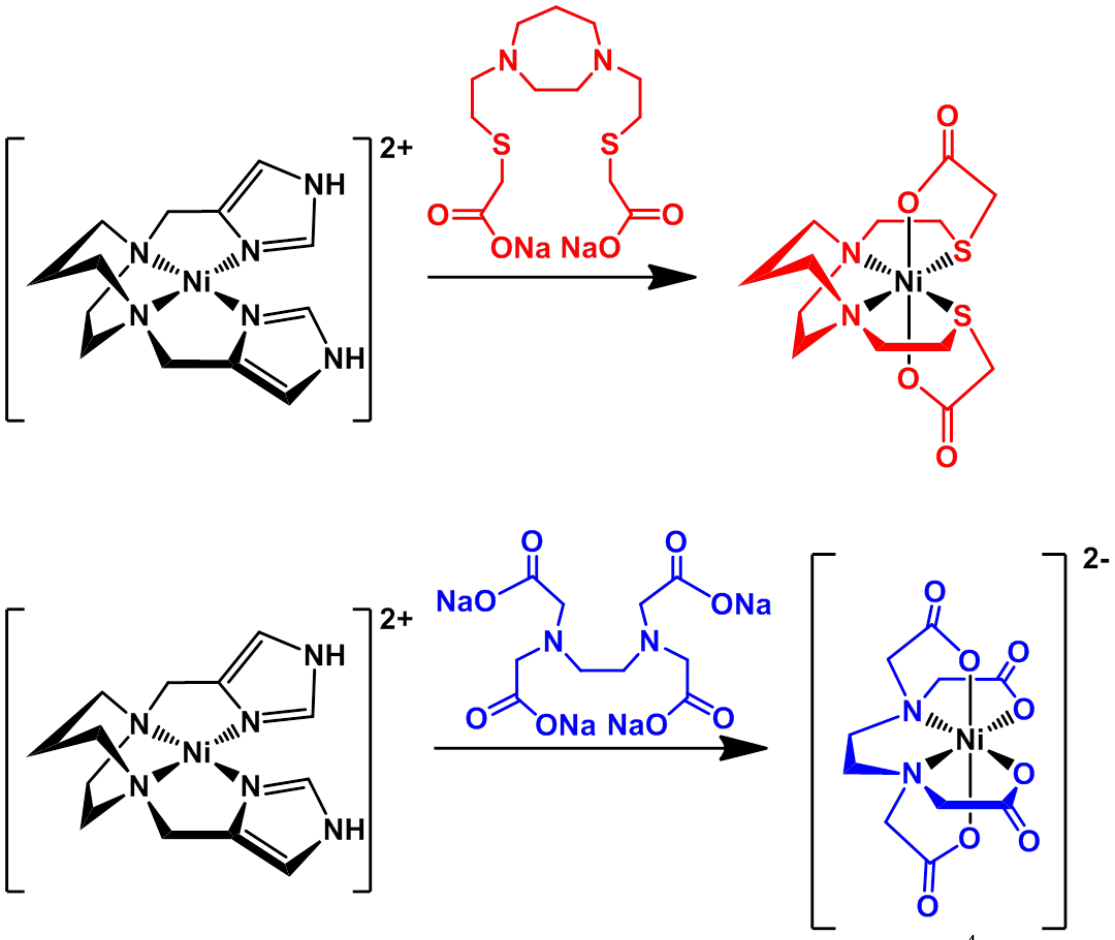

Figure B-1. Exchange reactions between a NiN_4 complex and $EDTA^{4-}$ and $N_2S_2^{2-}$ ligands. Products were confirmed by UV-Vis and mass spectrometry.

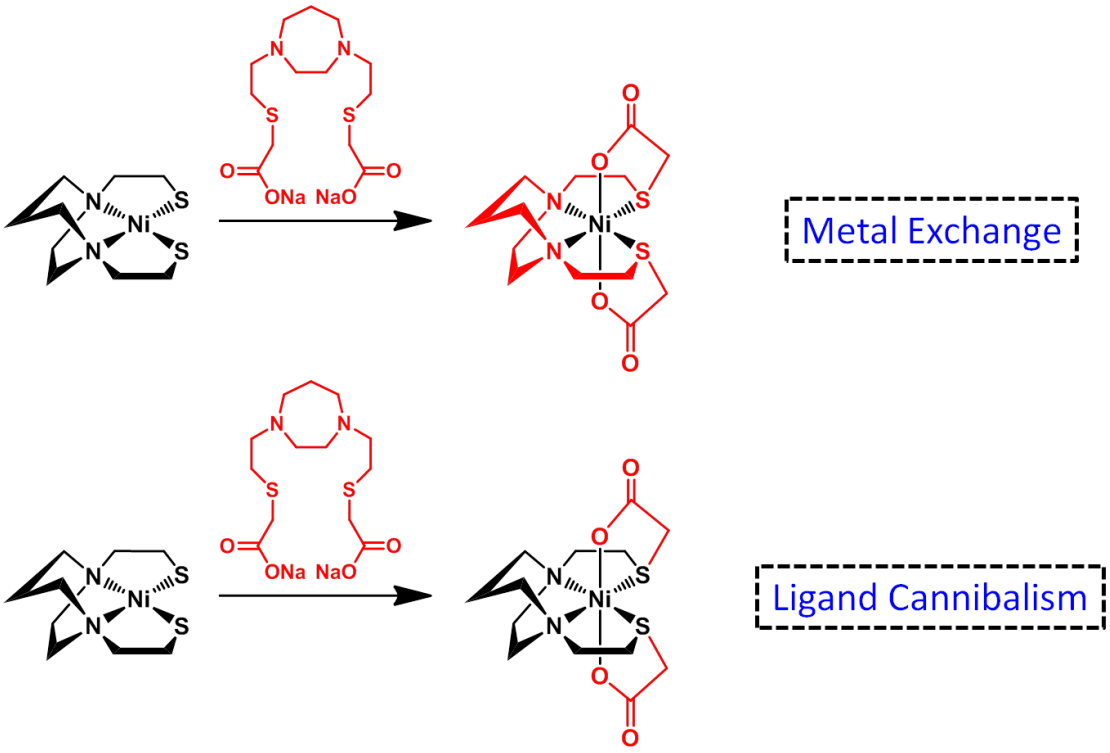

Figure B-2. Exchange reaction between NiN_2S_2 complex and the hexadentate $N_2S_2O_2^{2-}$ ligand. Product was confirmed by UV-Vis and mass spectrometry. The reaction could result from metal exchange or ligand cannibalism as shown in the figure. Further investigation indicated cannibalism is the class.

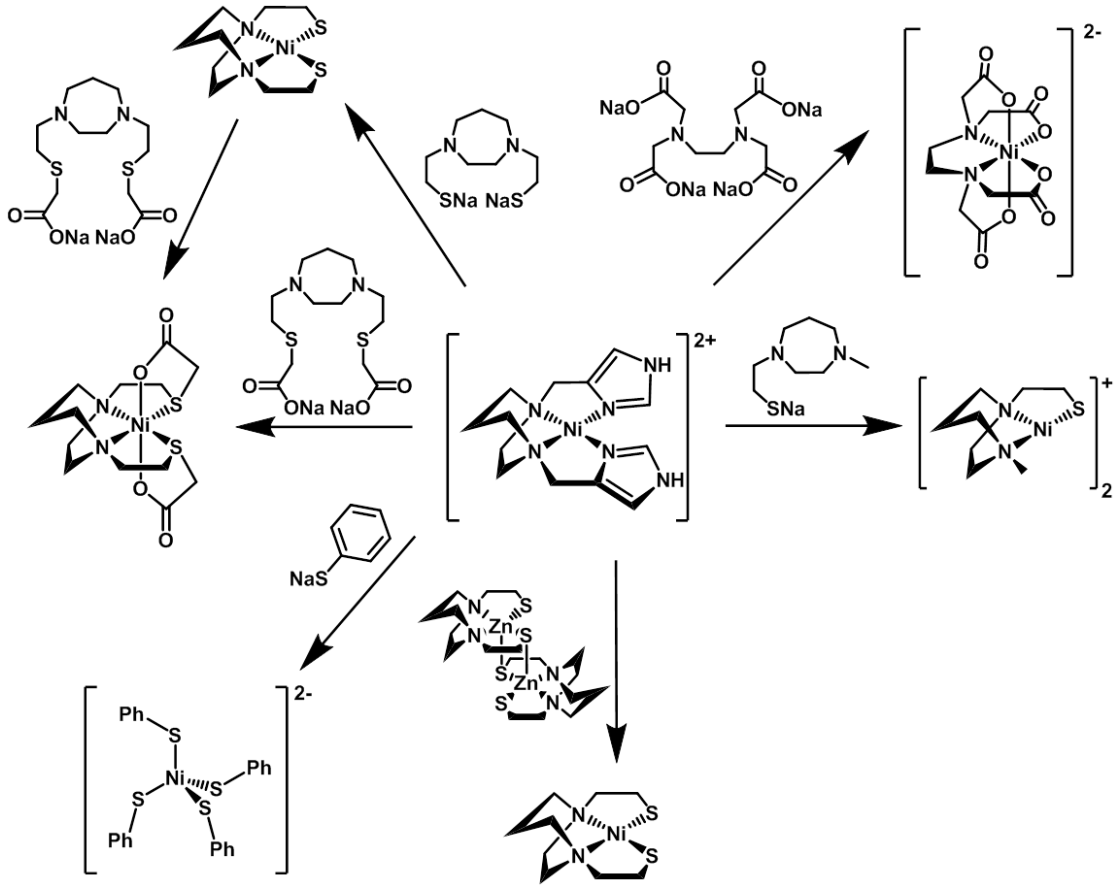

Figure B-3. Summation of ligand exchange reactions successfully performed. All products were confirmed by UV-Vis and mass spectroscopy.

APPENDIX C

MOLAR ABSORBTIVITY VALUES USED TO CALCULATE EQUILIBRIUM CONSTANTS

	359	**497**	**527**	**564**	**575**
Co-1'-Ac_2	------	25.276	25.791	21.955	18.908
Ni-1'-Ac_2	27.471	-----	-----	-----	22.997
$Co(NO_3)_2$	-----	5.9088	6.792	2.3874	1.3945
$Ni(NO_3)_2$	0.7249	-----	-----	-----	0.2541

APPENDIX D

DERIVATION OF EQUATIONS USED TO CALCULATE EQUILIBRIUM CONSTANTS

$$A_1 = \varepsilon_1 * c_1$$

$$A_2 = \varepsilon_2 * c_2$$

$$A_1 + A_2 = A_{total}$$

$$\varepsilon_1 * c_1 + \varepsilon_2 * c_2 = A_{total}$$

$$c_1 = \frac{mol\ Co(NO_3)_2}{V_{total}}$$

$$c_2 = \frac{mol\ Co1'Ac_2}{V_{total}}$$

$$x + y = initial$$

$$\varepsilon_1 * \frac{x}{V_{total}} + \varepsilon_2 * \frac{initial - x}{V_{total}} = A_{total}$$

$$mol\ Ni(NO_3)_2 + mol\ Ni1'Ac_2 = mol\ initial\ Ni(NO_3)_2 = Z$$

$$mol\ Co(NO_3)_2 + mol\ Co1'Ac_2 = mol\ initial\ Co1'Ac_2 = Z$$

$$mol\ Co1'Ac_2 + mol\ Ni1'Ac_2 = mol\ initial\ mol\ Co1'Ac_2 = Z$$

$$mol\ Co(NO_3)_2 + mol\ Co1'Ac_2 = mol\ Co1'Ac_2 + mol\ Ni1'Ac_2$$

$$K = \frac{[Ni1'Ac_2][Co(NO_3)_2]}{[Co1'Ac_2][Ni(NO_3)_2]} = \frac{[Ni1'Ac_2][Ni1'Ac_2]}{[Co1'Ac_2][Ni(NO_3)_2]} = \frac{[Ni1'Ac_2][Ni1'Ac_2]}{[Z - Ni1'Ac_2][Z - Ni1'Ac_2]}$$